FRACTURES IN WATER MAINS - THE EFFECT OF LONGITUDINAL BENDING

THOMAS REGAN

A THESIS SUBMITTED FOR THE DEGREE OF
DOCTOR OF PHILOSOPHY AT
THE CITY UNIVERSITY, LONDON

THE DEPARTMENT OF
CIVIL ENGINEERING

JUNE 1982

CONTENTS

LIST OF TABLES

LIST OF TABLES

LIST OF TABLES

LIST OF TABLES

LIST OF FIGURES

LIST OF FIGURES

LIST OF FIGURES

LIST OF FIGURES

ACKNOWLEDGEMENTS

The writer carried out the work described in this Thesis under the sponsorship of The Science Research Council, and would also like to acknowledge the assistance of The Metropolitan Water Board and The Metropolitan Water Division of The Thames Water Authority.

The writer would like to thank his supervisors, Dr. N. P. Roberts and later Dr. P. R. S. Speare, who kindly stepped in on the retirement of Dr. Roberts, both of The City University, for the help and encouragement they have given, and [redacted] of The Metropolitan Water Division who acted as a liaison between the two bodies.

The writer would like to thank the many technicians in the University for their help in the experimental work and also the many members of the Staff of The Metropolitan Water Division for their help in the collection and analysis of the mains fracture data, especially the members of the Computing Department, the Library and last but not least the members of The Distribution Drawing Office.

The writer would also like to thank [redacted] of The City University who typed this Thesis.

DECLARATION

I grant powers of descretion to the University Librarian to allow this Thesis to be copied in whole or in part without further reference to me.

This permission covers only single copies made for study purposes, subject to normal conditions of acknowledgement.

ABSTRACT

A brief history of water distribution mains and the materials used is given together with a review of research into the fracture of water mains. Although much was known about the fracture of pipes there has not been a systematic study of failures to investigate the primary causes.

An analysis of mains fracture data shows that for small and medium size pipes, there are two primary fracture triggering mechanisms, corrosion and longitudinal bending, and a variety of secondary mechanisms. A flow chart linking the primary and secondary fracture triggering mechanisms with the type of fracture they produce is given.

The effect of longitudinal bending is analysed first by using an elastic model to obtain design formulae, by which the performance of various materials and pipe sizes can be compared. The formulae are also used to investigate the vulnerability of spun and ductile iron to the onset of fissure corrosion. The effect of a concentrated surface load is also investigated and found to be a secondary effect for small and medium size mains.

A second mathematical model is described in which the ground can have a non-linear pressure-displacement relationship and the pipeline material a non-linear stress-strain relationship. The model was used to investigate the effect of differential displacement on pipelines in non-homogeneous soils and from the results obtained recommendations are made with regard to pipe laying procedures.

Experimental investigations into the effect of differential displacement on a buried pipeline are described and the results compared with those obtained from the second mathematical model.

Finally as the major causes of fractures are known, the economics of mains replacement are discussed with regard to finding a fracture regression curve or base fracture rate with which to formulate a replacement policy.

LIST OF SYMBOLS AND ABBREVIATIONS

A	Cross-sectional area
A'	Fracture growth rate coefficient
$\underset{\sim}{A}$	Coefficient matrix
A_{pc}	Region in which fibres are inelastically strained in compression
A_{pt}	Region in which fibres are inelastically strained in tension
a	Basic elemental length
a_c	Depth of inelastic front on compression side
a_e	Depth of elastic section
a_i	Length of ith element
a_t	Depth of inelastic front on tension side
a_1	Distance between supports A and B
a_2	Distance between supports B and C
B	Height of inelastic front above centre of pipe
B_i	Height of inelastic front above centre of pipe at ith node
B_j	Iteration value of B_i
$\underset{\sim}{b}$	Vector of imposed differential displacements
$\underset{\sim}{b}_1$	Vector of imposed differential displacements and rotations
C_a	Constant dependent on area under consideration
C_b	Cost of repairing a specified main
C_d	Cost of relining per specified length of main
$C_m(t)$	Cost of repairing the fractures in a specified length of main in year t
C_p	Cost of prelining per specified length of main
C_r	Cost of replacement per specified length of main
C_s	Cost of sleeving per specified length of main
c_i	Variable equal to $a^4 k_i/6EI$
c_o	Boundary value of c_i
c_1	Distance of upper surface from centroid

LIST OF SYMBOLS AND ABBREVIATIONS

c_2	Distance of lower surface from centroid
D_c	Mean coil diameter of a spring
d	External diameter of pipe
d'	Distance of centroid from point of zero stress
d_a	Displacement
d_i	Displacement at the ith node
d_s	Specified pipe diameter
d_w	Diameter of wire in a spring
d_o	Boundary value of d_i
d_1	Displacement at first node
E	Modulus of elasticity
$E(v, \phi)$	Incomplete elliptic integral of the second kind
$E(v, \frac{\pi}{2})$	Complete elliptic integral of the second kind
E_i	Modulus of elasticity of ith beam element
E_m	Modulus of elasticity of a specified material
e	Length of circular arc
e_1	Length of elliptical arc
$F(b)$	Indefinite integral of dimensionless parameter of bending moment
F_i	Variable equal to $g_{i-1}^2 g_i$
f_i	Imposed differential displacement at ith node
f_o	Boundary value of f_i
G	Modulus of rigidity of a spring
G_i	Variable equal to $g_{i-1} + g_i$
g_i	Ratio a_i/a
g_o	Boundary value of g_i
H	Horizontal scale factor
H_i	Variable equal to $g_{i-1} g_i^2$

LIST OF SYMBOLS AND ABBREVIATIONS

h_i	Ratio $EI/E_i I_i$
h_o	Boundary value of h_i
I	Second moment of area
I_c	Second moment of area with respect to elastic-inelastic boundary 2- 2 of area A_{pc}
I_i	Second moment of area of ith beam element
I_s	Second moment of area for a specified pipe size
I_t	Second moment of area with respect to elastic-inelastic boundary 1-1 of area A_{pt}
i	Nodal number
k	Modulus of foundation x width of beam
k_A	Ground resistance above a pipeline
k_B	Ground resistance below of pipeline
k_i	Foundation modulus at ith node
k_o	Modulus of foundation (ground resistance)
L	Distance between points of maximum bending moments - differential ground displacement distance between points of zero displacement - point loading
L_p	Length of pipe
L_1	Variable equal to $4(2 - \ell_1)$
L_2	Variable equal to $g_1^2 c_1(\ell_2 + 2)$
L_3	Variable equal to $g_1^2 h_1(\ell_1 + 4)$
L_4	Variable equal to $\ell_2 - 2$
ℓ_1	Ratio m_1'/m_o'
ℓ_2	Ratio d_1/d_o
M	Bending moment

LIST OF SYMBOLS AND ABBREVIATIONS

M_I	Idealized bending moment
M_{max}	Maximum bending moment
M_r	Rupture bending moment
M_y	Least squares straight line y-intercept
m	Bending moment
m_A	Bending moment at support A
m_B	Bending moment at support B
m_C	Bending moment at support C
m_i	Bending moment acting at ith node
m_i'	Variable equal to $a^2 m_i/6EI$
m_o'	boundary value of m_i'
N	Load acting at centroid of section
N(t)	Number of fractures per specified length of main in year t
N_c	Number of active coils of a spring
N_I	Idealized load
N_y	Gradient of least squares straight line
n	Number of nodes
n'	Distance of neutral axis from most strained tension fibre
n_s	Number of supports
n_1	Distance of upper surface from centroid
n_2	Distance of lower surface from centroid
P	Point load/total force due to displacement on negative side of the origin
P.F.A	Pulverised Fuel Ash
P_{GD}	Rupture shear, ground displacement
$P_m(t_r)$	Present value of repairs in a main from year t_p to year t_r
P_{PL}	Rupture shear, point loading
P_r	Rupture shear force

LIST OF SYMBOLS AND ABBREVIATIONS

$P_r(t_r)$	Present value in year t_p of replacing length of main in year t_r
P_{rsm}	Rupture shear for specified material and pipe size
$P_T(t_r)$	Total cost of repairing and replacing a main
P_x	x-parallax correction
P_y	y-parallax correction
p	reaction force of the foundation (pressure)
p_A	Displacement of support A
p_B	Displacement of support B
p_C	Displacement of support C
p_i	Foundation pressure acting at ith node
p_x	Vertical pressure at a point within the soil
Q	Shear force
Q_c	First moment of area with respect to elastic - inelastic boundary 2-2 of area A_{pc}
Q_s	Concentrated surface load
Q_t	First moment of area with respect to elastic - inelastic boundary 1-1 of area A_{pt}
q	External distributed loading
R	External radius of pipe
R'	Discount rate (non-inflationary)
R_A	Reaction at support A
R_B	Reaction at support B
R_C	Reaction at support C
r	Internal radius of pipe
r'	Base rate of failures
S	Elastic stress gradient
S_i	Variable equal to $2(F_i\ h_{i-1} + H_i\ h_i)$

LIST OF SYMBOLS AND ABBREVIATIONS

S_r	Spring rate
s_1	Distance of elemental length from elastic - inelastic boundary 1-1
s_2	Distance of elemental length from elastic - inelastic boundary 2-2
T_i	Variable equal to $g_{i-1}\ g_i\ G_i$
t	Time
$\tan\theta_B$	Gradient at support B
t_p	Present year
t_r	Year in which pipe will be replaced
t_r^*	Optimal replacement year
t_o	Base year
t_1	Possible time to first fracture
uPVC	Unplasticized Polyvinyl Chloride
V_L	Left hand side scale factor
V_R	Right hand side scale factor
v	Square root of the eccentricity of an ellipse
v_p	Appropriate scale factor
W_i	Force acting at ith node
x	Horizontal distance
$\underset{\sim}{x}$	Vector of unknown displacements and bending moments
x_p	Distance of point under consideration to origin
y	Displacement
y_o	Displacement of beam at origin
z	Depth of point below the surface
α	Shape factor
α_c	Ratio of compressive inelastic modulus and elastic modulus
α_p	Ratio of inelastic modulus and elastic modulus

LIST OF SYMBOLS AND ABBREVIATIONS

α_t	Ratio of tensile inelastic modulus and elastic modulus
β	Characteristic of the system
Δ	Total relative ground displacement
Δ_{GD}	Displacement, ground displacement
Δ_{PL}	Displacement, point loading
Δ_r	Rupture differential displacement
Δ_1	Half total relative ground displacement
δ	Vertical and horizontal deflection of pipe section
ε	Strain
ε_{ec}	Compressive yield strain
ε_{et}	Tensile yield strain
ε_1	Strain in most strained tension fibre
ε_2	Strain in most strained compression fibre
θ_i	Rotation at ith node due to ductility of pipe material
σ	Stress
σ'	Stress acting at centroid
σ_c	Stress acting in compression area A_{pc}
σ_{ec}	Compression yield stress
σ_{et}	Tension yield stress
σ_{max}	maximum stress
σ_r	Rupture stress
σ_{rm}	Rupture stress for a specified material
σ_t	Stress acting in tension area A_{pt}
ϕ	Angle subtended at centre of pipe by arc e
ϕ_i	Variable equal to $g_{i-1}\, g_i \left[g_i(c_{i-1}\, f_{i-1} + c_i\, f_i) + g_{i-1}(c_i\, f_i + c_{i+1}\, f_{i+1}) \right]$
ϕ_1	boundary value of ϕ_i

CHAPTER 1

INTRODUCTION

1.1 PROLOGUE

The fracture of water mains is a problem that water undertakings have come to live with. Every water distribution network suffers from failures of one form or another, at varying rates, depending on the location and the material composition of the pipes used in the reticulation.

The research into the causes of fractures in grey cast iron water mains was commissioned by The Metropolitan Water Board (now The Metropolitan Water Division of Thames Water) to ascertain the major types of fracture, their probable causes and whether or not any ameliorating action was possible.

1.2 HISTORY OF WATER DISTRIBUTION MAINS AND MATERIALS

The generally used method of supplying water to the people of London in the seventeenth century was in wooden pipes, (1). The pipes were mostly made of elm trunks which were bored by means of long augers and then countersunk at the thicker end (the butt) and tapered at the other end (the top). A joint was effected by driving the top of one pipe into the butt of another pipe.

Wooden pipes were in use for over two centuries but the service they gave was unsatisfactory. In spite of great care and ingenuity in producing perfectly fitting joints, the tapering of the wood gave it less resistance to decay and leakage consequently arose.

The bore of the pipes was generally limited to diameters under 8" and as the pipes were unable to withstand high pressures, their carrying capacity was small. In the eighteenth century it was not uncommon for four or more wooden pipes to be laid side by side in order to convey what is now taken by a single cast iron pipe.

By the early part of the nineteenth century improved pumping machinery made it possible to afford a supply to the upper storeys of houses and to provide more water for fire fighting. It then became evident that wooden pipes would be unable to stand up to these more exacting demands.

The useful life of wooden pipes was short and uncertain, varying from under 4 years to 25 years according to the soil in which they were laid. They seem to have survived longest in clay.

After the introduction of gas lighting it was found that wooden pipes absorbed gas from leaking gas mains and the water was, as a result, sometimes unfit for consumption.

These defects were effectively overcome by the use of cast iron pipes. They had been laid on a small scale during the eighteenth century but it was not until about 1785, (2), when Thomas Simpson invented the spigot and socket joint, that their use on a large scale became a practicable proposition.

The Metropolis Paving Act of 1817, provided that all new mains to be laid were to be of iron, but allowed at the same time the repair of existing wooden ones. The use of wooden pipes declined rapidly after this, although they did not disappear until the 1850's.

The early iron pipes were cast horizontally, or on the incline, in such a manner that, owing to the floating of cores, it often happened that there was considerable difference in the thickness of the pipes at different portions of the circumference, (3). They were not dipped or coated, so that they had no protection against the action of the water internally, nor against the action of the soil or other influences externally.

A great improvement was achieved by casting the pipes vertically in sand moulds with the sockets downwards, by which method an equal wall thickness was obtained together with the obviation of honeycombing in the metal, Boden (4). The pipes were then coated, while hot, in a bitumen solution, thus providing both internal and external protection.

Pipes cast in this manner were available from about 1850 onwards, Boden (4), and constitute the majority of pipes which are in service in the area covered by The Metropolitan Water Division of Thames Water.

The vertically cast iron pipe was standardised in the British Standard, BS 78:1938, (5).

In 1914, the French engineer, M. Sensaud de Lavaud began work on the centrifugal casting of pipes. The process was developed by The Stanton Ironworks Company Limited and production began in this country in 1922, Boden (4).

The manufacture of spun iron pipes involved the introduction of the iron into an inclined rapidly revolving water-cooled steel mould. The centrifugal action caused by the spinning ensuring uniformity of thickness and a freedom from defects which were difficult on occasion to avoid with vertically cast pipes.

The effect of spinning on the metal, when in a molten state, was to compact the particles of iron much more closely, thus producing greater tensile and transverse strength, (2).

The structure of a conventional centrifugally cast grey iron pipe consists predominantly of fine flake graphite in a ferritic matrix, Boden (4).

The centrifugally cast iron pipe is standardised in the British Standard, BS 1211:1958, (6).

Centrifugally span iron water mains were laid by The Metropolitan Water Board (now The Metropolitan Water Division of Thames Water) from about 1945 until 1970 , (7).

The addition, under carefully controlled conditions, of small quantities of magnesium to molten cast iron of low sulphur content changes the form of the graphite, from an inter-connected flake network, to the discrete nodules or spheriods, which characterise ductile iron, (8).

The effect of the change in graphitic form from flake to nodular is to produce a material which has a higher tensile strength, ductility and resistance to impact damage, Scholes and Fuller (9). These changes are reflected in the properties specified in British Standards BS 4622:1970, (10) and BS 4772:1971, (11), for grey and ductile iron pipes and fittings respectively.

Spun ductile iron pipes have been in use with The Metropolitan Water Division of Thames Water since 1970, (7).

Excluding individual service pipes, it was estimated that in 1950, 90% of the water distribution mains in Great Britain were made from cast iron materials, (12). The other 10% of water distribution mains were made from a variety of materials, namely steel and asbestos cement. In 1978, in The Metropolitan Water Division of Thames Water, 98% of the mains were made from cast iron materials, Reed (13).

Steel pipe has had a curious career in that it became popular in the late nineteenth century, only to fall into disfavour until after the First World War, (2). This was caused by the difficulty in protecting

the exterior and interior of a thin metallic membrane compared with the stout section of the cast iron pipe.

Steel pipes of small diameter can be made from the solid, but the larger diameters are made by welding together the edges of suitable curved plates, the sockets being formed later in a press. The thickness of the steel used is often controlled by the need to make the pipe stiff enough to keep its circular shape during storage, transportation and laying; but it is always less than the corresponding vertically cast, spun iron or ductile iron pipe, owing to the higher tensile strength of the steel.

Steel pipes have been used in The Metropolitan Water Division where extra strength has been required or in the larger sizes where they have proved to be cheaper than cast iron, but it has been necessary to protect these against corrosion wherever they have been laid. This has been done by bitumen sheathing or wrapping with special tape (7). By 1978, steel mains constituted about 1% of the mains in The Metropolitan Water Division, Reed (13).

Steel pipes for the water industry are covered by British Standard BS 534:1966, (14).

Asbestos cement, as a material, was first produced in 1900, and the production of asbestos cement pipes capable of withstanding internal pressure commenced in Italy in 1916. Asbestos cement pressure pipes were first manufactured in Britain in 1928, (2).

The properties of asbestos cement pipes include a high degree of insulation from heat, cold and electric current, immunity from decay, and freedom from incrustation. They have ample strength to resist normal external and internal loads and they harden and gain even greater strength with age, (15).

The factors of safety against bursting under pressure and against failure in longitudinal bending are less than those for spun iron pipes, (2).

Asbestos cement was first used in the area covered by The Metropolitan Water Division in about 1953 and again later when an improved joint was introduced. The material has disadvantages and has been restricted to mains other than in the carriageway roads, (7). A total of 2 km of asbestos cement mains had been laid by 1978, about 0·01% of the total length of mains in London, Reed (13).

Asbestos cement pipes suitable for use in the water industry are covered by British Standard BS 486:1973, (16).

The other materials now commonly used for manufacturing pipes for the conveyance of water are thermoplastics. The two most commonly used thermoplastics are uPVC (unplasticized Polyvinyl Chloride) and polythene. The choice between these two materials is determined largely by cost and pressure requirements, (17).

Both materials are considerably lighter than cast iron or asbestos cement and are highly resistant to attack which is of particular value in aggressive soils. 75 km of uPVC mains had been laid in

London by 1978, which constituted about 0·5% of the whole system, Reed (13).

uPVC pipes are controlled by British Standard, BS 3505:1968, (18) and polythene by BS 1972:1967, (19) and BS 3284:1967, (20).

1.3 PREVIOUS RESEARCH INTO WATER MAINS FAILURES

The causes of failures are of constant concern to the water industry, and at various times during the past 40 years many reports have been published both in Great Britain and abroad giving details of mains breakages.

In 1930, The Metropolitan Water Board, (3), reported that fractures of mains are caused by a variety of circumstances including:-

(i) change of temperature
(ii) traffic conditions
(iii) interference with the support of the mains during road operations or other works
(iv) deterioration of the iron by the surrounding soil
(v) the admission of water at low temperatures, during very cold weather, from exposed filter beds to mains lying in the ground at a temperature several degrees higher than that of the water entering the mains.

It is also stated in the above report that the majority of all types of fractures occurred in pipes of 3 in and 4 in diameters.

The above findings were similar to those of The Institution of Water Engineers in the United Kingdom, (21) and by Mabee, (22), in North America with regard to water mains.

In 1928, The Institution of Water Engineers analysed the fractures of 15 water authorities owning 4800 miles of mains and found that the average rate of fracture per mile per year was 0·11.

The findings in North America were similar to those in Great Britain except that it appeared that the American systems did not suffer as many fractures. In 1929, Detroit with a system of 2727 miles of mains had a rate of 0·044 fractures per mile per year, and in the year 1931 Chicago, with a system of 3692 miles of mains, had a rate of 0.038 fractures per mile per year.

The only new fact that emerges from a survey of most of the subsequent American papers on mains failures is that the cumulative rate of fracture per mile per year for cast iron water mains appears to be increasing. Garrity (23), gives the rate of failure in Detroit in over 3000 miles (1955) of mains as 0·2 fractures per mile per year and Galler (24) gives the rates for Detroit with 3393 miles of mains (average 1970-74) and Chicago with 4148 miles of mains (1973) as 0·396 and 0·073 fractures per mile per year respectively.

In the early 1970's, research into water mains failures took a different approach. Instead of classifying fractures by actual visible or notional cause, they were classified according to type, as indicated on a report of fractured mains form, Figure 1.1 or on a mains' record/ history card, Figure 1.2, that is either:

(i) longitudinal split

(ii) transverse (circumferential) split

(iii) blow out

(iv) holes and perforations

(v) ferrule fault

(vi) flange fault

(vii) collar, socket fault

(viii) plug fault

(ix) damaged pipe

(x) miscellaneous and unknown

In a survey of fractures in grey cast iron water mains, Bacon, Langley and Roberts (25), confirmed the previous findings (3) that the pipes most susceptible to failure were those with diameters of 6 in and less, and an analysis using the above type classification indicated that the predominant mode of fracture was the transverse split. Due to these findings they proposed that bending stress, however it may be caused, is a major factor causing fractures. The survey also states that there is a correlation connecting a drop in air temperature with an increase in transverse fractures.

The findings of the survey on fractures were investigated further and form the basis of reports by Roberts and Regan (26 - 28), in which it is postulated that there are two principal causes of fractures in small and medium diameter grey cast iron water mains, 300 mm and less:-

(i) corrosion

(ii) longitudinal bending

Ground loading can also be a principal fracturing mechanism, but this is only applicable to large diameter mains, 300 mm and over.

These findings lead to the present research into water mains' failures.

Thames Water

Metropolitan Water Division

REPORT OF FRACTURED MAIN

Report No. 17204

Location Address | Local Authority

Main Size

* Location Code

Area

Zone

Type of Fracture

PARTICULARS OF PIPE

Material

Thickness max ____ mm

Thickness min ____ mm

Condition

Protection

Depth (Cover) ____ m

* Length ____ m

* Direction

* Type of joints

* Distance from kero ____ m

Method of repair

LOCAL CONDITIONS

Ground surface type:-

Soil type by pipe:-

Bed type under pipe:-

* Adjacent apparatus:-

* and distance:- ____ m

* Ground O.D. level:-

* O.D. nearest pressure gauge:-

* Normal mains pressure max:-

* Normal mains pressure min:-

* Type of traffic:-

* Direction of traffic:-

Any additional information:-

PARTICULARS OF FRACTURE INCIDENT

Leakage notified by ____ of ____

to ____ at ____ am/pm on ____ 19__

Main isolated at ____ am/pm on ____ 19__

Incident reported verbally to ____ am/pm on ____ 19__

Incident reported to information room ____ am/pm on ____ 19__

Incident reported to Distribution office ____ am/pm on ____ 19__

Incident reported to M.P.H. Division ____ am/pm on ____ 19__

Escaping water entered following premises:-

Other apparatus affected:-

Approximate extent of damage to paving:-

Effect on supplies

Effect on traffic

Reported in media (radio, tv, press)

DATES OF PREVIOUS FRACTURES

Length of main subject to fractures listed above ____ m

Signed by ____ *(District Foreman)*

Date

Signed by ____ *(District Engineer)*

Date

Remarks of

* *See general instructions regarding asterisked entries*

PU 92

Date: *(Resident Engineer)*

FIG. 1.1 Report of fractured main

SIZE OF MAIN | DISTRICT PLAN NO.

WALK

RECORD OF MAIN AREA

STREET

LOCAL AUTHORITY

Card No.

Hydrant No.	O. D. Level	Zone	Pressure Static Head	Pressure Run Head	Date	GENERAL INFORMATION

OTHER MAINS IN STREET

(NOTE.—separate card should be used for each main).

PU 644

HISTORY OF MAIN

(Laying; Renewals; Repairs; Fractures; Openings; etc.)

DATE LAID.....19.....

DATE OF Fracture	DATE OF Other Work	WORK DONE (Length Laid, Etc.)	Burst Main Report	Location (Give Road Nos. if possible)	Depth	Position in footway, carriageway, etc. (give dimensions)	Condition (see code below)

CODE:—G=Good; S=Satisfactory; U=Unsatisfactory; B=Brittle; E=Electrolytic; GR=Graphitic; P=Pitted; UC=Uneven Casting.
(NOTE: More than one code sign can be used. When iron is other than "G" state whether "S" or "U."
Mark burst main column with asterisk if claim(s) for compensation received.)

FIG. 1.2 Mains record/history card

1.4 PRESENT RESEARCH INTO WATER MAINS FAILURES

An analysis of fracture data is given in Chapter 2, in which is set out the evidence that leads to the conclusion that there are two principal causes of fractures in small and medium diameter mains.

A flow chart of the fracture triggering mechanisms is also given, which has been constructed from the analysis of fracture data and from the theoretical analysis of the aspects that produce the various modes of fracture found in underground cast iron pipelines.

The effect of longitudinal bending on a buried pipeline is investigated by using the mathematical model of a beam on an elastic foundation subjected to a differential ground displacement. The resulting equations are completely linear elastic and as such can only be used to analyse the performance of materials with a linear stress-strain relationship.

The equations obtained from elastic model are used to calculate the values of the shear force and the differential ground displacement necessary to fracture sand cast grey iron and spun cast grey iron pipes for a range of soil resistances and pipe sizes. The relative performance with regard to fracturing when changing from one pipe size to another and when changing from one material to another is also investigated.

In the last decade a form of corrosion, known as fissure corrosion, has been identified, Harrison (29). Fissure corrosion occurs when a pipe that is suffering from graphitisation, (30), is stressed in tension, the stressing having the effect of intensely localising the graphitisation, thus producing trench-like fissures orientated normally to the principal tensile axis.

The equations obtained from the linear elastic model are used to demonstrate that the ground has the capacity, not only to produce the required stress level in spun iron pipes but also in ductile iron pipes.

The performance of asbestos cement pipes subjected to differential ground displacement is also analysed using the linear elastic model.

The effect of a point load acting on a surface pipeline is investigated using the mathematical model of a beam resting on an elastic foundation and this is extended to measure the effect of a concentrated surface load on a buried pipeline.

As the first model is entirely linear elastic, a second, more general, mathematical model is proposed. This model uses a 'force-displacement method' for analysing statically-indeterminate beams to simulate a buried pipeline subjected to a differential ground displacement. The general format of the model allows for a non-linear pressure-displacement relationship in the soil and a non-linear stress-strain relationship in the pipeline material.

Two experimental investigations into the effect of differential displacement on a buried pipeline are described and the results are compared with those obtained from the second mathematical model. The first experiment was a full scale test on a double length of pipe which was subjected to a series of incremental differential displacements whilst encased within an inelastic medium and the second was a test on a ductile pipe which was subjected to a series of incremental differential displacements whilst supported by sets of springs.

The second mathematical model is used to investigate three cases of non-homogeneous ground for a variety of pipeline materials and pipe sizes and from the results obtained recommendations are made with regard to pipe laying procedures.

As the major causes of fractures in water mains have been found, the economics of mains replacement are discussed. The basis of the replacement policy is that either a reliable fracture regression curve or a base fracture rate can be found, from known fracture data, and then used to determine which mains will need replacing. The relative economic merits of relining as opposed to relaying and of prelining and sleeving are also reviewed.

CHAPTER 2

ANALYSIS OF FRACTURE DATA

2.1 INTRODUCTION

The methods previously used for collating fracture data have hidden the basic factors that have placed water mains at risk. This is particularly true when dealing with small diameter mains.

The analysis of fractures by type of fracture, The City University (25 - 28), has indicated that there are four major modes of fracture in grey cast iron water mains:-

(i) transverse (circumferential) breaks, Figure 2.1
(ii) longitudinal splits, Figure 2.2
(iii) blow outs, Figure 2.3
(iv) holes and perforations, Figure 2.4

A summary of the results from The City University research is given in Table 2.1. Table 2.1 gives the numbers of the various types of fractures in cast and spun iron pipes for the Eastern 2(E2), Eastern 6 (E6), Kent 3(K3) and Western 5(W5) areas of The Metropolitan Water Board, now part of The Metropolitan Water Division of Thames Water, Figure 2.5, and the numbers of various types of fractures in cast and spun, and asbestos cement pipes for the Swindon area of The Cotswold Water Division of Thames Water, Figure 2.6. It is evident that the rate of each type of fracture varies greatly from one area to another. This variation is due to the nature of the soil surrounding the pipe, that is, whether the soil is corrosive or not. An indication of a corrosive area is a low rate of transverse fracture and a high rate

of holes and blow outs, such as the Eastern 2(E2) area of The Metropolitan Water Division.

The most outstanding features are the rate of transverse fractures and the vulnerability of small diameter mains to this mode of fracture, at least 90% of which occur in mains with diameters of 150 mm and less.

A graph of the rate of transverse fracture per km per 10 years for each of the areas against pipe size has been plotted, Figure 2.7. The rates of transverse fracture are for iron mains in all areas except Swindon, for which the rates of transverse fracture of all materials combined together are given and also the rates of transverse fracture for asbestos cement mains. The fracture rates for Eastern 6 and Western 5 have been scaled down by a factor of 10 in order to make the graph more compact. The scaling down does not effect the underlying relationship of an inverse proportionality between the rate of transverse fracture and pipe size, which is clearly demonstrated in the graph. The inverse proportionality indicates that mains with small diameters have a higher risk of fracture.

Three curves from the family of curves, Constant/P_r (Rupture shear force), which compare the theoretical weakness of a pipe in bending, dealt with in more detail in Chapter 3, have been added to the graph. There is a significant correspondence between the rate of fracture and the theoretical weakness in bending, which indicates that longitudinal bending is a primary mechanism by which pipes of small diameter are put at risk.

The fracture itself is usually triggered by some other influence such as a temperature differential, ground loading, water pressure or a combination of these.

FIG. 2.1 Transverse(circumferential) break

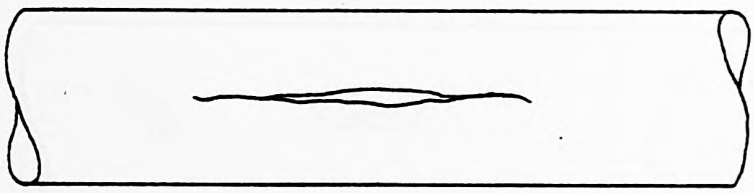

FIG. 2.2 Longitudinal split

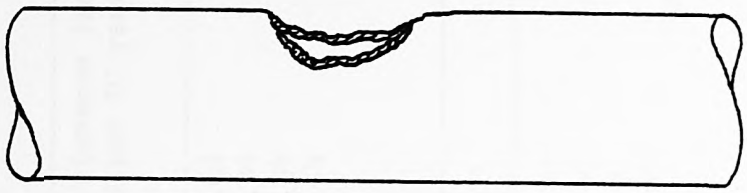

FIG. 2.3 Blow out

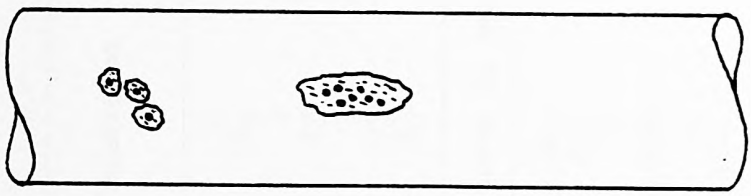

FIG. 2.4 Holes and perforations

TABLE. 2.1 Summary of fracture data

Area	Size	Type of fracture				Rate of transverse fracture per km.per 10 years
		Transverse	Longitudinal	Holes and Blow outs	All	
E2	75	7	4	1	12	0.68
	100	149	60	118	333	0.31
	125	2	4		6	0.34
	150	13	8	13	34	0.14
	>150	2	20	18	43	
	TOTAL	173	96	150	428	
	PERCENTAGE	40	22	35		
99% of transverse fractures in mains 150 mm and less						
E6	75	641	17	13	681	12.40
	100	446	22	16	490	4.40
	125	48	5	4	57	4.60
	150	106	11	10	128	2.60
	>150	37	15	13	65	
	TOTAL	1282	70	56	1425	
	PERCENTAGE	90	5	4		
97% of transverse fractures in mains 150 mm and less						

continued /...

TABLE. 2.1 Summary of fracture data

continued /...

K3	75	114	17	11	148	0.42
	100	268	66	81	446	0.16
	125	4	1	5	13	0.04
	150	12	6	28	50	0.02
	>150	1	8	13	46	
	TOTAL	400	98	139	708	
	PERCENTAGE	56	15	16		
99% of transverse fractures in mains 150 mm and less						
W5	75	85	11	20	119	4.04
	100	548	80	155	802	1.98
	125	52	7	14	74	3.38
	150	53	11	23	91	1.03
	>150	65	35	57	158	
	TOTAL	803	145	269	1246	
	PERCENTAGE	64	12	22		
92% of transverse fractures in mains 150 mm and less						

continued /...

TABLE. 2.1 Summary of fracture data

continued /...

SWINDON	50	9	1	23	39	0.46
CAST/	75	146	14	177	367	0.51
SPUN	100	74	5	45	132	0.38
	125	15			16	0.80
	150	18	3	13	41	0.23
	>150	5	12	33	58	
	TOTAL	267	35	291	653	
	PERCENTAGE	41	5	45		
95% of transverse fractures in mains 150 mm and less						
SWINDON	50	3			7	3.81
ASBESTOS	75	5		1	18	0.90
CEMENT	100	8		1	25	0.17
	125					
	150	2			4	0.20
	>150	1	1		11	
	TOTAL	19	1	2	65	
	PERCENTAGE	29	2	3		
95% of transverse fractures in mains 150 mm and less						

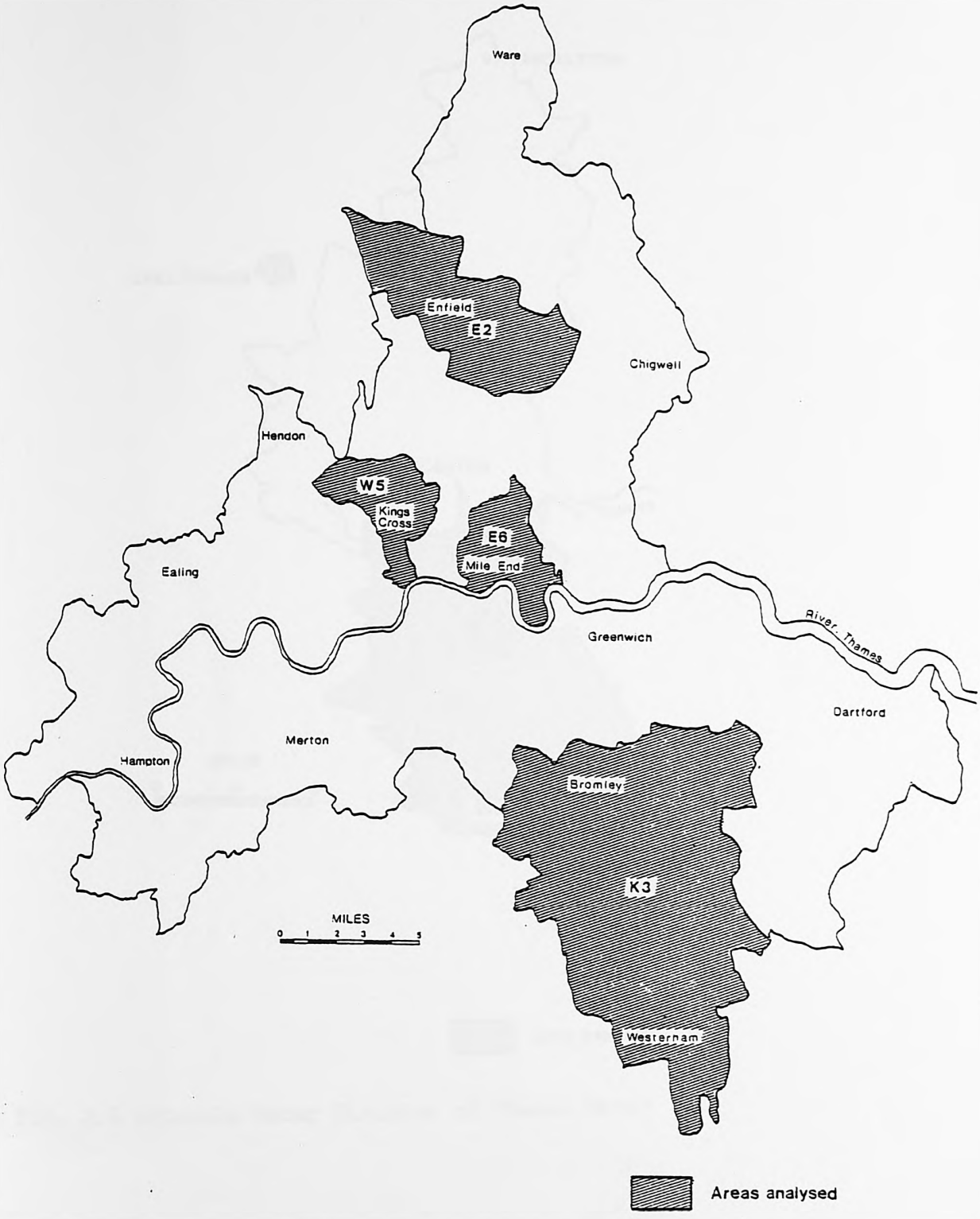

FIG. 2.5 The Metropolitan Water Board now part of The Metropolitan Water Division of Thames Water

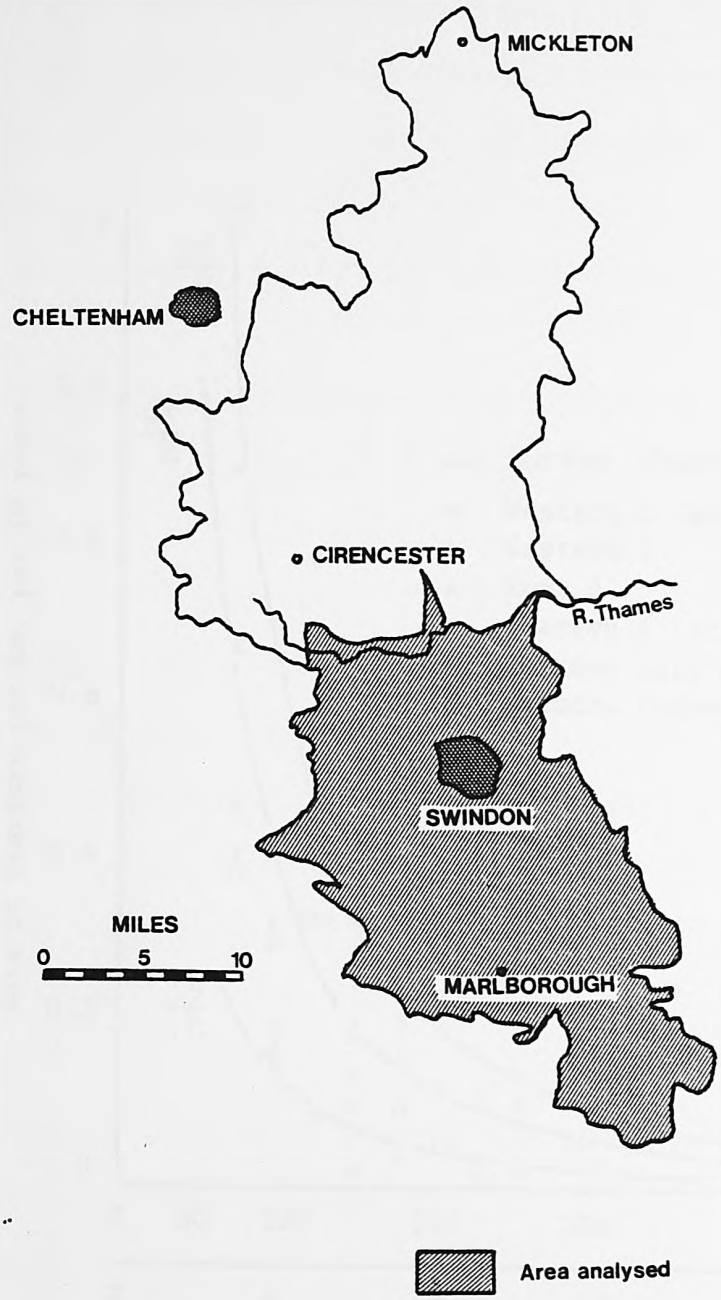

FIG. 2.6 Cotswold Water Division of Thames Water

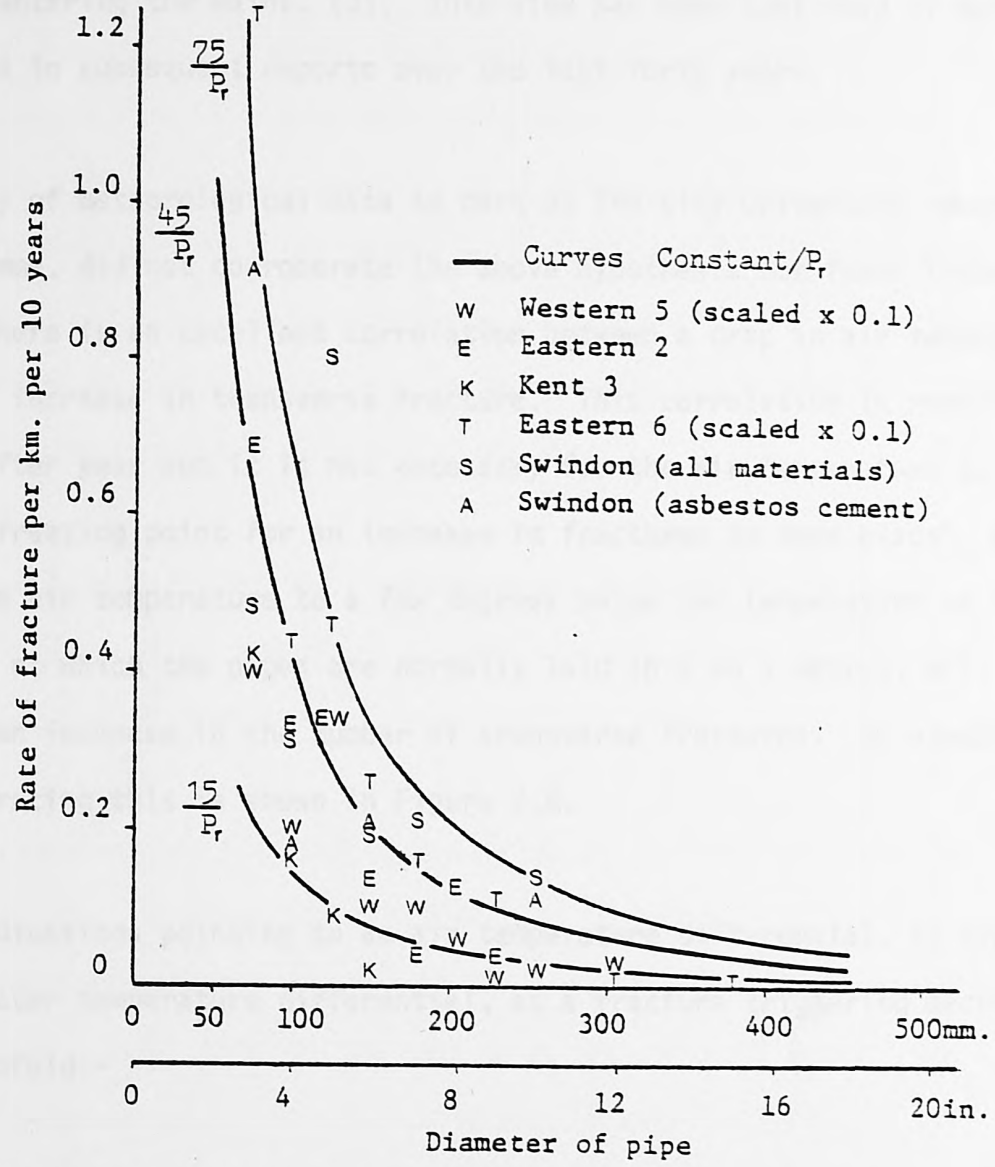

FIG. 2.7 Variations of rate of transverse fracture with size of pipe compared with theoretical weakness in bending

2.2 TEMPERATURE DIFFERENTIAL

It has been the general practice to assume that grey cast iron water mains are fractured during very cold weather by the admission of water at low temperatures, from exposed filter beds to mains lying in the ground at a temperature several degrees higher than that of the water entering the mains, (3). This view has been confirmed by many authors in subsequent reports over the last forty years.

A study of meteorological data as part of The City University research programme, did not corroborate the above hypothesis but found instead that there is an excellent correlation between a drop in air temperature and an increase in transverse fracture. This correlation is repeated year after year and it is not necessary for the air temperature to drop below freezing point for an increase in fractures to take place. A drop in air temperature to a few degrees below the temperature of the ground at which the pipes are normally laid (0·9 to 1 metre), will cause an increase in the number of transverse fractures. An example illustrating this is shown in Figure 2.8.

The indications pointing to an air temperature differential, as opposed to a water temperature differential, as a fracture triggering mechanism are twofold:-

(i) The rate of fracture of gas mains is similar to that of water mains; Mabee (22) gives the following statistics:-

Water:

Indianapolis	0·017 breaks per mile per year
Detroit	0·044 breaks per mile per year
Chicago	0·038 breaks per mile per year

Gas:

Indianapolis 0·052 breaks per mile per year

eliminating 3" diameter pipes, which are not in common use in the water industry in the above cities, gives a rate of 0·034 breaks per mile per year.

It has also been found, Lacey (31), that the rates of fracture per mile-year for gas mains vary inversely with the diameter of the pipe , which is the same as for water mains, and that the rates of fracture per mile-year for the period 1962/63 which included a very cold period are on average double those for the preceeding period 1961/62 and three times those for the period 1966/67 which had mild winter weather.

(ii) A sub-division of the fracture data in the Kent area (K3), into its well water and river water districts, failed to show any significant difference in the fracture rates, Table 2.2.

This is contrary to the findings reported by The Institution of Water Engineers (21) in which it is stated that the number of fractures per unit length of main is greater in mains conveying water from surface sources of supply, than in the case of mains carrying water from underground sources. The Institution's findings are based on the returns from 32 diverse authorities in the United Kingdom and as such, they could be displaying local influences, whereas the Kent data is from the same area and will therefore give a much better comparison of the rates of fracture.

A further exercise was to measure the kitchen tap water temperature, the water being delivered directly from the main, of various consumers, one of whom lived in the Kent well water area. It was found that the tap water temperature in the well water area showed a greater variation than the tap water temperature where the water was supplied from a river source although the well water was delivered into the mains system at a fairly constant temperature of about 10·3^{o}C, Roberts and Regan (28). This indicates that the temperature of the well water is being modified by the ground.

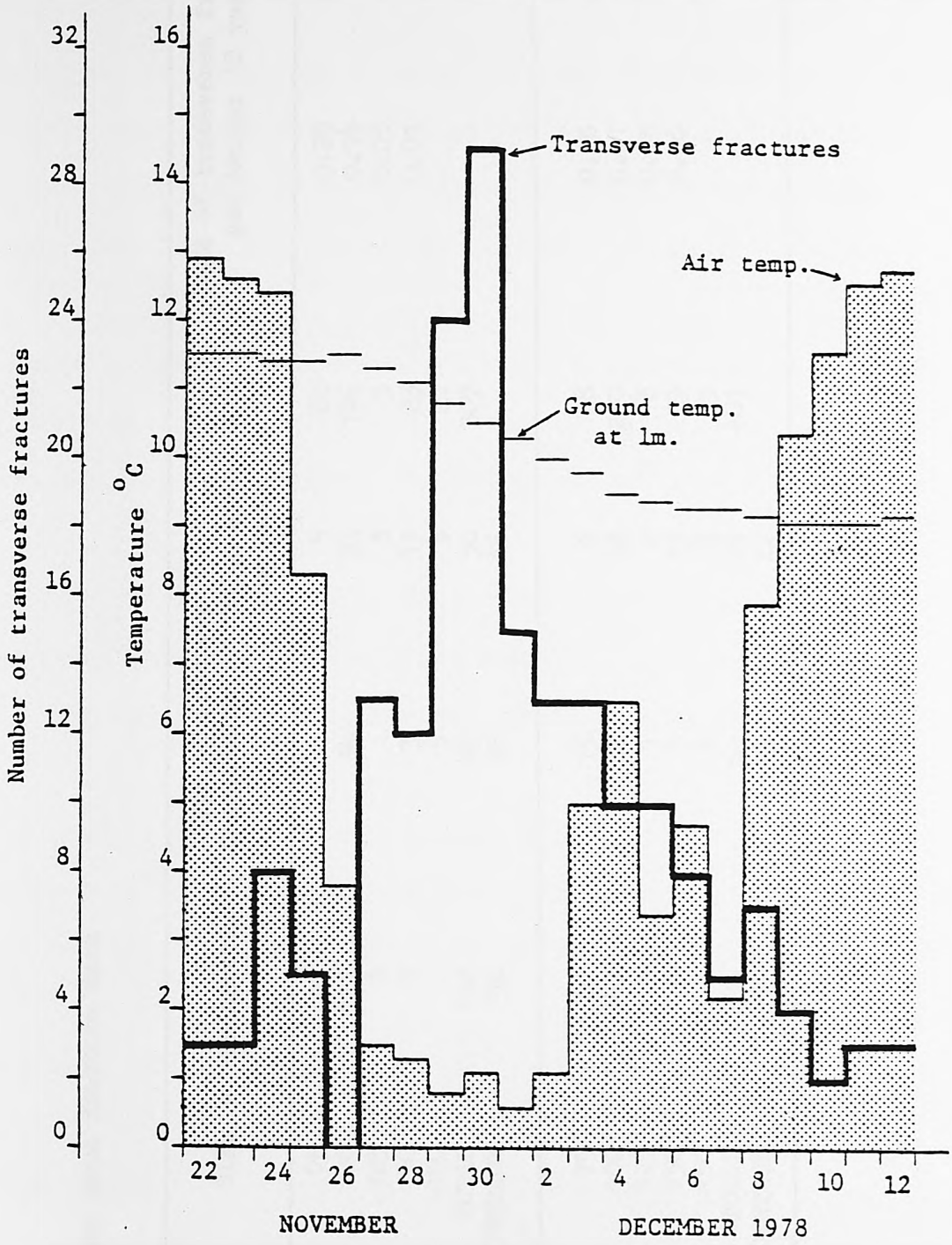

FIG. 2.8 Correspondence between number of transverse fractures and the variation in air and ground temperatures

TABLE. 2.2 Kent area fracture data

Area	Size	Type of fracture				Rate of transverse fracture per km.per 10 years
		Transverse	Longitudinal	Holes and Blow outs	All	
K3 WELL	75	47	4	5	60	0.29
	100	121	34	23	196	0.14
	125	1		3	5	0.05
	150	3	3	13	23	0.01
	>150		5	5	21	
	TOTAL	172	46	50	307	
	PERCENTAGE	56	15	16		
K3 RIVER	75	67	13	6	88	0.26
	100	147	32	58	250	0.11
	125	3	1	2	8	0.03
	150	9	3	15	29	0.06
	>150	1	3	8	25	
	TOTAL	228	52	89	401	
	PERCENTAGE	57	13	22		

2.3 GROUND LOADING

An increase in ground loading is usually the result of an external effect such as traffic loading or frost loading.

An increase in the volume or weight of traffic on a road which is not suitable, or has not been up-graded for the purpose , is usually followed by an increase in the rate of fracture of the water mains beneath the road. The reverse of the above situation is also true.

Potentially the most hazardous situation is occasioned by impulsive loading caused by vehicles passing over pot holes or parts of the road which have not been properly reinstated following excavations.

The effect of ground loading can only be a secondary effect in the fracture of small and medium sized pipes as the cross sections of these pipes are usually strong enough to withstand these loads.

Large diameter pipes are most susceptible to ground loading; it can be a primary or secondary fracture triggering effect, and as such, these pipelines must be laid in such a manner as to withstand these loads.

The theory for calculating earth and traffic loads on underground pipelines is well advanced, Clarke (32), and there are numerous design charts available for use by pipeline designers.

Examples where ground loading has been a primary cause of longitudinal fracture in mains with diameters of over 300 mm, (26) are:-

(i) A pipe, at about 1·2 m depth under the kerb on an arterial route roundabout which was constantly hit by vehicles.

(ii) A manhole built by another public service authority right on top of the water main.

The effect of frost loading on underground pipes has been investigated in North America, Smith (33) reports:

> "It is well known that when atmospheric temperature drops below 32F (0C) for several hours, shallow soil moisture freezes in lenses and water travels by capillary action from adjacent soil to these newly-formed lenses, swelling the water-soil mixture. If low temperatures persist, additional lenses are formed and additional expansion occurs...
>
> During the early stages of frost penetration, the shallow earth expands in all directions. The resulting lateral pressures lock the upper layers of earth into a bridge covering a broadened area. There is an upward expansion which may cause damage to streets, highways, and buildings and there is also the downward thrust which increases the vertical load on underlying pipe".

Smith's studies in Wheaton, Illinois, USA, were an extension of the original experiments carried out in Portland, Maine, USA, by Monie and Clark (34) who reported that by the time the frost had penetrated to a depth of 3 ft the recorded loading on a pipe, with an average depth of 3.75 ft, had doubled. Smith suspected a significant error,

because of the indeterminate value of pipe support by the earth beneath the pipe between the load cell supports. He subsequently found that as frost penetration reached a depth of 2 ft the recorded load per linear foot on a pipe at a depth of 4·5 ft had increased from an average of 400 lb to 725 lb, which again is almost double.

There is also a dramatic increase in the number of fractures during prolonged periods of sub-zero temperatures. During the period 23rd December 1962 - 6th February 1963 there was a prolonged cold spell in London when the mean temperature at Kew Gardens was below freezing point for the majority of the time. The total number of fractures recorded during that period was 3091, with the highest number in one day being 158, Metropolitan Water Board (35). The annual average for fractures per whole year at that time was 2200. The majority of fractures were transverse splits and occurred in small diameter pipes, 6" and less.

A correspondence between an extra loading due to frost and an increase in the number of fractures is indicated by the fact that the ground temperature, at a depth of 1 ft, recorded at Kew Gardens on 26th January 1963 was - 1·3^{o}C, the lowest recorded since records began in 1906.

The temperature recorded at a depth of 4 ft, the approximate depth at which pipes are normally laid was 4·1^{o}C on 26th January 1963 which is below the minimum monthly mean of 5·3^{o}C, Chandler (36).

2.4 FISSURE CORROSION

It has been reported by Harrison (29), that when iron pipes corrode, the graphite within the iron structure is unaffected by the corrosion process and conversion of the iron to a corrosion product around the graphite produces a coherent mass retaining the original geometry of the pipe; the process is termed 'graphitisation'. Graphitisation usually occurs in a general layer or as a plug intruding into the iron. However, when spun grey cast iron is stressed in tension, the graphitisation can become intensely localised, producing trench-like fissures orientated normally to the principal tensile axis, Figures 2.9 and 2.10.

Experimental work, Gray and Wilkins (37), indicates that spun iron pipes must be stressed to approximately 40% of their ultimate tensile stress before fissure corrosion occurs.

The level of corrosiveness of the environment seems to have little effect on the process of graphitic fissure corrosion, Harrison (29), and in most cases of failed pipe due to this type of corrosion have been found in moderate to non-agressive soils.

Graphitic fissure corrosion had not been seen up to 1976, Harrison (29), on either pit cast grey iron or ductile iron pipes in normal service. Stress assisted corrosion of ductile iron has, however, been produced under laboratory conditions.

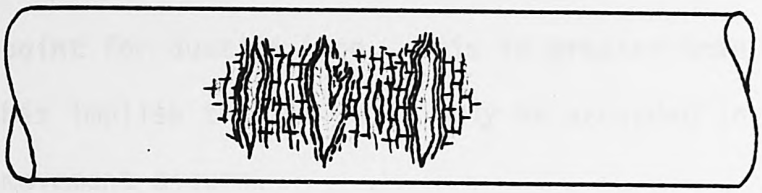

FIG. 2.9 Graphitic fissures on surface of pipe

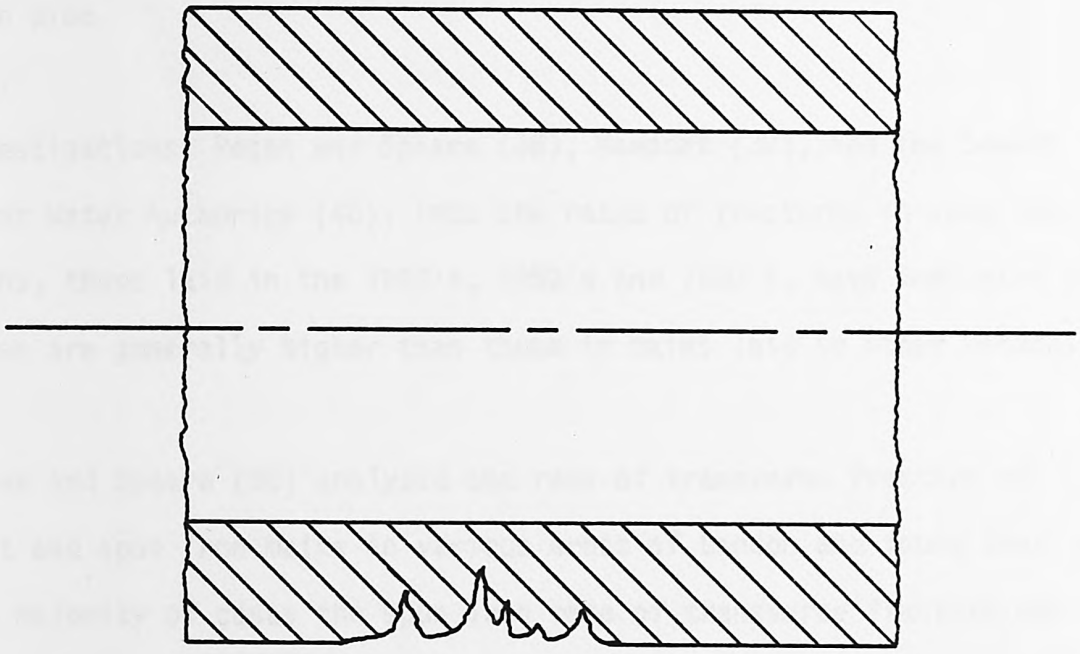

FIG. 2.10 Penetration of fissures into pipe wall

A form of localised grooving can be created in ductile iron experimentally, Gray and Wilkins (37), but all the features for formation differ significantly from those appropriate to spun iron, and to practical exposure conditions. Specifically, the range of environmental and corrosion rates are more confined as the threshold stress is very close to the yield point for ductile iron. This is greater than the design stress, and this implies that it could only be exceeded in pipes if gross ground movement occurs.

Gray and Wilkins (37) state further that both the tendency to form grooves and the rate of groove penetration diminish as the corrosion rate decreases and the use of loose polyethylene sleeving improves still further the prospect of preventing localised attack on ductile iron pipe.

Investigations, Regan and Speare (38), Newport (39), and The Severn Trent Water Authority (40), into the rates of fractures in spun iron mains, those laid in the 1940's, 1950's and 1960's, have indicated that these are generally higher than those in mains laid in other decades.

Regan and Speare (38) analysed the rate of transverse fracture of cast and spun iron mains in various areas of London and found that in the majority of cases the spun iron rate of transverse fracture was higher than the cast iron rate. The predominant subsoil in the areas analysed was clay, which is a very expansive soil and an ideal medium in which the mains can be put at risk due to fissure corrosion.

An analysis of fractures in mains laid in the 1940's and 1950's in Coventry and Rugby by The Severn Trent Water Authority (40) also shows that these mains have a higher rate.

Newport (39) analysed the rates of fractures in mains in five areas of Nottingham, one of which contained predominately spun iron mains. The rate of fracture for the spun iron mains area was found to be approximately four times greater than for pipes in the other older areas.

Pipes from The Severn Trent Water Authority have been examined by the Water Research Centre and fissure corrosion has been found to be the major cause of fracture, Parkinson (41). The pipe with the greatest attack of fissure corrosion had a maximum external corrosion pit depth of 0·9 mm with a corresponding maximum fissure crack length of 4·2 mm giving a total external attack of 5·1 mm. The pipe wall thickness was 7 mm, which shows the very damaging effect of this type of corrosion.

Parkinson also states that fissure corrosion is restricted to either the crown or the invert of the pipe which suggests that the tensile stresses causing it are not primarily attributable to the hydrostatic pressure but to the pipe/soil interaction.

2.5 TRANSVERSE FRACTURES

The effect of a drop in air temperature to a few degrees below that of the ground temperature, at pipe level, is diminished when the ground temperature is rising in the spring and summer and is magnified as the ground begins to cool in the autumn. In 1976 the ground was at its highest temperature for many years and started to fall about a month earlier than usual. As a result there was a one-month shift (from September to August) in the increase in transverse fractures.

The actual mechanism connecting air temperature to transverse fractures is the contraction of the pipe and not differential displacement of the ground. If the latter was the case then a sudden increase of air temperature might also give rise to an increase in transverse splits, but this is not the case. As a temperature change of $1^{o}C$ induces a stress in a restrained cast iron pipe of only about 1 N/mm^2, Roberts and Regan (28), it is clear that the effect of a drop in air temperature is a "last straw". The fact that the rate of transverse fracture per kilometer of pipe is inversely related to the bending strength proves that the primary stressing of the pipe is due to differential settlement. A large drop in the air temperature must superimpose a small additional tensile stress in the deflected pipes thus reaching the rupture stress. This action will be most pronounced when the pipes are cooling down after the peak of the ground temperature in the summer.

2.6 BLOW-OUTS, HOLES AND LONGITUDINAL SPLITS

Blow outs and holes in cast iron pipes are generally the result of long term corrosion; the rate of which varies from area to area depending on the corrosive nature of the soil.

A longitudinal split is the normal fracture mechanism due to ground loading of large diameter pipes, 300 mm and over. In small diameter pipes, a longitudinal split is more likely to be the by-product of long term corrosion.

These types of fracture will be sensitive to the pressure of the water in the pipes. Higher than normal pressure will cause a small increase in the hoop stress of the pipe. This is again a "last straw" effect and shows up in two ways:-

(i) The larger number of bursts known to occur in the early hours of the morning when the consumption is low and hence the water pressure is higher than during the daytime.

(ii) The increase in the number of blow outs, holes and longitudinal splits when water consumption, and thus water pressure due to increased pumping, is about average during the summer time.

When water pressure was reduced to save water in London during the drought of 1976, the number of blow outs, holes and longitudinal splits decreased dramatically, Roberts and Regan (27).

2.7 FRACTURE TRIGGERING MECHANISMS

The analysis of fractures in grey cast iron pipes by type and the subsequent investigation of the factors necessary to achieve the four principal modes of fracture, has revealed that for small and medium diameter pipes, 300 mm and less, there are two primary causes:

(i) Corrosion

(ii) Longitudinal bending

and four secondary triggering mechanisms:-

(i) An air/ground temperature differential

(ii) Ground loading

(iii) Fissure corrosion

(iv) Water pressure

In the case of large diameter mains, 300 mm and over, ground loading can be the primary cause of the pipe failing.

A flow chart linking the primary and secondary fracturing mechanisms to the modes of fracture which they can cause is given in Figure 2.11.

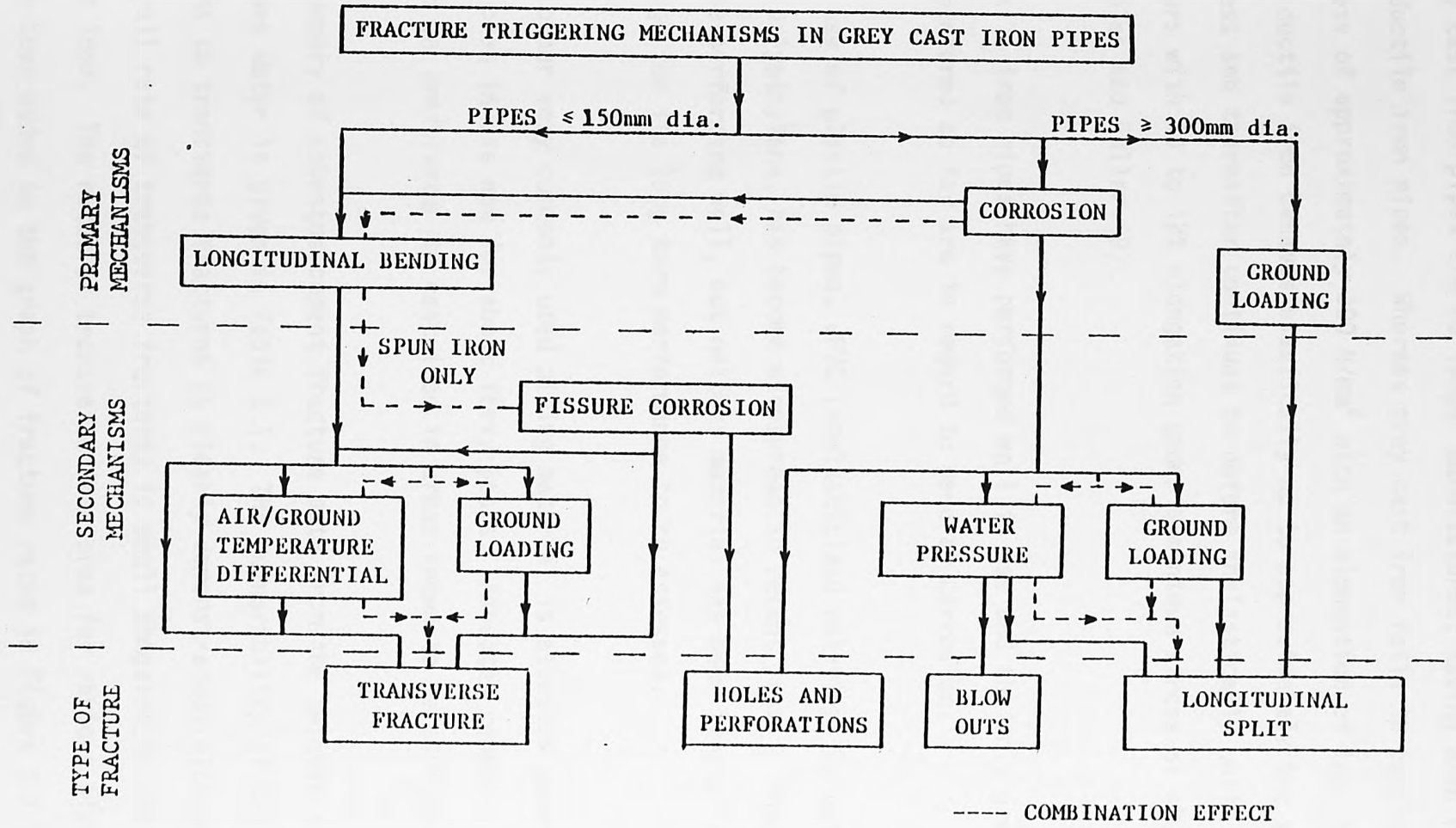

FIG. 2.11 Flow chart linking primary and secondary fracture triggering mechanisms with the type of fracture they produce

2.8 OTHER MATERIALS

Grey cast iron pipes are no longer manufactured, having been replaced by ductile iron pipes. Whereas grey cast iron fails in tension at a stress of approximately 200 N/mm^2 with an elongation of less than 1%, ductile iron behaves elastically up to approximately the same stress and thereafter continues to deform inelastically until failure occurs with 10 to 12% elongation under a minimum stress of 420 N/mm^2, Scholes and Fuller (9).

Ductile iron pipes have performed well in use and the only problems encountered so far are in regard to general corrosion.

The use of plastic pipes, uPVC (unplasticized polyvinyl chloride) and polyethylene, has become widespread in recent years. They appear to be performing well, but neither material has been in use long enough for its long term performance to be assessed.

The other very commonly used piping material is asbestos cement, which has been in use now for about forty years. Asbestos cement pipes were used in preference to cast iron in areas known to be corrosive.

A summary of asbestos cement fracture data from the Swindon area of Thames Water is given in Table 2.1. The vulnerability of small diameter mains to transverse fractures is clearly demonstrated, although the overall rate of transverse fractures is small compared to that for cast iron. The rates of transverse fractures for various pipe sizes have been added to the graph of fracture rates in Figure 2.7 and are consistent with the fact that for a brittle material the rate

of fracture per kilometer is inversely proportional to the diameter of the pipe.

The use of asbestos cement pipes as a replacement for cast iron pipes is further put in doubt by experiences on the continent of Europe, Coe (42). The authority in the City of Turin, Italy, which inherited a water distribution network with a high proportion of asbestos cement pipes, has decided not to lay any more as it was found that the fracture rate was three to four times higher than iron pipes. Asbestos cement pipes in Barcelona, Spain, have a fracture rate which is on average 1·3 times greater than cast iron. In Budapest, Hungary, in 1971 of 800 reported bursts, the ratio of asbestos cement to cast iron was about 2:1

2.9 SUMMARY

The primary fracture mechanisms of grey cast iron and spun cast iron water mains have been found and are for small and medium diameter pipes ($\leq$300 mm):

(i) longitudinal bending

(ii) corrosion

and for large diameter mains ($\geq$300 mm), ground loading.

Both corrosion and ground loading have been subjects of a great deal of research and their mechanisms and prevention are well known.

The effect of longitudinal bending on pipelines has received very little attention even though it is by far the major factor influencing the fracture of small and medium size diameter pipes.

The damaging effect of longitudinal bending is demonstrated in the analysis of fractures in two ways:-

(i) the majority of fractures in small diameter mains are transverse splits, as much as 90% of fractures in one of the areas analysed were transverse.

(ii) the rate of transverse fracture per kilometer per year has been shown to be inversely proportional to the pipe size and also to the theoretical weakness of the pipe in bending.

Due to the above findings, a theoretical study of the behaviour of buried pipelines subjected to longitudinal bending (its cause differential ground displacement) was undertaken. Both a linear and a non-linear mathematical model simulating the effect of differential ground displacement are described in the following chapters.

CHAPTER 3

ELASTIC MATHEMATICAL MODEL OF LONGITUDINAL BENDING

3.1 INTRODUCTION

The basic assumption made with regard to the elastic mathematical model is that the reaction forces of the foundation are proportional at every point to the deflection of the beam at that point. The above assumption enables the differential equation for the deflection line of a beam on an elastic foundation to be solved analytically for various modes of loading.

3.2 GROUND REACTION

Consider a beam which is supported along its entire length by a linear elastic medium which is subject to vertical forces acting in the principal plane of the symmetrical cross-section. The deflection of the beam will give rise to continuously distributed forces in the surrounding medium. It follows from the stated conditions that the intensity of the reaction force p and the deflection y at any point are related by

$$p = ky \quad \ldots \ldots \ldots \ldots \ldots \ldots \ldots \quad (3.1)$$

The stiffness of the surrounding medium is characterised by that force, which, distributed over a unit area, will cause a deflection equal to unity. This constant of the surrounding medium k_o, usually called the 'modulus of the foundation' or 'ground resistance', has dimensions ML^{-3}.

If the beam under consideration is a circular pipe with an outside diameter d, a unit deflection of the pipe will give rise to a reaction αdk_o in the surrounding medium, where α is a shape factor, used to account for the curved section of a pipe. Therefore at a point where the deflection of the pipe is y, the intensity of the reaction (per unit length of pipe) will be given by

$$p = \alpha dk_o y \quad \ldots \ldots \ldots \ldots \ldots \ldots \ldots \quad (3.2)$$

Taking $k = \alpha dk_o$, Equation (3.2) can be written as

$$p = ky \quad \ldots \ldots \ldots \ldots \ldots \ldots \ldots \quad (3.3)$$

3.3 THE DIFFERENTIAL EQUATION OF THE DEFLECTION LINE

Due to the deflection of a beam encased in a linear elastic medium, besides the vertical reactions, there may also be longitudinal forces due to the frictional reaction between the beam and the medium. For this analysis it will be assumed that the longitudinal frictional forces can be neglected, so that the resultant reaction forces will be vertical at every cross section.

Take an infinitely small element of the beam, Figure 3.1, enclosed between two vertical cross sections a distance dx apart and assume that this element is acted upon by an external distributed loading q.

The upward acting shearing force, Q, to the left of the cross section is considered to be positive, as is the corresponding bending moment, M which is a clockwise moment acting from the left of the element. Considering the equilibrium of the element in Figure 3.1, summation of the vertical forces gives

$$Q - (Q + dQ) + kydx - qdx = 0 \quad \ldots \quad \ldots \quad \ldots \qquad (3.4)$$

which gives

$$\frac{dQ}{dx} = ky - q \quad \ldots \quad \ldots \quad \ldots \quad \ldots \quad \ldots \quad \ldots \qquad (3.5)$$

Using the relationship $Q = \frac{dM}{dx}$, Equation (3.5) can be written as

$$\frac{dQ}{dx} = \frac{d^2M}{dx^2} = ky - q \quad \ldots \quad \ldots \quad \ldots \quad \ldots \quad \ldots \qquad (3.6)$$

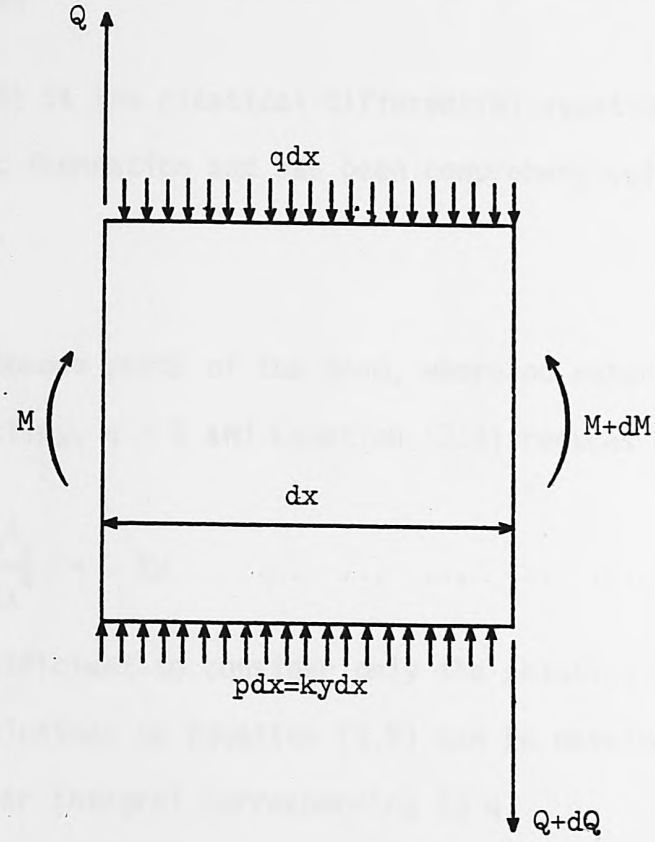

FIG. 3.1 Beam element

Using the known differential equation of a beam in bending, $EI \frac{d^2y}{dx^2} = - M$ and differentiating twice we obtain the equation

$$EI \frac{d^4y}{dx^4} = - \frac{d^2M}{dx^2} \quad \ldots \ldots \ldots \ldots \ldots \ldots \qquad (3.7)$$

Eliminating $\frac{d^2M}{dx^2}$ from Equation (3.6) and (3.7), we have

$$EI \frac{d^4y}{dx^4} = - ky + q \quad \ldots \ldots \ldots \ldots \ldots \qquad (3.8)$$

Equation (3.8) is the classical differential equation for a beam resting on an elastic foundation and has been comprehensively dealt with by Hetényi (43).

Along the unloaded parts of the beam, where no external distributed loading is acting, $q = 0$ and Equation (3.8) reduces to

$$EI \frac{d^4y}{dx^4} = - ky \quad \ldots \ldots \ldots \ldots \ldots \ldots \qquad (3.9)$$

It will be sufficient to consider only the solution of Equation (3.9), from which solutions to Equation (3.8) can be obtained by the addition of a particular integral corresponding to q.

The solution of Equation (3.9) is that of a linear fourth order differential equation which can be obtained using the method of differential operators to give the general solution for the deflection line as

$$y = e^{\beta x}(A \cos\beta x + B \sin\beta x) + e^{-\beta x}(C \cos\beta x + D \sin\beta x)$$

$$\ldots \ldots \ldots \ldots \ldots \ldots \qquad (3.10)$$

where $\beta^4 = \frac{k}{4EI}$

The variable β includes both the flexural rigidity of the pipe and the stiffness of the supporting foundation, and is called the characteristic of the system.

This solution is acceptable when dealing with a piping material which has a linear elastic stress-strain relationship and a brittle fracture mechanism. It is also applicable to the linear elastic part of any materials behaviour.

3.4 GROUND MOVEMENT

The effect of longitudinal bending on a buried pipeline can be obtained by considering the effect of a differential ground displacement on the buried pipeline.

Consider a semi-infinite pipeline, Figure 3.2, with one end at the origin O and of infinite length in the direction of x increasing, subjected to a point load P at the origin. The solution of Equation (3.10) in this case is

$$y = \frac{-2\beta P}{k} e^{-\beta x} \cos\beta x \quad \ldots \quad \ldots \quad \ldots \quad \ldots \quad \ldots \qquad (3.11)$$

If P is equated to the total force due to the displacement of the ground and the pipeline on the negative side of the origin and the x-axis is shifted, Figure 3.3, to the point

$$y_o = [y]_{x=o}$$

where from Equation (3.11)

$$y_o = \frac{-2\beta P}{k}$$

Shifting the x-axis to the point $y = y_o$, Equation (3.11) becomes

$$y = \frac{2\beta P}{k}(1 - e^{-\beta x}\cos\beta x) \quad \text{or} \quad y = \Delta_1(1 - e^{-\beta x}\cos\beta x)$$

$$\ldots \quad \ldots \quad \ldots \quad \ldots \quad \ldots \qquad (3.12)$$

where $\Delta_1 = \frac{2\beta P}{k}$

Δ_1 is numerically equal to the ground displacement on the negative side, Figure 3.4. The total relative ground displacement of the two halves is

$$\Delta = 2\Delta_1 = \frac{4\beta P}{k} \quad \ldots \quad \ldots \quad \ldots \quad \ldots \quad \ldots \qquad (3.13)$$

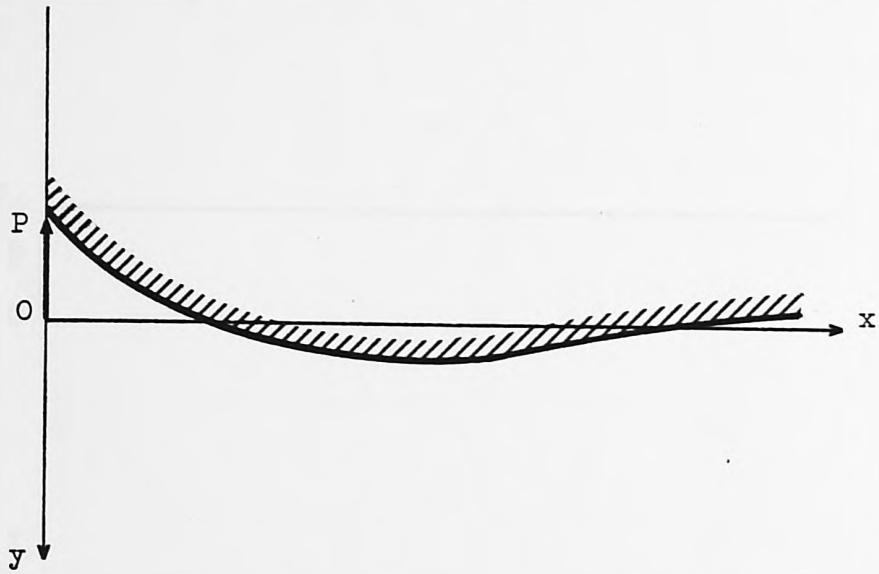

FIG. 3.2 Semi-infinite pipeline

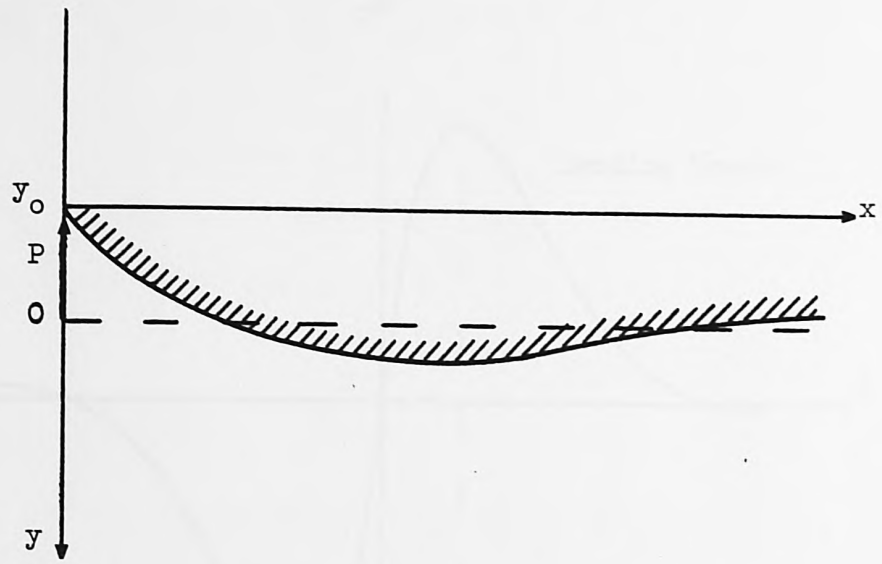

FIG. 3.3 Change of axis

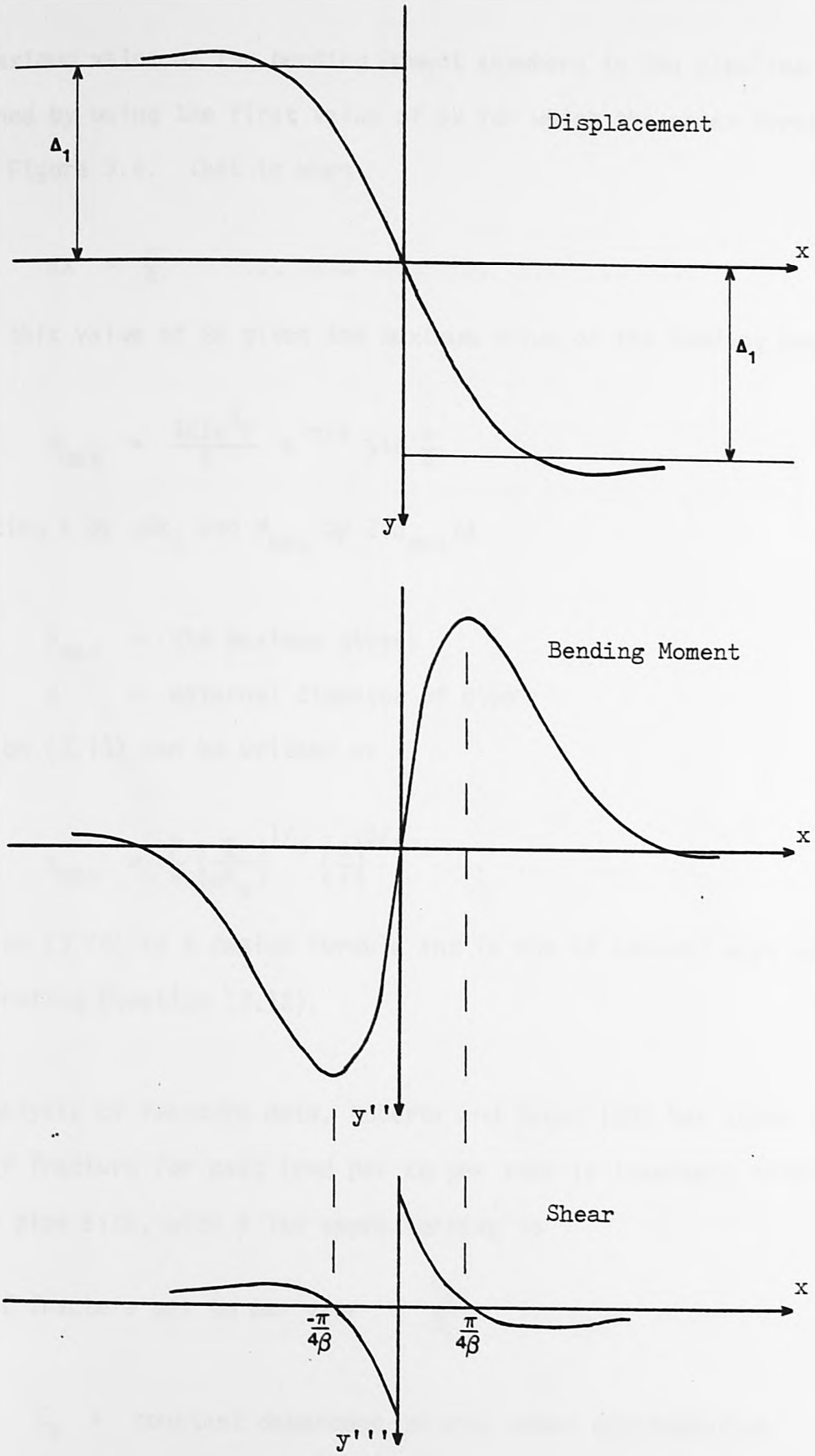

FIG. 3.4 Displacement, Bending Moment and Shear profiles

3.5 DERIVED DESIGN FORMULAE

The maximum value of the bending moment anywhere in the pipeline is obtained by using the first value of βx for which the shear force is zero, Figure 3.4. That is when

$$\beta x = \frac{\pi}{4} \quad \ldots \ldots \ldots \ldots \ldots \ldots \ldots \qquad (3.14)$$

Using this value of βx gives the maximum value of the bending moment as

$$M_{max} = \frac{4EI\beta^3 P}{k} e^{-\pi/4} \operatorname{Sin} \frac{\pi}{4} \quad \ldots \ldots \ldots \qquad (3.15)$$

Replacing k by $\alpha d k_o$ and M_{max} by $2I\sigma_{max}/d$

where

σ_{max} = the maximum stress

d = external diameter of pipe

Equation (3.15) can be written as

$$\sigma_{max} \simeq \frac{P}{4} \left\{\frac{E}{\alpha k_o}\right\}^{1/4} \left\{\frac{d}{I}\right\}^{3/4} \quad \ldots \ldots \ldots \ldots \qquad (3.16)$$

Equation (3.16) is a design formula and is one of several ways of interpreting Equation (3.12).

The analysis of fracture data, Roberts and Regan (28) has shown that the rate of fracture for cast iron per km per year is inversely proportional to the pipe size, with a law approximating to

$$\text{rate of fracture per km per year} = \frac{C_a}{M_r} \quad \ldots \ldots \ldots \qquad (3.17)$$

where

C_a = constant dependent on area under consideration

M_r = rupture bending moment

There must therefore be a correspondence between Equations (3.16) and (3.17). Equation (3.16) can be rearranged to calculate the force required to develop the rupture stress as

$$P_r = 4\sigma_r \left\{\frac{\alpha k_o}{E}\right\}^{1/4} \left\{\frac{I}{d}\right\}^{3/4} \quad \ldots \quad \ldots \quad \ldots \quad (3.18)$$

where suffix r denotes the rupture value.

Values of the rupture shear froce P_r are given in Table 3.1, for grey sand cast, Class C (σ_r = 185 N/mm^2) and spun cast, Class C (σ_r = 247 N/mm^3) iron and a range of soil (ground) resistances.

Table 3.1 shows that the force required to rupture a pipe increases with the size of the pipe in such a way that double the size of pipe demands three to five times the force.

Choosing constants of 15, 45 and 75, curves of the family of curves, Constant/Rupture shear force (P_r) for spun grey cast iron in a soil with resistance k_o = 0·25 N/mm^3 were added to Figure 2.7.

This clearly explains why the rate of fracture per km per year follows an inverse law. It is equivalent to stating that the possibility of developing a force large enough to fracture a brittle pipe (in bending) is inversely proportional to its magnitude.

Substitution of the rupture force P_r into the expression for the total relative displacement, Equation (3.13) becomes

$$\Delta_r = \frac{4\beta P_r}{k} = 8\sqrt{2}\,\sigma_r \left\{\frac{1}{\alpha E k_o}\right\}^{1/2} \left\{\frac{I}{d^3}\right\}^{1/2} \quad \ldots \quad (3.19)$$

TABLE. 3.1 Shear force P(kN) to develop rupture stress in various sizes of grey cast iron pipes (Shear force is proportional to rupture stress)

Soil resistance k_o N/mm³		0.025	0.1	0.25	1.0
Nominal pipe size in	mm	SAND CAST GREY IRON (185 N/mm²)			
3	75	33	47	59	84
4	100	52	74	93	131
5	125	79	112	140	198
6	150	109	142	178	252
8	205	187	265	333	470
12	305	402	570	716	1012
		SPUN GREY CAST IRON (247 N/mm²)			
3	75	37	55	68	97
4	100	61	85	107	151
5	125	91	126	158	224
6	150	123	175	219	310
8	205	206	296	372	527
12	305	441	633	795	1124

Table 3.2 gives the magnitude of the differential displacement over the length of pipe L which is involved. L is the distance between the positions of the maximum bending moments, and is obtained from Equation (3.14) as

$$L = 2x = \frac{\pi}{2\beta} \quad \ldots \quad \ldots \quad \ldots \quad \ldots \quad \ldots \quad \ldots \qquad (3.20)$$

Table 3.2 shows that the range of L is from 0·5 to 2·9 m as the pipe size increases and the soil becomes softer. As the length of a single cast iron pipe is about 4 m it is obvious that, even with flexible joints, a pipe can be put at risk by differential ground displacement.

The value of the shape factor α was taken to be unity in the analysis to eliminate it from Equations (3.18) and (3.19).

In order to investigate the shape factor, Roberts and Regan (28) conducted a series of tests in which short lengths of cast iron pipes were pressed into P.F.A (Pulverised Fuel Ash), (44). The gradients obtained from the load-penetration curves were compared with the load-penetration gradients obtained from plate bearing tests, (45) which were conducted on the P.F.A. A shape factor of approximately 0·9 was found to apply to the pipe cross section. The tests did not take into account any of the effects the size of the pipe may have on the value of the shape factor.

The value of α is also affected by the interaction between the pipe and the soil; that is, what type of coating the pipe has and whether or not the soil is cohesionless. It would therefore be necessary, if a better approximation is required, to carry out a thorough evaluation of α

TABLE. 3.2 The magnitude of the differential displacement Δ(mm) over the length of pipe L(m) which is involved (Displacement is proportional to the rupture stress and L is indipendent of the rupture stress)

Soil resistance k_o N/mm³		0.025		0.1		0.25		1.0	
Nominal pipe size in	mm	Δ(mm)	L (m)	Δ(mm)	L (m)	Δ(mm)	L (m)	Δ(mm)	L (m)
		SAND CAST GREY IRON (185 N/mm²)							
3	75	69.90	1.25	34.94	0.89	22.10	0.71	11.05	0.50
4	100	73.70	1.45	36.84	1.03	23.30	0.82	11.65	0.58
5	125	79.00	1.67	39.50	1.18	24.98	0.94	12.49	0.66
6	150	81.64	1.86	40.82	1.32	25.82	1.05	12.91	0.74
8	205	90.80	2.23	45.41	1.58	28.72	1.25	14.36	0.89
12	305	101.70	2.88	50.85	2.04	32.16	1.62	16.08	1.14
		SPUN GREY CAST IRON (247 N/mm²)							
3	75	85.20	1.18	42.60	0.84	26.93	0.67	13.47	0.47
4	100	89.12	1.39	44.56	0.98	28.18	0.78	14.09	0.55
5	125	94.30	1.59	47.15	1.12	29.82	0.89	14.91	0.63
6	150	99.10	1.76	49.55	1.25	31.34	0.99	15.67	0.75
8	205	107.76	2.09	53.88	1.49	34.08	1.18	17.04	0.84
12	305	120.16	2.70	60.08	1.91	38.00	1.52	19.00	1.08

for different soils, pipe sizes and pipe coatings to establish exact design values.

The lower values of the foundation modulus that are used are based on the values given by Terzaghi (46) and are in the range 0·025 to 0·1 N/mm^3. This range was thought to be too small, as it would imply that very large displacements would be required to rupture a pipe, Roberts and Regan (28). This is no longer the case as it is stated in (45) that the average value of the foundation modulus for road subgrades is 0·054 N/mm^3 and Morris (47) states that the majority of main breaks in Houston, Texas, USA are in the 2 - 6 in size and that vertical soil movement causes about 70% of all breaks. An offset of about 3 in is usually noted in the sheared ends. This value of offset corresponds to a soil resistance of approximately 0·025 N/mm^3, Table 3.2.

The upper values of the foundation modulus, 0·1 to 1·0 N/mm^3 are used as a paved road would be able to offer a far greater resistance due to the effect of the paving. The value of the foundation modulus given by references (45) and (46) are appropriate when the earth cover of the pipe is sufficient to neutralise the effect of the paving or when the pipe is being displaced away from the surface. The higher values of the foundation modulus are appropriate when the pipe has a shallow cover and is being displaced towards the road surface.

Recent research by The Transport and Road Research Laboratory, Symons (48), has indicated that underground pipelines may be put at risk, from differential displacement, due to adjacent trench excavations.

The effect of an adjacent excavation would be to differentially displace a shallow buried pipeline as shown in Figure 3.5. Progressive excavation of the trench would include temporary bending over the complete length of the pipeline located within the zone of ground movement. On completion of the trench, the central portion of the pipeline is likely to have been subjected to translation with permanent bending remaining towards the ends of the trench. In the longer term any increase in the density of the backfill could result in increased ground movement and pipe strains.

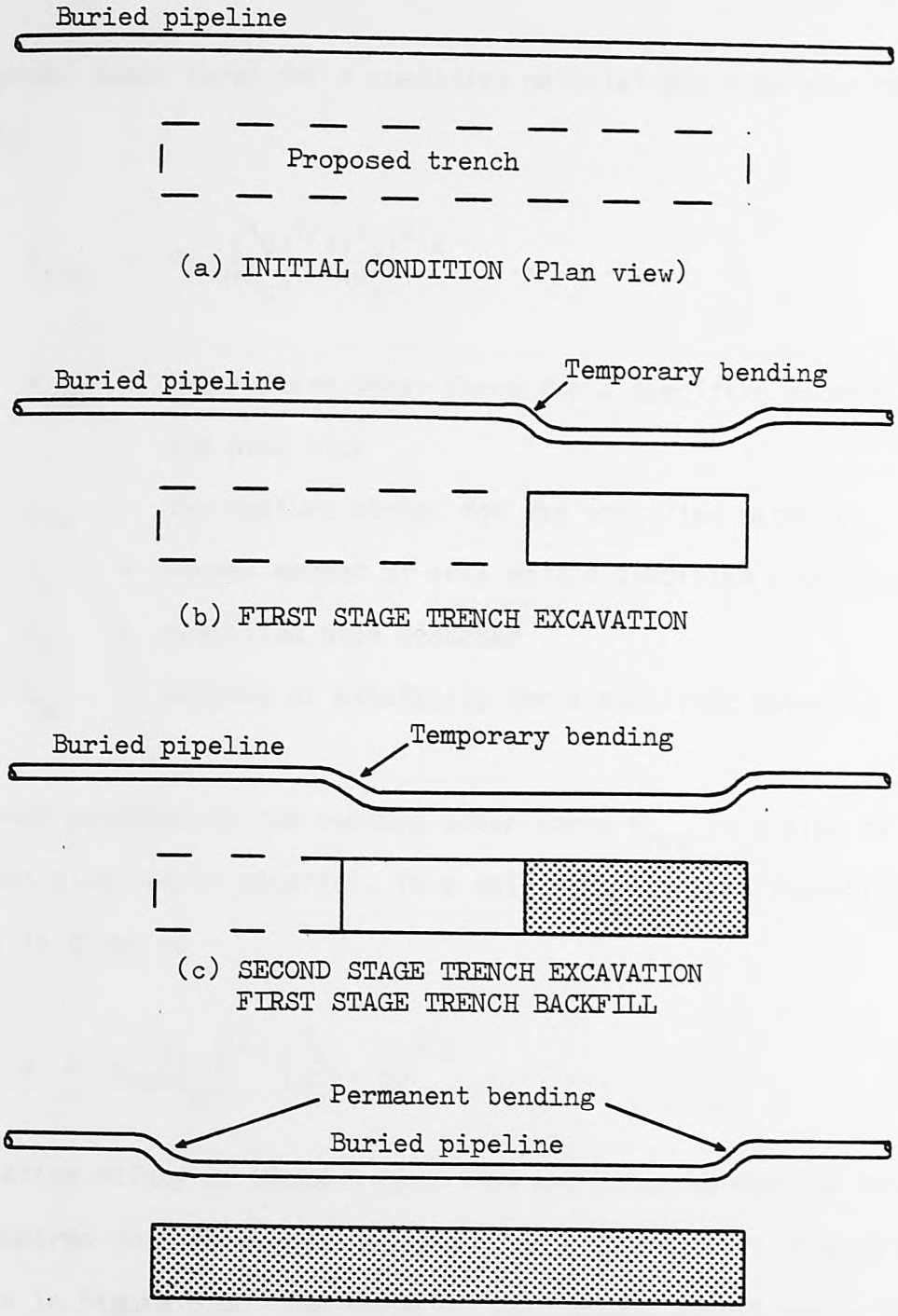

FIG. 3.5 Probable effect of trench construction on adjacent buried pipeline

3.6 COMPARISON OF VARIOUS MATERIALS

The relative safety in bending of various piping materials can be compared by using a modified version of Equation (3.18).

The rupture shear force for a specified material and pipe size is given by

$$P_{rsm} = 4\sigma_{rm}\left\{\frac{k_o}{E_m}\right\}^{1/4}\left\{\frac{I_s}{d_s}\right\}^{3/4} \quad \ldots \quad \ldots \quad \ldots \quad \ldots \qquad (3.21)$$

where

P_{rsm} = the rupture shear force for a specified material and pipe size

σ_{rm} = the rupture stress for the specified material

I_s = second moment of area of the specified pipe size

d_s = specified pipe diameter

E_m = modulus of elasticity for a specified material

The stress produced by the rupture shear force P_{rsm} in a pipe of a different size and/or material, in a soil with the same foundation modulus is given by

$$\sigma = \sigma_{rm}\left\{\frac{E}{E_m}\right\}^{1/4}\left\{\frac{I_s}{d_s} \cdot \frac{d}{I}\right\}^{3/4} \quad \ldots \quad \ldots \quad \ldots \quad \ldots \qquad (3.22)$$

The relative safety of Class C spun iron and Class K9 ductile iron pipe compared to a 75 mm (3") diameter Class C sand cast iron pipe is shown in Figure 3.6. The value of the rupture stress for a 75 mm diameter Class C sand cast iron pipe is used as a datum value, and the percentage of the rupture stress that this value of the shear force would produce in larger diameter pipes and pipes made from spun and ductile iron of various sizes have been calculated using Equation (3.17) and plotted, Figure 3.6.

Figure 3.6 shows that if sand cast iron was the only material available, and if the ground had the capacity to break a Class C 75 mm diameter pipe by longitudinal bending alone, then if a 100 mm or 150 mm pipe had been laid in its place, the percentage of the rupture stress developed in the pipes would have been 64 and 42 respectively.

By considering ductile iron as having a linear stress-strain relationship (the fact that ductile iron has a linear elastic stress-strain relationship up to its yield point of about 200 N/mm^2 and an inelastic relationship thereafter, makes it a safer material than indicated) it can be compared with both sand cast and spun iron in longitudinal bending. Figure 3.6 shows that for 75 mm pipes spun iron would have been stressed to within 91% of its rupture stress whereas ductile iron would have been stressed to 55% of its rupture stress.

A change from a 75 mm Class C sand cast iron pipe to a 150 mm Class K9 ductile iron pipe would result in a stress level of only 22%, which clearly shows the superiority of ductile iron pipes in resisting fracture due to longitudinal bending.

Relative safety curves with datum values of 100 mm and 150 mm Class C cast iron pipes are shown in Figures 3.7 and 3.8. Figure 3.8 shows that if ductile iron is used instead of sand cast iron, the longitudinal bending that would fracture a 150 mm sand cast iron pipe would produce a stress level of at most 75% in a ductile iron pipe.

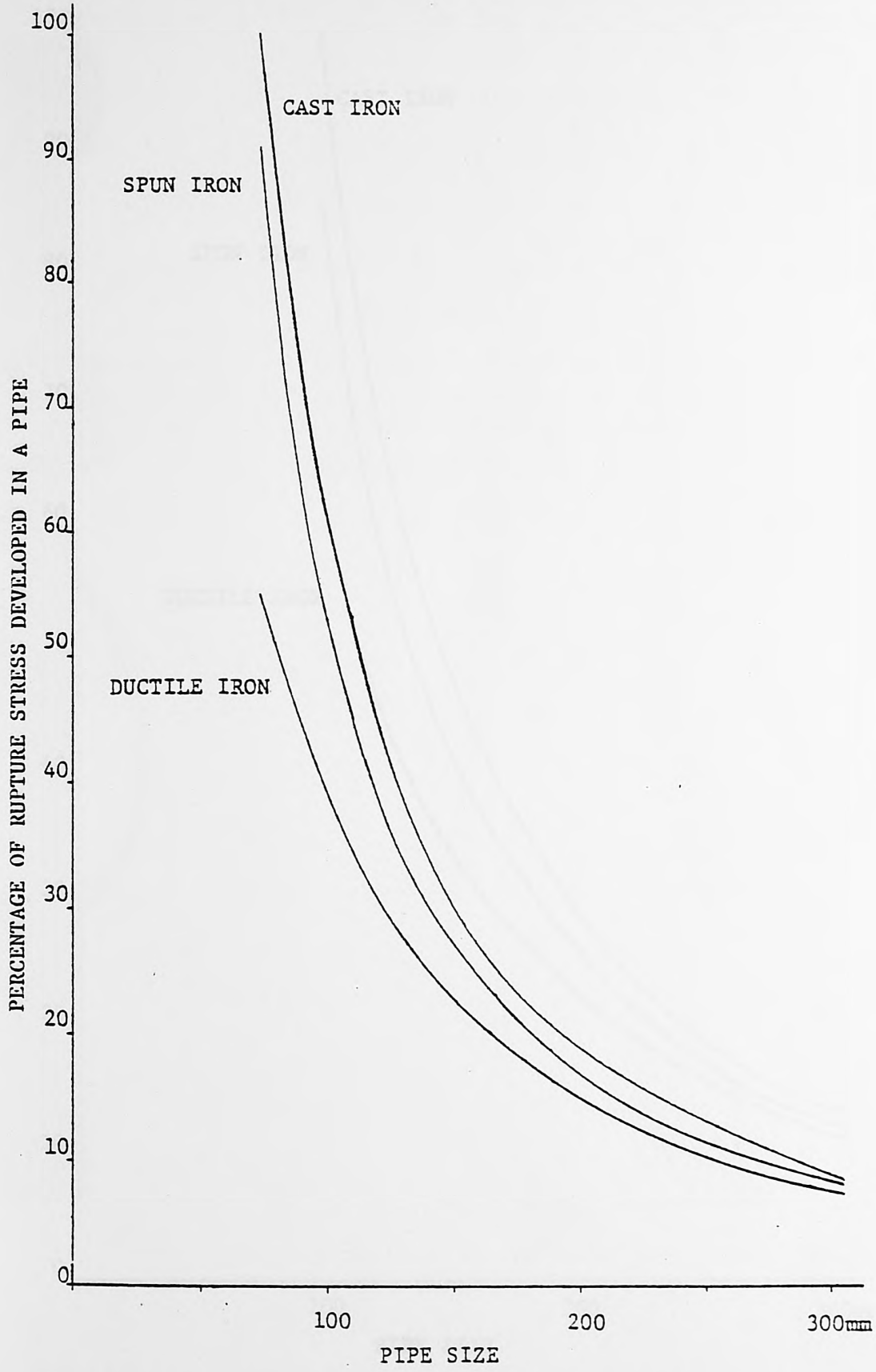

FIG. 3.6 Relative safety of other pipe materials and sizes compared to a 75mm sand cast iron pipe

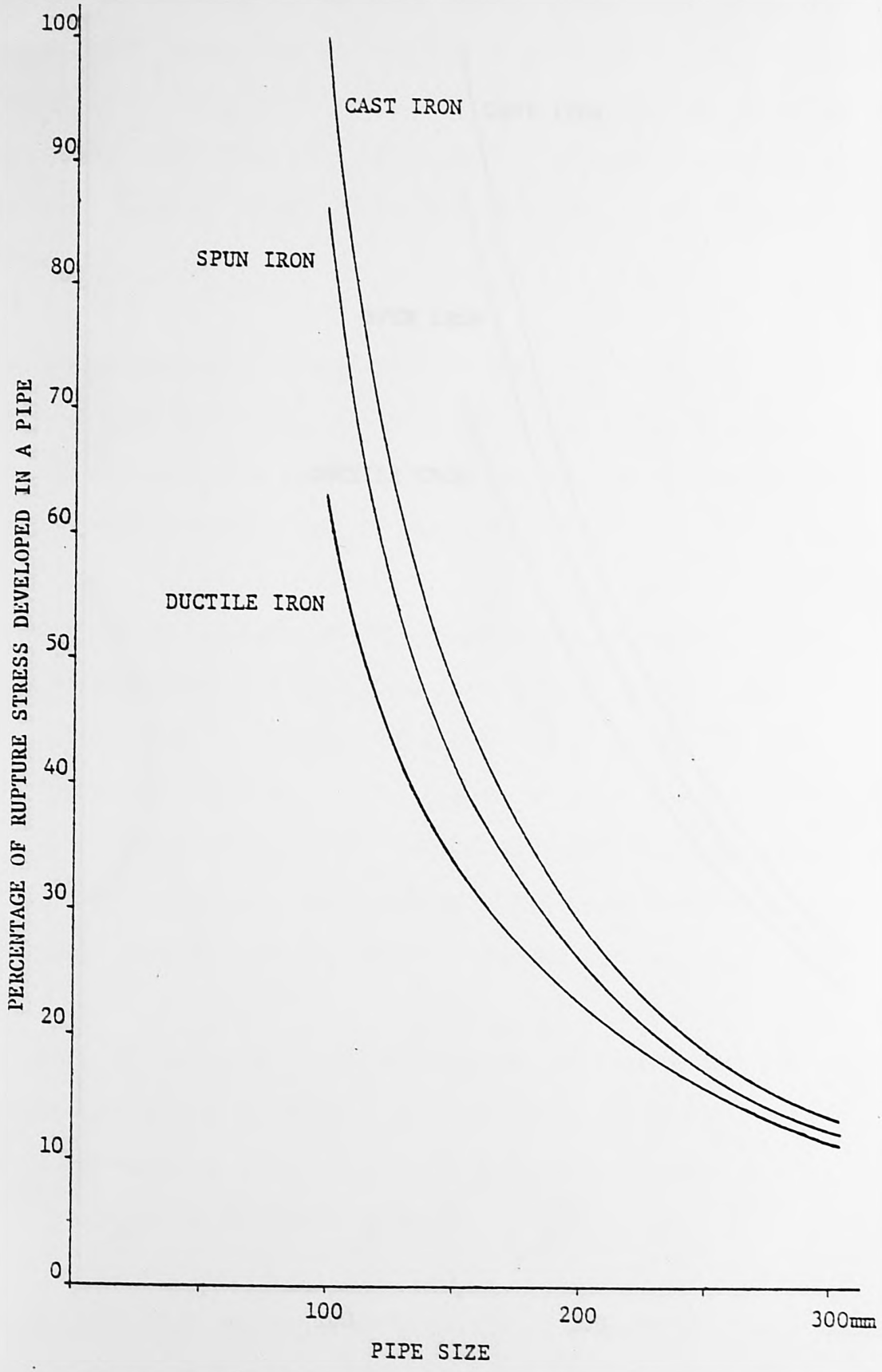

FIG. 3.7 Relative safety of other pipe materials and sizes compared to a 100mm sand cast iron pipe

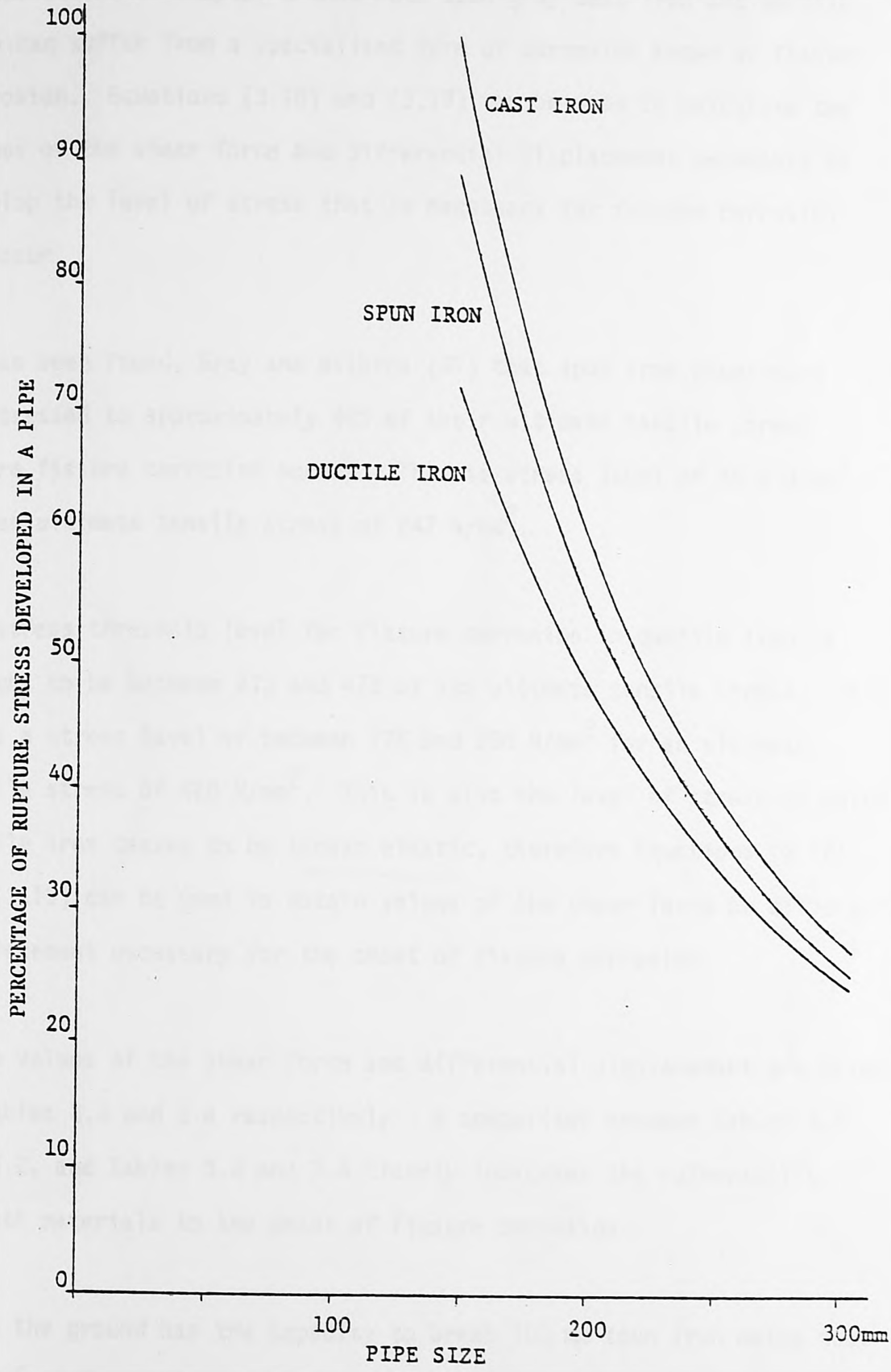

FIG. 3.8 Relative safety of other pipe materials and sizes compared to a 150mm sand cast iron pipe

3.7 FISSURE CORROSION

It was stated in Chapter 2 that both spun grey cast iron and ductile iron can suffer from a specialised form of corrosion known as fissure corrosion. Equations (3.18) and (3.19) can be used to calculate the values of the shear force and differential displacement necessary to develop the level of stress that is necessary for fissure corrosion to occur.

It has been found, Gray and Wilkins (37) that spun iron pipes must be stressed to approximately 40% of their ultimate tensile stress before fissure corrosion occurs. This is stress level of 98·8 N/mm^2 for an ultimate tensile stress of 247 N/mm^2.

The stress threshold level for fissure corrosion in ductile iron is thought to be between 41% and 47% of its ultimate tensile stress. This gives a stress level of between 175 and 200 N/mm^2 for an ultimate tensile stress of 420 N/mm^2. This is also the level of stress at which ductile iron ceases to be linear elastic, therefore Equations (3.18) and (3.19) can be used to obtain values of the shear force or differential displacement necessary for the onset of fissure corrosion.

These values of the shear force and differential displacement are given in Tables 3.3 and 3.4 respectively. A comparison between Tables 3.1 and 3.2, and Tables 3.3 and 3.4 clearly indicates the vulnerability of both materials to the onset of fissure corrosion.

Since the ground has the capacity to break 100 mm spun iron mains that are only a few months old with a transverse fracture, it is not surprising that fissure corrosion has been identified in this material.

Since ductile iron is linear elastic up to the point at which fissure corrosion occurs, Tables 3.3 and 3.4 can be used as a gauge as to whether the ground has the capacity to produce fissure corrosion in this material. It can immediately be seen from Tables 3.3 and 3.4 that the ground has the capacity, so it is almost certain that fissure corrosion will become a problem in ductile iron pipes of small nominal diameter.

TABLE. 3.3 Shear force P(kN) to develop the stress level at which fissure corrosion can occur

Soil resistance k_o N/mm^3		0.025	0.1	0.25	1.0
Nominal pipe size in	mm	SPUN GREY CAST IRON (98.8 N/mm^2)			
3	75	34.08	17.04	10.77	5.39
4	100	35.65	17.82	11.27	5.64
5	125	37.72	18.86	11.93	5.96
6	150	39.64	19.82	12.54	6.27
8	205	43.10	21.55	13.63	6.82
12	305	48.06	24.03	15.20	7.60
		DUCTILE GREY IRON (175 N/mm^2).			
3	75	55.40	27.70	17.52	8.76
4	100	56.66	28.33	17.92	8.96
6	150	58.88	29.44	18.62	9.31
8	205	60.08	30.04	19.00	9.50
12	305	64.38	32.19	20.36	10.18

TABLE. 3.4 The magnitude of the differential displacement Δ(mm) necessary to develop the stress level at which fissure corrosion can occur

Soil resistance k_o N/mm^3		0.025	0.1	0.25	1.0
Nominal pipe size in	mm	SPUN GREY CAST IRON (98.8 N/mm^2)			
3	75	15	22	27	39
4	100	24	34	43	60
5	125	36	50	63	90
6	150	49	70	88	124
8	205	82	118	149	211
12	305	176	253	318	450
		DUCTILE GREY IRON (175 N/mm^2)			
3	75	25	36	45	63
4	100	34	49	61	86
6	150	63	89	112	158
8	205	97	137	172	244
12	305	191	270	340	481

3.8 ASBESTOS CEMENT

Asbestos cement has a linear elastic stress-strain relationship and as such can be analysed using the elastic model. Equations (3.18),(3.19) and (3.20) can be used to calculate the rupture shear force, the magnitude of the differential displacement necessary to produce the rupture stress and the length of pipe which is involved. These values are given in Tables 3.5 and 3.6 for Class 25 pipes.

The tables show clearly that asbestos cement pipes are very susceptible to fracture from longitudinal bending. This confirms findings from the continent, Coe (42) that asbestos cement pipes fracture at a rate three to four times higher than iron pipes.

TABLE. 3.5 Shear force P(kN) to develop the rupture stress in various sizes of asbestos cement pipe

Soil resistance k_o N/mm^3		0.025	0.1	0.25	1.0
Nominal pipe size in	mm	ASBESTOS CEMENT (24 N/mm^2)			
3	75	6.4	9.1	11.4	16.2
4	100	10.7	15.1	19.0	26.9
6	150	23.5	33.2	41.8	59.1

TABLE. 3.6 The magnitude of the differential displacement Δ(mm) over the length of pipe L(m) which is involved

Soil resistance k_o N/mm^3		0.025		0.1		0.25		1.0	
Nominal pipe size in	mm	Δ(mm)	L (m)	Δ(mm)	L (m)	Δ(mm)	L (m)	Δ(mm)	L (m)
		ASBESTOS CEMENT (24 N/mm^2)							
3	75	18.68	0.90	9.34	0.64	5.91	0.51	2.96	0.36
4	100	20.59	1.07	10.30	0.76	6.51	0.60	3.26	0.42
6	150	24.00	1.39	12.00	0.98	7.59	0.78	3.80	0.55

3.9 POINT LOADING

The other common cause of fracture of pipes is point loading, either by rigid objects across the pipe (i.e. other pipes) or traffic flow over the pipe.

The solution of Equation (3.10) for a point load at the centre of an infinitely long pipe is

$$y = \frac{P\beta}{2k} e^{-\beta x}(\text{Cos}\beta x + \text{Sin}\beta x) \quad \ldots \quad \ldots \quad \ldots \quad (3.23)$$

which can be transformed to give

$$\sigma_r = \frac{P_r}{8} \left\{\frac{4E}{\alpha k_o}\right\}^{1/4} \left\{\frac{d}{I}\right\}^{3/4} \quad \ldots \quad \ldots \quad \ldots \quad \ldots \quad (3.24)$$

Comparing Equation (3.24) with Equation (3.16), for the same value of stress gives

$$P_{PL} = \sqrt{2}\, P_{GD}$$

where suffix PL indicates point load and GD indicates ground displacement.

The corresponding displacement relationship is

$$\Delta_{PL} = 0{\cdot}177\, \Delta_{GD}$$

Hence the fracture force is greater, but the displacement is much smaller. A comparison of the rupture conditions due to ground movement and a point load acting on spun grey cast iron pipes is given in Table 3.7. The pipe lengths tabulated are the distances between

TABLE. 3.7 Comparison of rupture conditions due to ground movement and a point load acting on spun grey cast iron pipes

Soil resistance k_o N/mm³		0.025			0.1			0.25			1.0		
Nominal pipe size in	mm	L m	P kN	Δ mm	L m	P kN	Δ mm	L m	P kN	Δ mm	L m	P kN	Δ mm
		GROUND MOVEMENT											
4	100	1.39	61	89	0.98	85	44	0.78	107	28	0.55	151	15
6	150	1.76	123	99	1.25	175	50	0.99	219	31	0.75	310	16
		POINT LOAD											
4	100	4.17	86	16	2.94	120	8	2.33	151	5	1.65	213	2
6	150	5.29	174	18	3.72	247	9	2.96	310	6	2.10	438	3

the positions of maximum bending moment for ground displacement and positions of zero displacement for point load.

The above analysis is for a pipeline laid on the surface of the ground. An analysis for the case of a buried pipeline has been dealt with by Pearson (49)in which he convolutes the distribution of vertical pressure on a buried pipe due to a concentrated surface load, Boussinesq's equation,

$$p_x = \frac{3Q_s}{2\pi z^2}\left[1 + \left(\frac{x}{z}\right)^2\right]^{-2\cdot5} \quad \ldots \quad \ldots \quad \ldots \quad \ldots \qquad (3.25)$$

where

p_x = vertical pressure at a point within the soil

Q_s = concentrated surface load

z = depth of the point below the surface

x = horizontal distance from the load to the point

with the second derivative of Equation (3.23) times EI using

$$P = \frac{p_x d}{\beta} \cdot d(\beta x) \quad \ldots \quad \ldots \quad \ldots \quad \ldots \quad \ldots \qquad (3.26)$$

to give the maximum longitudinal bending moment as

$$M_{max} = \frac{3dQ_s}{8\pi}(\beta z)^{-2}\int_{-\infty}^{\infty} e^{-\beta x}(\cos\beta x - \sin\beta x)\left[1 + \left(\frac{\beta x}{\beta z}\right)^2\right]^{-2\cdot5} d(\beta x) \quad \ldots \quad \ldots \quad \ldots \quad \ldots \qquad (3.27)$$

Letting $y = \beta x$ and $b = \beta z$ and

$$F(b) = \frac{3b^3}{4\pi}\int_0^{\infty} e^{-y}(\cos y - \sin y)\,(b^2 + y^2)^{-2\cdot5} dy \quad \ldots \quad \ldots \quad \ldots \quad \ldots \quad \ldots \qquad (3.28)$$

Equation (3.27) can be rewritten as

$$\frac{M_{max}}{Q_s d} = F(b) \quad \ldots \ldots \ldots \ldots \ldots \ldots \quad (3.29)$$

A graph of the dimensionless parameter of maximum bending moment, Equation (3.29), for an infinite rigid pipe beneath a concentrated surface load is given in Figure 3.9. This can be used to evaluate the maximum longitudinal bending moment in a pipe for a given soil resistance, depth and surface load.

By replacing M_{max} by $\frac{2\sigma_r I}{d}$ and rearranging, the value of the concentrated surface load, Q_s, which will produce the rupture stress, σ_r, in the pipeline is given by

$$Q_s = \frac{2\sigma_r I}{d^2 F(b)} \quad \ldots \ldots \ldots \ldots \ldots \ldots \quad (3.30)$$

Values of the concentrated surface load for various ground resistances and depths of cover for asbestos cement, Class 25, cast iron and spun iron, Class C, are given in Tables 3.8, 3.9 and 3.10 respectively.

The tables indicate that the most vulnerable material is asbestos cement and that at a depth of 500 mm in a very soft soil a static load of 204·5 kN (20·5 tons) would rupture a 100 mm diameter pipe and taking an impact factor of 1·5 this load is reduced to 136·7 kN (13·7 tons) for an uncorroded pipe. Corresponding values for cast iron and spun iron are 804·2 kN (80·7 tons) and 536·1 kN (53·8 tons), and 950·4 kN (95·4 tons) and 633·6 kN (63·6 tons) respectively.

As the normal specified minimum depth of cover for water mains is 900 mm, it is evident from the tables that at this depth it is impossible to produce the level of stress necessary to fracture even a 100 mm diameter asbestos cement pipe.

The above analysis deals only with the longitudinal bending moment produced in a pipe by a concentrated surface load and does not take into account earth loads superimposed on the pipe. The earth loading for small diameter pipes is insignificant compared with the stress caused in the pipe by a surface load, ANSI/AWWA C101 - 67 (R 1977) (50), but as the pipe diameter and depth of cover increase the more important earth loads become.

It is evident that small diameter pipes are primarily stressed in longitudinal bending by differential ground displacement and that secondary effects are produced by traffic and earth loads.

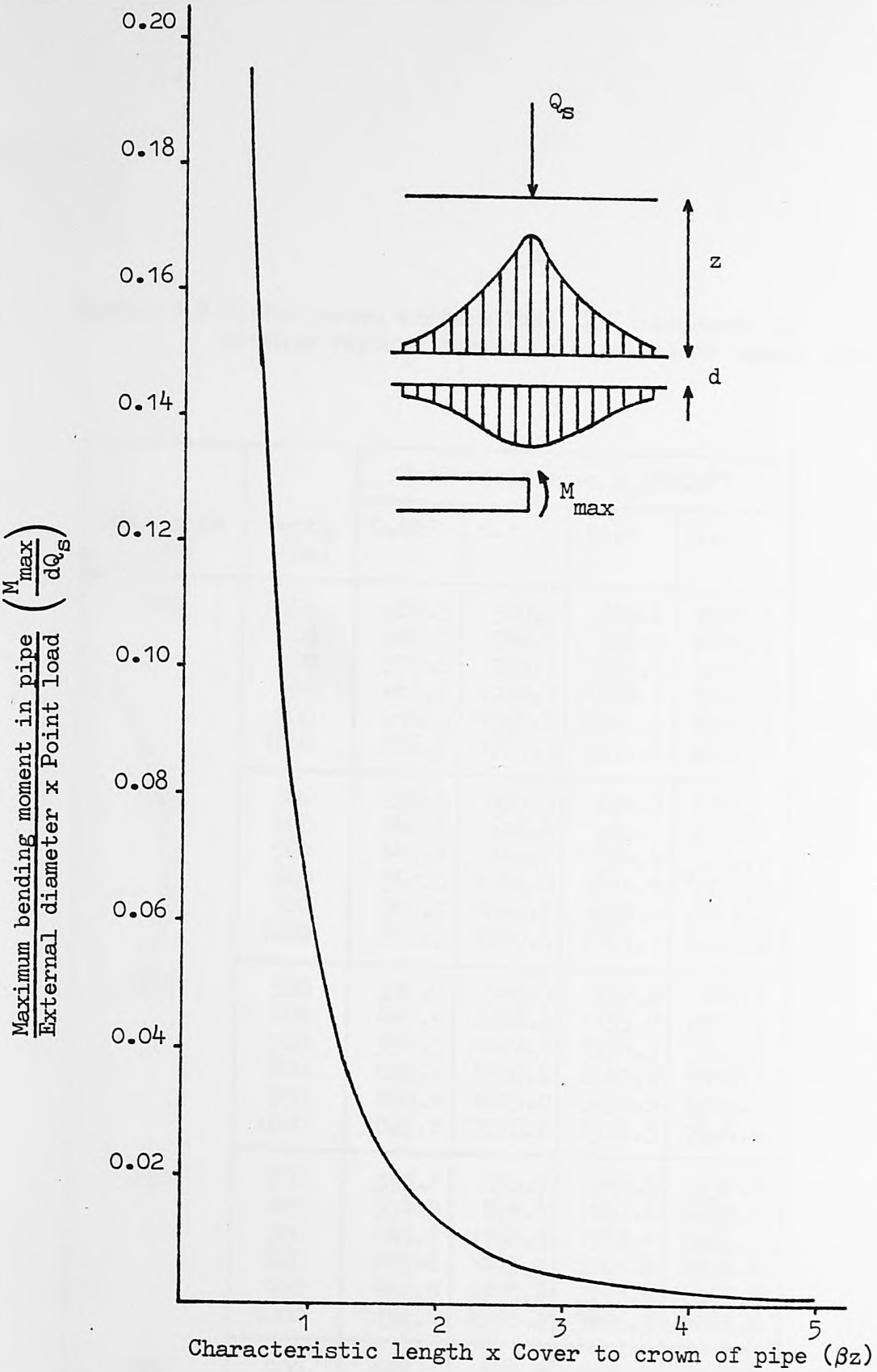

FIG. 3.9 Dimensionless parameter of bending moment for an infinite rigid pipe beneath a concentrated surface load

TABLE. 3.8 Concentrated surface load (kN) necessary to produce rupture stress in an asbestos cement pipe

Pipe size (mm)	Depth (mm)	Soil resistance k_o (N/mm³)			
		0.025	0.1	0.25	1.0
100	500	204.5	380.3	602.6	1325.7
	600	280.5	546.5	898.9	2110.4
	700	373.0	759.7	1293.3	3219.1
	800	484.6	1029.3	1808.8	4744.5
	900	618.2	1365.8	2471.9	6794.9
	1000	776.9	1781.3	3312.6	9495.4
150	500	256.3	451.3	684.0	1388.9
	600	342.2	626.4	980.1	2107.8
	700	443.4	842.6	1358.4	3080.7
	800	562.0	1106.8	1835.4	4370.7
	900	700.0	1426.5	2429.4	6051.0
	1000	859.7	1810.3	3161.1	8205.0
200	500	336.7	568.6	832.6	1586.1
	600	440.4	768.2	1155.7	2314.3
	700	559.5	1007.1	1554.5	3262.6
	800	695.6	1290.7	2041.8	4478.2
	900	850.4	1625.0	2631.6	6015.0
	1000	1025.7	2016.6	3339.5	7934.0
250	500	397.7	656.7	943.8	1735.7
	600	514.5	874.4	1287.4	2477.3
	700	646.7	1130.3	1703.1	3421.1
	800	795.6	1429.1	2201.8	4606.4
	900	962.9	1775.8	2795.4	6077.6
	1000	1150.1	2176.2	3496.9	7884.5
300	500	468.1	759.0	1074.1	1918.2
	600	600.2	998.5	1444.1	2687.1
	700	747.9	1275.7	1884.0	3646.2
	800	912.3	1594.8	2403.4	4828.9
	900	1094.9	1960.3	3012.5	6272.8
	1000	1297.0	2376.9	3722.4	8019.4

TABLE. 3.9 Concentrated surface load (kN) necessary to produce rupture stress in a cast iron pipe

Pipe size (mm)	Depth (mm)	Soil resistance k_o (N/mm^3)			
		0.025	0.1	0.25	1.0
100	500	804.2	1403.0	2110.8	4228.1
	600	1068.9	1936.2	3004.0	6363.7
	700	1379.1	2590.2	4137.3	9230.8
	800	1740.6	3384.4	5556.6	13006.5
	900	2159.3	4340.5	7313.8	17895.0
	1000	2641.8	5482.3	9466.9	24129.3
150	500	1039.1	1736.3	2520.4	4723.2
	600	1352.2	2330.1	3470.1	6821.4
	700	1709.2	3034.6	4631.7	9525.2
	800	2114.6	3864.6	6039.0	12958.8
	900	2572.9	4836.0	7729.2	17263.4
	1000	3089.3	5966.3	9743.6	22598.0
200	500	1268.5	2065.5	2933.6	5275.4
	600	1629.9	2725.1	3957.5	7422.9
	700	2034.9	3491.2	5180.3	10114.5
	800	2487.3	4376.0	6629.3	13448.5
	900	2990.9	5392.7	8334.6	17534.9
	1000	3550.0	6555.3	10329.0	22496.4
250	500	1474.7	2361.0	3305.6	5783.3
	600	1879.3	3080.3	4399.4	7995.5
	700	2327.4	3903.6	5684.1	10714.5
	800	2822.3	4841.4	7183.2	14022.9
	900	3367.4	5905.2	8922.3	18012.5
	1000	3966.3	7107.1	10929.2	22784.6
300	500	1696.6	2679.3	3708.0	6343.5
	600	2147.7	3464.1	4881.0	8644.1
	700	2642.4	4351.4	6239.4	11424.6
	800	3183.8	5350.5	7803.9	14756.4
	900	3774.7	6471.5	9596.9	18717.7
	1000	4418.6	7725.0	11642.3	23394.8

TABLE. 3.10 Concentrated surface load (kN) necessary to produce rupture stress in a spun iron pipe

Pipe size (mm)	Depth (mm)	Soil resistance k_o (N/mm³)			
		0.025	0.1	0.25	1.0
100	500	950.4	1674.2	2538.8	5160.0
	600	1269.2	2324.8	3639.5	7835.4
	700	1645.1	3128.4	5046.7	11457.6
	800	2085.5	4110.7	6821.5	16262.8
	900	2598.3	5300.1	9032.5	22524.3
	1000	3192.0	6728.3	11757.1	30554.5
150	500	1197.4	2019.1	2953.3	5614.2
	600	1565.0	2725.7	4095.0	8181.4
	700	1986.9	3570.3	5502.9	11519.9
	800	2468.6	4572.0	7221.2	15794.5
	900	3016.2	5751.6	9299.0	21193.1
	1000	3636.1	7132.2	11790.7	27927.7
200	500	1449.3	2379.0	3402.1	6197.8
	600	1869.6	3155.5	4619.0	8792.9
	700	2343.2	4063.5	6083.3	12074.7
	800	2875.0	5118.9	7831.0	16172.6
	900	3470.0	6338.7	9901.4	21232.4
	1000	4133.5	7741.4	12337.3	27416.9
250	500	1664.9	2685.8	3784.8	6704.3
	600	2129.5	3521.8	5068.0	9343.1
	700	2646.9	4485.0	6586.7	12615.7
	800	3221.2	5589.3	8371.3	16630.3
	900	3856.9	6846.2	10455.4	21507.8
	1000	4558.7	8280.5	12875.1	27382.5
300	500	1917.4	3048.4	4243.0	7339.4
	600	2435.1	3958.9	5615.6	10072.9
	700	3005.8	4994.6	7216.3	13404.5
	800	3633.0	6167.6	9072.0	17427.2
	900	4320.8	7490.9	11211.6	22244.1
	1000	5073.3	8978.1	13666.4	27968.4

CHAPTER 4

NON-LINEAR ELASTIC MATHEMATICAL MODEL OF LONGITUDINAL BENDING

4.1 INTRODUCTION

A discrete mathematical model is proposed, for the solution of the problem of differential ground displacement acting on an encased pipeline, in which it can be assumed that the ground has a non-linear pressure-displacement relationship and the pipeline is composed of elemental lengths with different moduli of elasticity and second moments of area.

The model employed is solved by using a force-displacement method which entails the setting up and solving a set of non-homogeneous simultaneous equations.

The model is initially solved for a linear elastic pipeline encased in a linear elastic foundation and from this solution, the non-linear cases are solved by iteration until convergence is achieved.

4.2 FOUNDATION AND PIPELINE MODEL

The foundation model is obtained by considering that the foundation can be represented by a series of springs that are joined to the pipeline. This is the same foundation model, Hetényi foundation, Kerr (51), that was used for the continuous linear elastic model dealt with in Chapter 2.

The pipeline model is obtained by considering that the deflected pipeline is divided into a number of elemental lengths which are released from the effects of continuity.

The model is solved using a force-displacement method which when applied to the model has the effect of restoring the continuity of the pipeline and maintining the equilibrium between the pipeline and the foundation.

4.3 FORCE-DISPLACEMENT EQUATIONS

The force-displacement solution is obtained by considering a beam resting on three or more supports, let A, B, C be any three consecutive supports, Figure 4.1, with AB = a_1 and BC = a_2, and A, B, C at a depth p_A, p_B and p_C respectively below the x - axis. Let R_A, R_B, R_C be the reactions at the supports and m_A, m_B, m_C the bending moments there. Since the beam is supported at ... A, B, C, ... there is a discontinuity in the shearing force at each of these supports, but the bending moment has no discontinuities.

The sign convention used gives m and R positive where they act as shown in Figure 4.1.

Between any pair of supports the differential equation is

$$E_i I_i \frac{d^4y}{dx^4} = 0 \quad \ldots \ldots \ldots \ldots \ldots \ldots \qquad (4.1)$$

since the only loading acting on the beam is at the supports.

Let suffix 1 represent the beam AB and suffix 2 the beam BC. Integrating Equation (4.1) for each section of the beam between the supports and fitting the solutions together at support B we have

$$-a_1 < x < 0 \qquad\qquad 0 < x < a_2$$

$$E_1 I_1 \frac{d^3y}{dx^3} = A_1 \qquad\qquad E_2 I_2 \frac{d^3y}{dx^3} = A_2 \qquad (4.2)$$

because of the discontinuity in the shear force at $x = 0$, we have the boundary condition at $x = 0$

$$- R_B = A_2 - A_1 \quad \ldots \quad \ldots \quad \ldots \quad \ldots \quad \ldots \quad \ldots \qquad (4.3)$$

Integrating Equation (4.2)

$$E_1 I_1 \frac{d^2y}{dx^2} = A_1x + B_1 \qquad E_2 I_2 \frac{d^2y}{dx^2} = A_2x + B_2$$

$$\ldots \quad \ldots \quad \ldots \quad \ldots \quad \ldots \quad \ldots \qquad (4.4)$$

At $x = 0$, the bending moment m is continuous and has the value m_B

$$m_B = B_1 = B_2 \quad \ldots \quad \ldots \quad \ldots \quad \ldots \quad \ldots \quad \ldots \qquad (4.5)$$

Integrating Equation (4.4)

$$E_1 I_1 \frac{dy}{dx} = \frac{A_1x^2}{2} + B_1x + C_1$$

$$E_2 I_2 \frac{dy}{dx} = \frac{A_2x^2}{2} + B_2x + C_2 \quad \ldots \quad \ldots \quad \ldots \qquad (4.6)$$

The gradient is continuous at $x = 0$, with a value $\tan\theta_B$

$$E_1 I_1 \tan\theta_B = C_1 \qquad E_2 I_2 \tan\theta_B = C_2 \quad \ldots \qquad (4.7)$$

Integrating Equation (4.6)

$$E_1 I_1 y = \frac{A_1x^3}{6} + \frac{m_Bx^2}{2} + xE_1 I_1 \tan\theta_B + D_1$$

$$E_2 I_2 y = \frac{A_2x^3}{6} + \frac{m_Bx^2}{2} + x E_2 I_2 \tan\theta_B + D_2 \quad \ldots \qquad (4.8)$$

Using Equations (4.4) we obtain the bending moments at A, C by putting $x = -a_1$, $+a_2$ respectively into the appropriate expression giving

$$-A_1 = \frac{m_A - m_B}{a_1} \qquad A_2 = \frac{m_C - m_B}{a_2} \quad \ldots \qquad (4.9)$$

From Equation (4.8) the deflections p_A , p_C at A, C are

$$E_1 I_1 p_A = -\frac{A_1 a_1^3}{6} + \frac{m_B a_1^2}{2} - a_1 E_1 I_1 \tan\theta_B + E_1 I_1 p_B$$

$$E_2 I_2 p_C = \frac{A_2 a_2^3}{6} + \frac{m_B a_2^2}{2} + a_2 E_2 I_2 \tan\theta_B + E_2 I_2 p_B$$

Eliminating A_1 , A_2 and $\tan\theta_B$ from these equations using Equations (4.9) and rearranging gives

$$\frac{a_1 m_A}{6E_1 I_1} + \frac{a_1 m_B}{3E_1 I_1} + \frac{a_2 m_B}{3E_2 I_2} + \frac{a_2 m_C}{6E_2 I_2} -$$

$$-\left(\frac{p_A - p_B}{a_1}\right) + \left(\frac{p_B - p_C}{a_2}\right) = 0 \quad \ldots \qquad (4.10)$$

The reaction at point B is obtained using

$$R_B = A_1 - A_2$$

and Equation (4.9) to give

$$R_B = -\left(\frac{m_A - m_B}{a_1}\right) - \left(\frac{m_C - m_B}{a_2}\right) \quad \ldots \ldots \ldots \qquad (4.11)$$

The case of an encased pipeline can now be solved using Equation (4.10) as an equation of continuity and Equation (4.11) as an equation of equilibrium in a force-displacement method for solving statically-indeterminate structures.

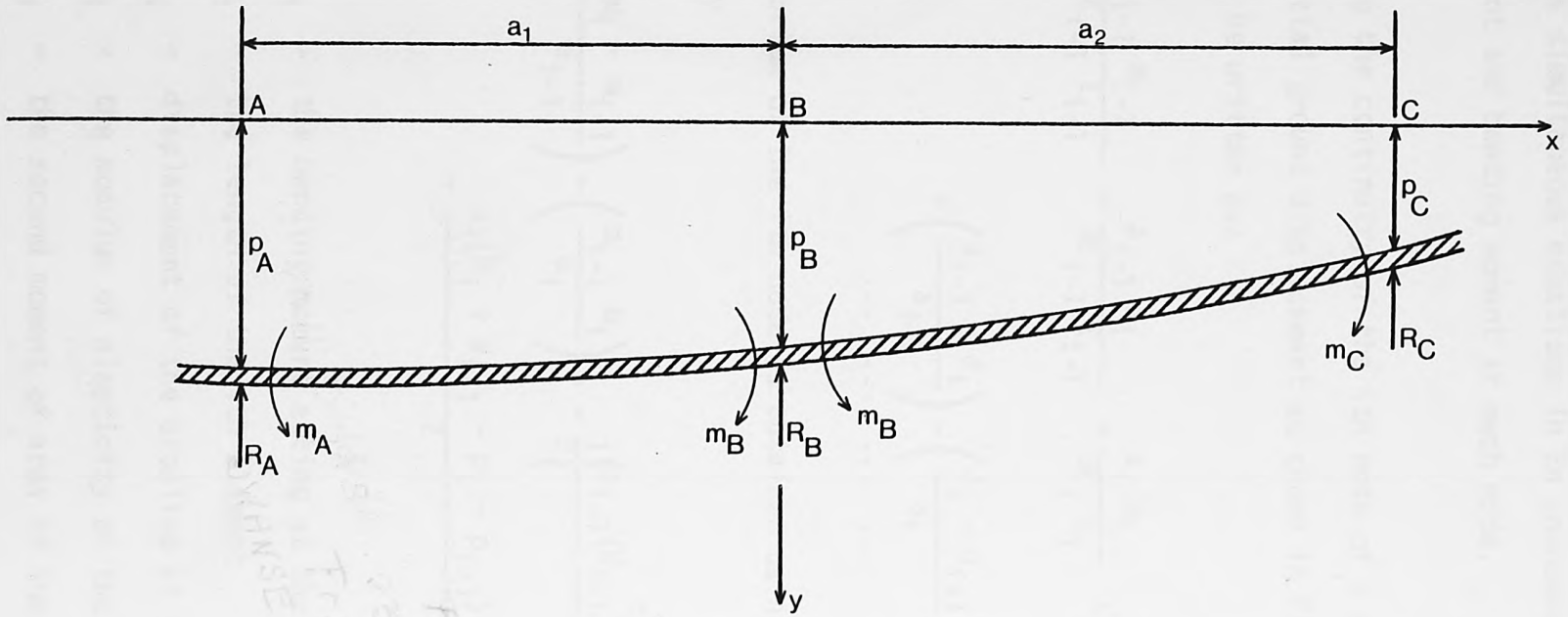

FIG. 4.1 Beam subjected to three moments and displacement of supports

4.4 FORCE-DISPLACEMENT EQUATIONS FOR AN ENCASED PIPELINE

If the pipeline is divided into n-1 elemental lengths, there will be n nodes and the pipeline-foundation model will consist of 2n non-homogeneous simultaneous equations in 2n unknowns, which will be the displacement and bending moment at each node.

Considering the continuity of the ith node of a pipeline subjected to a differential ground displacement as shown in Figure 4.2, Equation (4.10) can be written as:

$$\frac{a_{i-1}\, m_{i-1}}{6E_{i-1}\, I_{i-1}} + \frac{a_{i-1}\, m_i}{3E_{i-1}\, I_{i-1}} + \frac{a_i\, m_i}{3E_i\, I_i} + \frac{a_i\, m_{i+1}}{6E_i\, I_i} +$$

$$+\left(\frac{d_{i-1} - d_i}{a_{i-1}}\right) - \left(\frac{d_i - d_{i+1}}{a_i}\right) = 0 \qquad \text{(4.12)}$$

... ...

The equilibrium of the ith node is obtained using Equation (4.11) and is given by

$$\left(\frac{m_i - m_{i-1}}{a_{i-1}}\right) - \left(\frac{m_{i-1}\, m_i}{a_i}\right) = -\frac{1}{2}\left\{\frac{a_{i-1}(W_{i-1} + W_i - p_{i-1} - p_i)}{2} + \right.$$

$$\left. + \frac{a_i(W_i + W_{i+1} - p_i - p_{i+1})}{2}\right\} \quad \ldots \qquad \text{(4.13)}$$

where

m_i = the bending moment acting at the ith node

a_i = the length of the ith element

d_i = displacement of the pipeline at the ith node

E_i = the modulus of elasticity of the ith element

I_i = the second moment of area of the ith element

p_i = the foundation pressure acting at the ith node

W_i = force acting at the ith node which is dependent on the imposed differential displacement of the pipeline and the foundation modulus at that point

Taking $p_i = k_i d_i$ where k_i is the value of the foundation modulus at the ith node corresponding to a pressure p_i and a displacement d_i, and $W_i = k_i f_i$ where f_i is the imposed differential displacement at the ith node, Equations (4.12) and (4.13) can be rewritten as

Continuity

$$F_i\, h_{i-1}\, m'_{i-1} + S_i\, m'_i + H_i\, h_i\, m'_{i+1} + g_i\, d_{i-1} - G_i\, d_i + g_{i-1}\, d_{i+1} = 0 \quad \ldots \qquad (4.14)$$

Equilibrium

$$-4g_i\, m'_{i-1} + 4G_i\, m'_i - 4g_{i-1}\, m'_{i+1} + F_i\, c_{i-1}\, d_{i-1} + T_i\, c_i\, d_i + H_i\, c_{i+1}\, d_{i+1} = \phi_i \quad \ldots \quad \ldots \qquad (4.15)$$

where

$$c_i = \frac{a^4 k_i}{6EI}$$

$$g_i = \frac{a_i}{a}$$

$$h_i = \frac{EI}{E_i I_i}$$

$$m'_i = \frac{a^2 m_i}{6EI}$$

$$F_i = g_{i-1}^2\, g_i$$

$$G_i = g_{i-1} + g_i$$

$$H_i = g_{i-1}\, g_i^2$$

$$S_i = 2(F_i\, h_{i-1} + H_i\, h_i)$$

$$T_i = g_{i-1}\, g_i\, G_i$$

$$\phi_i = g_{i-1}\, g_i \left[g_i(c_{i-1}\, f_{i-1} + c_i\, f_i) + g_{i-1}(c_i\, f_i + c_{i+1}\, f_{i+1}) \right]$$

for $2 \leqslant i \leqslant n - 1$

The constant a is the basic elemental length, if the pipeline is divided into unequal elemental lengths a_i , then the relationship between a and a_i given above can be used. E and I are the linear elastic modulus of elasticity and second moment of area used to obtain the linear elastic solution, which is then used as a starting solution when dealing with the non-linear cases.

The boundary conditions for the pipeline at i=1 and i=n, can be obtained by assuming that the undefined displacements and bending moments in Equations (4.14) and (4.15) are a certain ratio, ℓ_1 , ℓ_2 of the preceding displacement and bending moment respectively.

For i=1, the unknown bending moment and displacement can be defined as

$$m'_o = \ell_1\, m'_1$$

$$d_o = \ell_2\, d_1$$

and if $g_o = g_1$

$$h_o = h_1$$

$$c_o = c_1$$

$$f_o = f_1$$

The equations of equilibrium and continuity can be written as:

Equilibrium

$$L_1 m'_1 - m'_2 + L_2 d_1 + g_1^2 c_2 d_2 = \phi_1$$

Continuity

$$L_3 m'_1 + g_1^2 h_1 m'_2 + L_4 d_1 + d_2 = 0$$

where

$$L_1 = 4(2 - \ell_1)$$

$$L_2 = g_1^2 c_1(\ell_2 + 2)$$

$$\phi_1 = g_1^2(3c_1 f_1 + c_2 f_2)$$

$$L_3 = g_1^2 h_1(\ell_1 + 4)$$

$$L_4 = \ell_2 - 2$$

Similar expressions can be obtained for the other boundary conditions at i = n.

The matrix equation

$$\underset{\sim}{A}\,\underset{\sim}{x} = \underset{\sim}{b} \quad \ldots \ldots \ldots \ldots \ldots \ldots \qquad (4.16)$$

Figure 4.3, of the indeterminate bending moments and displacements is formed by taking the equations of continuity, (4.14), as the even rows and the equations of equilibrium, (4.15), as the odd rows of matrix $\underset{\sim}{A}$, and the columns as alternatively bending moment and displacement. The resulting matrix is of band diagonal form with a maximum of six non-zero elements per row and column, all other elements being equal to zero. The matrix equation can be solved by any suitable method.

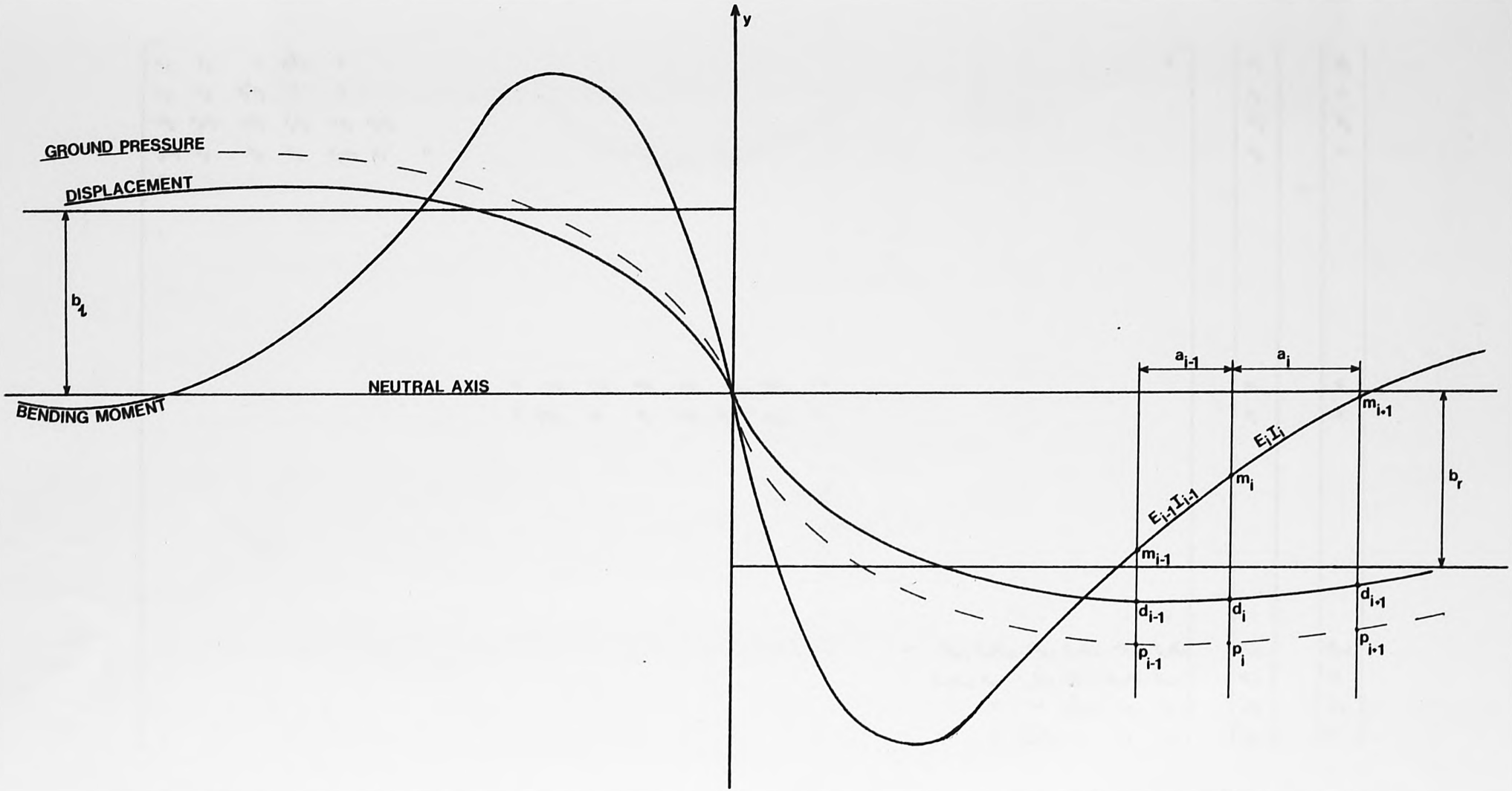

FIG. 4.2 Displacement, Bending Moment and Ground Pressure profiles of a pipeline subjected to differential ground movement

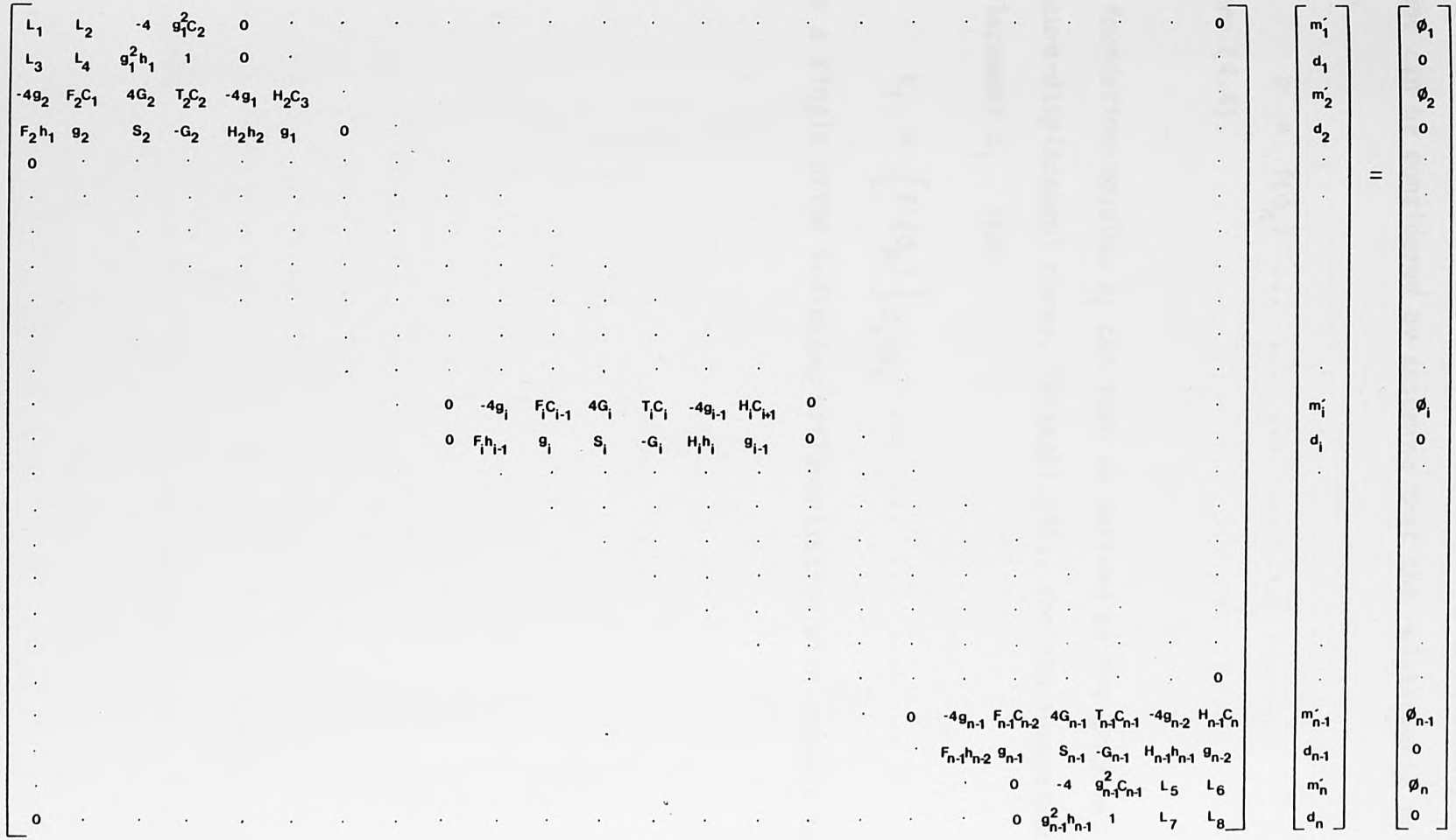

FIG. 4.3 Matrix equation $\underset{\sim}{A}\underset{\sim}{x}=\underset{\sim}{b}$

4.5 DETERMINATION OF FOUNDATION MODULUS, k_i

The case of a non-linear pressure-displacement relationship for the ground can be considered by assuming that the relationship is of the form

$$p = f(d_a) \quad \ldots \quad \ldots \quad \ldots \quad \ldots \quad \ldots \quad \ldots \quad \ldots \qquad (4.17)$$

Figure (4.4).

The foundation modulus k_i can then be defined as the gradient of the pressure-displacement curve, Terzaghi (46), for the foundation at a displacement d_i , then

$$k_i = \left[f'(d_a)\right]_{d_a=d_i} \quad \ldots \quad \ldots \quad \ldots \quad \ldots \quad \ldots \qquad (4.18)$$

where a single prime indicates differentiation with respect to d_a.

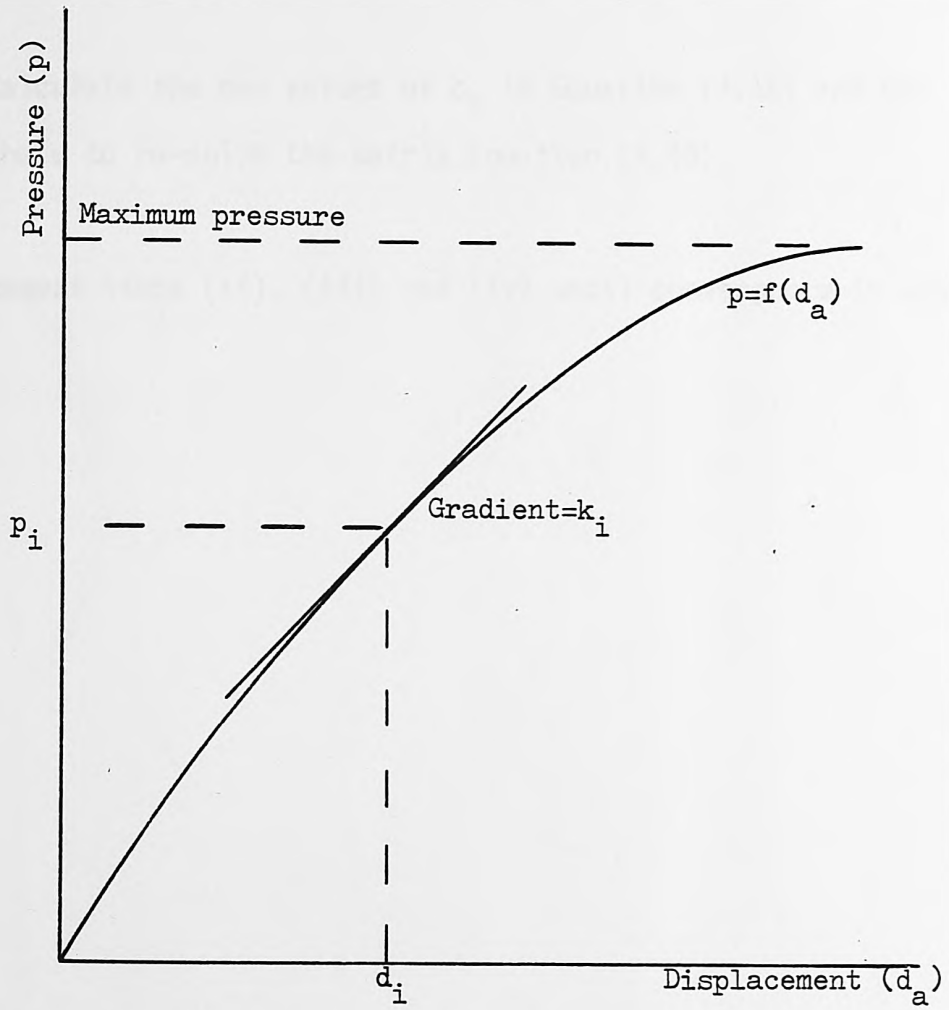

FIG. 4.4 Generalised ground pressure-displacement curve

4.6 SOLUTION PROCEDURE FOR NON-LINEAR GROUND

The following procedure is adopted when dealing with the case of non-linear pressure-displacement:

(i) Solve assuming linear elastic behaviour.

(ii) Using the values of the displacements obtained calculate the value of the foundation modulus k_i using Equation (4.18).

(iii) Calculate the new values of c_i in Equation (4.15) and use these to re-solve the matrix Equation (4.16).

(iv) Repeat steps (ii), (iii) and (iv) until convergence is achieved.

CHAPTER 5

FULL SCALE EXPERIMENTAL SIMULATION OF GROUND MOVEMENT

5.1 INTRODUCTION

In order to measure the effect of ground movement on a buried pipeline, surrounded by a fill material, a full scale experiment was designed by which a double length of pipe could be subjected to a differential displacement while encased within an elastic medium.

The experiment was carried out using two pipes joined by bolting their sockets together, in two 'trenches', 5·5 metres long by 0·3 metres wide by 0·4 metres deep, which were capable of containing a fill material. One trench box was rigidly secured to the concrete floor of the laboratory; the other was mounted on four proving rings, one at each corner, which could be jacked up or down relative to the floor, thus simulating ground movement, Figures 5.1 and 5.2.

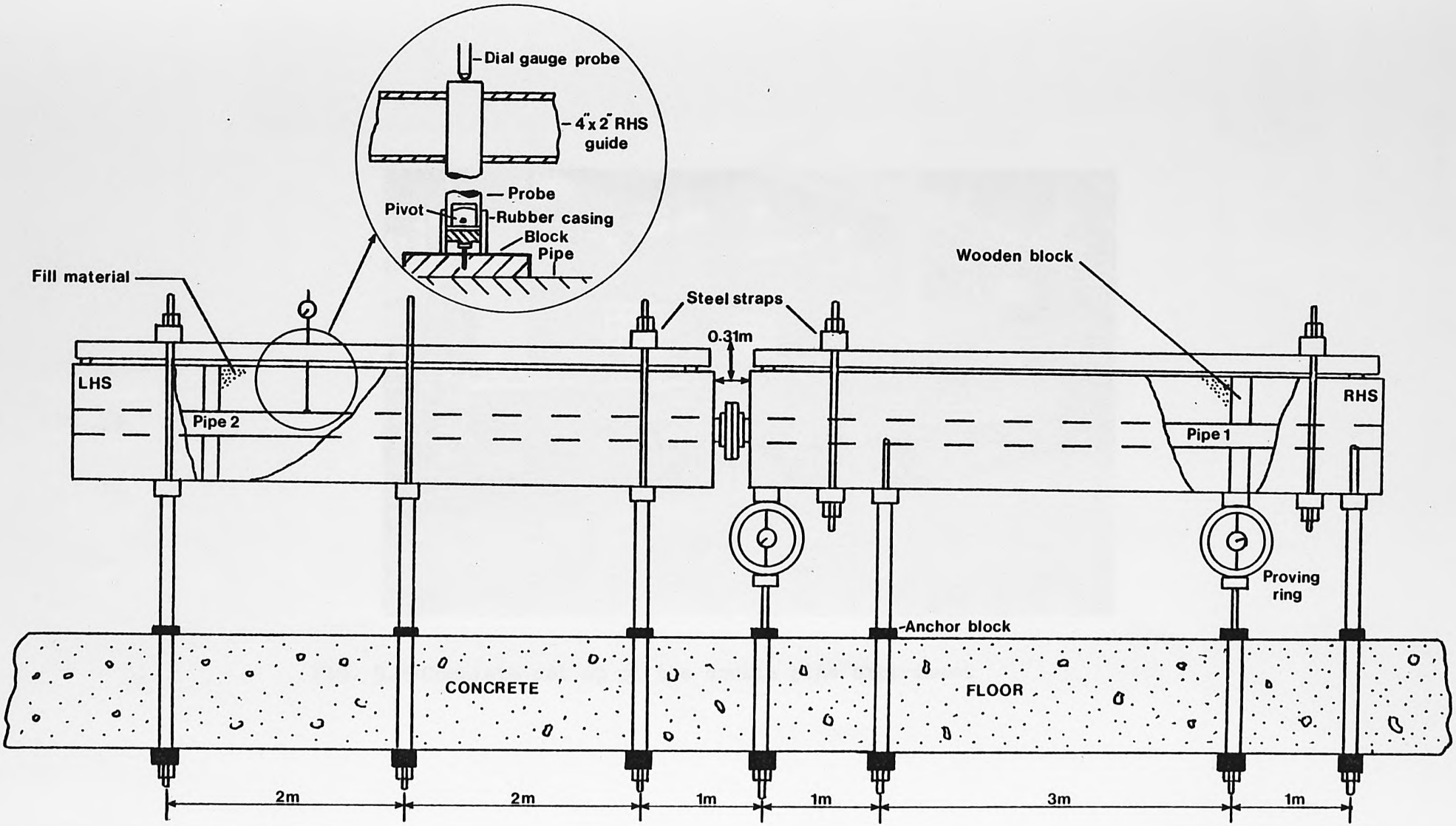

FIG. 5.1 Diagram of double pipe experiment

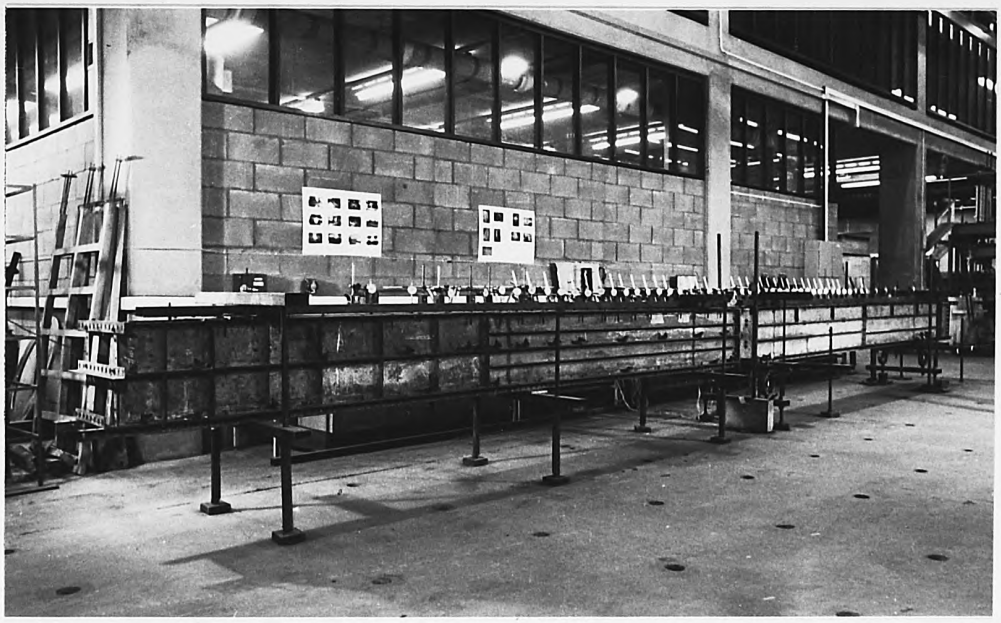

FIG. 5.2 Complete set up of the double pipe experiment

5.2 MEASUREMENT OF FILL STIFFNESS

The stiffness of the fill material was measured by an experiment in which short lengths of pipe surrounded by the fill material could be loaded in order to obtain sets load-displacement readings. The dimensions of the box containing the fill material were 0·6 m long by 0·3 m wide by 0·4 m deep, Figure 5.3.

The original fill material considered was Pulverised Fuel Ash (P.F.A). The P.F.A was obtained in powder form and this was mixed with water to produce a slurry so that it could then be poured around the pipe, which had been previously centralized in the box.

The P.F.A was allowed to set and samples were taken so that the moisture content could be calculated.

The pipe was displaced in a downward direction by means of a hydraulic ram connected to a proving ring, which was used to measure the applied loading. The displacement of the pipe was measured using two dial gauges, one at each end of the metal block. The displacement of the pipe was taken as the average of the two dial gauge readings, Figure 5.4.

The resulting load-displacement curves for P.F.A demonstrated that the material was non-linear. The gradient indicated that the stiffness of P.F.A was too high to be used with polythene pipes, which were to be used in the full scale experiment.

As an alternative fill material it was decided to use polystyrene beads due to their ease of use and low stiffness.

The load-displacement experiment was repeated using the polystyrene beads as the fill material. The box used in the experiment was half filled with the beads and the pipe was placed on the beads and centralized. The remainder of the box was then filled with the beads.

The experiment was repeated six times and the resulting load-displacement graphs are given in Figures 5.5 and 5.6. The load-displacement readings are given in Tables A1 to A6 in Appendix A.

In Test A the polystyrene beads were added until they were level with the top of the box, the lid was then secured before the test was started.

In Tests B to E, the polystyrene beads were replaced in the box before each test and added until their level was above the edges of the box. The box was then covered with its lid so that the polystyrene beads were compacted.

In Test F, the beads used in Test K were reused. The box was opened after Test K and the pipe was re-centralized. More beads were added to the box until they came above the edges. The lid was replaced and the test repeated.

A least squares straingh line, (52) of the form

$$\text{load} = M_y + (N_y \times \text{displacement})$$

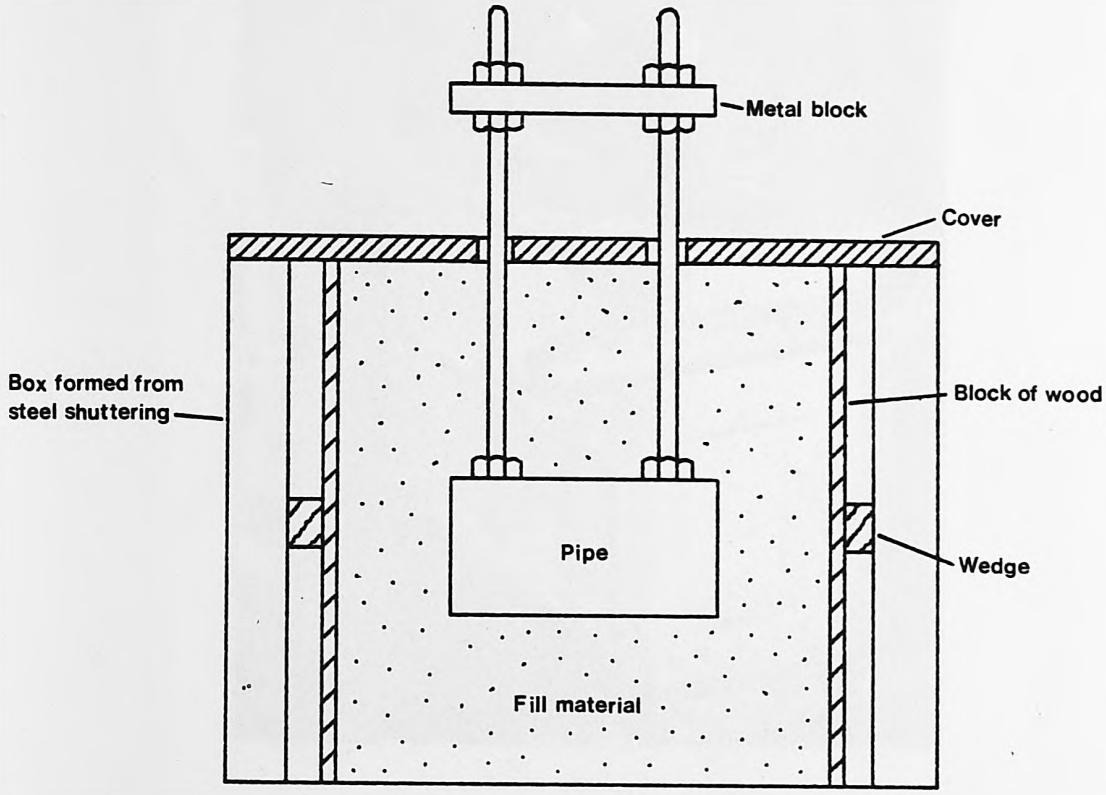

FIG. 5.3 Details of short pipe tests

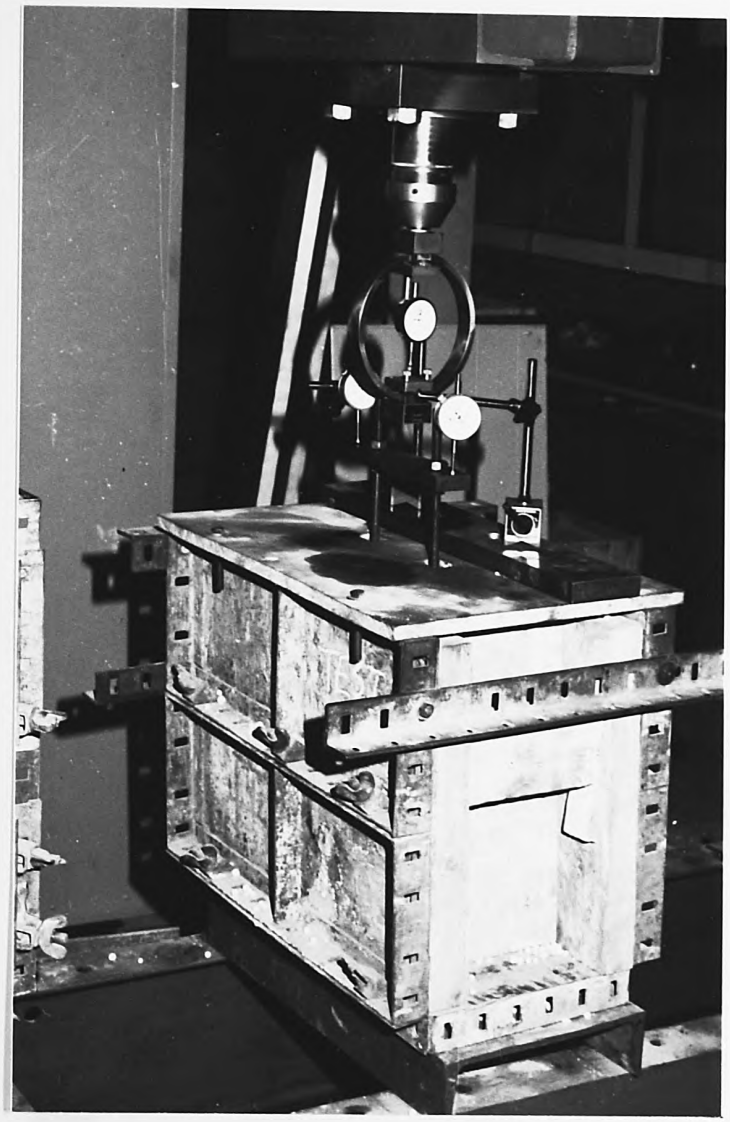

FIG. 5.4 Short pipe test in operation

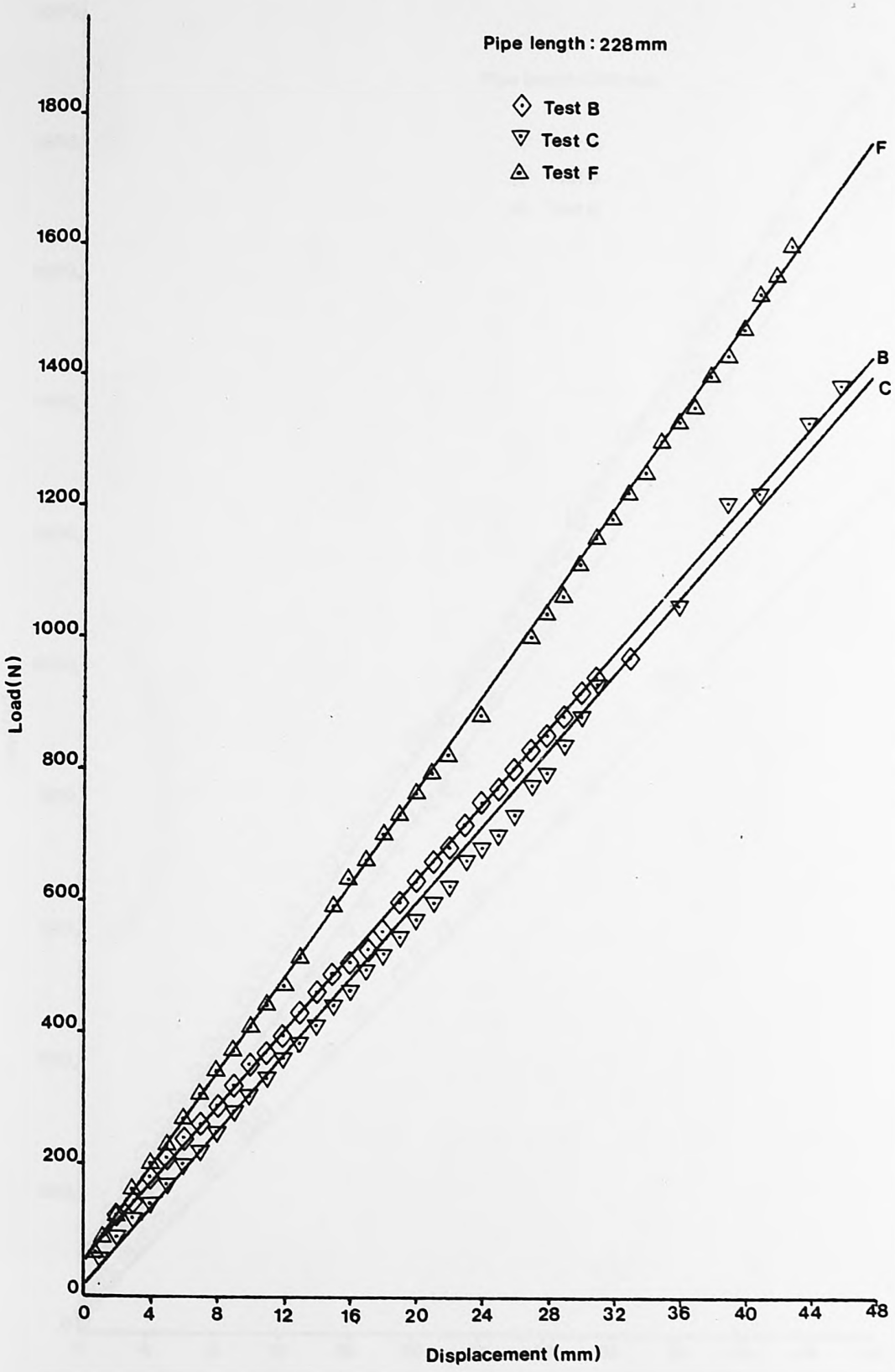

FIG. 5.5 Graphs of short pipe tests B,C and F with least squares straight lines

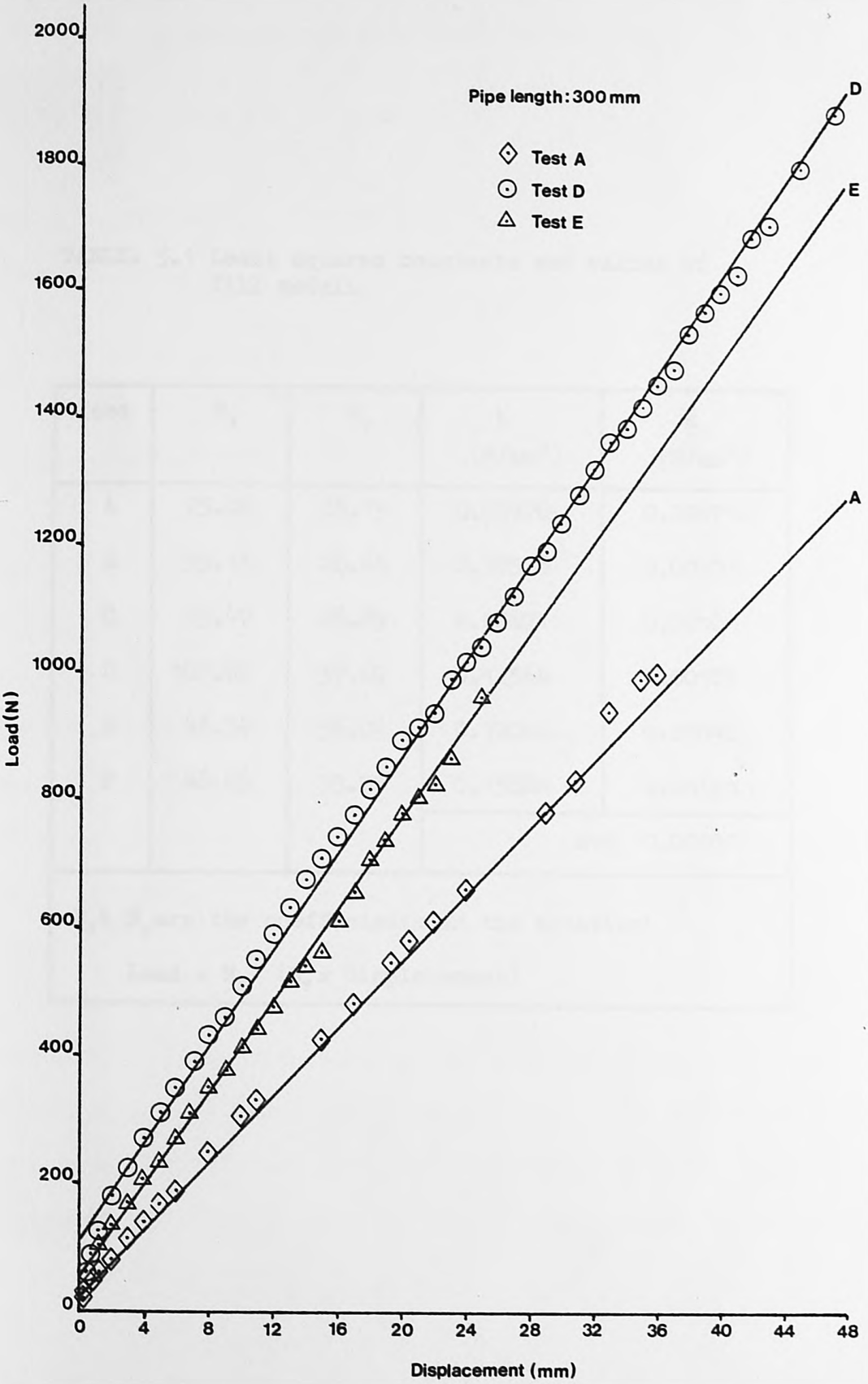

FIG. 5.6 Graphs of short pipe tests A,D and E with least squares straight lines

TABLE. 5.1 Least squares constants and values of fill moduli

Test	M_y	N_y	k (N/mm^2)	k_o (N/mm^3)
A	25.06	26.19	0.08970	0.00074
B	55.13	28.68	0.12578	0.00103
C	13.47	28.89	0.12671	0.00104
D	107.82	37.69	0.12564	0.00103
E	48.34	36.01	0.12004	0.00098
F	48.65	35.75	0.15680	0.00129
			Ave	0.00102

M_y & N_y are the coefficients in the equation:

Load = M_y + (N_y x Displacement)

where

M_y is the y-intercept (at x = 0)

N_y is the gradient of the straight line

was fitted to each set of readings.

The value of the fill stiffness for each set of readings is found using the formulae

$k = N_y$/pipe length

k_o = k/pipe diameter

and are given in Table 5.1

The average value of the fill stiffness k_o was found to be 0·00102 N/mm^3.

The value of the fill stiffness for Test A can be considered to be the lower limit as it was obtained without any compaction of the beads by the lid and the value obtained from Test F can be considered as an upper limit as it was obtained from a double compaction of the beads.

In the full scale experiment the beads were to be compacted as in Tests B to E, so the average value of k_o was used in Equation (3.14) to estimate the distance of the maximum bending moment from the flange of the pipe, in order to locate strain gauges around this point.

5.3 EXPERIMENTAL PROCEDURE

The strain gauges, Showa foil type F - 8 were stuck to the pipe in the positions shown in Figure 5.7. The gauges were wired up to a data logger and readings were taken for a set of known loading conditions, four point loading, Figure 5.8, in order to calculate the bending moments at each strain gauge and hence calibrate them.

To measure the displacements of the pipes, twenty-five hinged displacement rods were attached to each pipe. The rods were mounted on plastic blocks which were stuck to the pipe in such a way that the rods were hinged to pivot longitudinally to the pipe axis. This ensures that the rods remain vertical even when the pipe is bent. The first rod was placed at a distance of 200 mm from the flange and then initially with a spacing of 150 mm and finally with a spacing of 600 mm, Figures 5.1, 5.7 and 5.9.

The trench boxes were then half filled with the polystyrene beads along their entire lengths. The pipes were then positioned in the boxes in such a manner that the displacement rods were in a vertical position and the wooden retaining blocks 4·42 metres from the flanges. Using this distance in Equation (3.12) with the average value of the stiffness of the polystyrene beads, k_o = 0·00102 N/mm^3 gives a pipe displacement of approximately 0·03 mm, for a differential trench displacement of 30 mm, which if restrained would not unduly affect the overall displacement of the pipe.

The trenches could then be completely filled with the polystyrene beads, Figure 5.10. The trenches were overfilled so that the beads could be compressed by steel covers bolted to the tops of the

trenches in a similar manner to that used in the short pipe tests.

To retain the fill material and still allow the pipe freedom of movement at the flange end, a perspex faceboard was designed, Figure 5.11. The faceboard comprises of a base plate which is bolted to the box and a face plate with a circular hole, the diameter of the pipe, which is free to slide up or down in such a manner so as not to inhibit the free movement of the pipe.

The assembly of the apparatus was completed by mounting the dial gauges, one for each displacement rod, on a rectangular hollow section steel beam. Dial gauges mounted on stands were also used to measure the movement of the flange and the four corners of the moveable trench with respect to the concrete floor of the laboratory, Figure 5.12.

The moveable trench was taken off of its supports and allowed to rest on the proving rings overnight to allow the pipe and polystyrene beads to attain an equilibrium position. The zero readings of the strain gauges and dial gauges were then taken and used as the datum values in the subsequent experiment.

Differential ground movement was effected by lowering the moveable trench by jacking down the proving rings by increments of 6 mm until the trench was 30 mm below the datum level.

At each incremental level the readings on all the dial gauges were recorded and the deflected shapes of the pipes were derived, Tables B.1 to B.5 in Appendix B, which have been plotted, Figures 5.13 to 5.17.

The strain gauges attached to each pipe were read at each incremental level using a data logger and the readings were transposed using the calculated gauge constants to give the bending moment distributions, Tables B.6 to B.10 in Appendix B, which have been plotted, Figures 5.18 to 5.22.

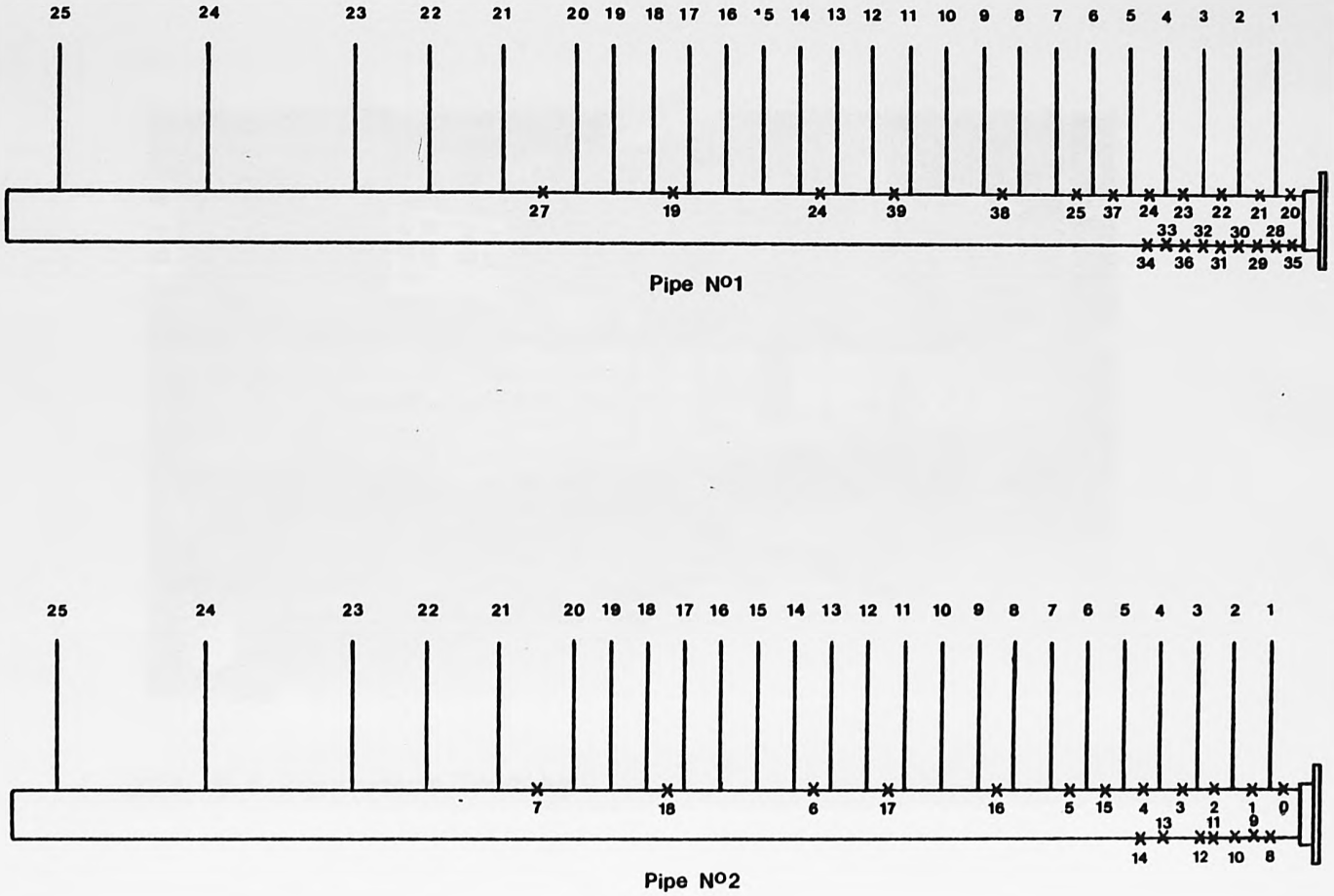

FIG. 5.7 Details of strain gauge and displacement rod positions

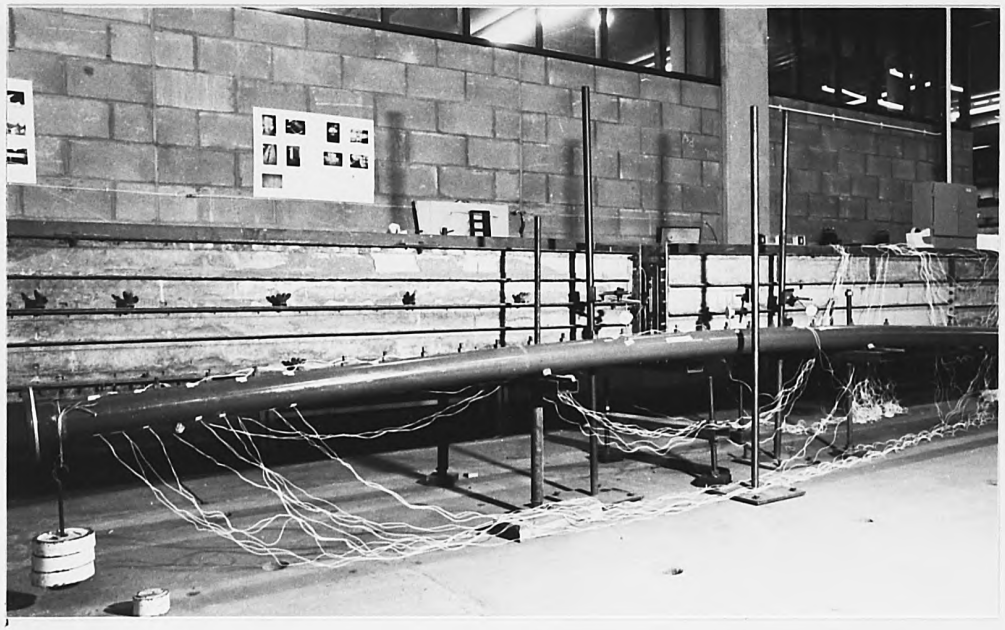

FIG. 5.8 Four point loading

FIG. 5.9 Detail of displacement rods as fixed to pipe

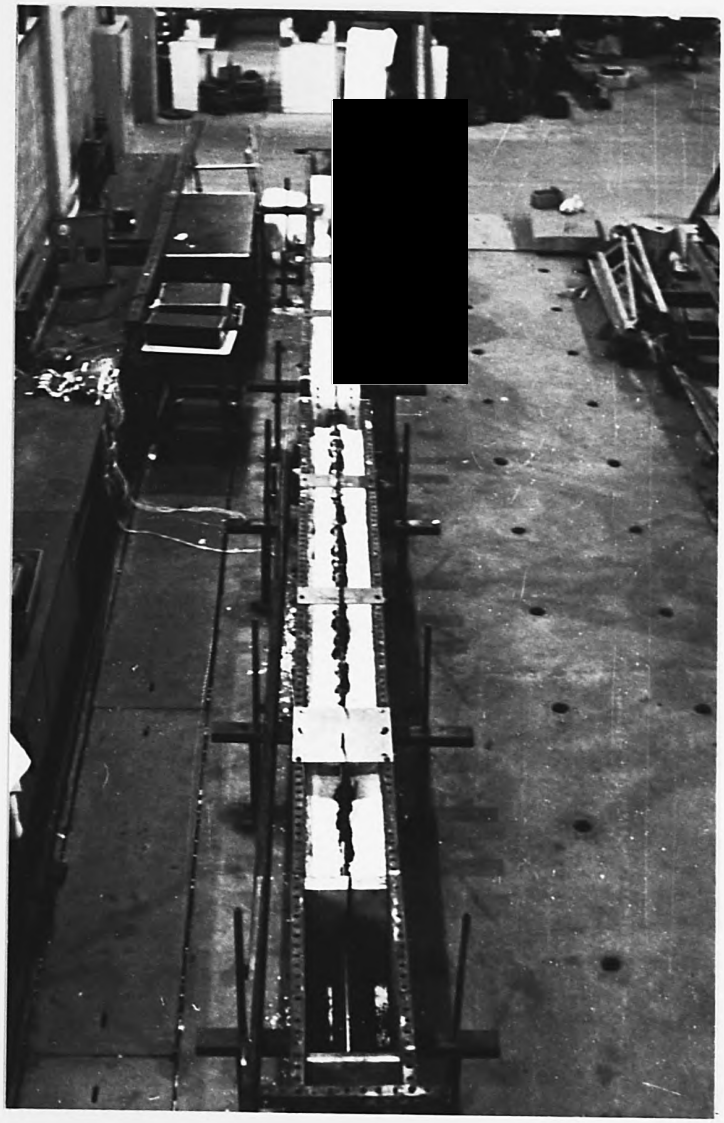

FIG. 5.10 Assembly of double pipe experiment

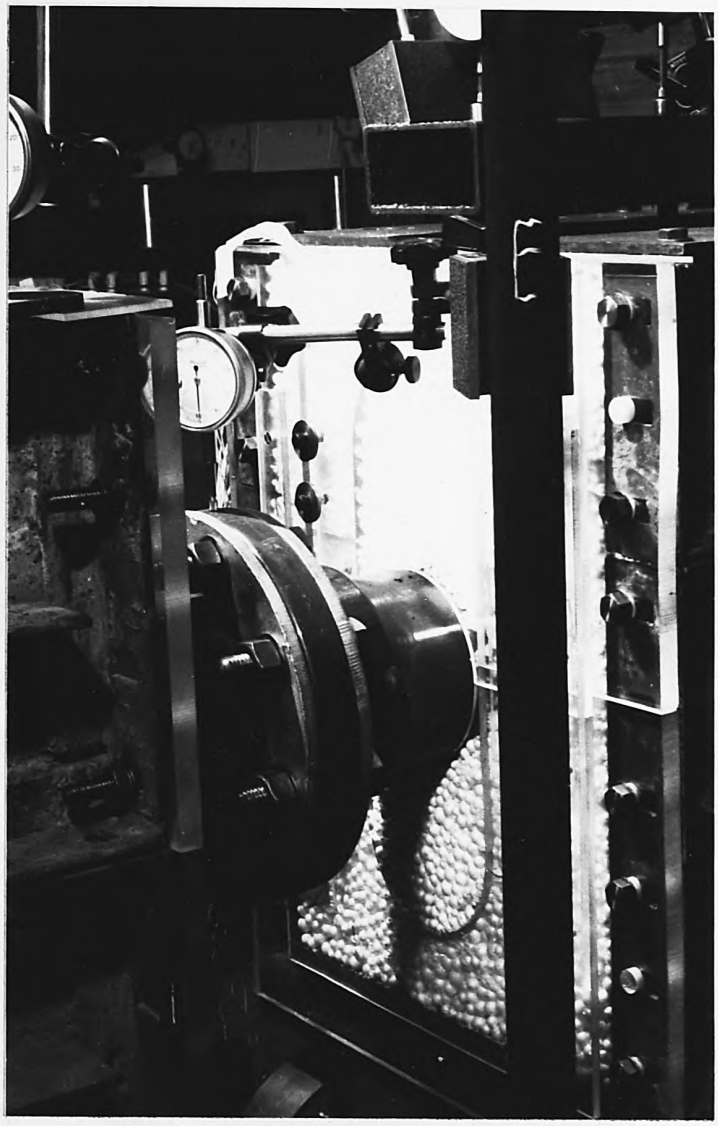

FIG. 5.11 Perspex faceboard and pipe flange

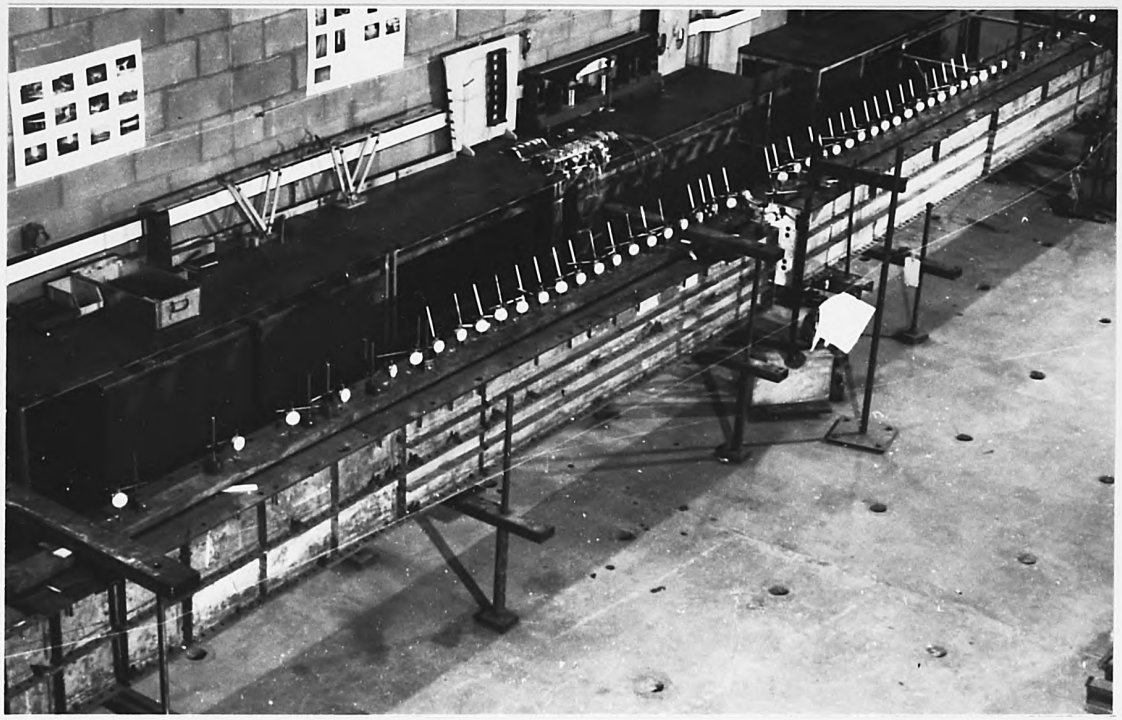

FIG. 5.12 Complete assembly of double pipe experiment

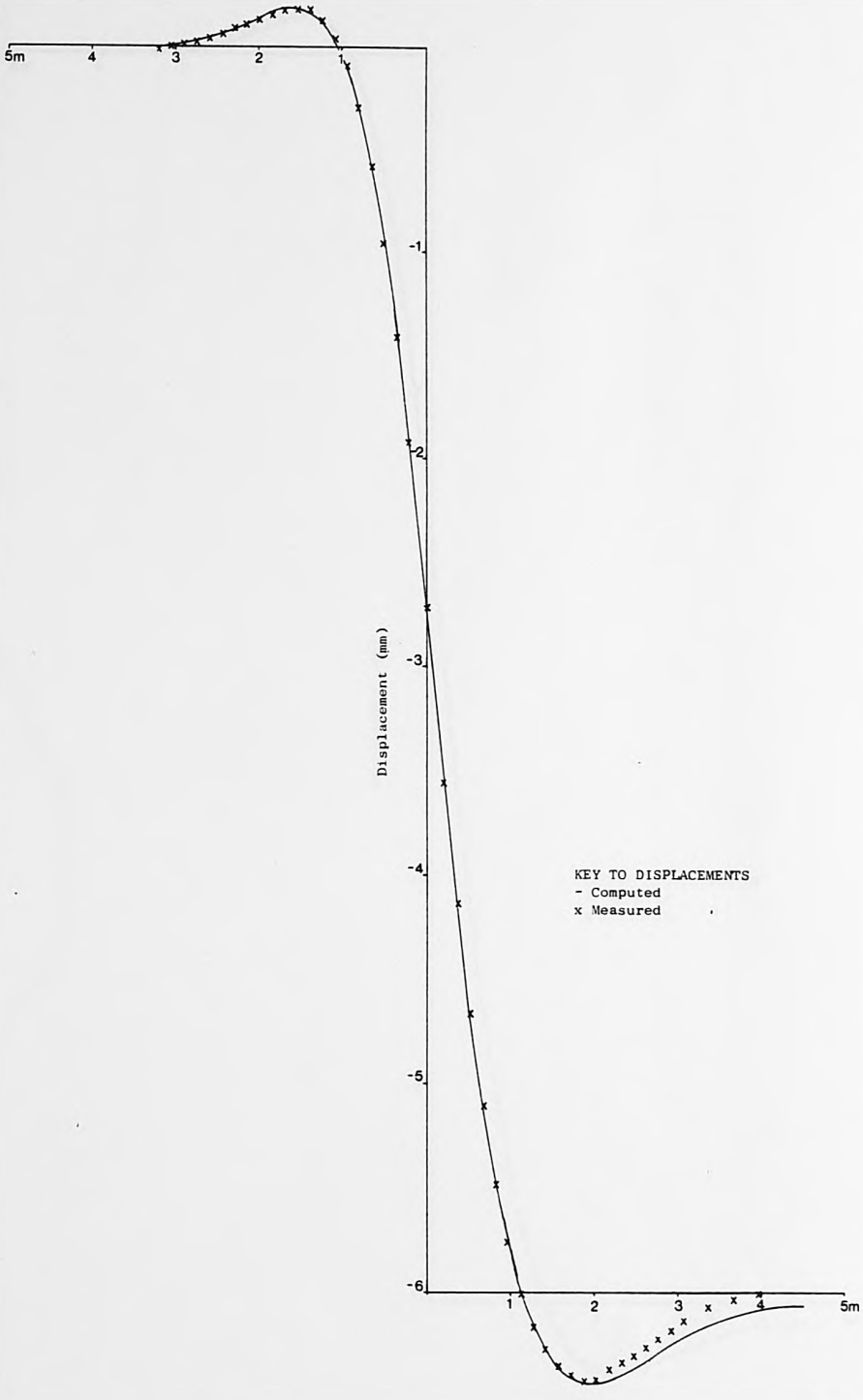

FIG. 5.13 Computed and experimental deflections for a trench displacement of -6 mm

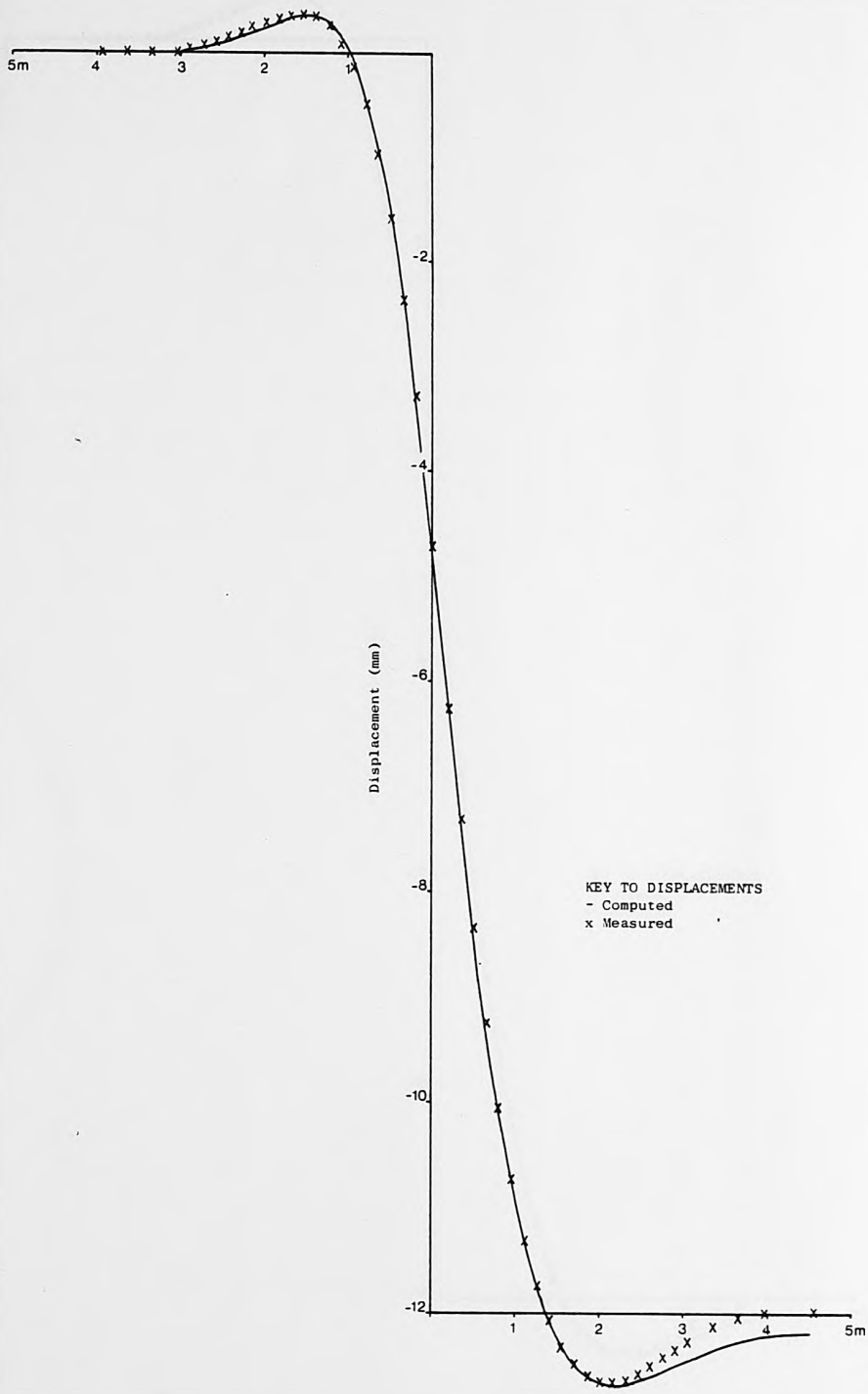

FIG. 5.14 Computed and experimental deflections for a trench displacement of -12 mm

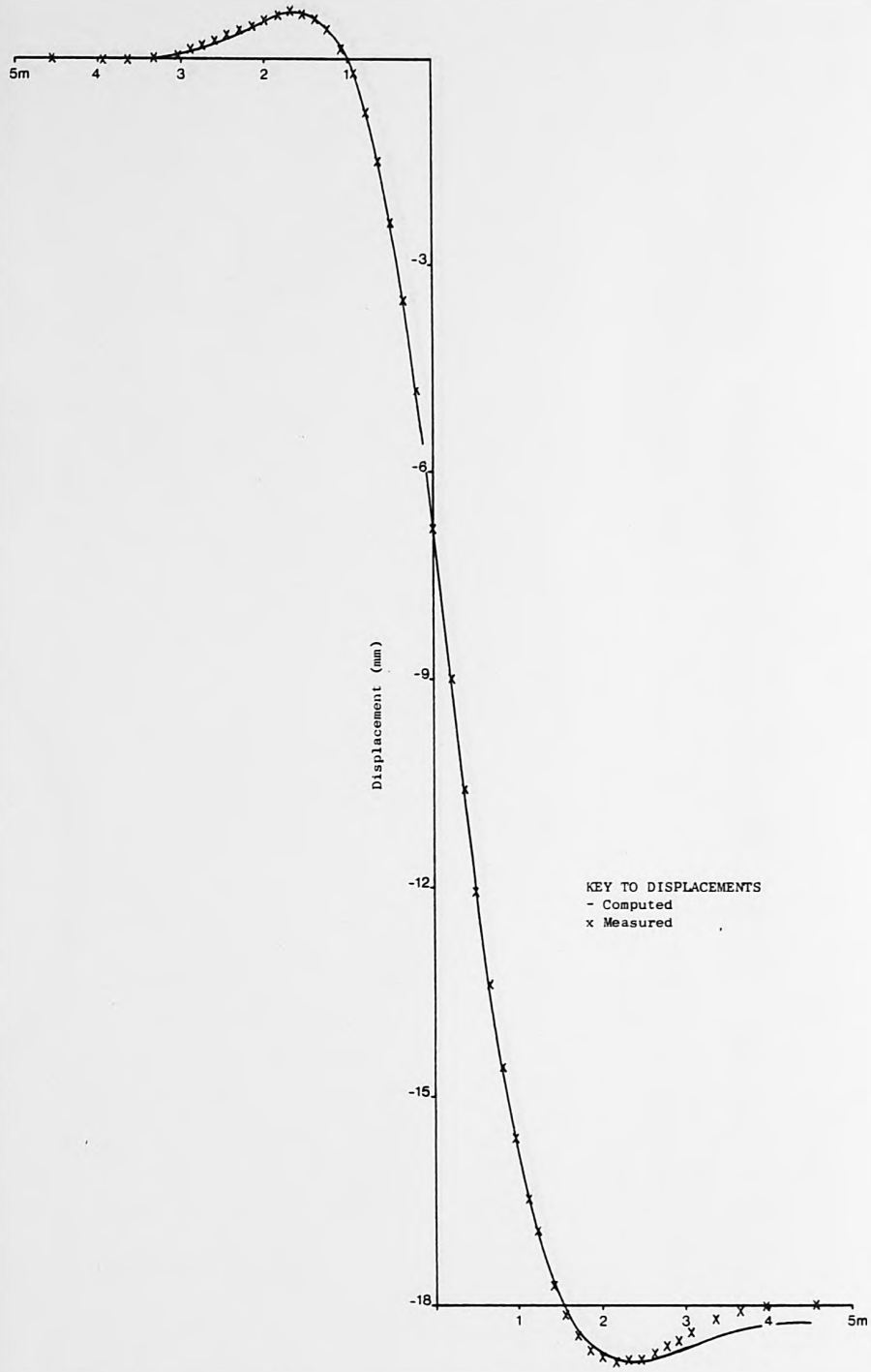

FIG. 5.15 Computed and experimental deflections for a trench displacement of -18 mm

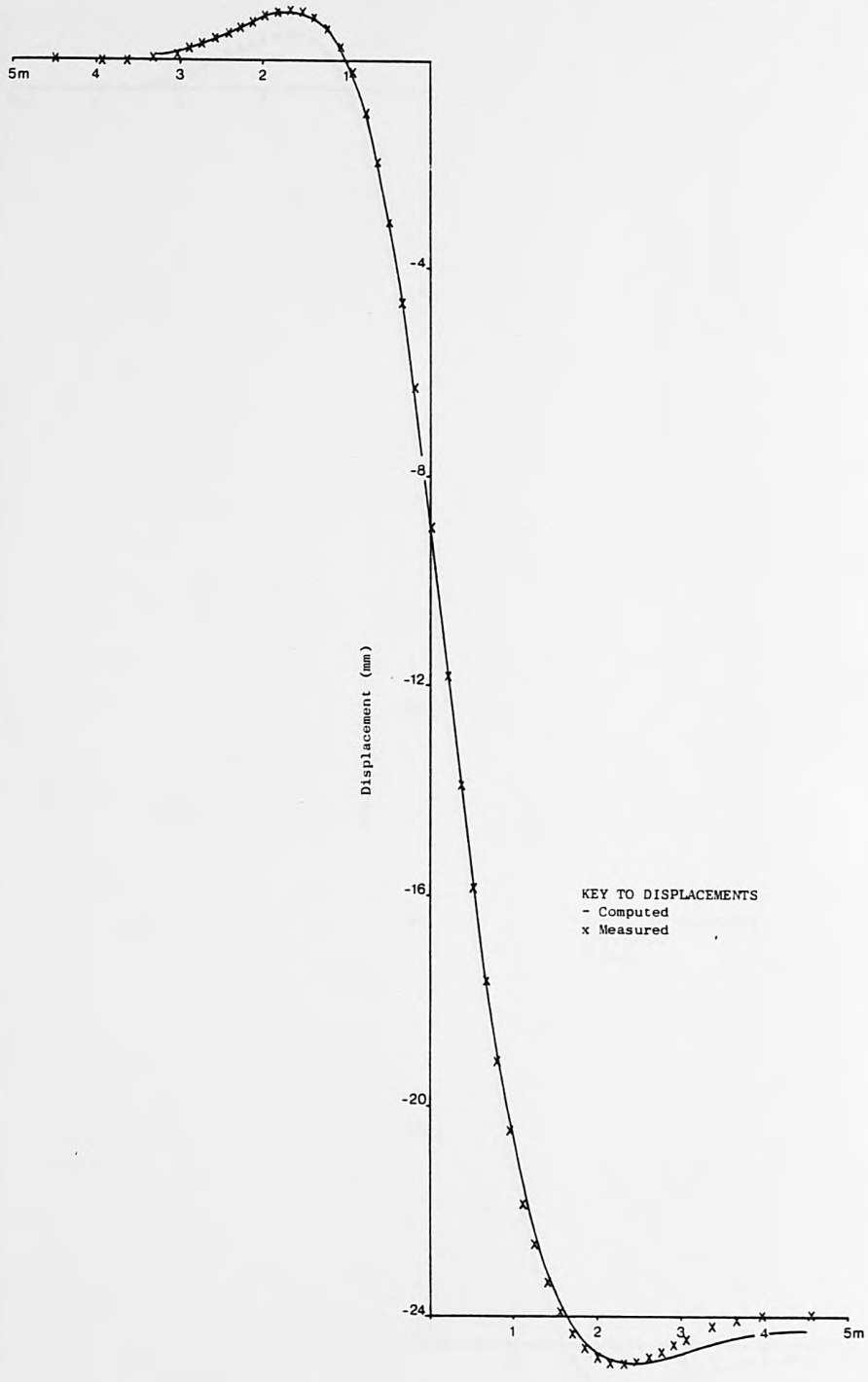

FIG. 5.16 Computed and experimental deflections for a trench displacement of -24 mm

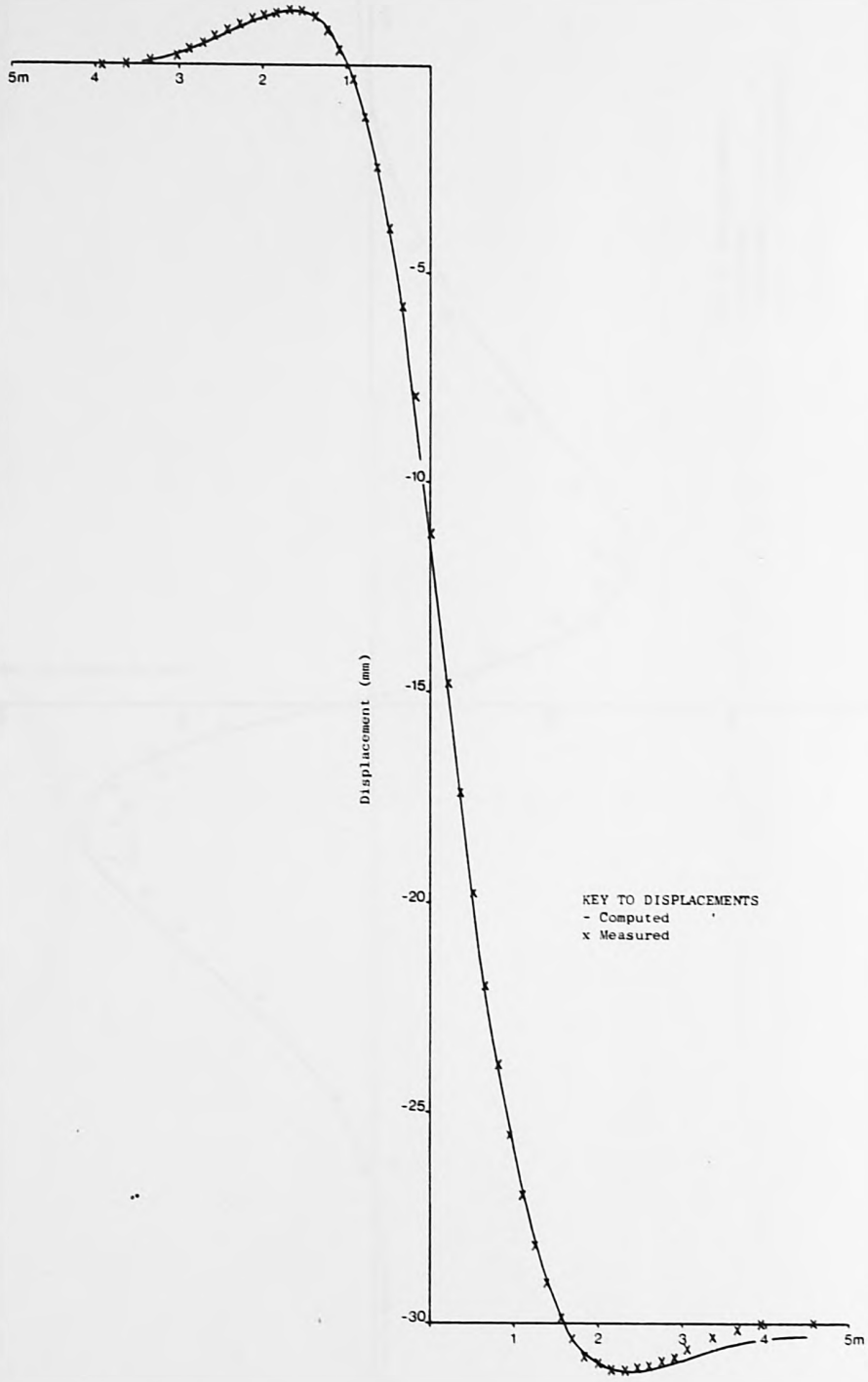

FIG. 5.17 Computed and experimental deflections for a trench displacement of -30 mm

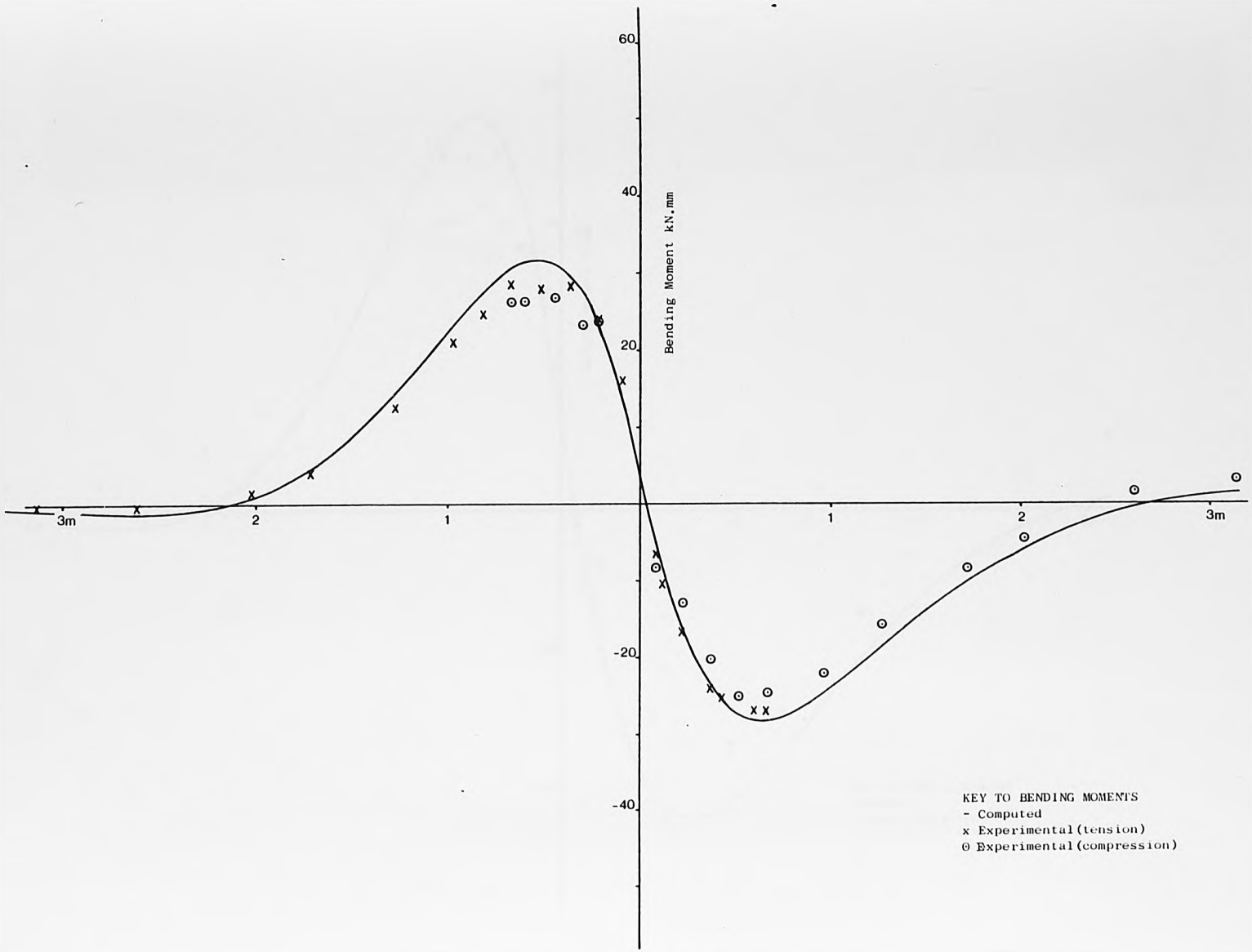

FIG. 5.18 Computed and experimental bending moments for a trench displacement of -6 mm

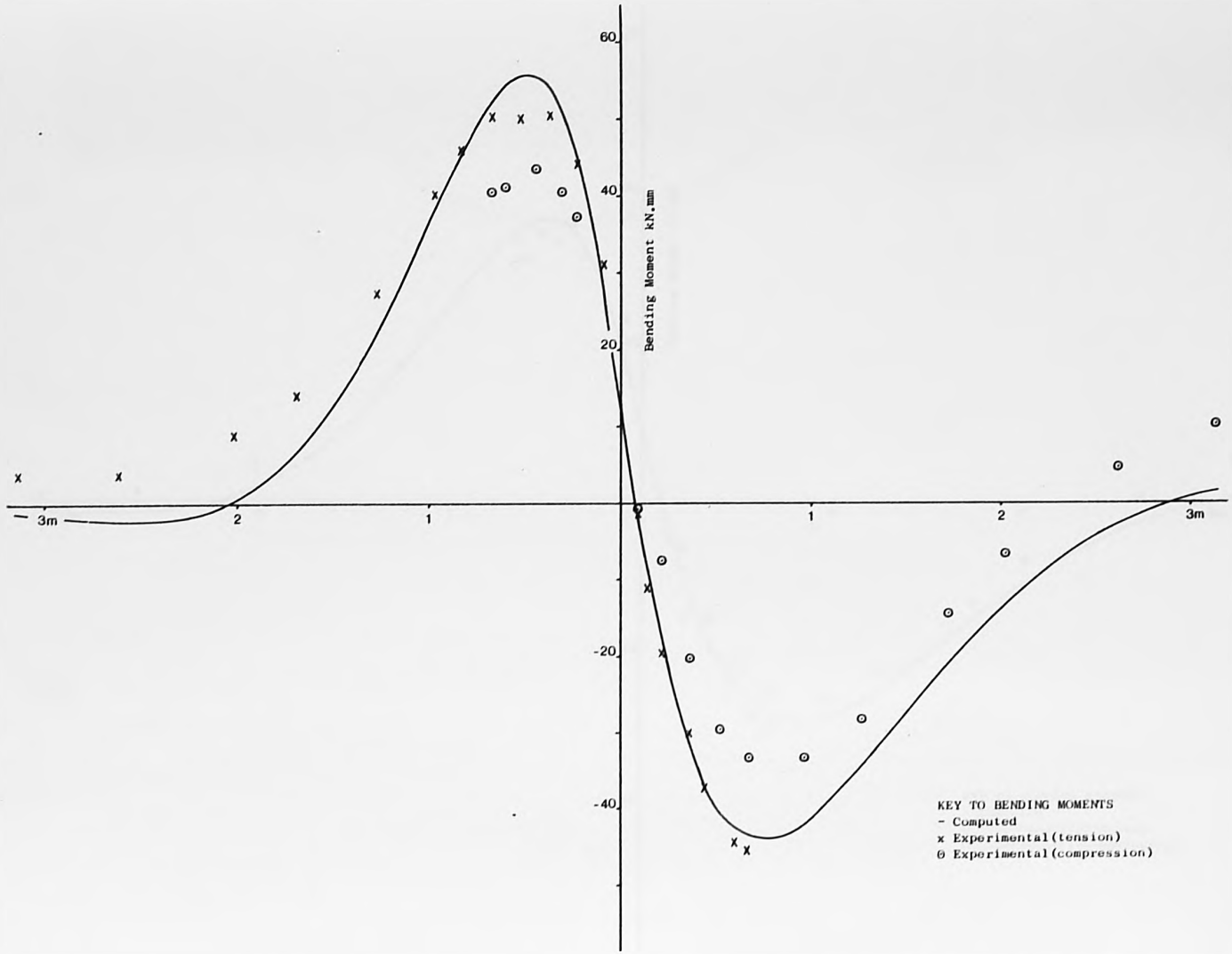

FIG. 5.19 Computed and experimental bending moments for a trench displacement of -12 mm

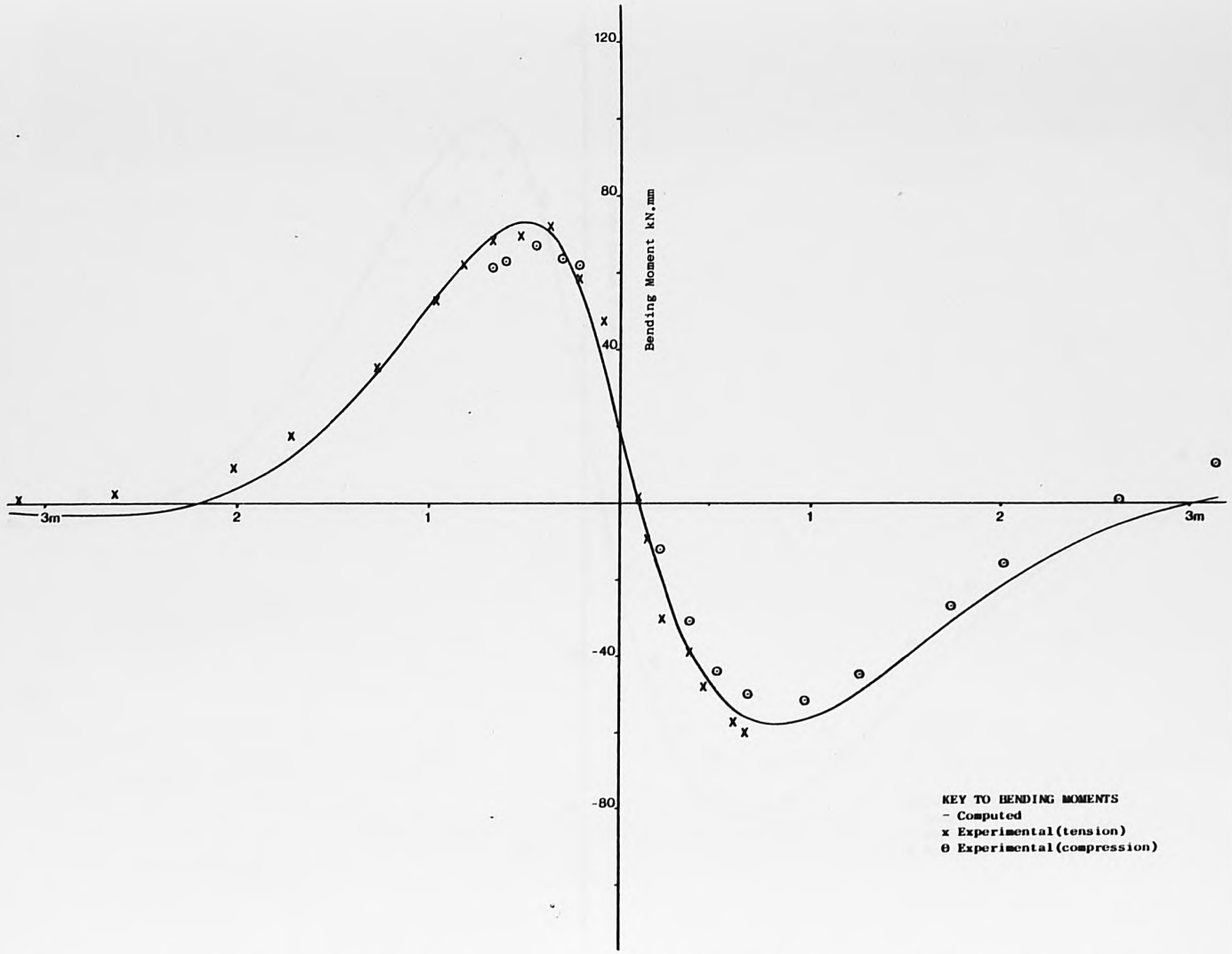

FIG. 5.20 Computed and experimental bending moments for a trench displacement of -18 mm

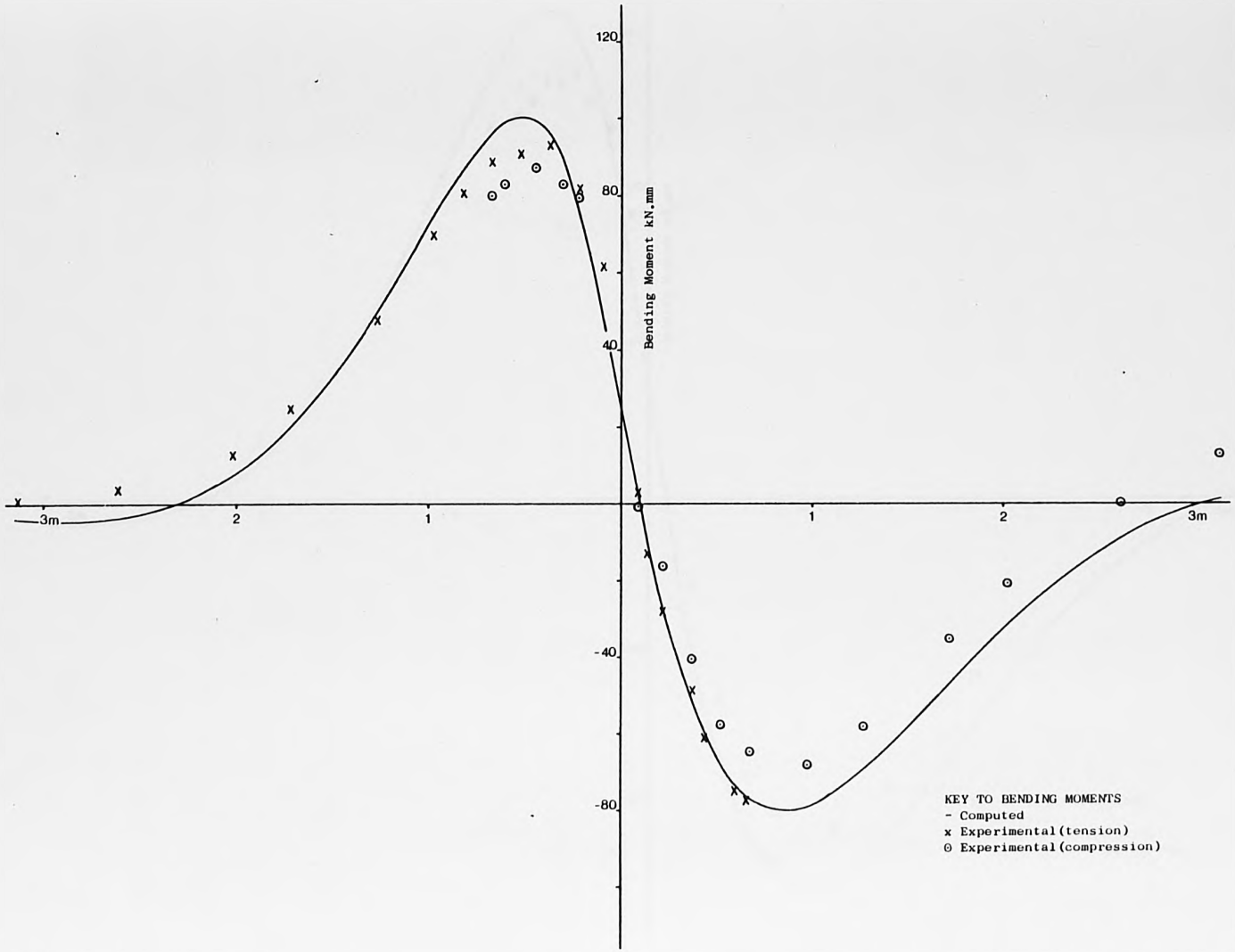

FIG. 5.21 Computed and experimental bending moments for a trench displacement of -24 mm

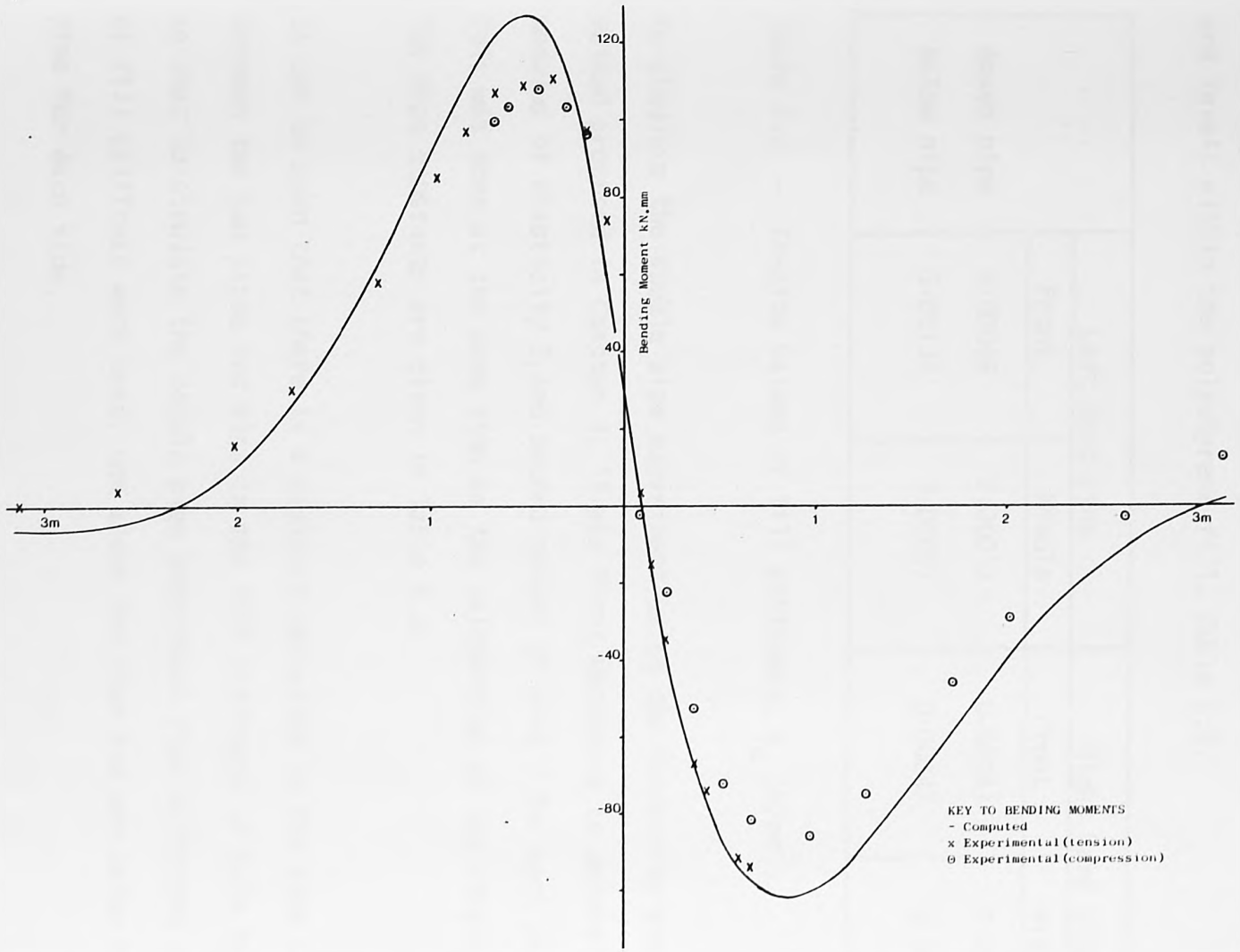

FIG. 5.22 Computed and experimental bending moments for a trench displacement of -30 mm

5.4 DISCUSSION OF EXPERIMENTAL RESULTS

Both the displacement and bending moment profiles showed a lack of antisymmetry, so the trenches were opened after the experiment to allow in-situ stiffness tests to be performed at different positions and levels within the polystyrene fill, Table 5.2.

	Left hand side		Right hand side	
	Front	Middle	Front	Middle
Above pipe	0·00049	0·00013	0·00041	0·00039
Below pipe	0·00134	0·00097	0·00047	0·00044

Table 5.2 - In-situ values of fill stiffness, k_o (N/mm^3).

To simulate the double pipe experiment using the force-displacenent method proposed in Chapter 4, it was first necessary to determine the modulus of elasticity E and second moment of area I for each pipe. This was done at the same time as the calibration of the strain gauges. The pipe constants are given in Table 5.3.

It can be seen that there is a distinct variation in the pipe constants between the two pipes and also in the fill stiffness of both trenches, so that to simulate the double pipe experiment four different values of fill stiffness were used, one above the pipe and one below the pipe for each side.

TABLE. 5.3 Pipe constants used in the computer simulation of double pipe experiment

Pipe constants	Left hand side	Right hand side
Exterior radius R(mm)	57.07	57.07
Interior radius r(mm)	52.13	51.89
Modulus of elasticity E_i(N/mm^2)	3239.96	3313.57
Second moment of area I_i(mm^4)	2531294.17	2637371.84
Linear values used		
Modulus of elasticity E(N/mm^2)	3285.0	3285.0
Second moment of area I(mm^4)	2576380.0	2576380.0

The values of the fill resistance, per incremental level, were calculated from the simultaneous solution of the equations of vertical equilibrium and the equilibrium of moments for each side, Table 5.4.

These values were used in Equation (4.16) to give the computed displacements and bending moments for each pipe at each incremental level, Tables C.1 to C.5 in Appendix C.

The computed and experimental results for the displacements and bending moments were plotted and are shown in Figures 5.13 to 5.17 and Figures 5.18 to 5.22 respectively.

The values of fill compressibility used in the computer sumulation give a correspondence, between the computed and experimental results, of maximum displacements to within 5% and maximum bending moments to within about 15%.

A further check on the accuracy of the simulation was made by calculating the vertical equilibrium and equilibrium of moments for each pipe at each incremental level, Table 5.5. It can be seen from the table that the vertical equilibrium and equilibrium of moments correspond to within 9% and 7% respectively.

A dial gauge mounted on a floor stand, used to measure any possible vertical moment of the static trench was also read at each incremental level and it was noted that the end of the trench nearest the flange of the pipes was displacing in a direction similar to that of the moveable trench.

TABLE. 5.4 Values of $k_o(N/mm^3)$ for above and below the pipe obtained from the simultaneous solution of the equations of vertical equilibrium and equilibrium of moments for each side and used in the computer simulation

Displacement (mm)	Position relative to pipe	Left hand side	Right hand side
-6	above	0.001353	0.000858
	below	0.001335	0.000253
-12	above	0.001272	0.000483
	below	0.001404	0.000239
-18	above	0.000760	0.000351
	below	0.001116	0.000266
-24	above	0.000645	0.000335
	below	0.001121	0.000330
-30	above	0.000552	0.000345
	below	0.001167	0.000344

TABLE. 5.5 Comparison of the conditions of equilibrium between the experimental and computer simulation results

Displacement (mm)	Equilibrium condition	Left hand side		Right hand side	
		Experimental	Simulation	Experimental	Simulation
-6	Vertical equilibrium	82.44	80.41	82.44	81.48
	Equilibrium of moments	426627.0	422867.5	422505.0	429494.6
-12	Vertical equilibrium	139.03	129.45	139.03	130.30
	Equilibrium of moments	736859.0	686295.8	695150.0	678058.0
-18	Vertical equilibrium	168.22	161.66	168.22	162.50
	Equilibrium of moments	887360.5	862600.4	845305.5	844403.8
-24	Vertical equilibrium	221.93	217.93	221.93	219.61
	Equilibrium of moments	1169571.1	1168923.9	1116307.9	1134546.2
-30	Vertical equilibrium	292.43	276.84	292.43	280.13
	Equilibrium of moments	1545492.5	1508591.2	1466536.4	1453820.8

The maximum displacement was found to be 0·04 mm when the moveable trench had been displaced 30 mm from the neutral position. This represents an error of about 0·5% in the reading for the first displacement rod. The trench was secured to the concrete floor at a distance of 600 mm from the pipe flange, such that any error in the readings of the pipe displacement will decrease as the distance from the pipe flange increases.

A dial gauge was also used to monitor the movement of the rectangular hollow steel section beam relative to the top of the trench. The maximum movement recorded by this gauge was 0·02 mm, which represents an error of about 0·25% in the reading for the first displacement rod.

Another source of error was the possibility of the pipe section becoming oval during the experiment. To test this hypothesis, strain gauges 11, 30 and 36 were placed at right angles to the other gauges.

It was noted that during the experiment these gauges indicated that the pipe section was attaining an elliptical shape. The effect of this would be to increase the projected area of contact and hence the relative foundation modulus. The resulting displacement of the pipe would then be less than in the case where the pipe section remained circular.

The maximum transverse stress measured on the pipe wall during the experiment was 2·431 N/mm^2 when the pipes had been differentially displaced by 30 mm. This level of stress represents about 5% of the tensile strength of the pipe as given by the manufacturer (53). As

a further check on the amount of ovality the pipe section may have sustained, the geometry of a circular section becoming elliptical was examined.

Consider a circular section, Figure 5.23, which has had its vertical radius reduced by small amount δ and its horizontal radius increased by the same small amount δ. The resulting cross section will be an ellipse with major and minor axes of $R + \delta$ and $R - \delta$ respectively.

The length of arc, e, subtended by an angle ϕ, for the circular section is given by

$$e = R\phi \quad \ldots \quad \ldots \quad \ldots \quad \ldots \quad \ldots \quad \ldots \quad \ldots \quad (5.1)$$

and for the ellipse by

$$e_1 = (R + \delta)\, E(v, \phi) \quad \ldots \quad \ldots \quad \ldots \quad \ldots \quad (5.2)$$

where $E(v, \phi)$ is the incomplete elliptic integral of the second kind defined by

$$E(v, \phi) = \int_0^{\phi} (1 - v^2 \sin^2\theta)^{1/2} d\theta \qquad 0 < v < 1$$

$$\ldots \quad \ldots \quad \ldots \quad \ldots \quad \ldots \quad (5.3)$$

and v is the square root of the eccentricity of the ellipse, given by

$$v = \frac{2(R\delta)^{1/2}}{R + \delta} \quad \ldots \quad \ldots \quad \ldots \quad \ldots \quad \ldots \quad (5.4)$$

Equation (5.3) can be solved by using the expansion of the uniformly convergent series of $(1 - x)^{1/2}$ with $x = v^2 \sin^2\theta$ and integrating term by term, Spiegel (54), to give the length of arc of an ellipse as

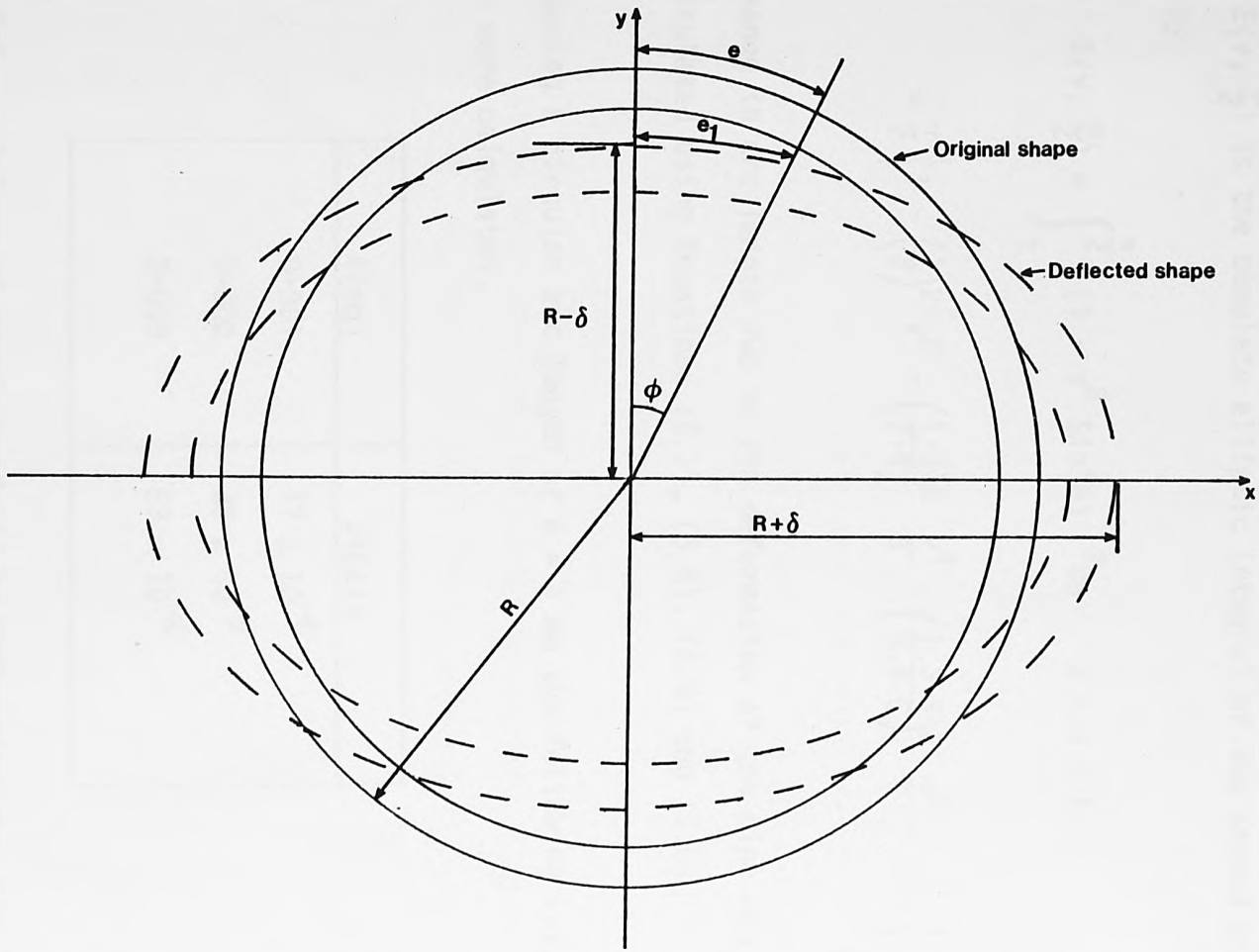

FIG. 5.23 Deformation of a pipe from a circular to an elliptical cross-section

$$e_1 = \frac{2(R + \delta)}{\pi}\left[\phi - \text{Cos}\phi\ \text{Sin}\phi\left(1 + \frac{2}{3}\text{Sin}^2\phi\right)\right] E(v, \tfrac{\pi}{2}) +$$

$$+ (R + \delta)\text{Cos}\phi\ \text{Sin}\phi\left[1 + \frac{2}{3}\left(1 - \frac{v^2}{4}\right)\text{Sin}^2\phi\right] \quad \ldots \qquad (5.5)$$

where $E(v, \frac{\pi}{2})$ is the complete elliptic integral of the second kind, given by

$$E(v, \tfrac{\pi}{2}) = \int_0^{\frac{\pi}{2}} (1 - v^2\ \text{Sin}^2\theta)^{1/2} d\theta \qquad 0 < v < 1$$

$$= \frac{\pi}{2}\left\{1 - \left(\frac{1}{2}\right)^2 v^2 - \left(\frac{1\cdot 3}{2\cdot 4}\right)^2 \frac{v^4}{3} - \left(\frac{1.3.5}{2.4.6}\right)^2 \frac{v^6}{5} - \ldots\right\}$$

$$\ldots \quad \ldots \quad \ldots \quad \ldots \quad \ldots \qquad (5.6)$$

The change in arc length due to the deformation of the pipe can now be calculated using Equations (5.1), (5.4), (5.5) and (5.6).

Considering a circular arc length of e = 1 mm the following values of strain were calculated,

δ (mm)	Strain
0·001	17×10^{-6}
0·002	35×10^{-6}
0·003	53×10^{-6}

Table 5.6 - Values of strain produced by deflecting the pipe section

and as the maximum value of strain measured during the experiment was 40×10^{-6}, it is evident from Table 5.6, that the ovality of the pipe will have very little effect on the deflections of the pipe as the diametrical change in length will be of the order 0·004 mm(0·007%).

To test whether or not the pipe is long enough to be considered infinite, Hetényi (43) gives the following relationship

$$L_p > \pi\left(\frac{4EI}{k_o d}\right)^{1/2} \quad \ldots \quad \ldots \quad \ldots \quad \ldots \quad \ldots \quad \ldots \quad (5.7)$$

where L_p is the length of the pipe.

Using the minimum value of k_o given in Table 5.4 and the pipe constants given in Table 5.3 in relationship (5.7) gives

$$L_p > 3{\cdot}425 \text{ m} \quad \ldots \quad \ldots \quad \ldots \quad \ldots \quad \ldots \quad \ldots \quad (5.8)$$

As the pipe was restricted by wooden blocks its effective length was 4·42 m, which satisfies the above relationship, so the pipe is long enough to be considered infinite.

The overall correspondence between the experimental and computed results indicates that the mathematical model is applicable in the case of a non-homogeneous foundation modulus.

5.5 THE EFFECT OF NON-HOMOGENEOUS SOIL

The mathematical model was used to investigate the effect of differential ground displacement on a pipeline in a non-homogeneous soil. Three cases of non-homogeneous soil were investigated, Figure 5.24. Case A in which the soil has a different resistance above the pipe than below, Case B in which the soil has a different resistance on the left hand side than the right hand side and Case C in which the soil resistance on the left hand side under the pipe is different from the rest.

The three cases correspond to the following real life situations:

Case A: when a layer of imported backfill of lower resistance is used above the pipe.

Case B: pipe built into a wall or concrete foundation, or the boundary between two distinct types of soil.

Case C: A hard layer in the soil, rock or another pipe, onto which the pipe has been laid.

Tables 5.7, 5.8 and 5.9 give the values of the differential displacement necessary to fracture various sizes of pipe, for a series of soil resistances, k_A above the pipe and k_B below the pipe, for asbestos cement, cast iron and spun iron pipes respectively.

The benefits of using a layer of a softer backfill material above a pipe when laying a pipeline are clearly demonstrated. A reduction in the resistance above the pipe from 1·0 to 0·025 N/mm^3 would necessitate the ground to be able to displace the pipeline by more than three times

the displacement necessary to fracture the pipeline in a homogeneous soil with a resistance of 1·0 N/mm^3.

The tables also clearly show that iron materials are better able to withstand the stresses imposed by differential displacement.

Table 5.10 gives the values of the differential displacement necessary to fracture 100 mm and 300 mm spun iron pipes for a series of soil resistances, k_A on the right hand side of the pipeline and k_B on the left hand side, Case B. The table shows that the displacement necessary to fracture the pipe decreases dramatically as the value of k_B increases indicating the very detrimental effect of allowing a pipeline to be built into a wall or concrete foundation.

It can also be seen that the solution for a 100 mm spun iron main with resistances of k_A = 0·025 and k_B = 1000·0 N/mm^3 has broken down. That is, the value of the ground resistance on the right hand side is ceasing to have an effect on the solution as the value of the displacement has started to decrease.

Table 5.11 gives the values of the differential displacement necessary to fracture 100 mm and 300 mm spun iron pipes for a series of soil resistances, k_B on the lower left hand side of the pipeline and k_A elsewhere, Case C. This table shows that the amount of differential displacement necessary to fracture the pipeline also decreases dramatically as the value of k_B increases though not as much as with Case B.

Tables 5.10 and 5.11 also indicate that if these situations are allowed to occur, such as laying one pipeline across another or building a manhole around the pipe, then even large diameter pipes are put at risk due to differential displacement and possible transverse fracture.

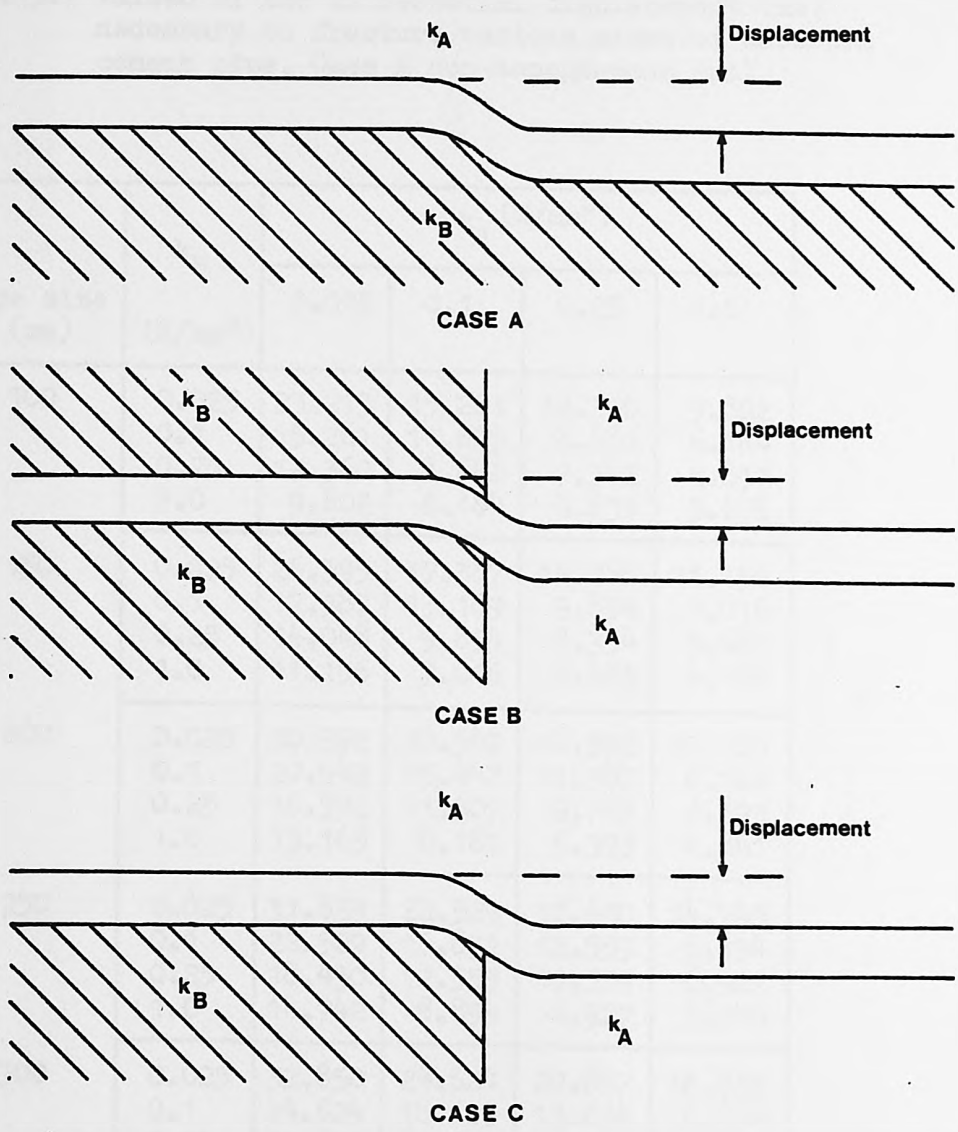

FIG. 5.24 The three cases of non-homogeneous soil analysed using the mathematical model

TABLE. 5.7 Values of the differential displacement (mm) necessary to fracture various sizes of asbestos cement pipe, Case A non-homogeneous soil

Pipe size (mm)	k_B (N/mm^3)	k_A (N/mm^3)			
		0.025	0.1	0.25	1.0
100	0.025	23.213	15.261	12.360	9.802
	0.1	15.261	11.605	8.682	6.184
	0.25	12.360	8.682	7.342	4.831
	1.0	9.802	6.184	4.831	3.678
150	0.025	26.595	17.387	14.048	11.156
	0.1	17.387	13.169	9.854	7.016
	0.25	14.048	9.854	8.334	5.481
	1.0	11.156	7.016	5.481	4.169
200	0.025	30.592	20.542	16.592	13.165
	0.1	20.542	15.443	11.507	8.182
	0.25	16.592	11.507	9.717	6.393
	1.0	13.165	8.182	6.393	4.861
250	0.025	31.839	22.529	18.430	14.742
	0.1	22.529	16.831	12.553	8.894
	0.25	18.430	12.553	10.559	6.927
	1.0	14.742	8.894	6.927	5.270
300	0.025	32.850	24.624	20.657	16.835
	0.1	24.624	18.105	13.654	9.674
	0.25	20.657	13.654	11.463	7.494
	1.0	16.835	9.674	7.494	5.693

TABLE. 5.8 Values of the differential displacement (mm) necessary to fracture various sizes of cast iron pipe, Case A non-homogeneous soil

Pipe size (mm)	k_B (N/mm^3)	k_A (N/mm^3)			
		0.025	0.1	0.25	1.0
100	0.025	81.725	53.495	43.189	34.282
	0.1	53.495	40.430	30.326	21.542
	0.25	43.189	30.326	25.578	16.839
	1.0	34.282	21.542	16.839	12.794
150	0.025	89.463	61.274	49.718	39.588
	0.1	61.274	46.005	34.268	24.325
	0.25	49.718	34.268	28.883	18.889
	1.0	39.588	24.325	18.889	14.445
200	0.025	91.901	67.952	56.620	45.871
	0.1	67.952	50.277	37.759	26.734
	0.25	56.620	37.759	31.718	20.746
	1.0	45.871	26.734	20.746	15.762
250	0.025	94.511	73.139	62.970	52.533
	0.1	73.139	52.289	40.176	28.651
	0.25	62.970	40.176	33.811	22.036
	1.0	52.533	28.651	22.036	16.731
300	0.025	100.660	79.103	70.167	60.645
	0.1	79.103	53.155	42.342	30.929
	0.25	70.167	42.342	35.521	23.494
	1.0	60.645	30.929	23.494	17.698

TABLE. 5.9 Values of the differential displacement (mm) necessary to fracture various sizes of spun pipe, Case A non-homogeneous soil

Pipe size (mm)	k_B (N/mm^3)	k_A (N/mm^3)			
		0.025	0.1	0.25	1.0
100	0.025	98.744	64.547	52.158	41.425
	0.1	64.547	48.898	36.590	26.070
	0.25	52.158	36.590	30.947	20.351
	1.0	41.425	26.070	20.351	15.479
150	0.025	108.094	72.732	58.771	46.651
	0.1	72.732	54.693	40.741	28.983
	0.25	58.771	40.741	34.392	22.626
	1.0	46.651	28.983	22.626	17.207
200	0.025	111.377	80.242	66.092	53.115
	0.1	80.242	59.789	44.671	31.633
	0.25	66.092	44.671	37.530	24.610
	1.0	53.115	31.633	24.610	18.712
250	0.025	112.672	85.570	72.504	59.571
	0.1	85.570	63.391	47.383	33.584
	0.25	72.504	47.383	39.787	26.004
	1.0	59.571	33.584	26.004	19.714
300	0.025	117.792	91.985	80.546	68.288
	0.1	91.985	64.104	50.084	36.068
	0.25	80.546	50.084	42.120	27.657
	1.0	68.288	36.068	27.657	20.868

TABLE. 5.10 Values of the differential displacement (mm) necessary to fracture 100mm and 300mm spun iron pipes, Case B non-homogeneous soil

Pipe size (mm)	k_B (N/mm^3)	k_A (N/mm^3)			
		0.025	0.1	0.25	1.0
100	1.0	34.390	23.563	19.295	15.479
	10.0	20.586	13.958	10.710	7.450
	100.0	7.068	6.256	5.436	4.082
	1000.0	1.505	1.516	1.506	1.441
300	1.0	55.738	32.168	26.063	20.868
	10.0	36.900	19.846	14.680	10.060
	100.0	15.658	11.400	8.958	6.007
	1000.0	3.497	3.355	3.194	2.791

TABLE. 5.11 Values of the differential displacement (mm) necessary to fracture 100mm and 300mm spun iron pipes, Case C non-homogeneous soil

Pipe size (mm)	k_B (N/mm^3)	k_A (N/mm^3)			
		0.025	0.1	0.25	1.0
100	1.0	41.311	25.958	20.261	15.479
	10.0	29.461	17.930	12.888	8.200
	100.0	12.848	9.862	7.889	5.274
	1000.0	3.750	3.176	2.816	2.331
300	1.0	68.288	36.068	27.545	20.868
	10.0	53.907	25.761	17.660	11.068
	100.0	28.764	17.709	12.780	7.717
	1000.0	8.492	6.830	5.840	4.400

CHAPTER 6

MATHEMATICAL SIMULATION OF DUCTILE PIPE MATERIALS

6.1 INTRODUCTION

In order to be a realistic model, the force-displacement method proposed must also be applicable in the case of a ductile pipe material. The simulation of a ductile pipe material is achieved by partially relaxing the continuity conditions, thus allowing a rotation to occur, at all nodes where the calculated value of the bending moment is greater than the yield value of the bending moment.

6.2 BASIC ASSUMPTIONS

The theory governing the inelastic bending of beams in this analysis is based on the following assumptions:

(i) The member is prismatic and the cross-section has at least one plane of symmetry.

(ii) The bending and axial loads are applied in the plane of symmetry.

(iii) Plane sections remain plane after the loads are applied.

(iv) The stress-strain relationship for each longitudinal fibre of each member is the same as that obtained from tension and compression specimens of the material.

(v) The cross-sectional dimensions of the members are small, relative to its length, so that the deformations due to shear may be neglected.

(vi) The initial residual stresses are negligible.

(vii) The deflections are small so that the curvature formula can be approximated by the second derivative of the deflection with respect to the distance along the beam.

6.3 GENERAL LOAD AND DEFORMATION RELATIONSHIPS

Smith and Sidebottom (55) have obtained general load and deformation relationships by considering a short section of a beam as shown in Figure 6.1, subjected to a bending moment M in the plane of symmetry (y-y axis), and to a load N acting at the centroid of the sectional area A. Let N and M be of sufficient magnitude to produce strains ε_1 and ε_2 in the most strained tension and compression fibres respectively and to locate the neutral axis at a distance n', from the most strained tension fibre. Since plane sections remain plane, the strain distribution is linear and is known. Using the strain distribution in Figure 6.1 and the continuous curve in the stress-strain diagram, Figure 6.2, the stress distribution can be constructed as shown in Figure 6.1.

The magnitude of N and M for this stress distribution may be obtained from the equations of equilibrium

$$N = \int \sigma \, dA$$

$$M = \int \sigma (n' - d') dA \qquad \ldots \ldots \ldots \ldots \ldots \qquad (6.1)$$

where d' is the distance of the centroid from the point of zero stress, Figure 6.1.

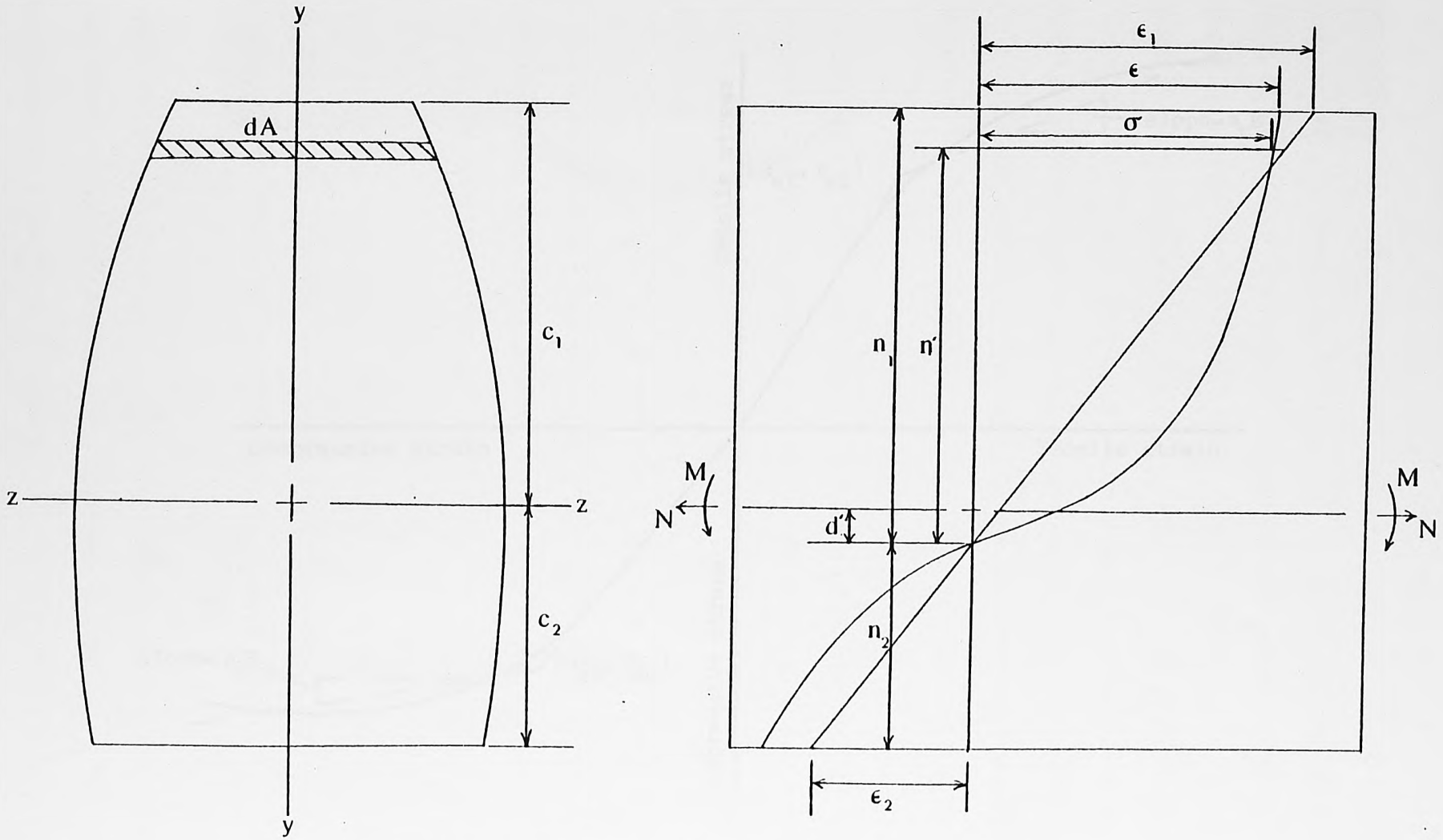

FIG. 6.1 Strain distribution

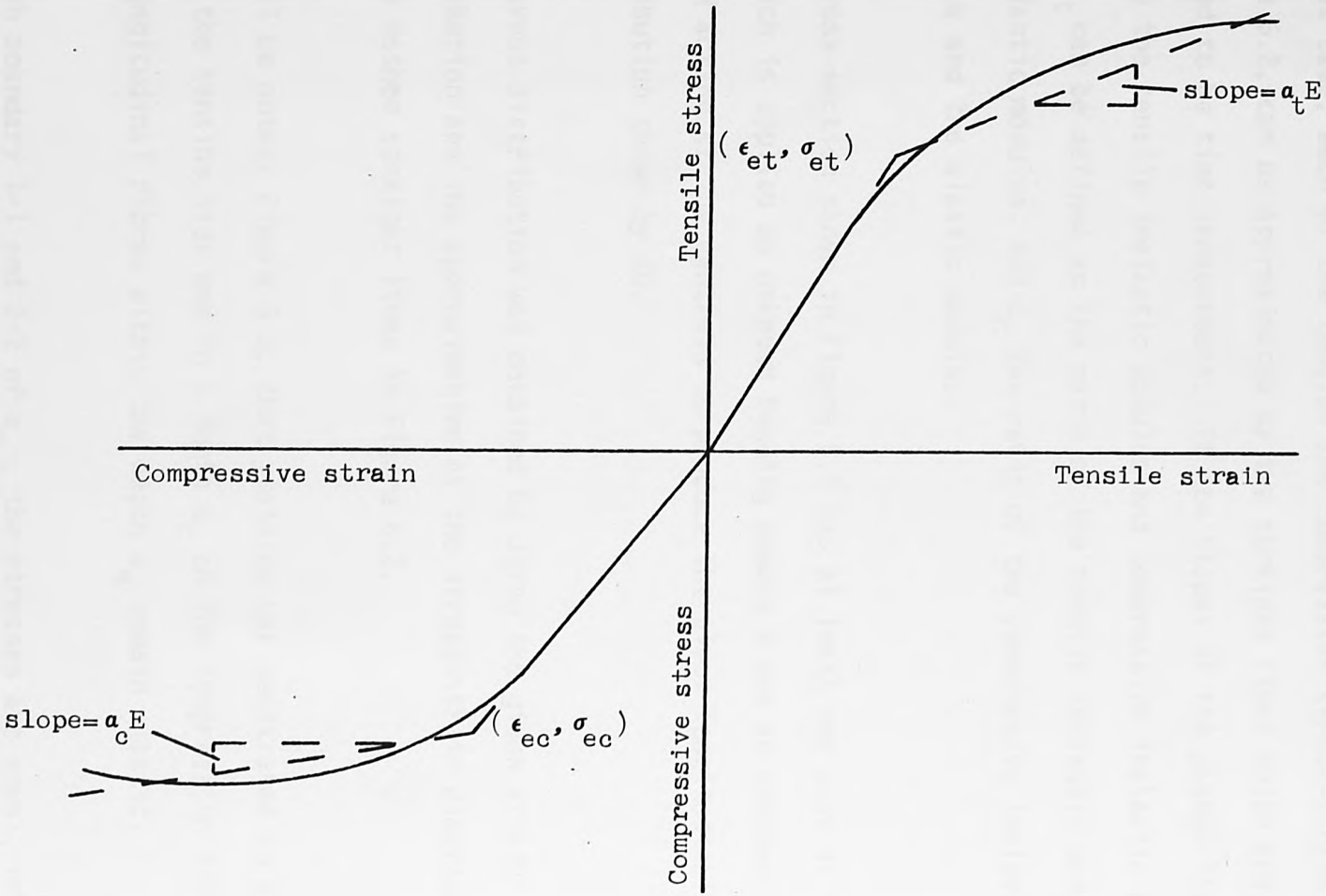

FIG. 6.2 Stress-strain relationship

6.4 LOAD AND DEFORMATION RELATIONSHIPS FOR TIME INDEPENDENT INELASTIC DEFORMATIONS

It is also further assumed that the inelastic deformation of the beam is not subject to the action of creep and is therefore time independent. In this case, each of the tension and compression stress-strain curves, Figure 6.2, can be approximated by two straight lines which are also assumed to be time independent. If the slopes of the dashed lines are called the tensile inelastic modulus and compressive inelastic modulus, then α_t can be defined as the ratio of the tensile inelastic modulus and the elastic modulus, and α_c the ratio of the compressive inelastic modulus and the elastic modulus.

The cross-section shown in Figure 6.3 has at least one axis of symmetry in which is applied an unknown bending moment M and an unknown axial load N acting at the centroid to produce the given longitudinal stress distribution shown by AD.

The stress distribution was obtained by using the given strain distribution and the approximation of the stress-strain diagram, shown by the dashed straight lines in Figure 6.2.

It will be noted, Figure 6.3, that yielding has penetrated to a depth a_t on the tension side and to a depth a_c on the compression side. The longitudinal fibres within the depth a_e remain elastic.

At each boundary 1-1 and 2-2 of a_e , the stresses are equal, respectively, to the tension and compression yield stresses σ_{et} and σ_{ec} which occur simultaneously, as defined in Figure 6.3. Between the elastic -

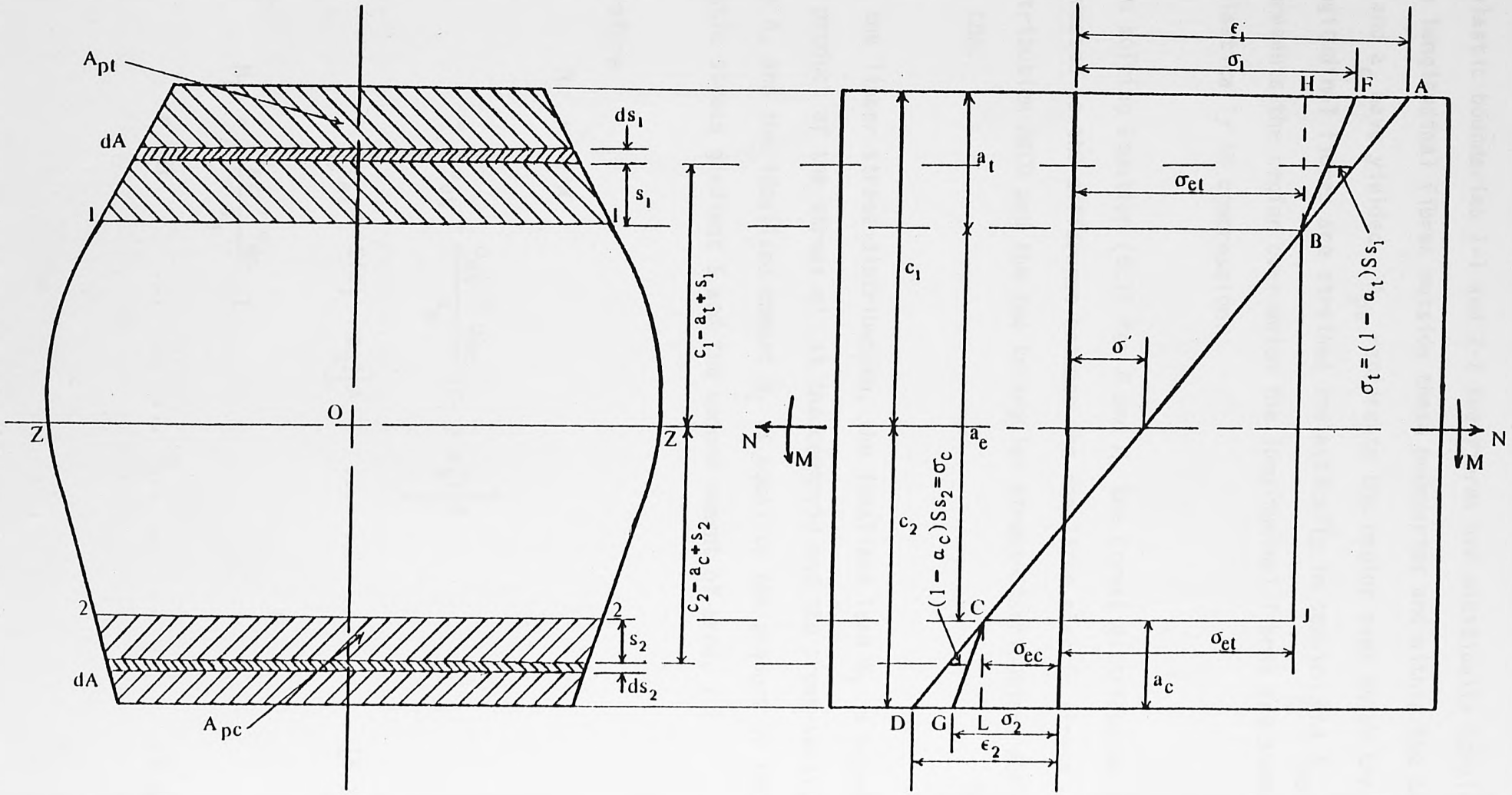

FIG. 6.3 Stress-strain distribution in a section

inelastic boundaries 1-1 and 2-2 the fibres are elastically strained. The longitudinal fibres outside these boundaries and within the depths a_t and a_c have yielded. A_{pt} represents the region over which the longitudinal fibres are strained inelastically in tension and A_{pc} represents the region over which the longitudinal fibres are strained inelastically in compression.

When solving Equation (6.1) for N and M, the stress distribution is expressed as the difference between the idealized elastic stress distribution ABCD and the two triangular stress-distributions ABF and CDG.

For the linear stress distribution, the idealized load N_I is equal to the product of the stress σ' at the centroid and the cross-sectional area A, and the idealized moment M_I is equal to the product of the elastic stress gradient S and the second moment of area, I.

Therefore

$$N_I = \sigma' A$$

$$= \left[\sigma_{et} - \frac{\sigma_{et} + \sigma_{ec}}{a_e}(c_1 - a_t)\right] A$$

$$= \left[\sigma_{et} - S(c_1 - a_t)\right] A \quad \ldots \quad \ldots \quad \ldots \qquad (6.2)$$

and

$$M_I = \frac{\sigma_{et} + \sigma_{ec}}{a_e} I$$

$$= SI \quad \ldots \quad \ldots \quad \ldots \quad \ldots \quad \ldots \quad \ldots \qquad (6.3)$$

where c_1 is the distance of the upper surface from the centroid.

Then we have

$$N = N_I - \int_o^{a_t} \sigma_t \, dA + \int_o^{a_c} \sigma_c \, dA \quad \ldots \qquad (6.4)$$

and

$$M = M_I - \int_o^{a_t} (c_1 - a_t + s_1)\sigma_t \, dA - \int_o^{a_c} (c_2 - a_c + s_2)\sigma_c \, dA$$

$$\ldots \quad \ldots \quad \ldots \quad \ldots \quad \ldots \qquad (6.5)$$

where

c_2 is the distance of the lower surface from the centroid

σ_t is the stress at a distance s_1 from the boundary 1-1

σ_c is the stress at a distance s_2 from the boundary 2-2

The stress represented by HF is equal to $\alpha_t E(\varepsilon_1 - \varepsilon_{et})$ and by LG is equal to $\alpha_c E(\varepsilon_2 - \varepsilon_{ec})$.

But

$$\frac{\varepsilon_1 - \varepsilon_{et}}{a_t} = \frac{\varepsilon_{et} + \varepsilon_{ec}}{a_e}$$

and

$$\frac{\varepsilon_2 - \varepsilon_{ec}}{a_c} = \frac{\varepsilon_{et} + \varepsilon_{ec}}{a_e}$$

Therefore the stress represented by AF is equal to $(1 - \alpha_t)\, S\, a_t$ and by DG is equal to $(1 - \alpha_c)\, S\, a_c$.

Now, from triangles AFB and CDG, respectively and from the previously obtained stresses AF and DG, we have the stresses σ_t and σ_c at distances s_1 and s_2, respectively, from the boundaries 1-1 and 2-2 as follows

$$\sigma_t = (1 - \alpha_t)\, S\, s_1 \quad \ldots \quad \ldots \quad \ldots \quad \ldots \qquad (6.6)$$

$$\sigma_c = (1 - \alpha_c)\, S\, s_2 \quad \ldots \quad \ldots \quad \ldots \quad \ldots \qquad (6.7)$$

Substituting the values for σ_t and σ_c from Equations(6.6) and (6.7) into Equations (6.4) and(6.5) we have

$$N = \left[\sigma_{et} - S(c_1 - a_t)\right]A - (1 - \alpha_t)\, S \int_o^{a_t} s_1\, dA +$$

$$+ (1 - \alpha_c)S \int_o^{a_c} s_2\, dA \quad \ldots \quad \ldots \quad \ldots \qquad (6.8)$$

and

$$M = SI - (1 - \alpha_t)S \int_o^{a_t} (c_1 - a_t + s_1)s_1\, dA -$$

$$- (1 - \alpha_c)S \int_o^{a_c} (c_2 - a_c + s_2)s_2\, dA$$

$$\ldots \quad \ldots \quad \ldots \quad \ldots \quad \ldots \qquad (6.9)$$

The above expressions for N and M, Equations (6.8) and (6.9) can be further modified to give the following expressions

$$N = \left[\sigma_{et} - S(c_1 - a_t)\right] A - (1 - \alpha_t)S\, Q_t + (1 - \alpha_c)\, S\, Q_c$$

$$\ldots \quad \ldots \quad \ldots \quad \ldots \quad \ldots \qquad (6.10)$$

$$M = SI - S(1 - \alpha_t)\left[(c_1 - a_t)Q_t + I_t\right] -$$

$$- S(1 - \alpha_c)\left[(c_2 - a_c)Q_c + I_c\right] \quad \ldots \quad \ldots \qquad (6.11)$$

where

Q_t = the first moment with respect to the elastic - inelastic boundary 1-1 of the area A_{pt}.

Q_c = the first moment with respect to the elastic - inelastic boundary 2-2 of the area A_{pc}.

I_t = the second moment with respect to the elastic - inelastic boundary 1-1 of the area A_{pt}.

I_c = the second moment with respect to the elastic - inelastic boundary 2-2 of the area A_{pc}.

6.5 DEFORMATION RELATIONSHIPS FOR A PIPE SECTION

Considering a pipe with external and internal radii of R and r respectively made from a homogeneous material with similar properties in tension and compression and using the stress-strain distribution shown in Figure 6.4, together with the condition

$$N = 0$$

the following relationships hold

$$\alpha_t = \alpha_c = \alpha_p \text{(ratio of inelastic and elastic moduli)}$$

$$a_t = a_c$$

$$Q_t = Q_c$$

$$I_t = I_c$$

$$c_1 = c_2 = R$$

$$S = \frac{\sigma_{et}}{B}$$

where $B = R - a_t$

Using the above relationships with Equation (6.11), we have

$$M = \frac{\sigma_{et}}{B}\left[I - 2(1 - \alpha_p)(B\, Q_t + I_t)\right] \quad \ldots \quad \ldots \qquad (6.12)$$

which gives the value of the inelastic bending moment in the pipe when the inelastic front has penetrated to a depth a_t from the outer surface or a distance B from the centre.

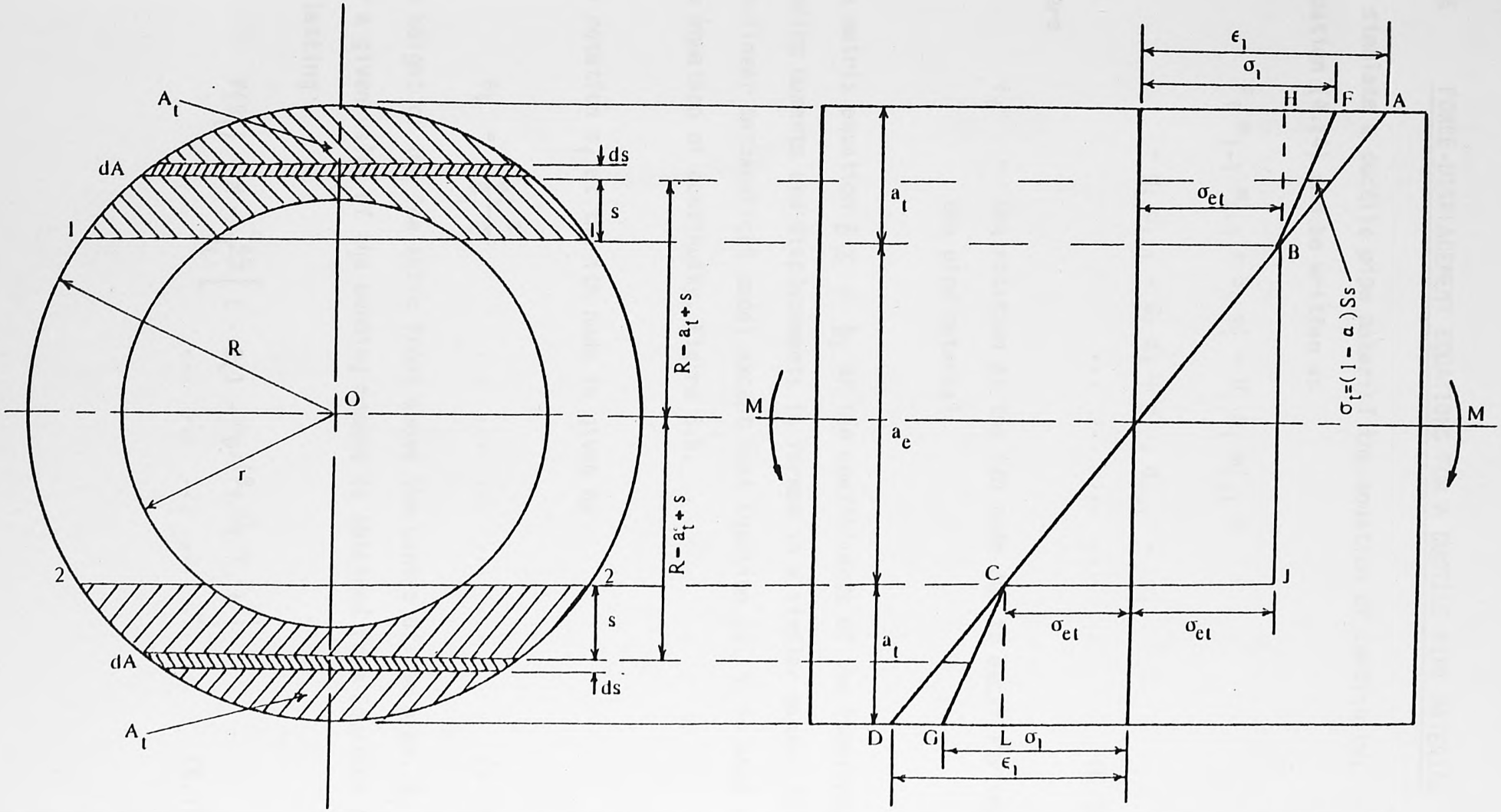

FIG. 6.4 Stress-strain distribution in a pipe

6.6 FORCE-DISPLACEMENT EQUATIONS FOR A DUCTILE PIPE MATERIAL

To simulate a ductile pipe material the equation of continuity, Equation (4.14) can be written as

$$F_i\, h_{i-1}\, m'_{i-1} + S_i\, m'_i + H_i\, h_i\, m'_{i+1} + $$

$$+ g_i\, d_{i-1} - G_i\, d_i + g_{i-1}\, d_{i+1} = \theta_i \qquad \text{... ... ...} \qquad (6.13)$$

where

θ_i = the rotation at the ith node due to ductility in the pipe material.

The matrix equation $\underset{\sim}{A}\ \underset{\sim}{x} = \underset{\sim}{b}_1$ of the coefficients of the indeterminate bending moments and displacements is formed in a similar manner to the non-linear mathematical model except that Equation (6.13) is used as the equation of continuity, Figure 6.5.

The rotation θ_i at the ith node is given by

$$\theta_i = \frac{\sigma_{et}\, a_i}{B_i\, E} \qquad \text{... ... ...} \qquad (6.14)$$

The height of the inelastic front above the centre of the pipe, B_i for a given value of the bending moment is obtained from Equation (6.12) by letting

$$f(B_i) = M - \frac{\sigma_{et}}{B_i}\left[I - 2(1 - \alpha_p)(B_i\, Q_t + I_t)\right] \qquad \text{... ... ...} \qquad (6.15)$$

and using the Newton-Raphson iteration scheme, Ralston (56),

$$B_{j+1} = B_j - \frac{f(B_j)}{f'(B_j)} \quad \ldots \quad \ldots \quad \ldots \quad \ldots \qquad (6.16)$$

where a single prime indicates differentiation with respect to B.

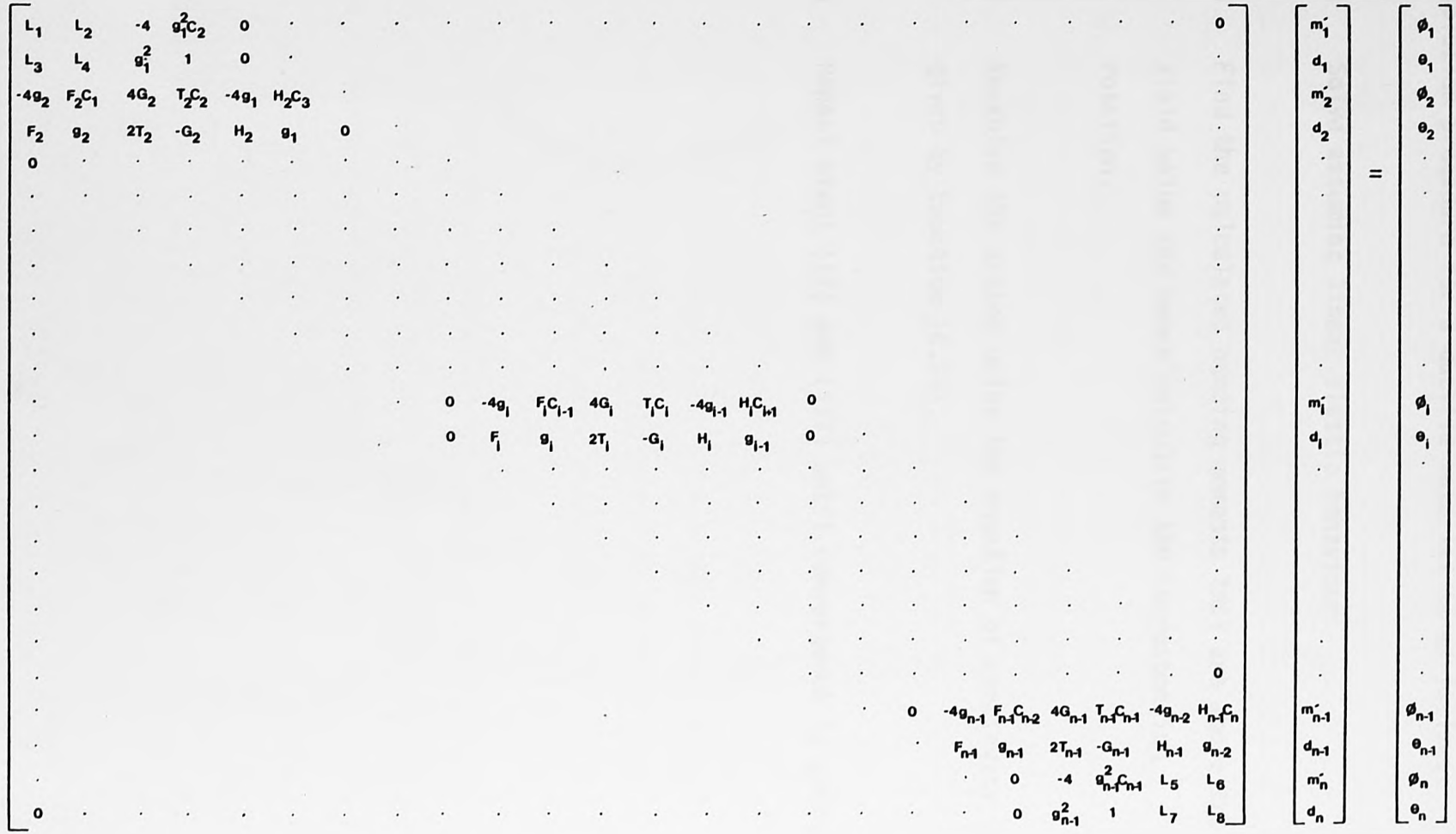

FIG. 6.5 Matrix equation $\underset{\sim}{A}\underset{\sim}{x}=\underset{\sim}{b}_1$

6.7 SOLUTION PROCEDURE FOR A DUCTILE MATERIAL

The solution procedure for a ductile material is as follows:

(i) Solve assuming linear elastic behaviour.

(ii) Find the calculated bending moments that are above the yield value and hence calculate the corresponding rotation.

(iii) Re-solve the system using the equation of continuity given by Equation (6.13).

(iv) Repeat steps (ii) and (iii) until convergence is achieved.

CHAPTER 7

EXPERIMENTAL SIMULATION OF GROUND MOVEMENT ACTING ON A DUCTILE PIPE

7.1 INTRODUCTION

In order to measure the effect of ground movement on a buried ductile pipeline, an experiment was designed by which a pipe of ductile material could be subjected to a differential displacement when supported by sets of springs.

The experiment was carried out using a thin walled small diameter annealed copper tube which was suspended at 48 points, each of which comprised of a pair of springs above and below the pipe, Figure 7.1. The springs were connected to metal plates held in a Hi-tech frame. The plates could be raised or lowered thus simulating ground movement, Figure 7.2. After each movement of the plates a photograph was taken using a Zeiss UMK Terrestrial Photogrammetric Camara. The resulting photographs were later analysed using a Stecometer.

Before the experiment could be carried out it was first necessary to measure the stiffness of the springs and to obtain a load-strain curve for the annealed copper pipe material.

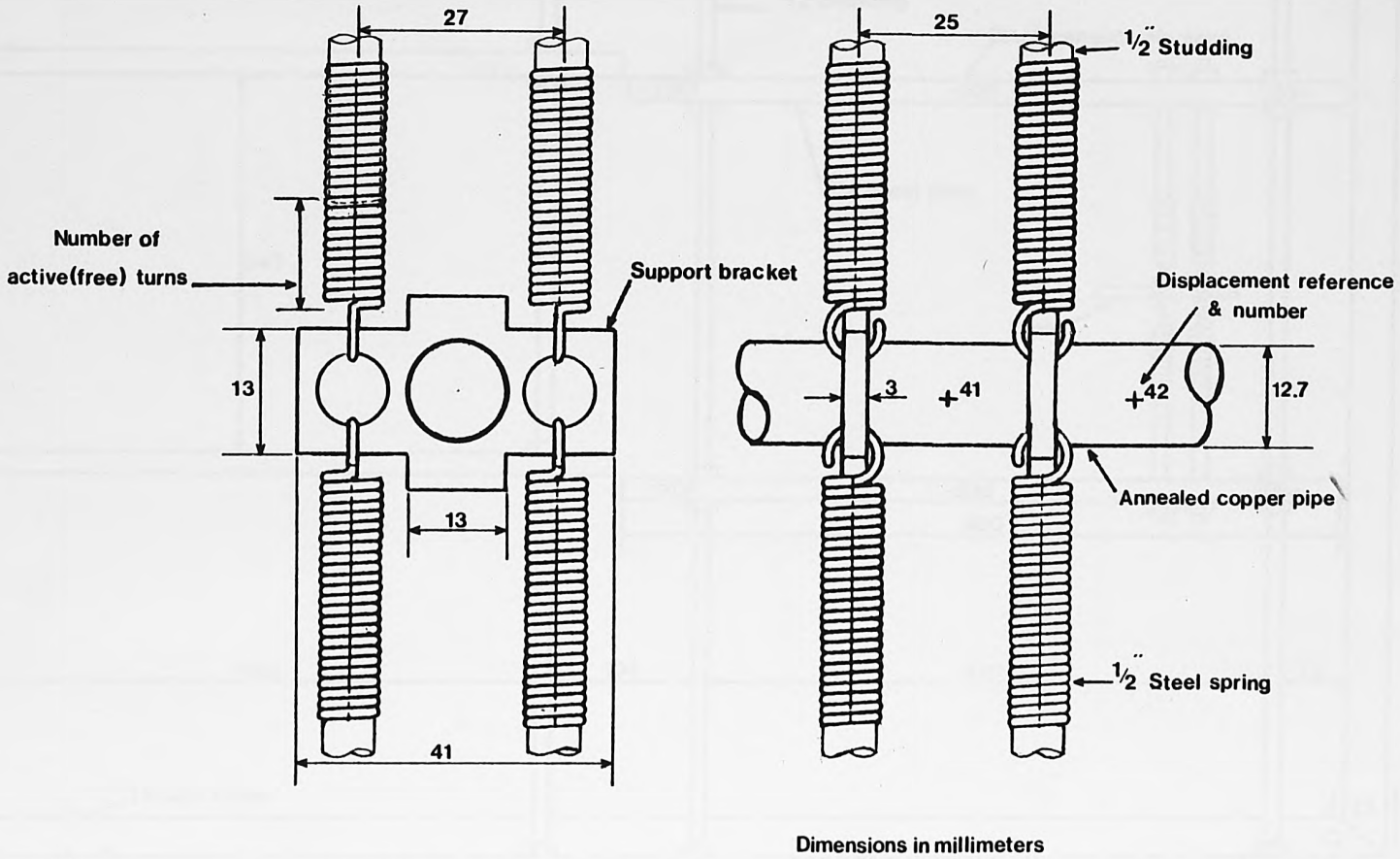

FIG. 7.1 Detail of springs and support brackets

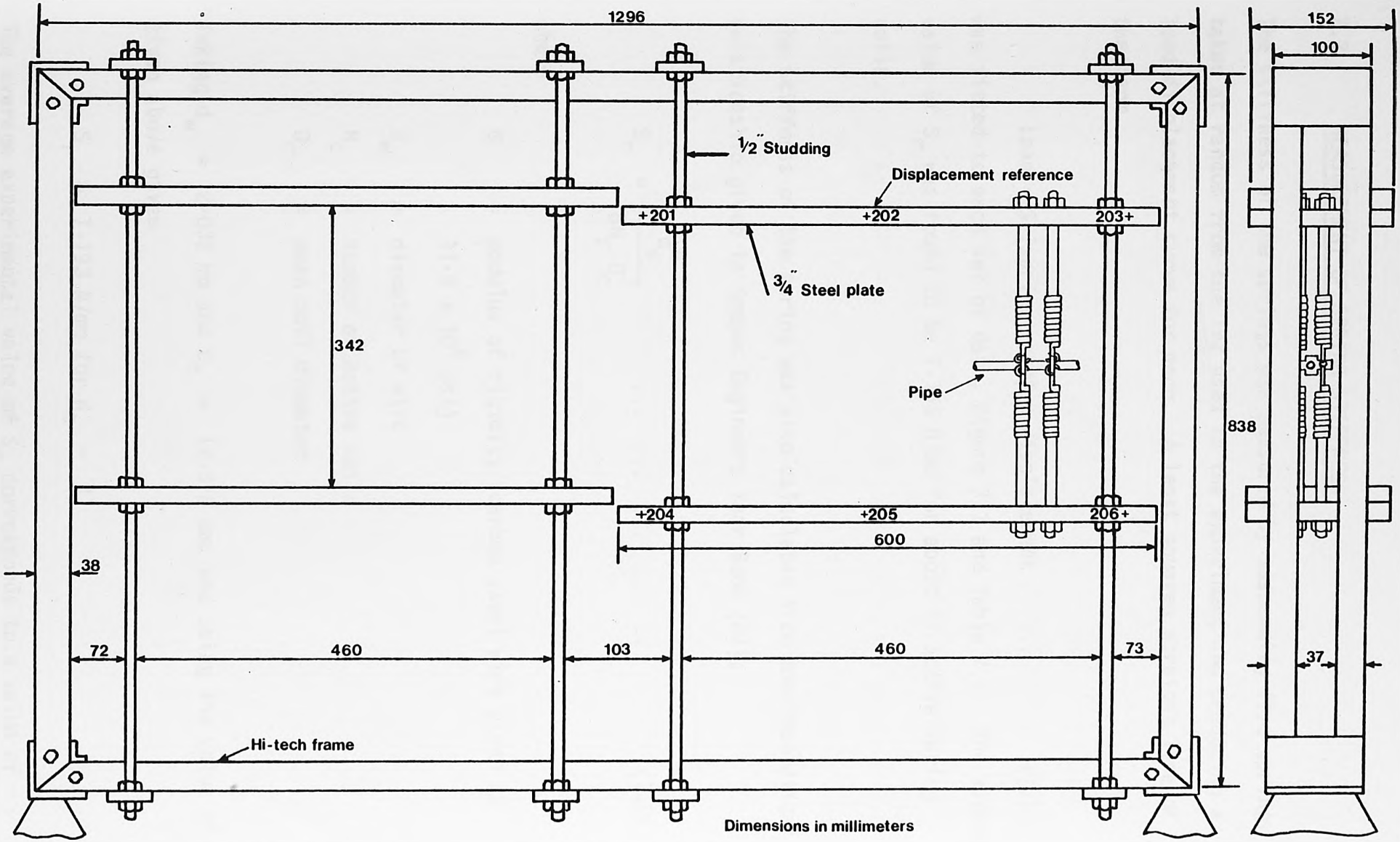

FIG.7.2 Detail of whole experimental frame

7.2 MEASUREMENT OF SPRING STIFFNESS

The stiffness of the springs was measured by suspending five springs taken at random from the 192 used in the experiment and producing a load-displacement curve for each. A least squares straight line of the form

$$\text{Load} = S_r(\text{spring rate}) \times \text{displacement} \quad \ldots \quad (7.1)$$

was fitted to each set of data, Figure 7.3 and Table 7.1. The average value of S_r was found to be 7·156 N/mm for about 11 active spring coils.

The stiffness of the spring was also calculated from the theoretical relationship given in Kempes Engineers Year Book (57),

$$S_r = \frac{G\, d_w^4}{8 N_c\, D_c^3} \quad \ldots \quad \ldots \quad \ldots \quad \ldots \quad \ldots \quad (7.2)$$

where

G = modulus of rigidity (carbon steel wire given as $11{\cdot}5 \times 10^6$ psi)

d_w = diameter of wire

N_c = number of active coils

D_c = mean coil diameter

Taking $d_w = 2{\cdot}032$ mm and $D_c = 12{\cdot}878$ mm, and using the value of G given above gives

$$S_r = 7{\cdot}193 \text{ N/mm for } N_c = 11$$

The average experimental value of S_r corresponds to a value of $N_c = 11{\cdot}0566$

The spring rate can be converted into the reaction modulus of supporting foundation, in N/mm of deflection per mm of pipe, by using the relationship given by Thoms (58),

$$k = \frac{n_s S_r}{L_p} \quad \ldots \quad \ldots \quad \ldots \quad \ldots \quad \ldots \quad \ldots \qquad (7.3)$$

where

n_s = number of supports (96 pairs of springs)

S_r = spring rate

L_p = length of pipe used in experiment (1200 mm)

which gives a value to k of 1·143 N/mm^2 when using the experimental value of the spring rate. This corresponds to a soil stiffness, k_o, of 0·09 N/mm^3 when k is divided by the diameter of the copper tube, 12·7 mm.

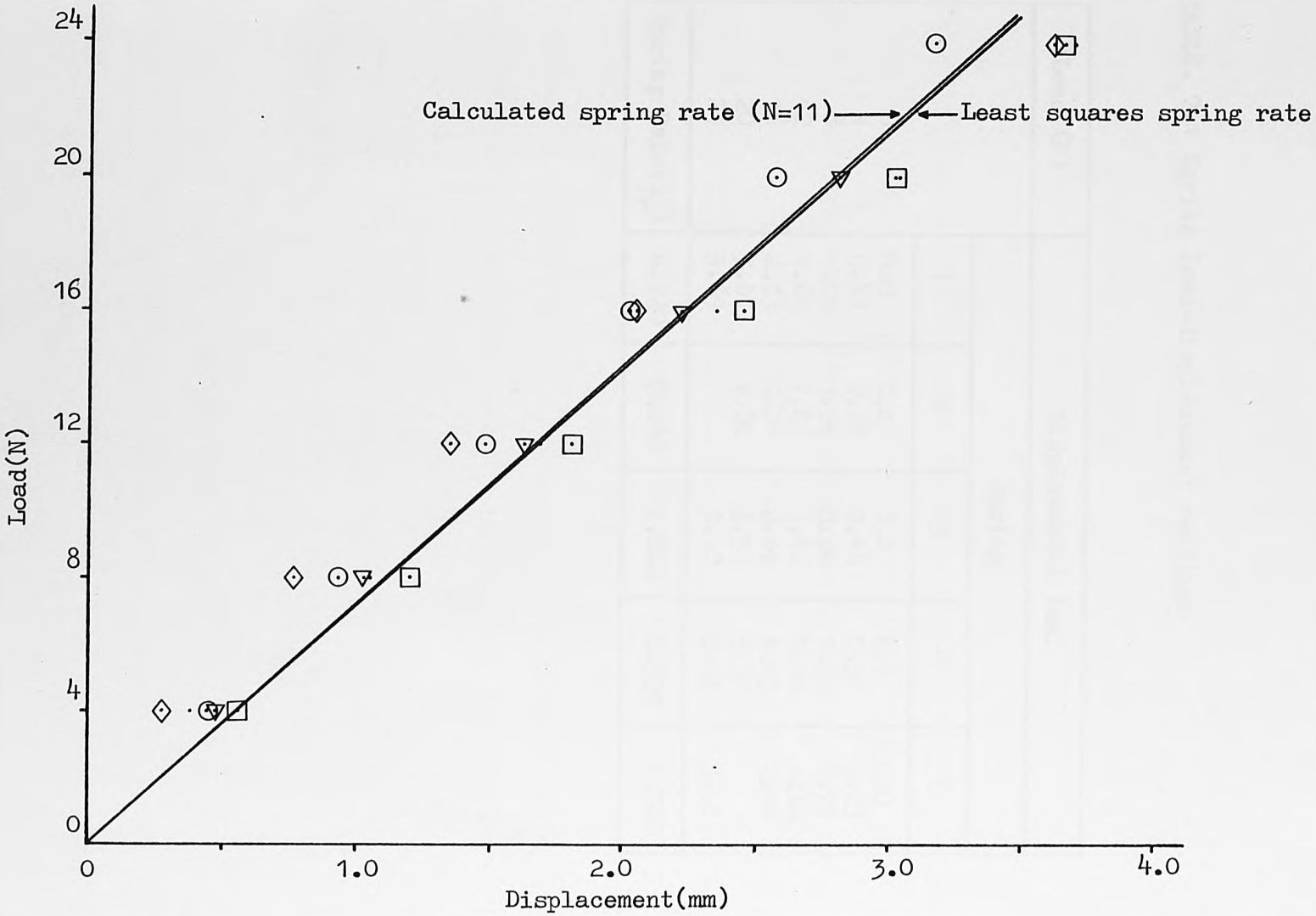

FIG. 7.3 Spring load-displacement curve

TABLE. 7.1 Spring load-displacement readings

Load (N)	Displacement (mm)				
	Spring				
	1	2	3	4	5
0	0.0	0.0	0.0	0.0	0.0
4	0.41	0.48	0.45	0.56	0.28
8	1.05	1.04	0.94	1.20	0.78
12	1.69	1.63	1.48	1.80	1.36
16	2.35	2.21	2.02	2.45	2.04
20	3.01	2.80	2.56	3.02	
24	3.69		3.15	3.65	3.62
Spring Rate(S_r)	6.720	7.263	7.820	6.599	7.380

7.3 STRESS-STRAIN RELATIONSHIP OF THE COPPER TUBE

Two methods were used to investigate the stress-strain relationship of the copper tube. Firstly, in the elastic region, the EI value was determined using the method of 4-point loading, and secondly, load-strain curves were obtained by performing tensile tests on an Instron Universal Testing Machine.

Altogether nine 4-point loading tests were performed on the copper tubes and the average value of the elastic modulus, E, was found to be $1{\cdot}342 \times 10^5$ N/mm^2 with a range of values between $1{\cdot}210 \times 10^5$ and $1{\cdot}519 \times 10^5$ N/mm^2.

Two tensile tests were performed on the annealed copper tube using the Instron Universal Testing Machine to load the specimens at a uniform rate. The extensions of the specimens were measured using two extensometers, one of 4" for one test and one of 6" for the other. To stop the jaws of the testing machine crushing the ends of the copper tubes, tapered cylindrical metal inserts were machined to support the ends in the jaws, Figure 7.4. The inserts were tapered so as to stop the premature failure of the specimen which would occur due to the sharp untapered sides of the inserts cutting into the copper.

The measured loads and extensions are given in Tables 7.2 and 7.3 and are shown graphically as load-strain curves in Figures 7.5 and 7.6.

Fitting a least squares straight line to each set of data for the range of load 0 to 300 N gives values of the elastic modulus, E, of $1{\cdot}382 \times 10^5$ and $1{\cdot}325 \times 10^5$ N/mm^2 for the 4" and 6" gauges respectively.

The grand average of the elastic modulus, using the values obtained from the 4-point loading tests and the tensile tests is $1{\cdot}344 \times 10^5$ N/mm^2. This was the value of E which was used in the computer analysis of the experimental simulation of ground movement acting on a ductile pipe.

A two straight lines approximatin of the load-strain curve for the copper tube material was obtained from the load-strain graph, Figure 7.5, by using the straight line corresponding to the elastic modulus and by choosing the second straight line for the curve obtained using the 6" extensometer such that the line was about 3% below the measured loads for the mid range values of strain and was about 3% above the measured loads for the end range values of strain, as indicated on the graph. This line is about 4% above the measured loads for the curve obtained using the 4" extensometer.

The gradient of the second straight line is 12716·67, which gives an inelastic modulus, defined in Chapter 6, of 627·55 N/mm^2. This gives a value to the ratio of the inelastic and elastic moduli, α_p used in Equation (6.12), of 0·00467. The yield stress, σ_{et}, used in the same Equation, has a value of 65·14 N/mm^2.

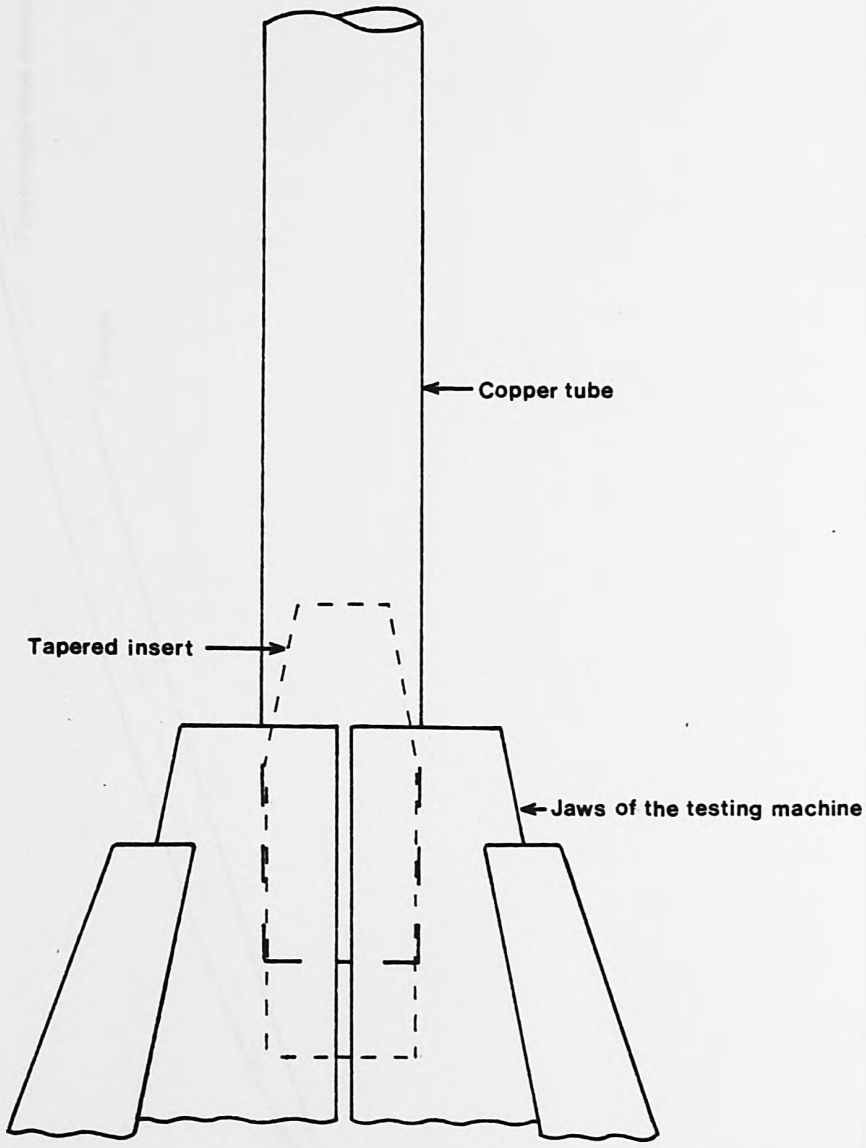

FIG. 7.4 Detail of tapered insert

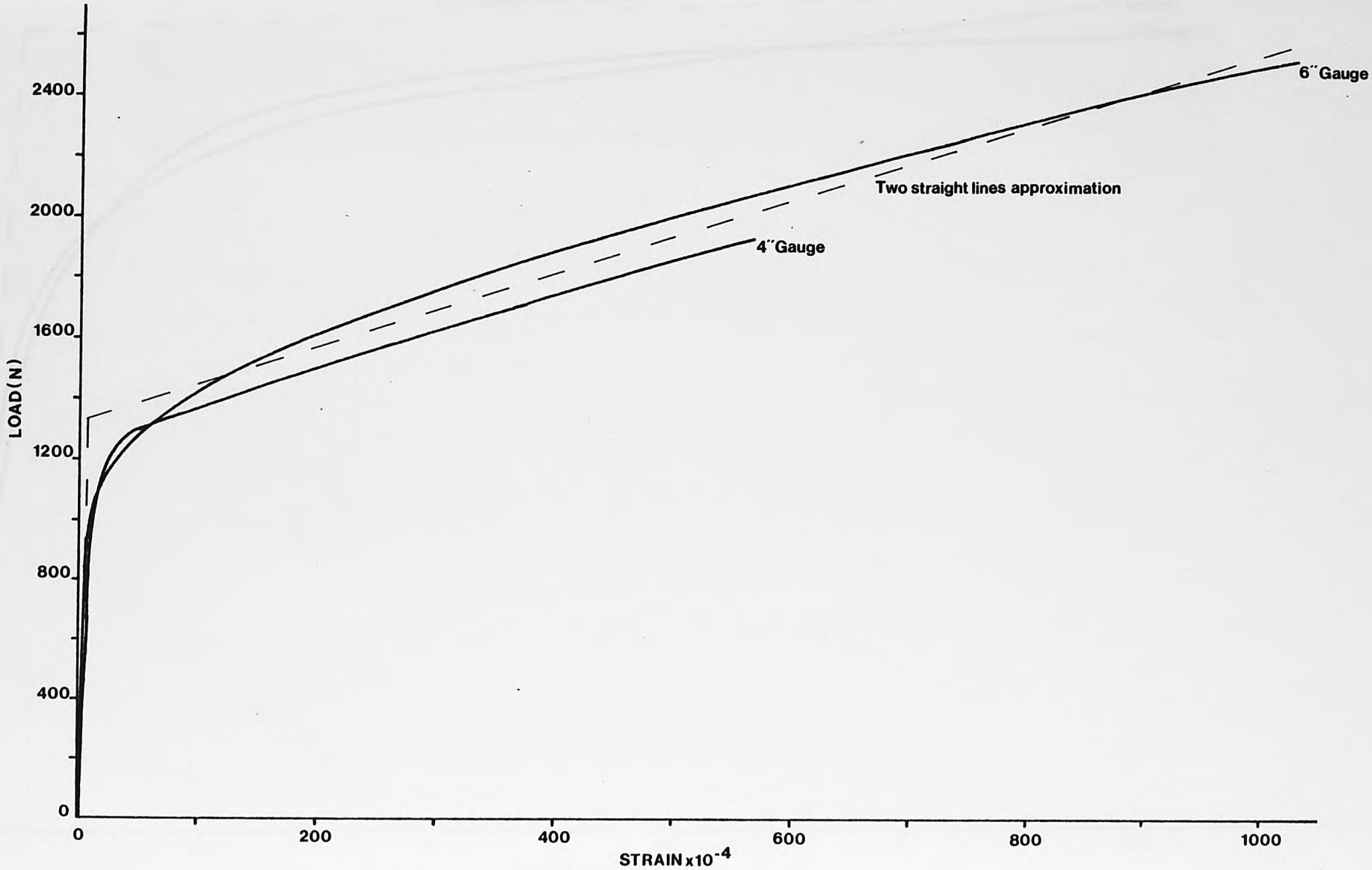

FIG. 7.5 Complete load-strain curves

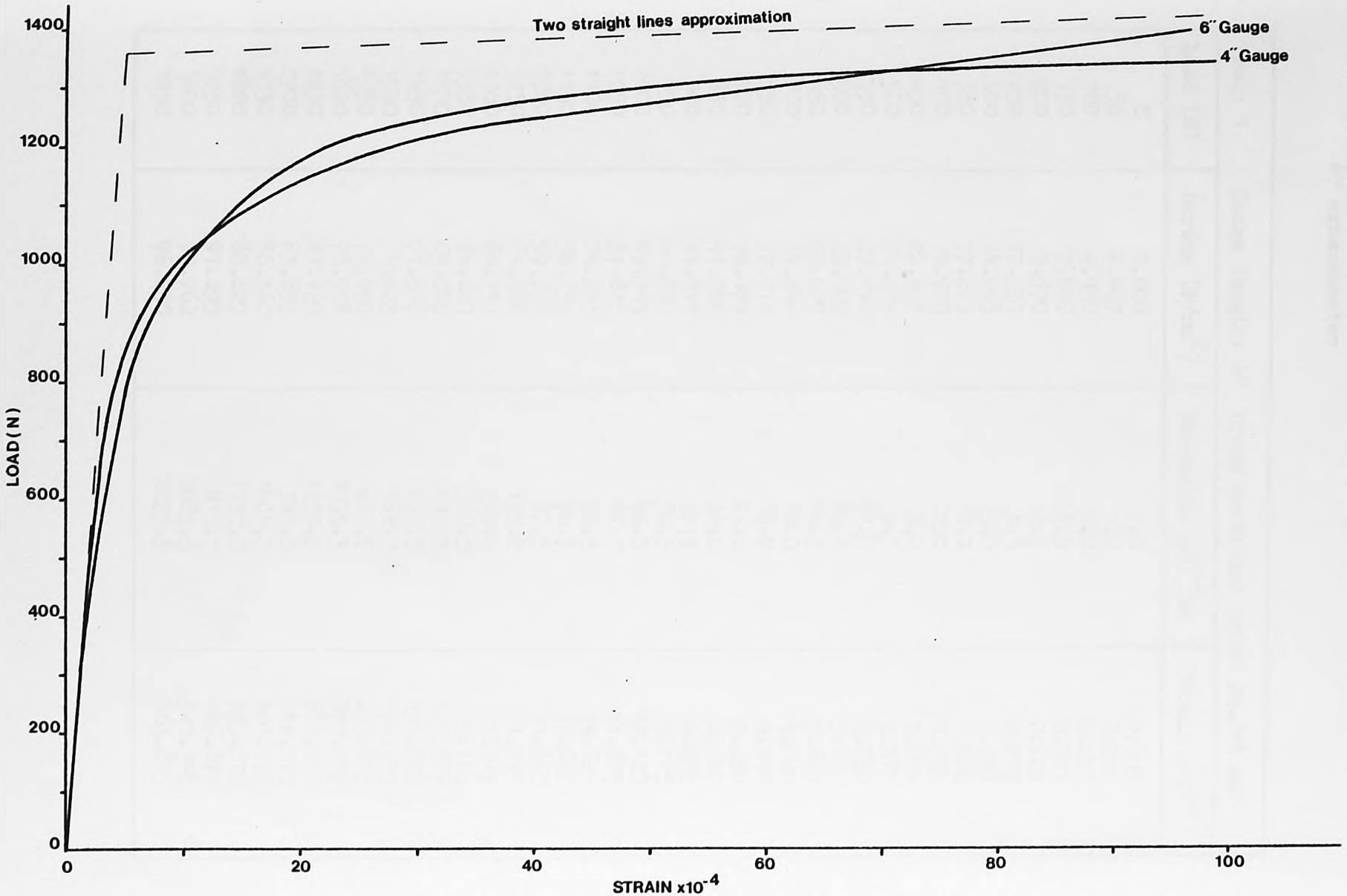

FIG. 7.6 Section of load-strain curve showing greater detail of lower strain levels

TABLE. 7.2 Load, stress, extension and strain values - 4" extensometer

Test: 1	Gauge length: 4"	Cross sectional area: 20.264 mm^2	
Load (N)	Stress (N/mm^2)	Extension $x10^{-4}$ mm	Strain $x10^{-4}$
0	0.000	0.0	0.000
50	2.467	1.0	0.250
100	4.935	1.0	0.250
150	7.402	1.5	0.375
200	9.870	2.5	0.625
250	12.337	3.5	0.875
300	14.805	5.0	1.250
350	17.272	6.0	1.500
400	19.739	7.0	1.750
450	22.207	8.0	2.000
500	24.674	9.5	2.375
550	27.142	11.0	2.750
600	29.609	12.5	3.125
650	32.077	14.5	3.625
700	34.544	16.0	4.000
750	37.011	18.0	4.500
800	39.479	21.0	5.250
850	41.946	24.0	6.000
900	44.414	27.5	6.875
950	46.881	32.5	8.125
1000	49.349	40.5	10.125
1050	51.816	47.5	11.875
1100	54.283	58.5	14.625
1150	56.751	70.5	17.625
1200	59.218	87.5	21.875
1250	61.686	125.5	31.375
1300	64.153	205.5	51.375
1350	66.621	380.5	95.125
1400	69.088	495.5	123.875
1450	71.555	635.5	158.875
1500	74.023	785.5	196.375
1550	76.490	935.5	233.875
1600	78.958	1095.5	273.875
1650	81.425	1235.5	308.875
1700	83.893	1385.5	346.375
1750	86.360	1605.5	401.375
1800	88.827	1735.5	433.875
1850	91.295	1915.5	478.875
1900	93.762	2085.5	521.375
1950	96.230	2255.5	563.875

TABLE. 7.3 Load, stress, extension and strain values - 6" extensometer

Test: 2	Gauge length: 6"	Cross sectional area: 20.264 mm^2	
Load (N)	Stress (N/mm^2)	Extension $x10^{-4}$ mm	Strain $x10^{-4}$
0	0.000	0.0	0.00
50	2.467	1.0	0.17
100	4.935	2.0	0.33
150	7.402	3.0	0.50
200	9.870	4.5	0.75
250	12.337	5.5	0.92
300	14.805	7.0	1.17
350	17.272	8.0	1.33
400	19.739	9.5	1.58
450	22.207	11.0	1.83
500	24.674	12.5	2.08
550	27.142	14.0	2.33
600	29.609	15.5	2.58
650	32.077	17.5	2.92
700	34.544	19.5	3.25
750	37.011	22.0	3.67
800	39.479	26.0	4.33
850	41.946	30.0	5.00
900	44.414	35.0	5.83
1000	49.349	54.0	9.00
1050	51.816	74.0	12.33
1100	54.283	97.0	16.17
1150	56.751	122.0	20.33
1200	59.218	163.0	27.17
1250	61.686	242.0	40.33
1300	64.153	362.0	60.33
1350	66.621	460.0	76.67
1400	69.088	560.0	93.33
1450	71.555	670.0	111.67
1500	74.023	830.0	138.33
1550	76.490	965.0	161.50
1600	78.958	1145.0	190.83
1650	81.425	1344.0	224.00
1700	83.893	1561.0	260.17
1750	86.360	1769.0	294.83
1800	88.827	1981.0	330.17
1850	91.295	2202.0	367.00
1900	93.762	2400.0	400.00

continued /...

TABLE. 7.3 Load, stress, extension and strain values -
6" extensometer

			continued /...
1950	96.230	2641.0	440.17
2000	98.697	2947.0	491.17
2050	101.165	3212.0	535.33
2100	103.632	3450.0	575.00
2150	106.099	3743.0	623.83
2200	108.567	3991.0	665.17
2250	111.034	4273.0	712.17
2300	113.502	4523.0	753.83
2350	115.969	4843.0	807.17
2400	118.437	5195.0	865.83
2450	120.904	5525.0	920.83
2500	123.371	5827.0	971.17
2550	125.839	6150.0	1025.17

7.4 EXPERIMENTAL PROCEDURE

The apparatus for the experimental bending of the copper tube was assembled by attaching the steel plates, from which the springs were suspended, to the Hi-tech frame by means of 8 lengths of studding which were secured top and bottom by brackets, Figure 7.2. It was important that the plates started the experiment as parallel as possible. This was achieved by the use of a precise engineers' level.

In order to set the spring rate exactly the same for each spring, a "mini-rule" was made with graduations at every 1/12th of an inch (the pitch of the ½" studding onto which the springs were screwed). Each spring was set such that it would have about 11 active (free) spring coils.

Once the springs had been set they were mated into the plates, with the hooks of the springs paralleled to the plates by using a precision level. This was only necessary for the top springs, as the bottom ones would fall naturally into place once the pipe had been installed.

Great care was necessary when installing the annealed copper tube as any bending would cause work hardening. The first procedure was to mount the 48 support brackets at suitable intervals on the pipe, as nearly as possible coinciding with the intervals of the hooks on the springs.

The pipe was then carefully inserted between the struts and the ends of the frame, and moved into position. The hooks on the top springs were then connected to the brackets.

Due to the fact that there was some distortion of the pipe, not all of the springs were carrying the weight of the pipe, it was necessary to adjust the springs until they were carrying, as nearly as possible, equal loads. The bottom springs could now be connected and allowed to hang loosely. Any slack on the bottom bolts being taken in by adjusting them until they were lying flush with the plate.

It was necessary to establish suitable controls on the apparatus before any photographs could be taken. Three sets of controls were used, one to give the overall scaling factors enabling the photographic values to be translated into actual values, one to measure the displacements of the plates and one to measure the displacement of the pipe.

Since the camera was to remain stationary relative to the frame throughout the experiment, the only axes to have an effect on the interpretation of the photographs are in the plane of the frame itself. The control chosen for the frame plane was a grid of known dimensions, Figure 7.7, which was superimposed between the frame and the camera at a known distance from the frame.

The control used for the plates was a set of six crosses marked and numbered on white painted areas of the plates, Figure 7.2, and the control used for the pipe was 47 crosses marked and numbered on the white painted pipe, between the support brackets. The whitened surfaces were sprayed with a matt non-reflective varnish to prevent any possible glare from the photoflood bulbs used when taking the photographs.

In order to get the best detail possible on the photographic negative, the camera was set at its point of nearest focus, about 1·4 metres from the plates, care being taken to ensure that the horizontal axes of the

negative was as parallel as possible to the plane of the frame. The vertical axes of the negative was set by sighting the camera onto a point on one of the studs at the level of the pipe adjacent to point reference 24. This was to serve as a check to ensure no movement of the camera or frame had taken place during the experiment.

The pipe was bent by lowering the plates on the right hand side by increments of 10 mm until they were 40 mm below their starting positions. At each incremental level, including the starting position, a photograph was taken using the Zeiss UMK Terrestrial Photogrammetric Camera, Figures 7.8 to 7.12. The main criteria when moving the plates was that they should be kept as parallel as possible to their original position. To achieve this the plates were lowered and then levelled using an engineers level and an accurately calibrated rule.

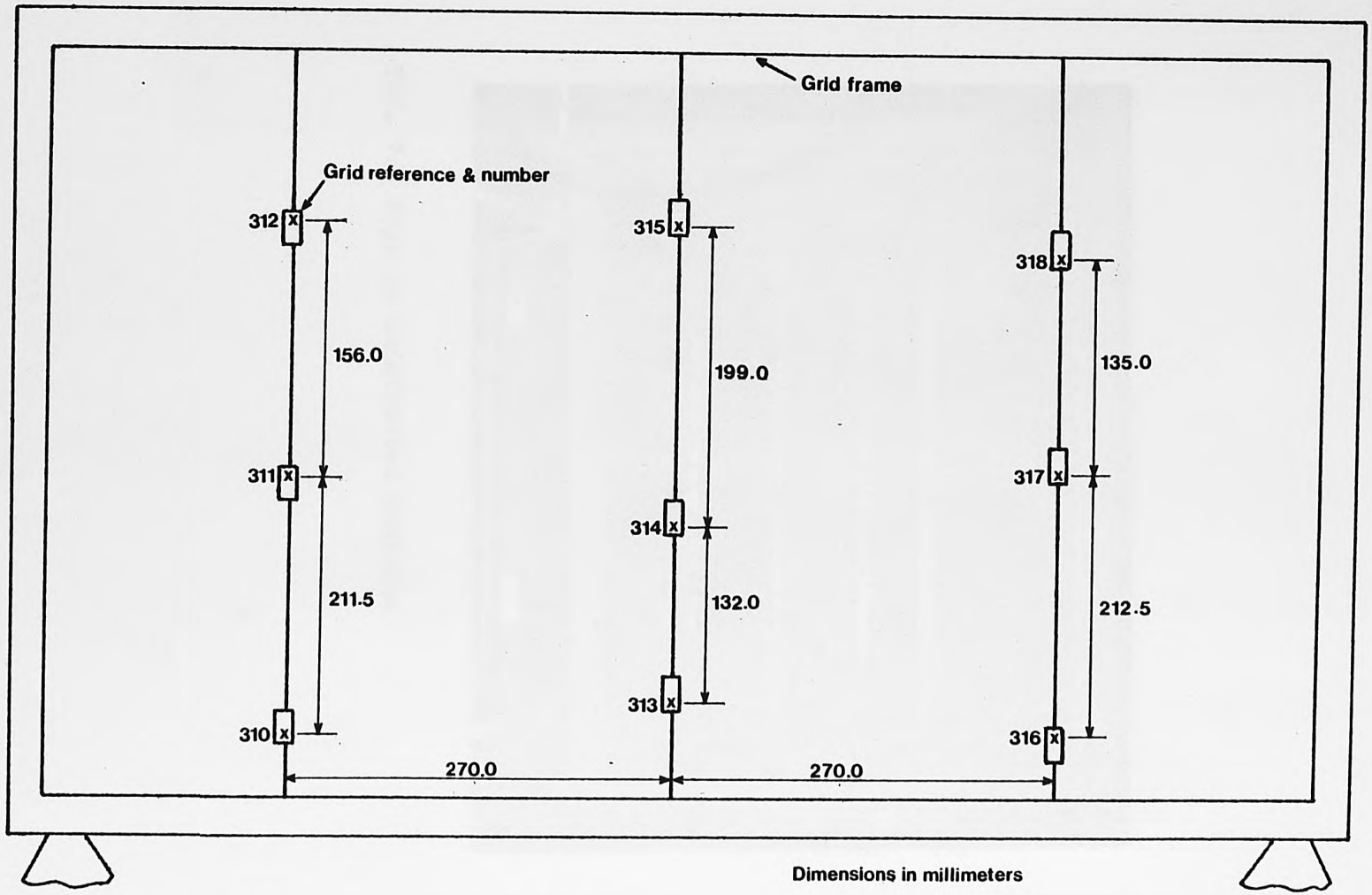

FIG. 7.7 Control grid

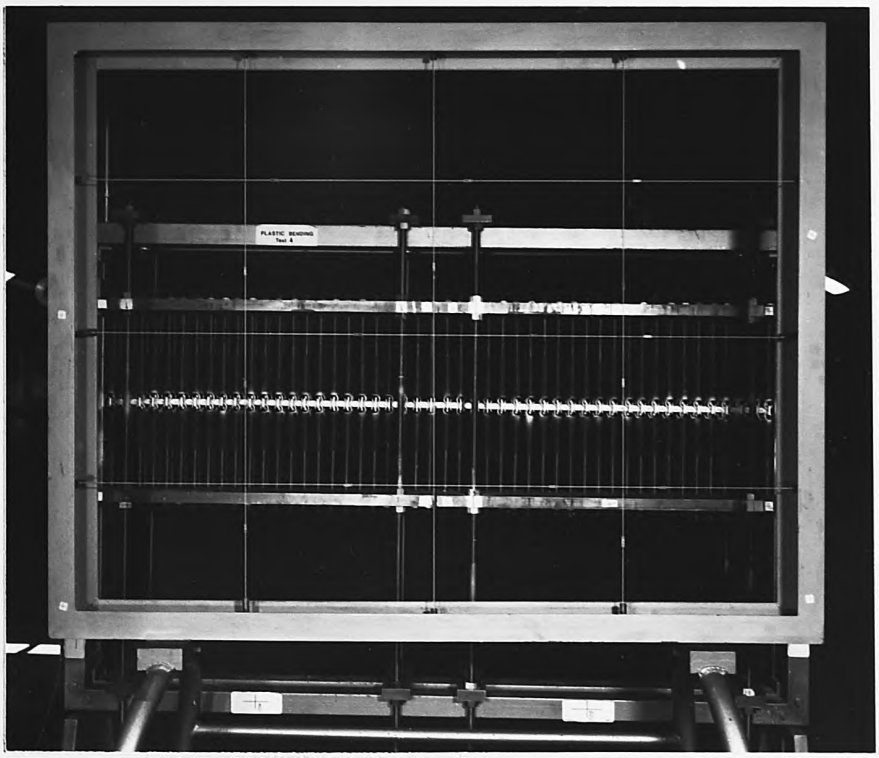

FIG. 7.8 Pipe in undeflected position

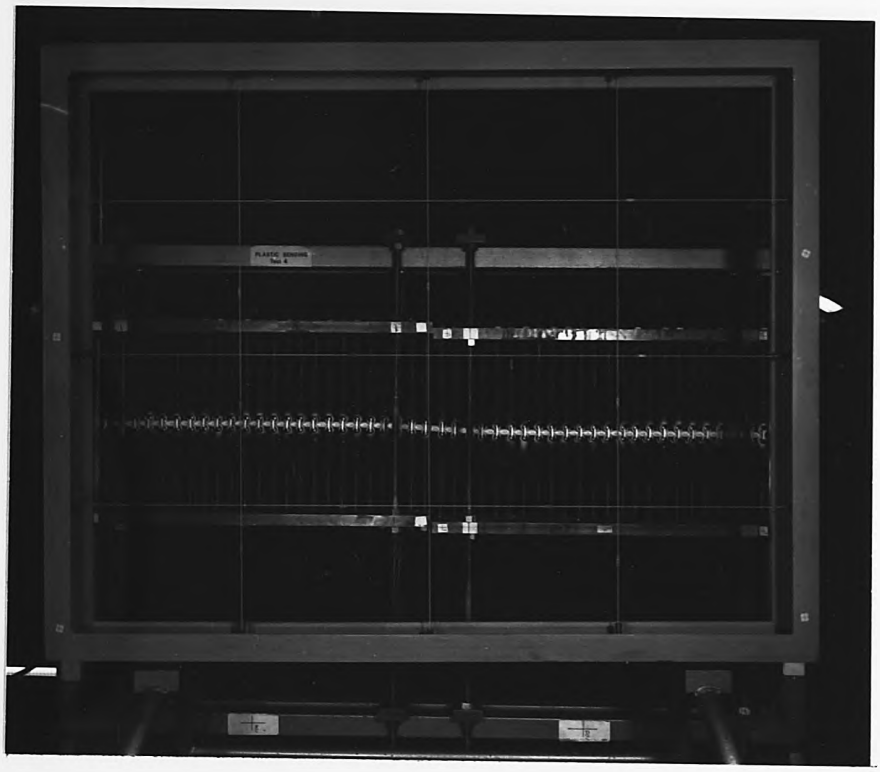

FIG. 7.9 Pipe in first displacement position

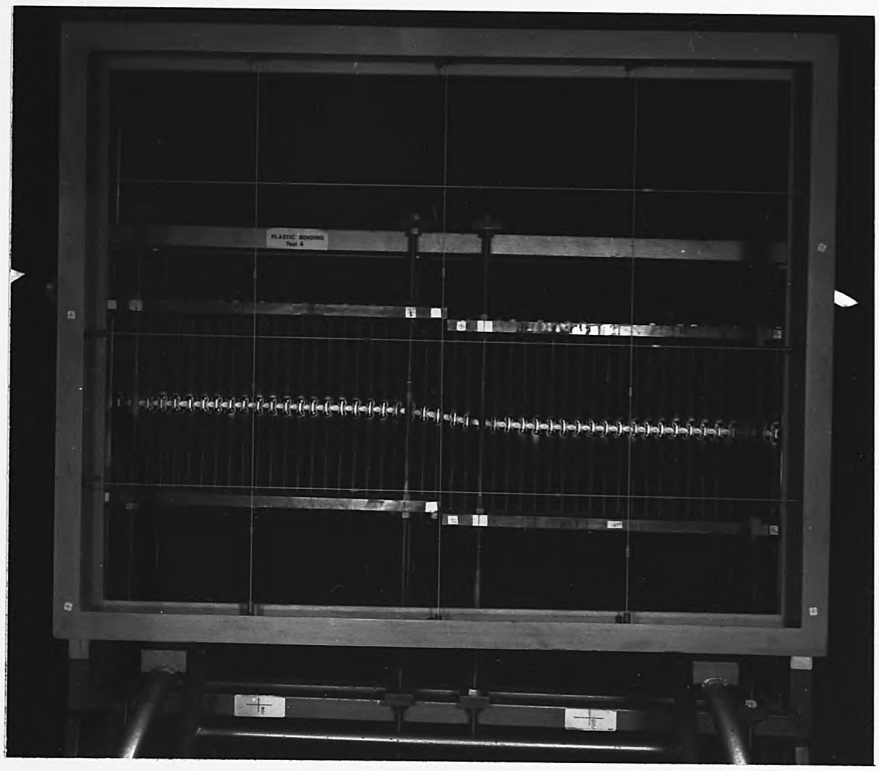

FIG.7.10 Pipe in second displacement position

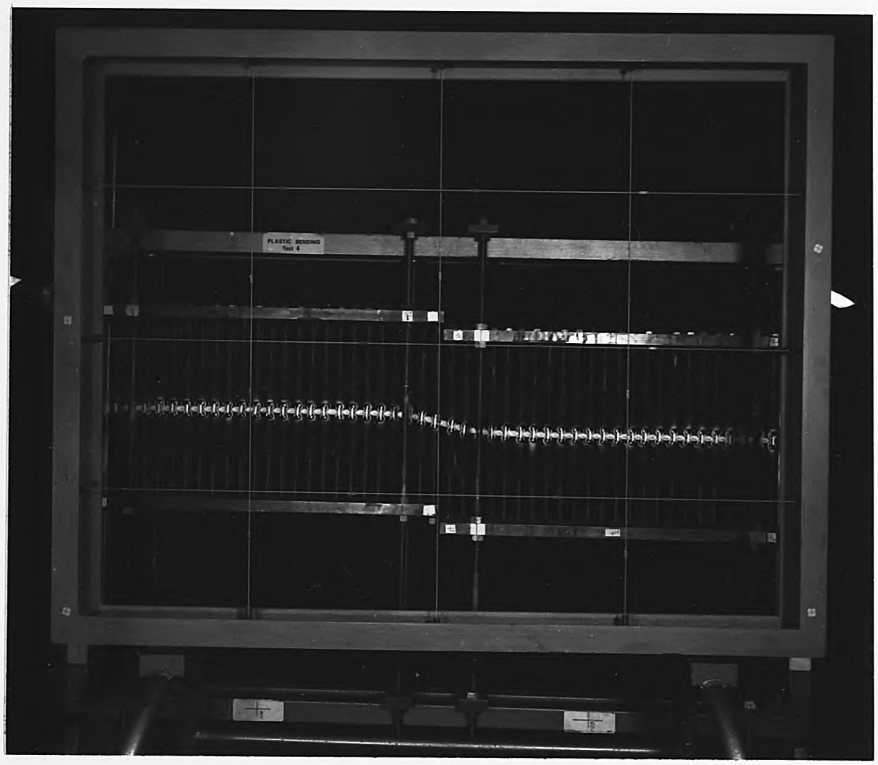

FIG. 7.11 Pipe in third displacement position

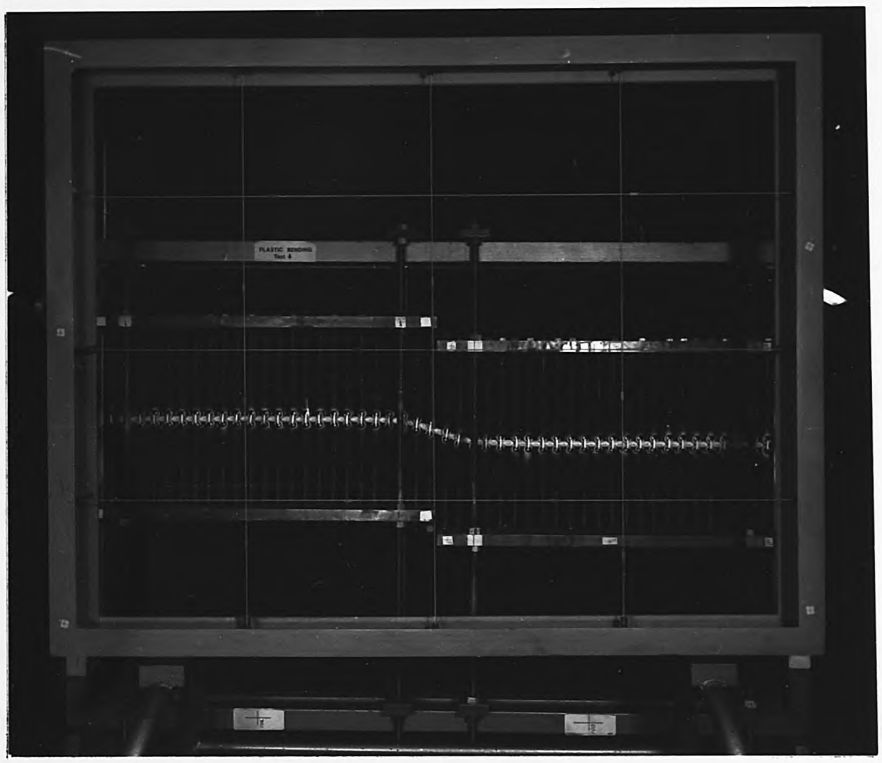

FIG. 7.12 Pipe in fourth displacement position

7.5 PHOTOGRAMMETRIC INTERPRETATION

The photographic negatives were analysed on a stecometer, which gives the overall x and y coordinates and also the changes in parallax, P_x and P_y between two points A and A', when the point A has been deflected to point A', Figure 7.13. It is the change in parallax which gives the displacements of the plates and the pipe.

When observing the negatives in the viewfinder, there appears to be a small circle in the image. If this circle lies in the same plane as the point under examination there has been no change in parallax. Rotation of the P_x control of the stecometer enables the operator to coincide the circle with the plane of any point under examination.

In order that P_x be the major parallax correction, it was necessary to orientate the photographic plates on the stecometer such that the pipe length was in the direction of the y-axis. The only corrections to P_y which were necessary were to compensate for any non-vertical displacement of the pipe. This orientation was chosen for its simplicity and speed in taking the readings from the photographic plates.

The values from the stecometer are only a set of arbitrary values, and thus have to be interpreted into actual values by the use of the photogrammetric control points on the grid frame. This was achieved by a computer analysis which was facilitated by a punch tape output from the stecometer.

The objective of the analysis was to determine the real displacements of the plates and the pipe. The real distances between the grid control points were known and by comparison with the values found from the stecometer it was possible to establish vertical and horizontal scale factors for the photograph.

However, since there may have been rotations about the x or y axes or both, or that the plane of the photographic plate may not have been parallel to the plane of the frame, two vertical scale factors were used, Figure 7.14. The left hand side scale factor, V_L was found using the known distance between the control grid points 310 and 312, Figure 7.7 and the right hand side scale factor V_R was found using the points 316 and 318. The horizontal scale factor, H, was found using the known distance between the points 310 and 316.

A linear interpolation equation of the form

$$v_p = \left(\frac{V_R - V_L}{H} \right) x_p + V_L$$

where

x_p = distance of point under consideration from the origin

v_p = appropriate scale factor

was then used to calculate the appropriate scale factor for any particular point.

It was found that the two vertical scale factors were practically the same, a difference of about 0·75%, which indicates that the photographic plane and the frame plane can be considered to be parallel to each other and also the unlikelihood of any rotations in the frame plane.

A computer programme was written to translate the stecometer readings into the actual plate and pipe displacements which are given in Appendix D, Table D.1 to D.4 and are shown graphically in Figures 7.15 to 7.18.

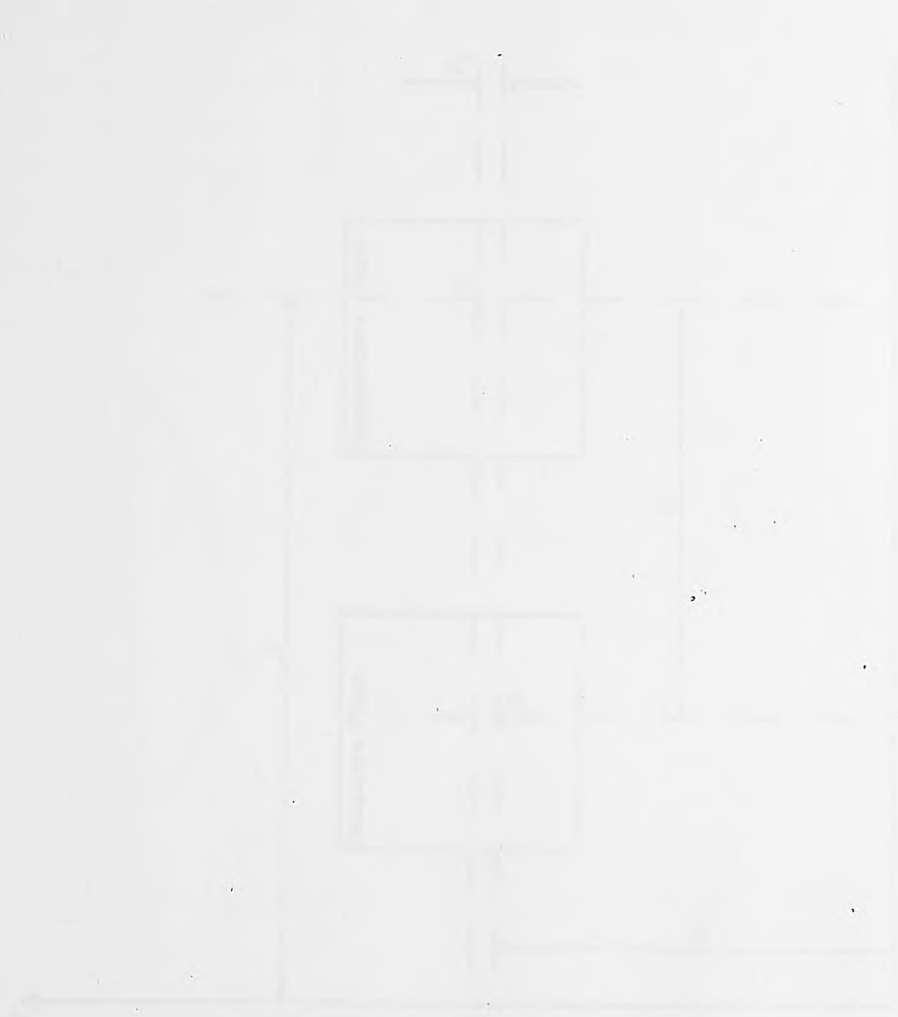

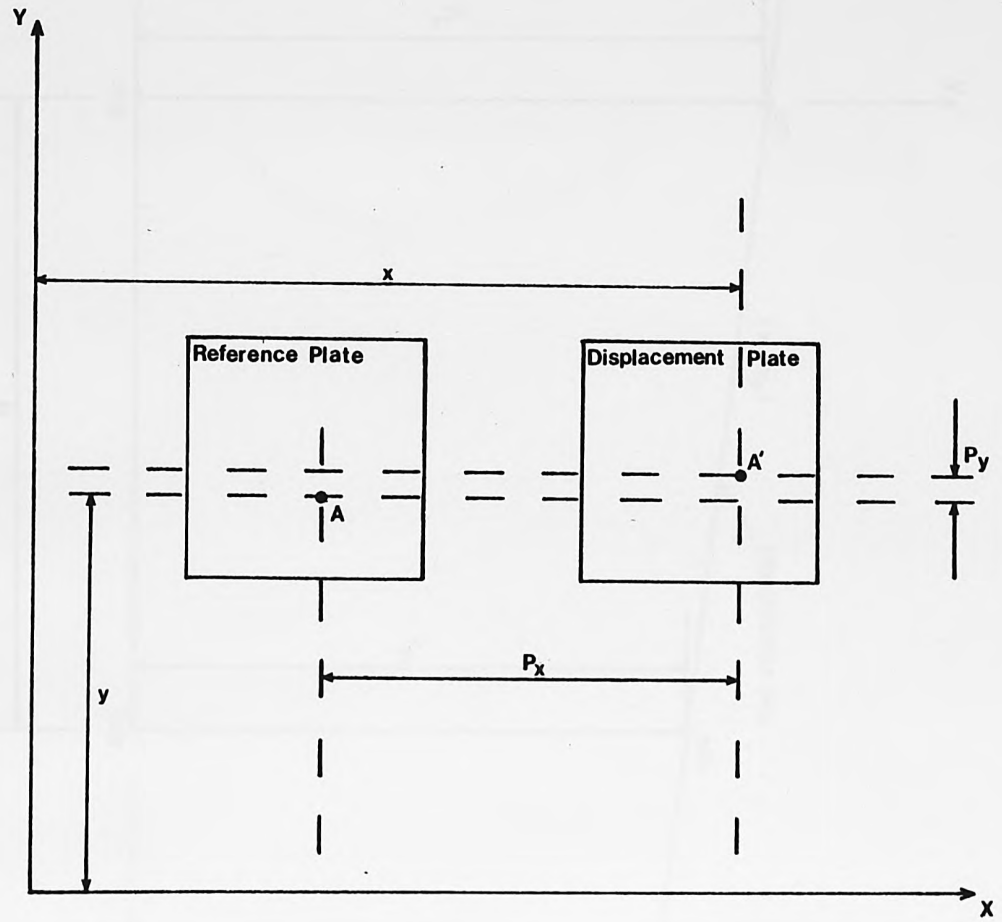

FIG. 7.13 Stecometer reference axes used in the photogrammetric interpretation of the photographic negatives

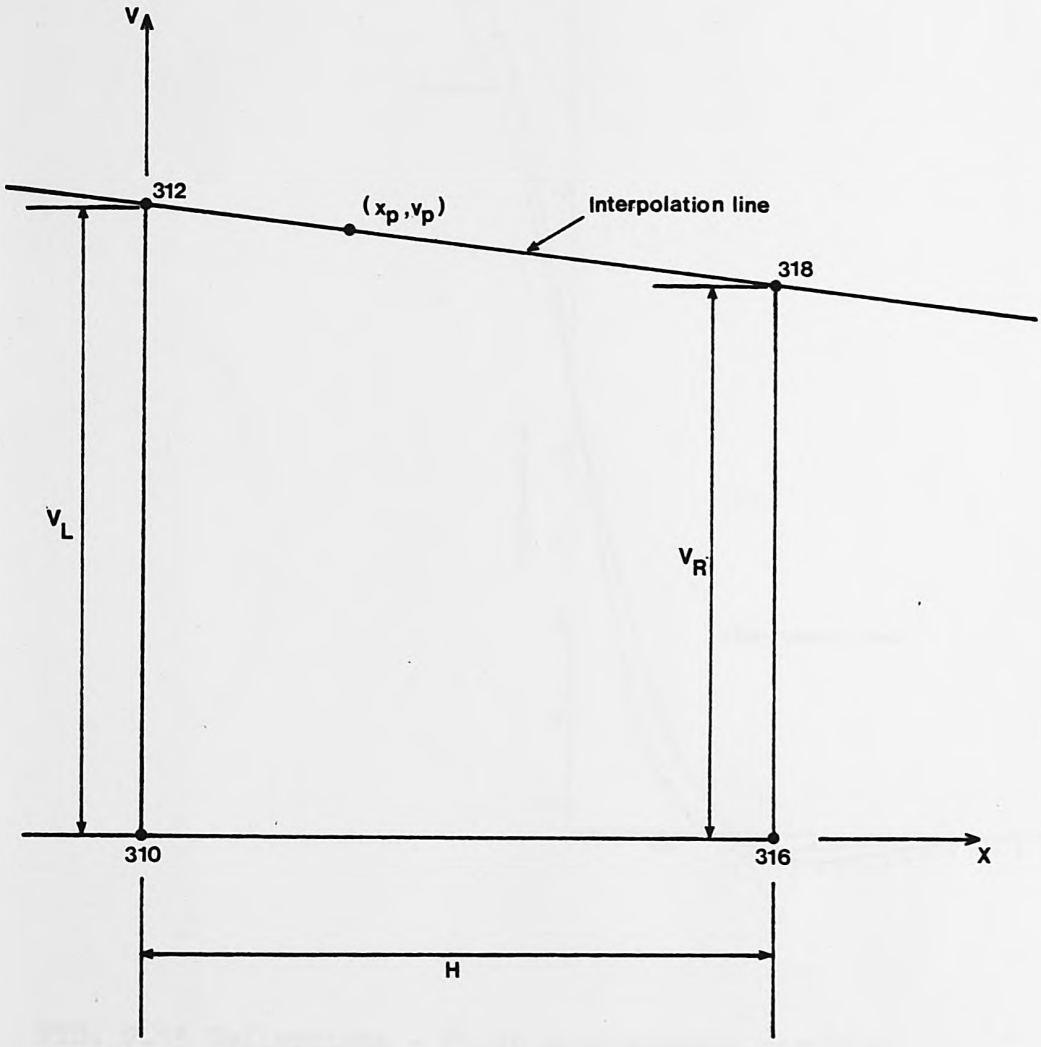

FIG. 7.14 Linear interpolation line for calculating the appropriate scale factors

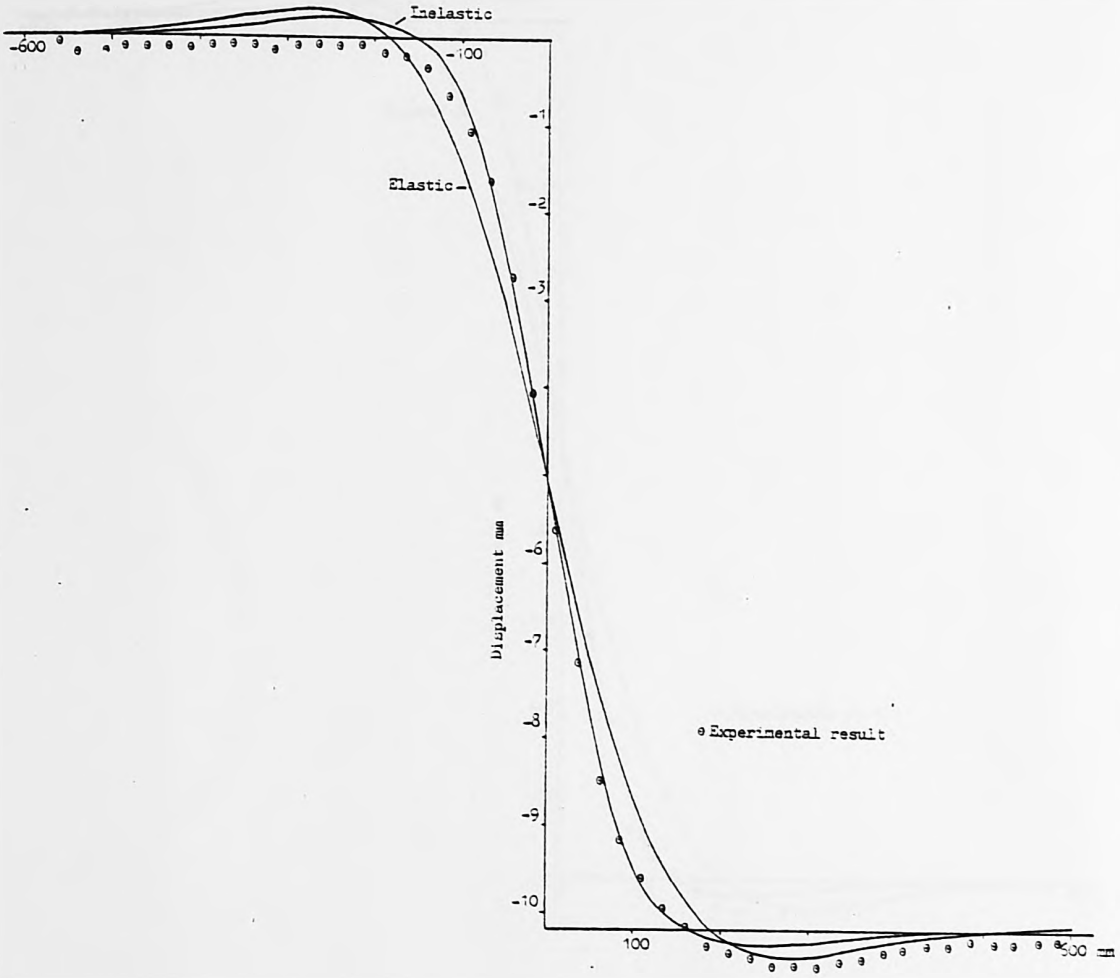

FIG. 7.15 Deflections - First displacement position

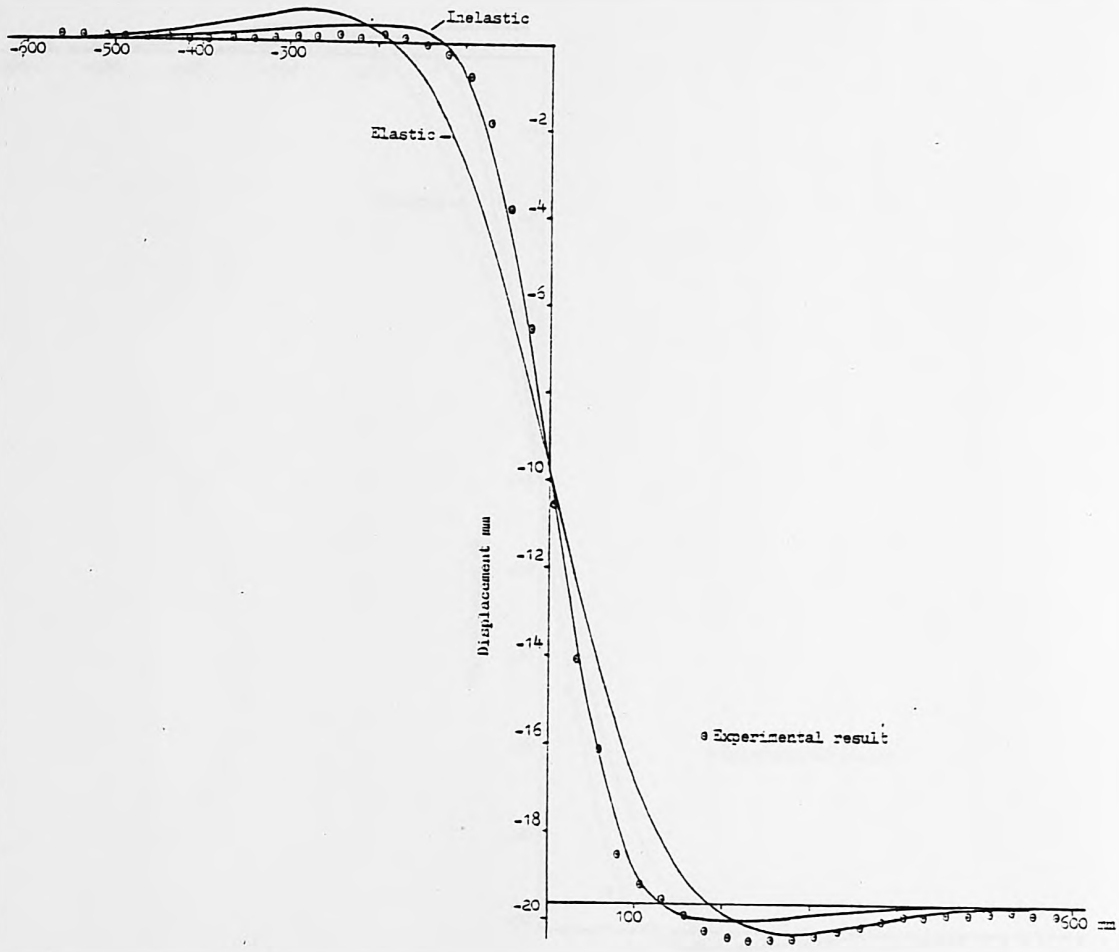

FIG. 7.16 Deflections - Second displacement position

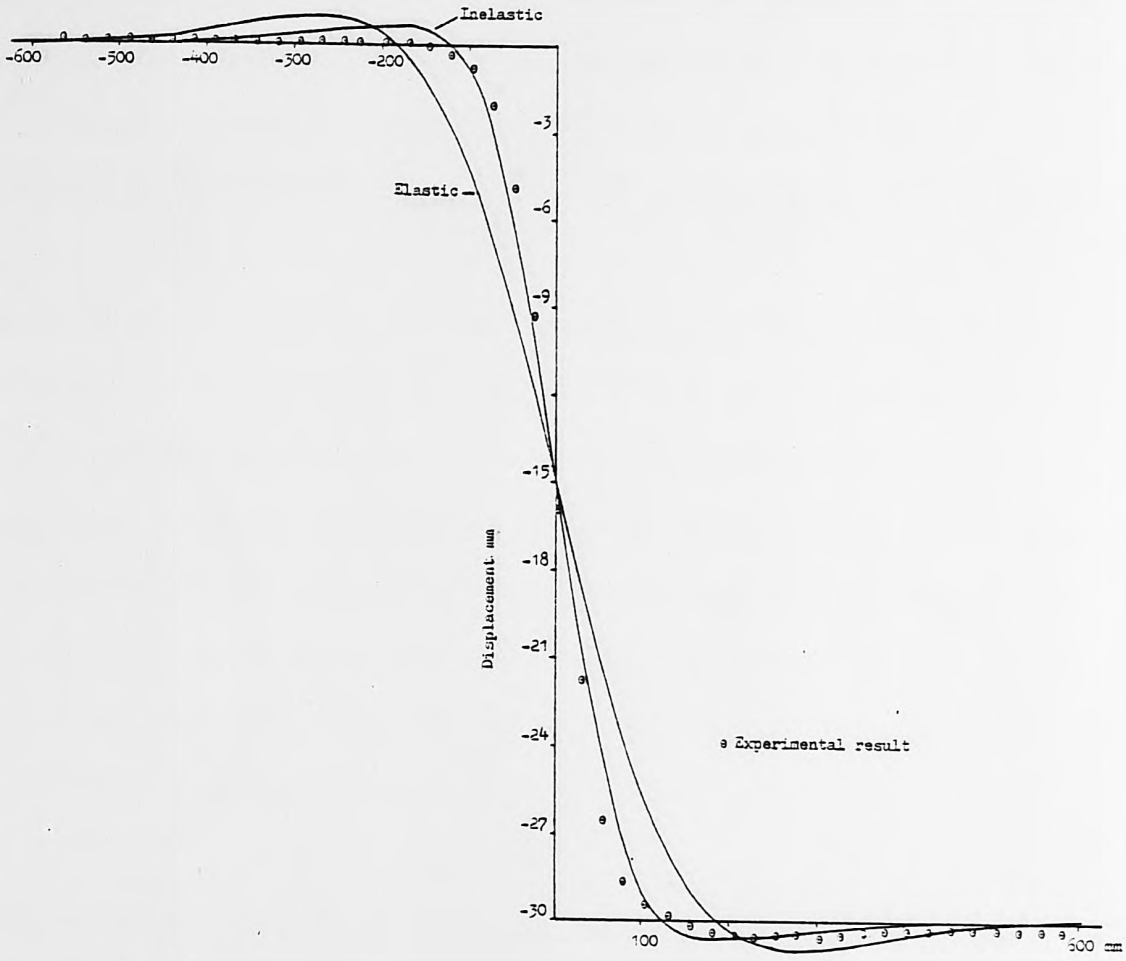

FIG. 7.17 Deflections - Third displacement position

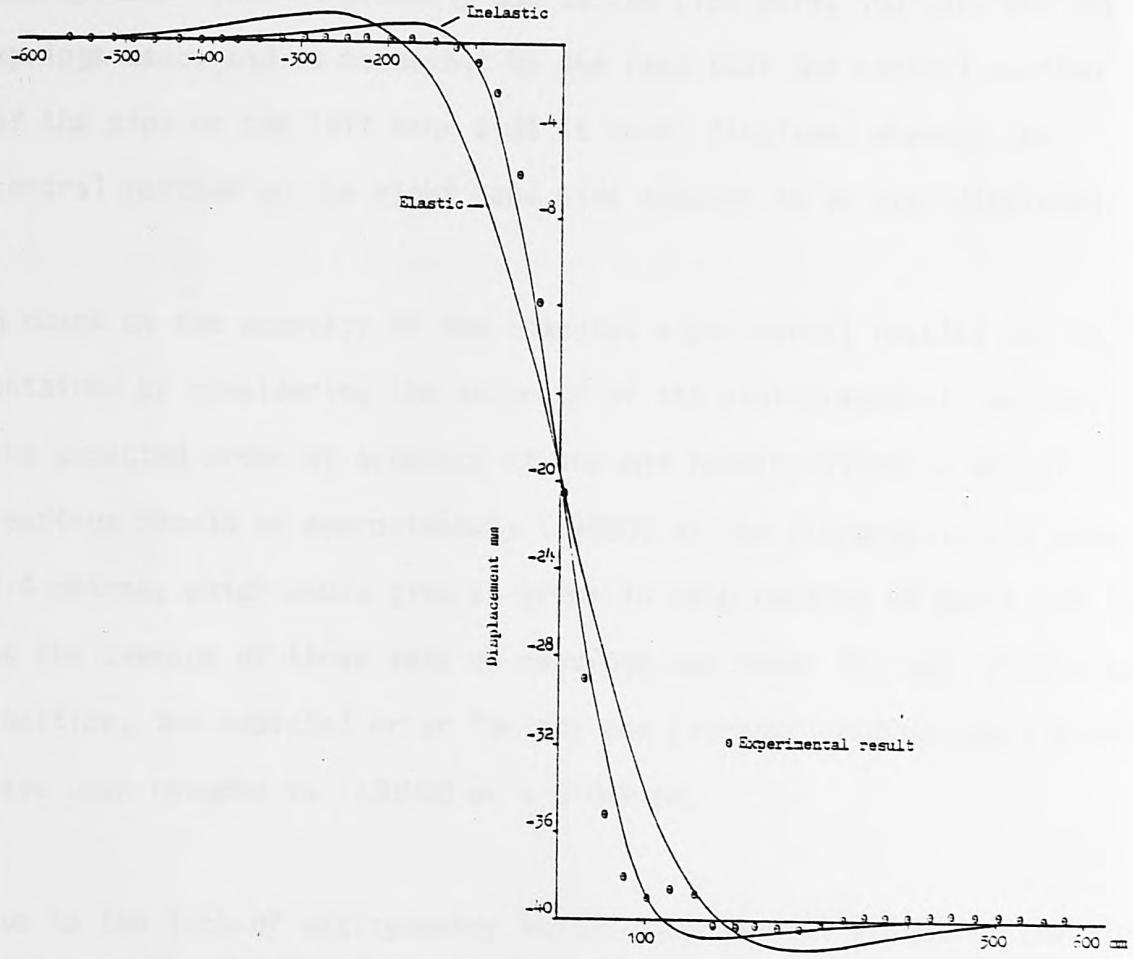

FIG. 7.18 Deflections - Fourth displacement position

7.6 DISCUSSION OF EXPERIMENTAL RESULTS

It is noticeable from Figures 7.15 to 7.18 that there is a lack of antisymmetry in all the displacement profiles. This suggests that the method of loading the pipe, that is, by lowering the plates on the right hand side, is not distributing the load uniformly throughout the system. This is probably due to the pipe being too soft for the springs used, and is borne out by the fact that the central portion of the pipe on the left hand side is under displaced whereas the central portion on the right hand side appears to be over displaced.

A check on the accuracy of the computed experimental results can be obtained by considering the accuracy of the photogrammetric method. The expected order of accuracy of any one reading within a set of readings should be approximately 1:10000 of the distance to the camera, 1·4 metres, which would give an error in each reading of about ± 0·14 mm. As the average of three sets of readings was taken for each displacement position, the expected error for any one averaged reading could probably have been reduced to 1:30000 or ± 0·045 mm.

Due to the lack of antisymmetry in the experimental values of the pipes displacements there is no conclusive evidence of their validity or non-validity in this case.

The mathematical model proposed to simulate the effect of differential ground displacement on a ductile pipe material was used with the experimental values of the ground resistance k_o , the elastic modulus E, the ratio of the inelastic and elastic moduli α_p and the yield stress σ_{et}. The linear elastic and inelastic values of

displacement and bending moment are given in Tables E.1 to E.4, Appendix E and Tables F.1 to F.4, Appendix F, respectively. The displacements have been added to Figures 7.15 to 7.18 and the bending moments are shown graphically in Figures 7.19 to 7.22.

Figures 7.15 to 7.22 show that the proposed model is simulating the expected reaction of a ductile material to an imposed differential displacement, both the deflections and bending moments are being redistributed from the linear elastic solution. It will also be noted from the figures that there is a fair degree of correspondence between the computed and experimental results in the region 100 mm each side of the origin.

Tables F.1 to F.4 also show that the depth of the inelastic front is penetrating further into the pipe and its range increasing with greater differential displacement, hence with loading on the pipe, which is consistent with known theoretical considerations, Timoshenko (59).

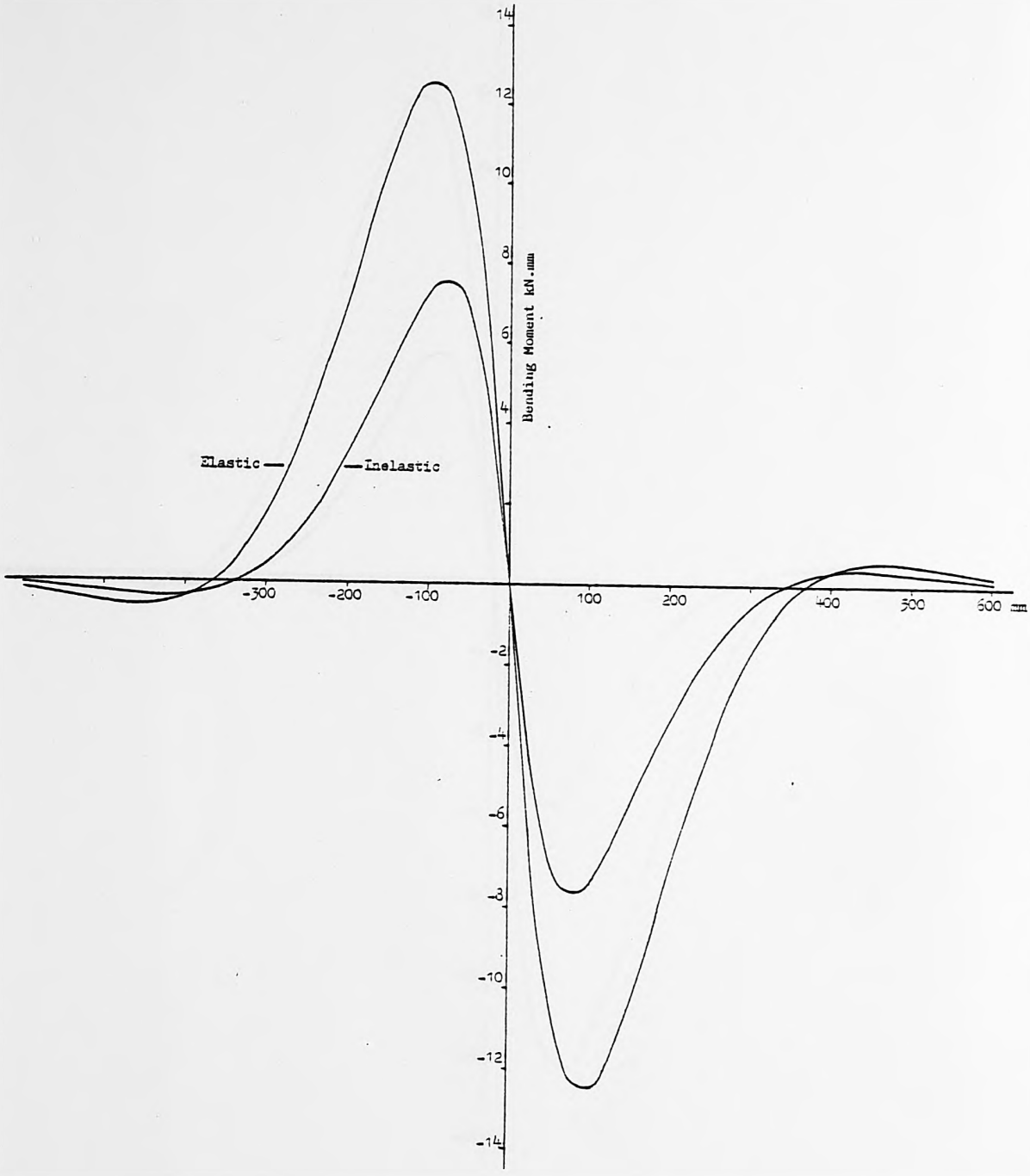

FIG. 7.19 Bending Moments - First displacement position

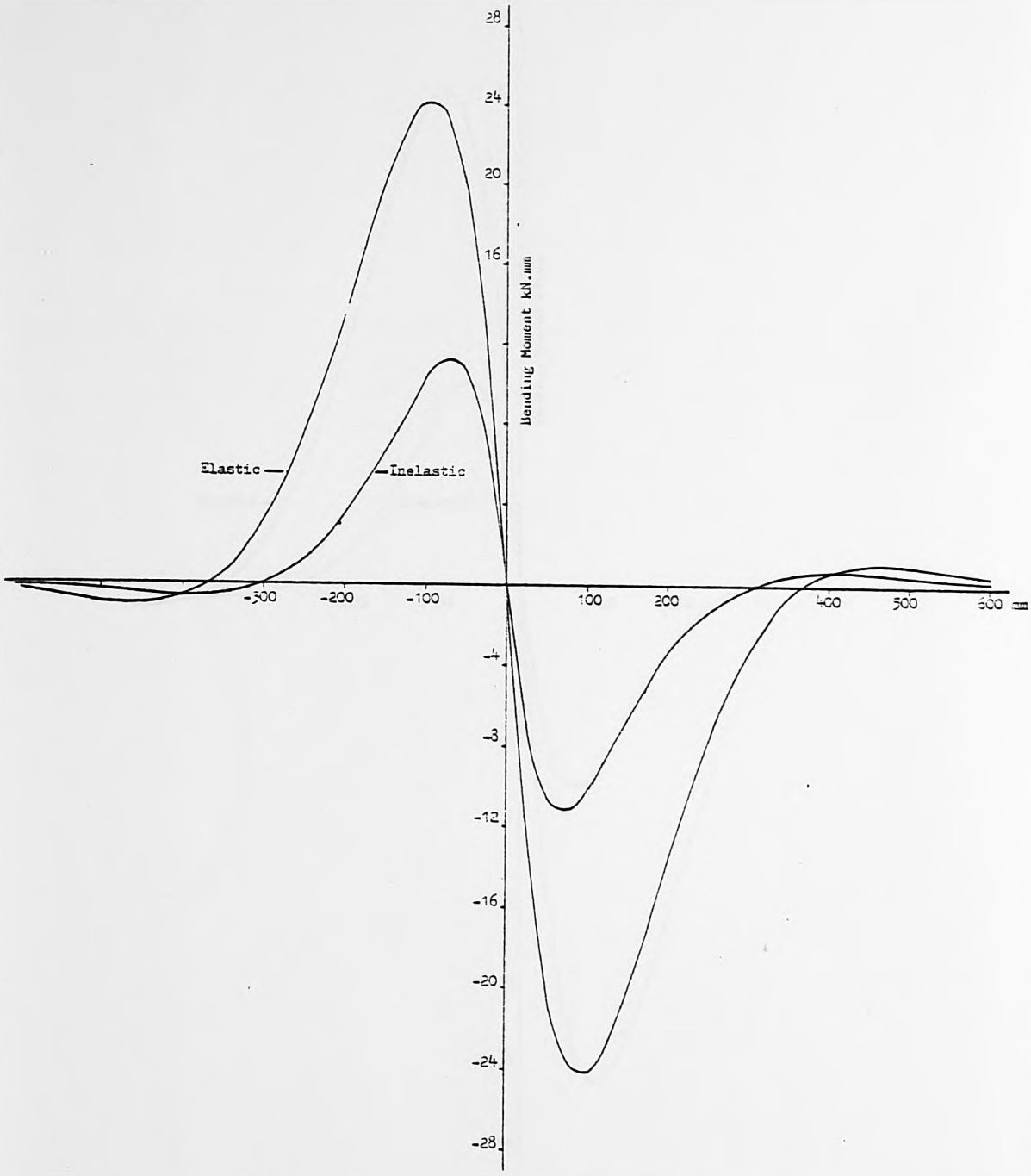

FIG. 7.20 Bending Moments - Second displacement position

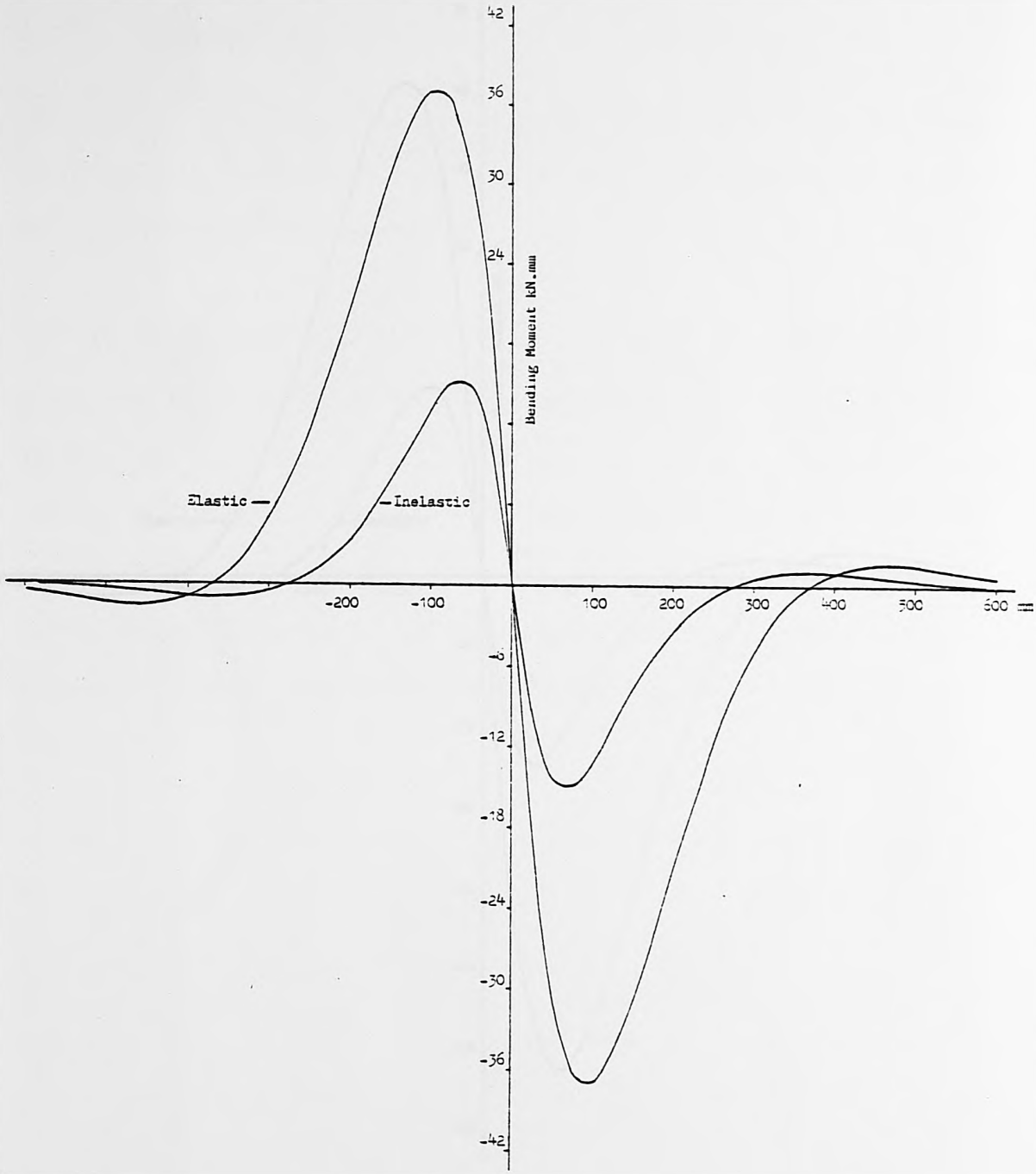

FIG. 7.21 Bending Moments - Third displacement position

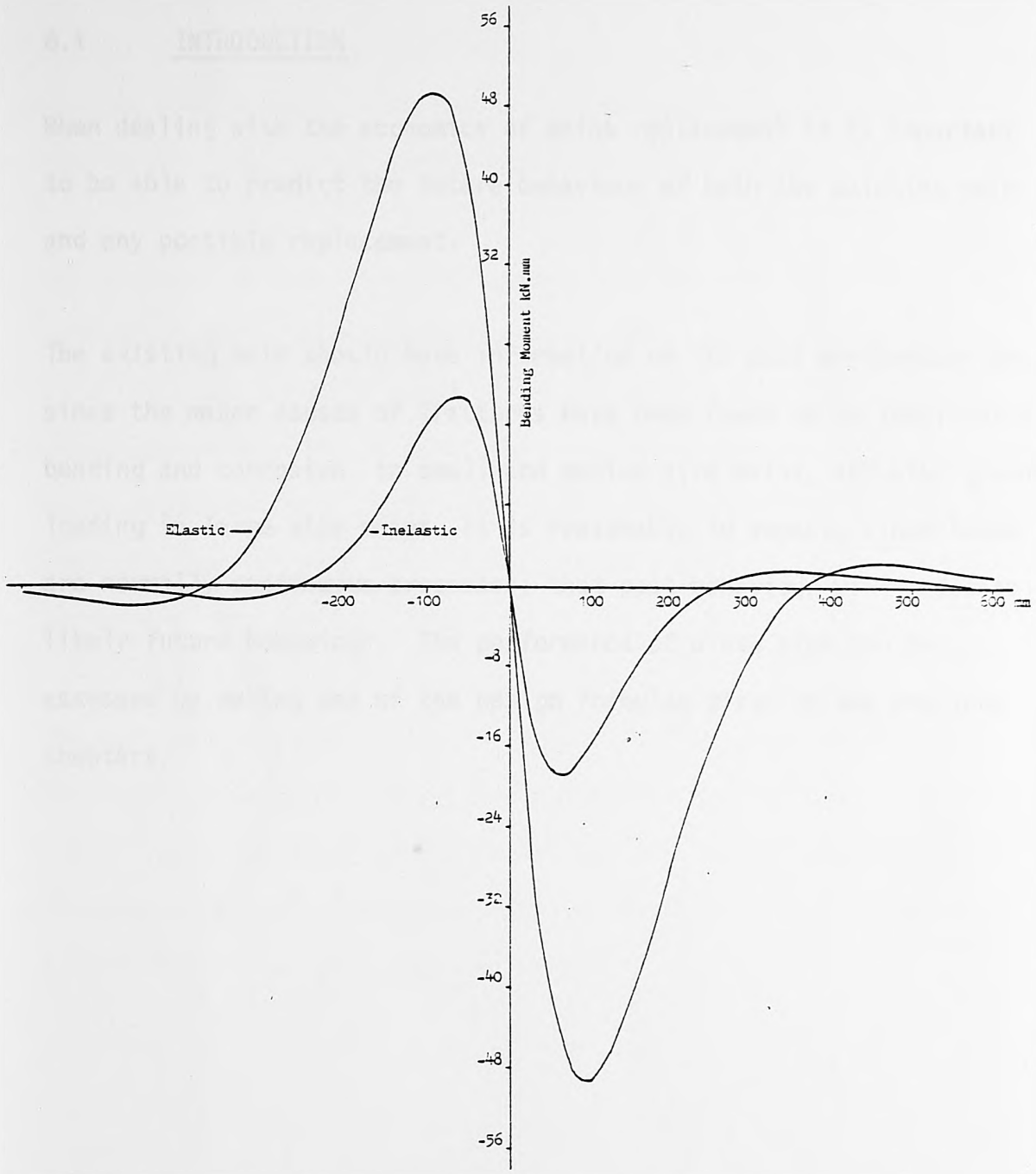

FIG. 7.22 Bending Moments - Fourth displacement position

CHAPTER 8

ECONOMICS OF MAINS REPLACEMENT

8.1 INTRODUCTION

When dealing with the economics of mains replacement it is important to be able to predict the future behaviour of both the existing main and any possible replacement.

The existing main should have information on its past performance and since the major causes of fractures have been found to be longitudinal bending and corrosion, in small and medium size mains, and also ground loading in large size mains, it is reasonable to expect, since these are normally continuous processes, that past behaviour will indicate likely future behaviour. The performance of a new pipe can be assessed by making use of the design formulae given in the previous chapters.

8.2 PIPE LIFETIME

In the discussion of mains replacement criteria the term 'pipe lifetime' is often used and values for the useful lifetime of various pipeline materials have been quoted. The term 'pipe lifetime' is a vague concept because pipes suffer from increasing deterioration rather than what can be termed sudden death.

The decrease in pipe strength is sometimes based on theoretical considerations relating corrosion with time. These are inaccurate since they are normally based on the assumption that failure occurs at the first penetration of corrosion. Romanoff (60) and Kirby (61) both quote evidence that a fully graphitised pipe can often have considerable strength, and in areas with little ground loading or movement the pipe may have a long residual life.

The economic lifetime of a pipe is the time until the point where continuing with the existing pipe would mean a greater cost than installing a new one. At this point problems such as fractures, discoloured water, flow and pressure problems will have increased to such a level that replacement is necessary.

8.3 REPLACEMENT POLICIES

In a draft report by The Severn Trent Water Authority (40), it is stated that statistics on the performance of mains in existing systems tend to indicate two principal types of burst patterns, Figure 8.1, in which Lines (1) and (2) are typical of iron and asbestos cement and indicate continual repair rather than replacement because the failure rate is constant. Line (3) is more typical of uPVC and shows a continuously increasing failure rate which implies a replacement age.

The replacement policy recommended by the report is to determine an acceptable failure rate and use this as a basis for replacement, by comparing a main's current failure rate, obtained from the history of each main, with this base value. An estimation of the base rate would involve the examination of the pattern of failures over several years since the weather can have a great effect on it.

In economic terms the time to replace a main is the point when the expected cost of the failures in the next year is equal to that of putting off replacement for one year. The estimate of the base rate of failure is then given by

$$r' = \frac{C_r R'}{C_b} \qquad \ldots \ldots \ldots \ldots \ldots \qquad (8.1)$$

where r' = base rate of failure

C_r = cost of replacement per specified length of main

C_b = cost of repair of specified main

R' = discount rate

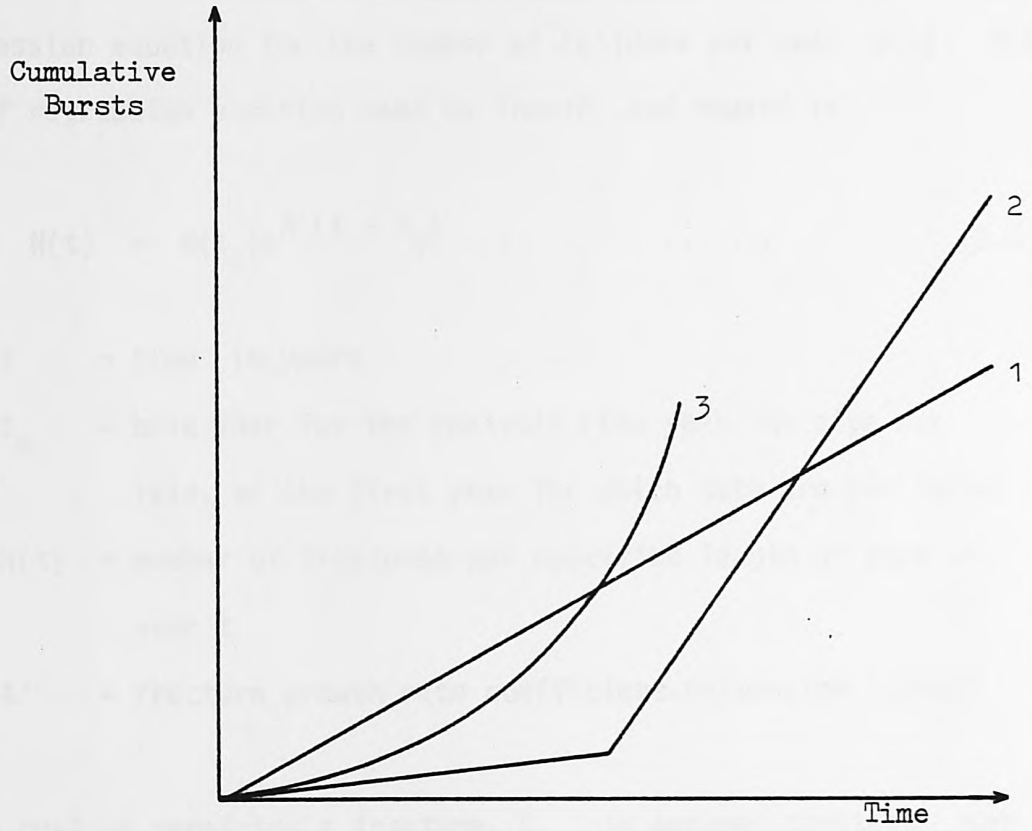

FIG. 8.1 Burst patterns as given by Severn Trent Water Authority

A different approach to a mains replacement policy is taken by Shamir and Howard (62), who produced a regression equation for forecasting the number of future failures in a particular length of pipe. An economic analysis, by which the optimal time for replacement is determined, can then be undertaken using the regression equation.

Pipe fracture data for a single pipe, several pipes with similar characteristics or the whole area of a network can be used to develop a regression equation for the number of failures per year, N(t). The form of regression equation used by Shamir and Howard is

$$N(t) = N(t_o)e^{A'(t - t_o)} \quad \ldots \quad \ldots \quad \ldots \quad \ldots \qquad (8.2)$$

where t = time in years

t_o = base year for the analysis (the year the pipe was laid, or the first year for which data are available).

$N(t)$ = number of fractures per specified length of pipe in year t

A' = fracture growth rate coefficient (dimension 1/year)

If the cost of repairing a fracture, C_b, is assumed constant over time, then the cost of repairing the fractures in a specified length of pipe in the future year t is

$$C_m(t) = C_b\, N(t_o)e^{A'(t - t_o)} \quad \ldots \quad \ldots \quad \ldots \qquad (8.3)$$

If the present year is denoted by t_p, and the (non-inflationary) discount rate is R', then the present cost of repairing fractures is

$$\frac{C_m(t)}{(1 + R')^{t - t_p}}$$

If t_r is the year in which the pipe will be replaced, then the present value of repairs from year t_p to year t_r for the specified length of pipe is

$$P_m(t_r) = \sum_{t=t_p}^{t_r} \frac{C_b\, N(t_o) e^{A'(t - t_o)}}{(1 + R')^{t - t_p}} \quad \ldots \quad (8.4)$$

If the new pipe will not incur any fractures, then $P_m(t_r)$ represents all future maintenance cost. If the new pipe is expected to have fractures, Equation (8.4) can be modified to take into account any assumed fracture regression equation.

The cost of replacing a specified length of pipe, expressed in the same constant cost as C_b is C_r. The present value in year t_p of replacing specifield length of pipe in year t_r is

$$P_r(t_r) = \frac{C_r}{(1 + R')^{t_r - t_p}} \quad \ldots \ \ldots \ \ldots \quad (8.5)$$

The optimal timing for replacement is then that year for which the total cost

$$P_T(t_r) = P_r(t_r) + P_m(t_r) = \frac{C_r}{(1 + R')^{t_r - t_p}} +$$

$$+ \sum_{t=t_p}^{t_r} \frac{C_b\, N(t_o) e^{A'(t - t_o)}}{(1 + R')^{t - t_p}} \quad \ldots \quad (8.6)$$

is a minimum.

Differentiating Equation (8.6) with respect to t_r, setting equal to zero and solving, gives the optimal value of $t_r(t_r^*)$ as

$$t_r^* = t_o + \frac{1}{A'} \text{Ln} \left[\frac{\text{Ln}(1 + R')C_r}{N(t_o)C_b} \right] \quad \ldots \quad \ldots \qquad (8.7)$$

The analysis can be carried out in similar manner if a linear or polynomial form of growth is found to fit the fracture data.

If the increase in fractures is linear and is given by

$$N(t) = N(t_o)A' (t - t_o) \quad \ldots \quad \ldots \quad \ldots \quad \ldots \qquad (8.8)$$

then the optimal timing for replacement would be given by

$$t_r^* = t_o + \frac{\text{Ln}(1 + R')C_r}{A'N(t_o)C_b} \quad \ldots \quad \ldots \quad \ldots \quad \ldots \qquad (8.9)$$

Assuming the optimal time for replacement in Equation (8.9) is $t_o + 1$ years and t_o is the present year then

$$A'N(t_o) = \frac{C_r}{C_b} \text{Ln}(1 + R') \quad \ldots \quad \ldots \quad \ldots \quad \ldots \qquad (8.10)$$

which gives a base rate of failure similar to the one used by The Severn Trent Water Authority (40), Equation (8.1). The only difference being, the difference in value between R' and Ln(1 + R'), which is minimal for small values of R'. For example, if the cost of repairing a fracture is £350 and the cost of relaying 100 metres of this main is £35 per metre, then the ratio C_r/C_b is 10 and using this in Equations(8.1) and (8.10) gives the following rates of failure per year per 100 metres of main

For R' = 5% r = 0·5 and $A'N(t_o)$ = 0·49

R' = 10% r = 1·0 and $A'N(t_o)$ = 0·95

If the rates of fracture of individual pipes or groups of pipes is known, then the use of Equations (8.1) or (8.10) will give an estimate of which of these pipes will need replacing in the forthcoming year. A more comprehensive investigation of the pipe network system would be gained by the use the analysis suggested by Shamir and Howard (62) as this, once the requisite fracture regression equations have been determined, would provide information on pipes needing replacement in the near future.

The model proposed is non-inflationary, so in years of high inflation the model should be used many times so as to compensate for the change in interest rates, and any mains that have been proposed for replacement within a specified time period should be re-examined for possible earlier replacement or for deferment as costs permit.

8.4 ECONOMICS OF RELAYING OR RELINING

When a water main is suffering from increasing fractures through internal corrosion there are two possible remedies:

(i) Relaying

(ii) Relining

Assuming that relining is possible without seriously damaging or weakening the pipe then it is possible to calculate the time period that the relining would have to last for it to be worthwhile to defer replacement. The Severn Trent Water Authority (40) gives the following equation

Let C_d = cost of relining per specified length of main

Then $$C_r = \frac{C_r}{(1 + R')^t} + C_d \quad \ldots \quad \ldots \quad \ldots \quad \ldots \qquad (8.11)$$

which gives

$$t = \frac{\text{Ln}\left(\frac{C_r}{C_r - C_d}\right)}{\text{Ln}(1 + R')} \quad \ldots \quad \ldots \quad \ldots \quad \ldots \quad \ldots \qquad (8.12)$$

t is the time period relining would have to last for it to be economical.

If the cost of relaying 100 metres of mains is £35 per metre and the cost of relining with cement-mortar is £10 per metre then with a 5% discount rate, t = 7 years and with a 10% discount rate, t = 3.5 years. Since cement-mortar lining will last considerably longer than these figures, it will be in most cases, cheaper to reline.

It is further stated that the decision to replace the main rather than reline it will depend on the ability of the main to withstand the lining process and the best measure of this is the extent of graphitisation. If the fracture rate of the main is already near the replacement rate given by Equation (8.1) or (8.10), then early replacement will be better than relining.

If it has been decided to lay a new main then due consideration must be given to which pipe material will be the most suitable. An analysis of the type and rate of fractures in the old main will give information as to whether the area suffers from ground movement or corrosion or both and whether the pipe has internal corrosion problems or not.

The choice of materials in the water industry, except in special circumstances, is usually limited to three; ductile iron, asbestos cement and uPVC.

Ductile iron is the strongest of the three but is also the most expensive and can corrode both internally and externally. Both can be greatly reduced, at extra cost, by external sleeving and internal lining.

Both asbestos cement and uPVC need careful handling during storage, transportation and laying and can be easily damaged by accident once laid. Asbestos cement can be attacked by certain soils (those containing sulphates in particular) and there are important health aspects with regard to the use of this material. uPVC deteriorates with age, is susceptible to failure due to surge and has special backfill requirements for large diameters.

8.5 ECONOMICS OF PRELINING AND SLEEVING

If the material chosen when relaying is ductile iron then the economics of prelining and sleeving can be investigated as follows.

If C_p = cost of prelining per specified length of main

C_s = cost of sleeving per specified length of main

then the equation which gives the number of years, t, that an unlined pipe would have to be in service with no internal corrosion problems for it to be economical to lay an unlined pipe as opposed to a prelined pipe and reline it when necessary is

$$C_r = (C_r - C_p) + \frac{C_d}{(1 + R')^t} \quad \ldots \quad \ldots \quad \ldots \qquad (8.13)$$

which on rearrangement gives

$$t = \frac{Ln(C_d) - Ln(C_p)}{Ln(1 + R')} \quad \ldots \quad \ldots \quad \ldots \quad \ldots \qquad (8.14)$$

If the cost of relining 100 metres of main is £10 per metre and of prelining is £1 per metre, then at a discount rate of 5% the unlined pipe would have to last 47 years, and at a discount rate of 10%, 24 years. It can be seen that laying unlined pipes can only be justified economically in cases where it is certain that there would be no internal problems for a considerable number of years.

In the case of sleeving, suppose a corrosive soil might lead to the first failure after t_1 years, then for polythene sleeving to be economical it would have to delay this failure to a number of years, t, given by the equation

$$C_r + \frac{C_b}{(1 + R')^{t_1}} = (C_r + C_s) + \frac{C_b}{(1 + R')^{t}}$$

... ... (8.15)

which gives

$$t = \frac{\text{Ln}\left[C_b(1 + R')^{t_1}\right] - \text{Ln}\left[C_b - C_s(1 + R')^{t_1}\right]}{\text{Ln}(1 + R')}$$

... ... (8.16)

If the cost of a fracture is £350 and the cost of sleeving 100 metres of main is £1 per metre and the soil may cause this length of main to have a fracture after 10 years, then the use of polythene sleeving would have to delay this fracture until 22 years, discounting at 5% and 24 years discounting at 10%, which is a plausible decrease in the rate of corrosion. In a less aggressive soil, where the first burst might not occur until after the 20th year, bursts would have to be delayed indefinitely with a 10% discount rate or until after 49 years with a 5% discount rate. In this case sleeving would not be economically advantageous.

8.6 FRACTURE DATA BASE

The economic analysis of mains replacement relies on the premise that the rate of fracture of a particular pipe is known. This is not always the case with every water undertaking, therefore it is suggested that a history and record of fractures for each main should be maintained. The data base could be a manual system, but the best results would probably be obtained from a computerised system.

The advantage of a computerised system being, its faster subsequent analyses of the stored data. A history, fracture and maintenance data base has been set up for use in one of the areas of British Gas, Trewin, Robinson and Howell (63), who report its many varied uses, not only to produce a history of the fractures that have occurred on the main but also to produce maintenance work sheets for the labour force, comparative costings and any other information that may be necessary for further analyses.

The importance of a record system is paramount if the state of a rectriculation is ever required to be monitored, not necessarily a computerised system but a system, ideally a universal system of base records. A system based on the record/history of mains card and fracture report form, Figures 1.1 and 1.2 would provide such, a basic, although may be not ideal, system.

CHAPTER 9

CONCLUSIONS

9.1 ANALYSIS OF FRACTURE DATA

An analysis of the types of fracture experienced by cast and spun iron water mains has indicated that the majority fail due to a transverse split.

The other major types of fracture are longitudinal splits, blow outs, and holes and perforations.

The rate of each type of fracture varies from one location to another depending on whether the soil is corrosive or not.

The highest rates of transverse fracture occur in small diameter mains and decrease with an inverse proportionality as the size of the main increases.

There is a correspondence between the rate of transverse fracture and the theoretical weakness of the pipe in bending which indicates that longitudinal bending is a primary mechanism in pipe fractures.

The other primary mechanisms for the fracture of small and medium sized mains is corrosion, and for large diameter mains, ground loading.

A correlation between a drop in air temperature to a few degrees below that of the ground at a depth at which water mains are normally laid (0·9 to 1·0 metres) and an increase in the rate of transverse fracture has also been found. It is not necessary for the air temperature to drop below freezing point for the phenomenon to occur, but if it does then an even more dramatic increase in the rate of transverse fracture is observed. Similar experiences have been noted in gas mains.

Ground loading usually occurs as the result of an external influence, such as traffic or frost loading.

An increase in the rate of fracture of water main(s) is usually experienced in roads, which are not suitable and/or have not been upgraded due to diversions, when the volume or weight of traffic is increased. The reverse is also true.

The effect of frost loading has been investigated in the USA and it was found that by the time frost penetration had reached 2 ft, the recorded load on a pipe with a cover of 4·5 ft had almost doubled.

An example of the dramatic increase in the rate of transverse fractures during prolonged periods of sub-zero temperatures was observed in London during the winter of 1962/63, when over a period of 46 days, 3091 fractures were recorded compared to the then annual average of 2200 fractures.

A correspondence between an extra loading due to frost and an increase in the number of fractures is indicated by the fact that the ground at the Kew Observatory in London was frozen to a depth of at least 1 ft.

Ground loading, is a secondary effect in small and medium size mains, as the cross-section of these pipes is usually strong enough to withstand the extra pressure, its effect is only damaging after the pipe has been stressed by longitudinal bending or the strength of the pipe has been reduced by the effects of corrosion.

The usual result of ground loading is to produce a longitudinal split in a large diameter main and either a transverse or longitudinal split in a small or medium diameter main.

A form of corrosion known as fissure corrosion has been found in spun iron mains. Its prerequisites being both graphitisation and longitudinal stress.

Investigations into the rate of transverse fracture in spun iron mains indicates that they are fracturing at a higher rate than cast iron mains. Fissure corrosion has been found to be an additional cause of transverse fractures in spun iron mains.

The other much used pipe material for which there is sufficient fracture information to be able to draw reliable conclusions is asbestos cement.

This is also a brittle material and an analysis of fracture data shows the same vulnerability to transverse fractures in small diameter mains as with cast and spun iron.

There is insufficient information regarding the performance of the newer pipe materials, ductile iron and plastics, for any reliable analyses to be carried out.

9.2 ELASTIC MATHEMATICAL MODEL OF LONGITUDINAL BENDING

A linear elastic mathematical simulation of the effect of longitudinal bending on a buried pipeline, using the theory of a beam on an elastic foundation, was used to develop design formulae.

The design formulae were used to give values of the rupture shear force and the differential displacement necessary to fracture various sizes of cast iron and spun iron pipes in homogeneous soils of various stiffnesses.

The distance between the points of maximum bending moment induced in the pipe by differential displacement was also calculated, and it was found that this distance was less than the length of a single pipe which indicates that even with flexible joints a pipe can be put at risk by this mode of bending.

One way in which outside interference may put pipelines at risk from differential displacement is due to adjacent trench excavations.

The model was also used to compare the performance of different iron pipeline materials and pipe sizes in the elastic range. The superiority of ductile iron pipe in resisting fracture due to longitudinal bending is clearly demonstrated.

The formulae were used to show that the ground has the capacity to produce the level of stress, by differential displacement, in both spun and ductile iron pipes, at which fissure corrosion is known to occur.

Asbestos cement pipes were also analysed and were found to be very susceptible to fracture from longitudinal bending.

The case of a point load acting on a surface pipeline was investigated and a comparison was made between the values of shear or displacement necessary to fracture a pipeline in this mode of bending and that of differential displacement. A pipeline built on the surface would definitely be at risk from traffic loading.

The effect of a concentrated surface load acting on a buried pipeline was obtained by convoluting the Boussinesq equation for the distribution of vertical pressure on a buried pipeline due to a concentrated surface load and the equation for a point load acting on a pipeline resting on an elastic medium. The results obtained indicate that the concentrated surface load necessary to fracture a pipeline laid with normal cover (0.9 to 1.0 metres) would not normally be able to be produced by current axle loads. The results did however indicate that 100 mm diameter asbestos cement pipe was vulnerable if laid with a depth of cover of 500 mm or less.

9.3 NON-LINEAR ELASTIC MATHEMATICAL MODEL OF LONGITUDINAL BENDING

The formulae derived from the theory of a beam on an elastic foundation are entirely linear elastic so a discrete mathematical model is proposed in which it can be assumed that the ground has a non-linear pressure-displacement relationship and the pipeline is composed of elemental lengths with different moduli of elasticity and second moments of area.

9.4 FULL SCALE EXPERIMENTAL SIMULATION OF GROUND MOVEMENT

An experiment was designed by which a double length of pipe could be subjected to a series of incremental differential displacements while enclosed within an elastic medium.

The surrounding medium, polystyrene beads, was in fact found to be non-linear and values of its resistance, per incremental level, were calculated from the simultaneous solution of the equations of vertical equilibrium and equilibrium of moments for each pipe.

The values calculated were used in the non-linear mathematical model to produce a series of displacements and bending moments which when compared with the experimental values indicate the validity of the model in this case.

The model was used to obtain the differential displacements necessary to fracture various sizes of asbestos cement, cast iron and spun iron mains in a range of non-homogeneous soil.

The analysis clearly demonstrates that if pipelines are laid in such a manner that there is a softer backfill material above the pipe than below the pipe, or vice versa, then the chances of a transverse fracture are greatly reduced.

The detrimental effect of allowing a pipeline to be built into a material with a large resistance, such as a brick wall, or to be laid across a material with a large resistance, such as another pipeline is also demonstrated.

9.5 MATHEMATICAL SIMULATION OF DUCTILE PIPE MATERIALS

The non-linear elastic mathematical model of longitudinal bending was extended to deal with ductile pipe materials, whose time independent stress-strain curves could be approximated by two straight lines.

9.6 EXPERIMENTAL SIMULATION OF GROUND MOVEMENT ACTING ON A DUCTILE PIPE

An experiment was designed by which a pipe of ductile material could be subjected to a series of incremental differential displacements while supported by sets of springs.

The experimental values of the pipe and spring constants were used in the non-linear mathematical model, extended to deal with ductile pipe materials, and showed that the proposed model was simulating the expected response of a ductile material to differential displacement.

The experimental deflection profiles displayed a lack of antisymmetry which indicated that the pipe was not distributing the load uniformly. There was a fair correspondence between the experimental and computed values in the area around the origin.

9.7 ECONOMICS OF MAINS REPLACEMENT

The primary causes of fractures in water mains have been identified, so it is possible, either to construct a regression equation for the number of future fractures in a particular length of pipe or to determine an overall base fracture rate and use either as the basis of a mains replacement policy.

The advantage of using the regression equation approach is that the subsequent analysis would not only indicate pipes that would need replacing in the next year but would also give an overall picture of pipes needing replacement in the near future.

Formulae are given for assessing the economics of:

i) relining a main as opposed to relaying it

ii) if a new main is to be laid whether it is advantageous to, preline it, sleeve it, or both.

CHAPTER 10

RECOMMENDATIONS

10.1 INTRODUCTION

The recommendations made are in two parts:

(i) for water undertakings in particular and covers, fracture data analysis, replacement policy and pipe laying practice

(ii) further research.

10.2 FRACTURE DATA ANALYSIS

The analysis of fracture data should not be an exercise that is performed every now and then. It should be carried out at least annually, so that any significant change in the pattern of fractures can be quickly recognised and monitored.

To facilitate such an analysis, a fracture data base should be initiated and a fracture report form introduced which will contain the maximum amount of information available about the many parameters which have an effect on buried pipelines.

The use of The Ordnance Survey National Grid Reference to 12 figures, 6 each of eastings and northings, is also recommended, as this will uniquely define the position of the fracture and the other information contained on a fracture report form even when all other surface detail has been obliterated.

10.3 REPLACEMENT POLICY

The fracture data base should be used as the basis of a mains replacement policy.

The use of a fracture regression curve for a single main or a group of mains will not only give the projected replacement years but can also be used to give an estimate of the state of the system both at present and in the future.

10.4 PIPE LAYING PRACTICE

When designing and laying pipelines, the effect of differential displacement should be taken into account. This can be done either by using the design formulae or tables given, and will probably mean using a stronger pipe material, or a larger pipe size, or an imported softer backfill material.

Great care should also be exercised in avoiding the laying of a main on any hard object or other service, or having these laid on a main.

10.5 FURTHER RESEARCH

The cause and effect of fissure corrosion in spun iron mains is known, but its detection is difficult, so the sampling programme already started should be continued and possibly enlarged, to find out the true extent of the problem and also to investigate the techniques for the detection of this form of corrosion.

Fissure corrosion in ductile iron should also be investigated to find its exact conditions of occurrence and therefore its possible control.

A programme of mains monitoring should be initiated in which certain pipes would be selected for instrumentation, to measure such effects as:

(i) the correlation between a drop in air temperature and the increase in transverse fractures

(ii) traffic and frost loading

(iii) the effect of adjacent deep excavations

The mathematical model of a ductile pipe should be investigated further as such a model is necessary for comparing the reaction of various materials to the effects of differential displacement.

The investigations should include extending the model to simulate materials with time dependent stress-strain curves, changes in the temperature of the surrounding soil and the effect of ovality in the pipe cross-section.

APPENDIX A

Readings from short pipe tests

TABLE. A.1 Short pipe test A

Test: A Fill: Polystyrene beads Pipe: Length=300.0 mm Diameter=121.9 mm		
Reading	Displacement (mm)	Load (N)
1	0.0	0.0
2	0.19	17.1
3	0.35	28.5
4	0.56	34.2
5	0.85	48.5
6	1.39	61.6
7	1.93	79.8
8	2.54	99.8
9	3.06	114.4
10	3.57	124.3
11	4.08	138.0
12	4.58	151.1
13	5.08	168.2
14	5.58	179.6
15	6.11	193.9
16	6.89	216.7
17	7.52	231.0
18	8.06	250.9
19	9.22	282.3
20	10.18	308.0
21	11.17	336.5
22	12.26	359.3
23	13.73	393.5
24	14.93	427.7
25	16.66	461.9
26	17.04	484.8
27	18.13	507.6
28	19.42	547.5
29	20.64	581.7
30	21.87	610.2
31	22.88	638.7
32	24.09	667.3
33	25.49	701.5
34	26.59	735.7
35	27.82	758.5
36	29.13	787.0
37	30.67	826.9
38	33.22	941.0
39	34.85	986.6
40	35.69	998.0

TABLE. A.2 Short pipe test B

Test: B Fill: Polystyrene beads Pipe: Length=228.0 mm Diameter=121.9 mm		
Reading	Displacement (mm)	Load (N)
1	0.0	0.0
2	0.05	10.8
3	0.28	41.4
4	0.68	70.7
5	1.00	85.0
6	1.32	98.4
7	1.59	110.6
8	1.85	119.8
9	2.29	128.9
10	2.79	137.4
11	3.28	157.4
12	3.78	176.8
13	4.28	191.1
14	4.80	200.8
15	5.30	216.7
16	5.80	235.5
17	6.30	244.7
18	6.80	256.6
19	7.30	277.7
20	7.83	284.6
21	8.33	299.4
22	8.82	310.8
23	9.32	327.9
24	9.84	342.2
25	10.33	356.4
26	10.84	366.4
27	11.33	379.3
28	11.84	390.7
29	12.82	427.7
30	13.83	456.2
31	14.83	486.2
32	15.80	504.7
33	16.90	523.3
34	17.85	547.5
35	18.87	594.3
36	19.87	628.5
37	20.70	655.9
38	21.90	681.4
39	22.91	712.9
40	23.91	746.3

continued /...

TABLE. A.2 Short pipe test B

continued /...

41	24.93	764.2
42	25.92	796.7
43	26.93	831.2
44	27.95	852.6
45	28.93	884.0
46	29.94	915.3
47	30.94	941.0
48	32.28	969.5

TABLE. A.3 Short pipe test C

Test: C Fill: Polystyrene beads Pipe: Length=228.0 mm Diameter=121.9 mm		
Reading	Displacement (mm)	Load (N)
1	0.0	0.0
2	0.93	54.2
3	1.48	74.1
4	1.97	85.6
5	2.45	102.7
6	2.99	119.8
7	3.45	131.2
8	4.00	142.6
9	4.48	156.8
10	5.07	171.1
11	5.65	188.2
12	6.17	202.5
13	6.73	216.7
14	7.75	245.2
15	8.77	273.7
16	9.75	299.4
17	10.76	327.9
18	11.82	356.4
19	12.78	379.3
20	13.82	404.9
21	14.89	436.3
22	15.93	459.1
23	16.92	490.5
24	18.00	519.0
25	19.03	547.5
26	20.07	570.3
27	21.08	596.0
28	22.08	621.6
29	23.16	664.4
30	24.08	684.4
31	25.17	701.5
32	26.17	732.8
33	27.12	778.5
34	28.10	798.4
35	29.14	838.3
36	30.95	878.3
37	31.14	906.8
38	32.27	938.1
39	33.54	980.9
40	35.91	1049.4

continued /...

TABLE. A.3 Short pipe test C

continued /...

41	37.20	1112.1
42	39.14	1206.1
43	41.01	1220.4
44	44.03	1328.8
45	45.98	1388.7

TABLE. A.4 Short pipe test D

Test: D Fill: Polystyrene beads Pipe: Length=300.0 mm Diameter=121.9 mm		
Reading	Displacement (mm)	Load (N)
1	0.0	0.0
2	0.13	28.5
3	0.47	68.4
4	0.69	91.2
5	1.10	122.6
6	1.49	151.1
7	1.91	176.8
8	2.44	199.6
9	2.94	222.4
10	3.46	245.2
11	4.05	273.7
12	4.63	296.6
13	5.22	319.4
14	5.72	336.5
15	6.20	359.3
16	6.66	379.3
17	7.19	396.4
18	7.69	416.3
19	8.19	433.4
20	8.68	453.7
21	9.18	467.7
22	10.17	516.1
23	11.17	553.2
24	12.18	590.3
25	13.10	630.2
26	14.15	675.8
27	15.15	710.0
28	16.13	741.4
29	17.12	775.6
30	18.11	815.5
31	19.09	849.7
32	20.08	889.7
33	21.06	915.3
34	22.08	935.3
35	23.06	989.5
36	24.05	1015.1
37	25.07	1038.0
38	26.10	1078.0
39	27.08	1120.6
40	28.08	1169.1

continued /...

TABLE. A.4 Short pipe test D

continued /...

41	29.08	1192.0
42	30.06	1235.0
43	31.07	1283.2
44	32.07	1323.1
45	33.07	1365.9
46	34.05	1385.8
47	35.05	1420.0
48	36.07	1454.3
49	37.07	1477.1
50	38.06	1534.0
51	39.06	1568.0
52	40.07	1596.8
53	41.05	1631.1
54	42.05	1691.0
55	43.03	1711.0
56	45.03	1802.0
57	47.04	1888.0

TABLE. A.5 Short pipe test E

Test: E Fill: Polystyrene beads Pipe: Length=300.0 mm Diameter=121.9 mm		
Reading	Displacement (mm)	Load (N)
1	0.0	0.0
2	0.15	22.8
3	0.34	42.8
4	0.47	54.2
5	0.61	65.6
6	0.94	84.1
7	1.18	97.0
8	1.46	108.4
9	1.94	131.7
10	2.44	151.1
11	2.94	166.8
12	3.42	183.9
13	3.93	203.9
14	4.45	216.7
15	4.92	231.0
16	5.42	248.1
17	5.90	269.5
18	6.40	288.0
19	6.89	305.1
20	7.39	323.6
21	7.86	340.8
22	8.37	356.4
23	8.88	373.5
24	9.37	390.7
25	9.87	407.8
26	10.36	423.4
27	10.86	439.1
28	11.34	456.2
29	11.84	473.3
30	12.33	490.5
31	12.82	510.4
32	13.31	521.8
33	13.84	536.1
34	14.31	554.6
35	14.80	558.9
36	15.28	584.6
37	15.78	604.5
38	16.77	655.8
39	17.78	701.5
40	18.78	735.7

continued /...

TABLE. A.5 Short pipe test E

continued /...

41	19.74	775.6
42	20.87	804.1
43	22.18	826.9
44	23.18	867.2
45	25.00	958.1

TABLE. A.6 Short pipe test F

Test: F Fill: Polystyrene beads Pipe: Length=228.0 mm Diameter=121.9 mm		
Reading	Displacement (mm)	Load (N)
1	0.0	0.0
2	0.19	22.8
3	0.43	39.9
4	0.78	65.6
5	1.27	91.2
6	1.76	115.5
7	2.26	138.3
8	2.76	159.7
9	3.26	176.8
10	3.76	195.3
11	4.25	212.4
12	4.74	229.5
13	5.25	246.7
14	5.74	262.3
15	6.25	282.3
16	6.74	299.4
17	7.22	316.5
18	7.73	333.6
19	8.24	350.7
20	8.71	367.8
21	9.23	383.5
22	9.73	404.9
23	10.24	416.3
24	10.72	433.4
25	11.23	449.1
26	11.73	460.5
27	12.73	507.6
28	13.73	547.5
29	14.73	587.4
30	15.72	621.6
31	16.73	651.6
32	17.72	690.1
33	18.72	721.4
34	19.73	758.5
35	20.74	784.2
36	21.70	807.0
37	22.72	844.0
38	23.73	878.3
39	24.74	926.7
40	25.73	966.7

continued /...

TABLE. A.6 Short pipe test F

continued /...

41	26.71	995.2
42	27.72	1029.4
43	28.72	1060.8
44	29.72	1106.4
45	30.72	1144.9
46	31.72	1176.2
47	32.71	1214.7
48	33.70	1246.1
49	34.72	1291.7
50	35.70	1325.9
51	36.67	1348.8
52	37.70	1391.5
53	38.67	1425.8
54	39.68	1465.7
55	40.68	1519.8
56	41.67	1554.1
57	42.66	1596.8

APPENDIX B

Derived deflections and bending moments,
full scale experiment

TABLE. B.1 Derived deflections for trench displacement -6mm

Distance along pipe (mm)	Left hand side Displacement (mm)	Right hand side Displacement (mm)
0	-2.715	-2.715
200	-1.935	-3.560
350	-1.420	-4.130
500	-0.960	-4.665
650	-0.585	-5.105
800	-0.315	-5.485
950	-0.100	-5.770
1100	0.040	-6.020
1250	0.130	-6.175
1400	0.180	-6.280
1550	0.180	-6.360
1700	0.180	-6.395
1850	0.155	-6.425
2000	0.135	-6.405
2150	0.120	-6.380
2300	0.085	-6.350
2450	0.065	-6.315
2600	0.030	-6.270
2750	0.020	-6.230
2900	0.005	-6.190
3050	-0.010	-6.145
3350	-0.015	-6.075
3650	-0.005	-6.040
3950	-0.010	-6.010
4550	0.000	-6.005
5150	0.000	-6.005

TABLE. B.2 Derived deflections for trench displacement -12mm

Distance along pipe (mm)	Left hand side Displacement (mm)	Right hand side Displacement (mm)
0	-4.725	-4.725
200	-3.305	-6.260
350	-2.390	-7.320
500	-1.610	-8.365
650	-0.985	-9.270
800	-0.515	-10.070
950	-0.150	-10.750
1100	0.080	-11.320
1250	0.240	-11.760
1400	0.335	-12.080
1550	0.360	-12.335
1700	0.360	-12.505
1850	0.320	-12.615
2000	0.285	-12.660
2150	0.250	-12.670
2300	0.195	-12.640
2450	0.140	-12.580
2600	0.100	-12.515
2750	0.060	-12.440
2900	0.035	-12.360
3050	-0.010	-12.285
3350	-0.015	-12.140
3650	-0.005	-12.060
3950	-0.015	-12.010
4550	0.000	-12.005
5150	0.000	-12.015

TABLE. B.3 Derived deflections for trench displacement -18mm

Distance along pipe (mm)	Left hand side Displacement (mm)	Right hand side Displacement (mm)
0	-6.840	-6.840
200	-4.850	-9.020
350	-3.540	-10.570
500	-2.420	-12.070
650	-1.505	-13.405
800	-0.805	-14.595
950	-0.250	-15.620
1100	0.130	-16.490
1250	0.390	-17.190
1400	0.550	-17.730
1550	0.620	-18.155
1700	0.645	-18.450
1850	0.610	-18.665
2000	0.565	-18.775
2150	0.470	-18.825
2300	0.420	-18.815
2450	0.335	-18.765
2600	0.260	-18.685
2750	0.185	-18.605
2900	0.125	-18.510
3050	0.020	-18.410
3350	0.000	-18.210
3650	-0.035	-18.095
3950	-0.035	-18.030
4550	-0.005	-18.010
5150	0.000	-18.025

TABLE. B.4 Derived deflections for trench displacement -24mm

Distance along pipe (mm)	Left hand side Displacement (mm)	Right hand side Displacement (mm)
0	-8.990	-8.990
200	-6.355	-11.855
350	-4.630	-13.920
500	-3.140	-15.885
650	-2.000	-17.650
800	-1.015	-19.205
950	-0.270	-20.550
1100	0.230	-21.915
1250	0.580	-22.650
1400	0.800	-23.370
1550	0.900	-23.955
1700	0.935	-24.375
1850	0.880	-24.665
2000	0.830	-24.840
2150	0.710	-24.920
2300	0.620	-24.940
2450	0.505	-24.895
2600	0.395	-24.805
2750	0.290	-24.715
2900	0.200	-24.610
3050	0.065	-24.490
3350	0.015	-24.225
3650	-0.035	-24.115
3950	-0.040	-24.035
4550	-0.010	-24.000
5150	0.000	-24.025

TABLE. B.5 Derived deflections for trench displacement -30mm

Distance along pipe (mm)	Left hand side Displacement (mm)	Right hand side Displacement (mm)
0	-11.255	-11.255
200	-7.990	-14.825
350	-5.840	-17.370
500	-3.990	-19.810
650	-2.470	-21.985
800	-1.290	-23.905
950	-0.340	-25.570
1100	0.325	-27.020
1250	0.790	-28.185
1400	1.090	-29.110
1550	1.245	-29.890
1700	1.305	-30.370
1850	1.270	-30.800
2000	1.195	-30.985
2150	1.060	-31.110
2300	0.950	-31.140
2450	0.800	-31.100
2600	0.650	-30.995
2750	0.500	-30.890
2900	0.365	-30.770
3050	0.190	-30.630
3350	0.075	-30.350
3650	-0.025	-30.170
3950	-0.045	-30.060
4550	-0.010	-30.000
5150	-0.005	-30.025

TABLE. B.6 Derived bending moments for trench displacement -6mm

Distance along pipe (mm)	Left hand side Bending Moment (kN.mm)	Distance along pipe (mm)	Right hand side Bending Moment (kN.mm)
TENSION		COMPRESSION	
94.5	15.76	94.0	-8.34
219.5	24.07	219.0	-12.80
368.0	28.35	369.0	-20.38
518.0	27.84	519.0	-25.18
668.0	28.33	669.0	-24.78
817.0	24.63	817.0	GAUGE NOT WORKING
968.0	20.87	969.0	-22.12
1268.0	12.40	1269.0	-15.85
1720.0	4.21	1719.0	-8.53
2018.0	1.44	2019.0	-4.56
2618.0	-0.59	2619.0	1.54
3143.0	-0.73	3144.0	3.08
COMPRESSION		TENSION	
		94.0	-6.62
144.5	GAUGE NOT WORKING	144.0	-11.37
219.5	23.62	219.0	-16.74
294.5	23.09		
		369.0	-24.36
444.5	26.77	444.0	-25.53
594.5	26.44	594.0	-27.10
669.5	26.17	669.0	-27.37

TABLE. B.7 Derived bending moments for trench displacement -12mm

Distance along pipe (mm)	Left hand side Bending Moment (kN.mm)	Distance along pipe (mm)	Right hand side Bending Moment (kN.mm)
TENSION		COMPRESSION	
94.5	30.83	94.0	-0.76
219.5	44.01	219.0	-7.53
368.0	50.32	369.0	-20.38
518.0	49.98	519.0	-29.75
668.0	50.13	669.0	-33.30
817.0	45.74	817.0	GAUGE NOT WORKING
968.0	40.29	969.0	-33.56
1268.0	27.29	1269.0	-28.53
1720.0	14.04	1719.0	-14.73
2018.0	8.66	2019.0	-6.84
2618.0	3.54	2619.0	4.61
3143.0	3.66	3144.0	10.02
COMPRESSION		TENSION	
		94.0	-1.47
144.5	GAUGE NOT WORKING	144.0	-11.37
219.5	37.22	219.0	-19.78
294.5	40.40		
		369.0	-30.26
444.5	43.42	444.0	-37.54
594.5	41.02	594.0	-44.42
669.5	40.38	669.0	-45.62

TABLE. B.8 Derived bending moments for trench displacement -18mm

Distance along pipe (mm)	Left hand side Bending Moment (kN.mm)	Distance along pipe (mm)	Right hand side Bending Moment (kN.mm)
TENSION		COMPRESSION	
94.5	47.27	94.0	0.0
219.5	57.07	219.0	-12.05
368.0	72.30	369.0	-30.95
518.0	69.25	519.0	-44.25
668.0	68.29	669.0	-50.33
817.0	61.93	817.0	GAUGE NOT WORKING
968.0	52.53	969.0	-51.87
1268.0	35.56	1269.0	-45.18
1720.0	17.55	1719.0	-27.13
2018.0	9.38	2019.0	-15.95
2618.0	2.36	2619.0	0.77
3143.0	0.73	3144.0	10.02
COMPRESSION		TENSION	
		94.0	1.47
144.5	GAUGE NOT WORKING	144.0	-9.85
219.5	62.27	219.0	-30.43
294.5	63.49		
		369.0	-39.12
444.5	67.30	444.0	-48.05
594.5	62.99	594.0	-57.97
669.5	61.32	669.0	-60.07

TABLE. B.9 Derived bending moments for trench displacement -24mm

Distance along pipe (mm)	Left hand side Bending Moment (kN.mm)	Distance along pipe (mm)	Right hand side Bending Moment (kN.mm)
TENSION		COMPRESSION	
94.5	61.66	94.0	-0.76
219.5	81.83	219.0	-16.56
368.0	92.85	369.0	-40.76
518.0	90.67	519.0	-57.98
668.0	88.63	669.0	-65.04
817.0	80.23	817.0	GAUGE NOT WORKING
968.0	69.80	969.0	-68.65
1268.0	47.96	1269.0	-58.65
1720.0	24.57	1719.0	-35.65
2018.0	12.99	2019.0	-21.27
2618.0	3.54	2619.0	0.00
3143.0	0.73	3144.0	12.33
COMPRESSION		TENSION	
		94.0	2.94
144.5	GAUGE NOT WORKING	144.0	-12.13
219.5	79.44	219.0	-28.15
294.5	82.97		
		369.0	-48.72
444.5	88.28	444.0	-61.56
594.5	82.77	594.0	-75.29
669.5	80.02	669.0	-77.56

TABLE. B.10 Derived bending moments for trench displacement -30mm

Distance along pipe (mm)	Left hand side Bending Moment (kN.mm)	Distance along pipe (mm)	Right hand side Bending Moment (kN.mm)
TENSION		COMPRESSION	
94.5	73.99	94.0	-2.28
219.5	96.96	219.0	-22.59
368.0	110.57	369.0	-52.84
518.0	108.52	519.0	-72.48
668.0	106.79	669.0	-82.08
817.0	96.41	817.0	GAUGE NOT WORKING
968.0	84.91	969.0	-86.19
1268.0	57.89	1269.0	-75.30
1720.0	30.19	1719.0	-46.50
2018.0	15.88	2019.0	-29.62
2618.0	3.54	2619.0	-3.08
3143.0	0.00	3144.0	12.33
COMPRESSION		TENSION	
		94.0	3.68
144.5	GAUGE NOT WORKING	144.0	-15.16
219.5	96.62	219.0	-35.00
294.5	103.18		
		369.0	-67.17
444.5	107.82	444.0	-74.33
594.5	103.28	594.0	-91.85
669.5	99.46	669.0	-94.29

APPENDIX C

Computed deflections and bending moments,
full scale experiment

TABLE. C.1 Computed deflections and bending moments for trench displacement -6mm

Distance along pipe (mm)	Left hand side		Right hand side	
	Displacement (mm)	Bending Moment (kN.mm)	Displacement (mm)	Bending Moment (kN.mm)
0	-2.735	3.54	-2.735	3.54
150	-2.136	17.86	-3.344	-10.78
300	-1.584	27.34	-3.927	-20.84
450	-1.104	31.34	-4.457	-26.30
600	-0.708	31.47	-4.924	-28.32
750	-0.398	29.11	-5.317	-27.93
900	-0.166	25.31	-5.639	-26.00
1050	-0.004	20.89	-5.895	-23.23
1200	0.100	16.40	-6.090	-20.17
1350	0.160	12.22	-6.234	-17.11
1500	0.186	8.57	-6.334	-14.20
1650	0.188	5.54	-6.397	-11.50
1800	0.175	3.16	-6.430	-9.06
1950	0.153	1.37	-6.440	-6.89
2100	0.126	0.12	-6.432	-5.00
2250	0.099	-0.70	-6.411	-3.39
2400	0.074	-1.17	-6.381	-2.05
2550	0.052	-1.38	-6.346	-0.95
2700	0.034	-1.41	-6.308	-0.08
2850	0.020	-1.31	-6.270	0.59
3000	0.009	-1.14	-6.234	1.08
3150	0.001	-0.94	-6.200	1.42
3300	-0.004	-0.73	-6.170	1.63
3450	-0.007	-0.53	-6.143	1.74
3600	-0.009	-0.36	-6.122	1.74
3750	-0.009	-0.21	-6.105	1.67
3900	-0.009	-0.10	-6.092	1.53
4050	-0.009	-0.02	-6.083	1.32
4200	-0.009	0.03	-6.077	1.07
4350	-0.009	0.05	-6.074	0.76
4500	-0.009	0.04	-6.073	0.40

TABLE. C.2 Computed deflections and bending moments for trench displacement -12mm

Distance along pipe (mm)	Left hand side		Right hand side	
	Displacement (mm)	Bending Moment (kN.mm)	Displacement (mm)	Bending Moment (kN.mm)
0	-4.739	12.89	-4.739	12.89
150	-3.630	35.83	-5.886	-9.90
300	-2.625	50.63	-7.008	-26.58
450	-1.768	55.82	-8.058	-37.03
600	-1.075	54.49	-9.006	-42.56
750	-0.543	49.13	-9.835	-44.34
900	-0.158	41.69	-10.541	-43.38
1050	0.101	33.55	-11.125	-40.58
1200	0.260	25.65	-11.595	-36.65
1350	0.342	18.53	-11.962	-32.19
1500	0.367	12.49	-12.239	-27.62
1650	0.354	7.61	-12.437	-23.17
1800	0.318	3.88	-12.570	-18.99
1950	0.269	1.17	-12.650	-15.14
2100	0.217	-0.67	-12.686	-11.69
2250	0.166	-1.79	-12.689	-8.66
2400	0.120	-2.37	-12.668	-6.04
2550	0.081	-2.56	-12.629	-3.84
2700	0.050	-2.47	-12.580	-2.01
2850	0.026	-2.21	-12.524	-0.55
3000	0.009	-1.86	-12.467	0.60
3150	-0.003	-1.48	-12.411	1.46
3300	-0.010	-1.11	-12.356	2.06
3450	-0.014	-0.77	-12.314	2.44
3600	-0.016	-0.48	-12.275	2.63
3750	-0.016	-0.25	-12.243	2.65
3900	-0.016	-0.08	-12.219	2.52
4050	-0.015	0.04	-12.201	2.26
4200	-0.014	0.10	-12.190	1.87
4350	-0.013	0.12	-12.184	1.36
4500	-0.013	0.08	-12.182	0.73

TABLE. C.3 Computed deflections and bending moments for trench displacement -18mm

Distance along pipe (mm)	Left hand side		Right hand side	
	Displacement (mm)	Bending Moment (kN.mm)	Displacement (mm)	Bending Moment (kN.mm)
0	-6.930	17.77	-6.930	17.77
150	-5.381	46.23	-8.531	-10.46
300	-3.966	65.12	-10.107	-31.66
450	-2.741	72.50	-11.597	-45.73
600	-1.730	71.87	-12.960	-53.98
750	-0.932	66.12	-14.173	-57.66
900	-0.332	57.57	-15.226	-57.84
1050	0.096	47.92	-16.116	-55.49
1200	0.380	38.30	-16.850	-51.40
1350	0.548	29.38	-17.441	-46.25
1500	0.627	21.48	-17.901	-40.55
1650	0.642	14.77	-18.246	-34.73
1800	0.611	9.29	-18.494	-29.06
1950	0.552	5.00	-18.660	-23.71
2100	0.477	1.77	-18.758	-18.80
2250	0.396	-0.53	-18.803	-14.39
2400	0.317	-2.05	-10.54	-10.54
2550	0.244	-2.96	-18.782	-7.22
2700	0.179	-3.38	-18.736	-4.44
2850	0.124	-3.44	-18.677	-2.16
3000	0.079	-3.26	-18.611	-0.35
3150	0.044	-2.93	-18.545	1.05
3300	0.018	-2.50	-18.481	2.08
3450	0.000	-2.03	-18.423	2.78
3600	-0.013	-1.56	-18.373	3.18
3750	-0.021	-1.12	-18.332	3.33
3900	-0.025	-0.74	-18.299	3.25
4050	-0.027	-0.43	-18.276	2.97
4200	-0.028	-0.20	-18.262	2.49
4350	-0.028	-0.05	-18.254	1.83
4500	-0.028	0.01	-18.251	1.00

TABLE. C.4 Computed deflections and bending moments for trench displacement -24mm

Distance along pipe (mm)	Left hand side		Right hand side	
	Displacement (mm)	Bending Moment (kN.mm)	Displacement (mm)	Bending Moment (kN.mm)
0	-9.105	25.17	-9.105	25.17
150	-7.101	63.55	-11.177	-12.86
300	-5.266	89.27	-13.220	-41.71
450	-3.668	99.65	-15.160	-61.28
600	-2.339	99.28	-16.945	-73.22
750	-1.280	91.97	-18.544	-79.05
900	-0.470	80.79	-19.942	-80.15
1050	0.118	68.07	-21.135	-77.71
1200	0.519	55.32	-22.128	-72.78
1350	0.769	43.37	-22.936	-66.19
1500	0.899	32.63	-23.573	-58.65
1650	0.938	23.35	-24.059	-50.71
1800	0.913	15.60	-24.415	-42.79
1950	0.845	9.34	-24.660	-35.20
2100	0.750	4.47	-24.815	-28.15
2250	0.642	0.84	-24.897	-21.78
2400	0.532	-1.73	-24.922	-16.16
2550	0.426	-3.41	-24.906	-11.31
2700	0.329	-4.39	-24.860	-7.22
2850	0.243	-4.82	-24.795	-3.86
3000	0.171	-4.84	-24.720	-1.16
3150	0.112	-4.58	-24.641	0.92
3300	0.065	-4.12	-24.565	2.45
3450	0.030	-3.54	-24.495	3.51
3600	0.004	-2.92	-24.434	4.15
3750	-0.013	-2.30	-24.383	4.41
3900	-0.025	-1.69	-24.343	4.35
4050	-0.031	-1.16	-24.315	4.00
4200	-0.035	-0.72	-24.297	3.37
4350	-0.036	-0.37	-24.287	2.49
4500	-0.037	-0.13	-24.284	1.36

TABLE. C.5 Computed deflections and bending moments for trench displacement -30mm

Distance along pipe (mm)	Left hand side		Right hand side	
	Displacement (mm)	Bending Moment (kN.mm)	Displacement (mm)	Bending Moment (kN.mm)
0	-11.365	31.47	-11.365	31.47
150	-8.834	80.51	-13.981	-17.10
300	-6.517	113.19	-16.558	-53.84
450	-4.501	126.11	-19.001	-78.62
600	-2.825	125.30	-21.247	-93.61
750	-1.488	115.76	-23.255	-100.79
900	-0.467	101.52	-25.005	-101.94
1050	0.276	85.57	-26.496	-98.94
1200	0.784	69.74	-27.733	-92.09
1350	1.101	54.95	-28.735	-83.52
1500	1.266	41.68	-29.522	-73.79
1650	1.316	30.15	-30.119	-63.58
1800	1.282	20.46	-30.553	-53.45
1950	1.192	12.57	-30.849	-43.78
2100	1.066	6.36	-31.031	-34.83
2250	0.922	1.65	-31.124	-26.77
2400	0.773	-1.76	-31.147	-19.70
2550	0.628	-4.07	-31.120	-13.62
2700	0.494	-5.48	-31.056	-8.53
2850	0.375	-6.19	-30.970	-4.37
3000	0.272	-6.36	-30.870	-1.06
3150	0.187	-6.14	-30.773	1.48
3300	0.119	-5.64	-30.676	3.33
3450	0.065	-4.98	-30.588	4.58
3600	0.026	-4.21	-30.511	5.31
3750	-0.002	-3.41	-30.447	5.59
3900	-0.021	-2.61	-30.398	5.46
4050	-0.032	-1.88	-30.362	4.98
4200	-0.038	-1.23	-30.340	4.18
4350	-0.041	-0.70	-30.328	3.08
4500	-0.042	-0.29	-30.324	1.68

APPENDIX D

Derived deflections, ductile pipe experiment

TABLE. D.1 Derived deflections. First displacement position

Displacement position: 1

Plate displacements Upper: -9.983 -10.049 -10.190
Lower: -10.187 -10.175 -10.361

Average plate displacement: -10.157

Reference	Distance(mm)	Displacement(mm)
1	-558.8	-0.089
2	-533.3	-0.201
3	-507.5	-0.179
4	-484.2	-0.135
5	-460.0	-0.136
6	-434.9	-0.135
7	-410.8	-0.145
8	-386.1	-0.099
9	-362.1	-0.085
10	-337.6	-0.107
11	-313.0	-0.160
12	-287.9	-0.102
13	-263.4	-0.069
14	-238.8	-0.101
15	-216.9	-0.089
16	-190.8	-0.178
17	-164.8	-0.233
18	-139.5	-0.346
19	-114.8	-0.667
20	-90.2	-1.095
21	-66.1	-1.654
22	-41.4	-2.756
23	-18.2	-4.084
24	10.0	-5.629
25	36.3	-7.168
26	62.0	-8.472
27	85.0	-9.158
28	109.1	-9.591
29	135.4	-9.962
30	160.7	-10.184
31	185.6	-10.389
32	210.4	-10.460
33	234.5	-10.513
34	258.7	-10.610
35	284.0	-10.614
36	309.2	-10.630
37	335.2	-10.549
38	359.4	-10.528
39	383.1	-10.455
40	407.8	-10.409
41	434.0	-10.373
42	459.1	-10.381
43	484.2	-10.321
44	511.1	-10.355
45	535.6	-10.348
46	561.2	-10.325
47	584.9	-10.303

TABLE. D.2 Derived deflections. Second displacement position

Displacement position: 2

Plate displacements Upper: -19.651 -19.531 -19.317
Lower: -19.604 -19.756 -19.934

Average plate displacement: -19.632

Reference	Distance(mm)	Displacement(mm)
1	-563.8	-0.080
2	-538.2	-0.065
3	-512.5	-0.080
4	-489.1	-0.079
5	-465.0	-0.014
6	-439.8	-0.041
7	-415.7	0.020
8	-391.1	-0.009
9	-367.0	-0.019
10	-342.5	0.011
11	-318.0	0.028
12	-292.9	0.090
13	-268.3	0.090
14	-243.8	0.120
15	-221.8	0.089
16	-195.7	0.145
17	-169.8	0.095
18	-144.4	-0.097
19	-119.8	-0.335
20	-95.1	-0.786
21	-71.1	-1.827
22	-46.3	-3.832
23	-23.1	-6.555
24	5.1	-10.536
25	31.3	-14.094
26	57.0	-17.102
27	80.1	-18.562
28	104.2	-19.157
29	130.4	-19.553
30	155.8	-19.898
31	180.7	-20.250
32	205.5	-20.407
33	229.6	-20.480
34	253.8	-20.431
35	279.1	-20.427
36	304.3	-20.375
37	330.3	-20.226
38	354.4	-20.124
39	378.1	-19.996
40	402.9	-19.915
41	429.0	-19.895
42	454.2	-19.854
43	479.2	-19.852
44	506.1	-19.813
45	530.7	-19.813
46	556.2	-19.852
47	579.9	-19.832

TABLE. D.3 Derived deflections. Third displacement position

Displacement position: 3

Plate displacements Upper: -30.056 -30.110 -30.147
Lower: -29.397 -29.863 -30.465

Average plate displacement: -30.006

Reference	Distance(mm)	Displacement(mm)
1	-565.3	-0.089
2	-539.7	0.001
3	-514.0	-0.080
4	-490.6	-0.112
5	-466.5	-0.099
6	-441.3	-0.060
7	-417.2	-0.079
8	-392.6	-0.070
9	-368.6	-0.070
10	-344.0	-0.050
11	-319.5	0.005
12	-294.4	0.034
13	-269.8	0.062
14	-245.3	0.063
15	-223.3	0.066
16	-197.3	0.033
17	-171.3	0.006
18	-146.0	-0.079
19	-121.3	-0.400
20	-96.6	-0.870
21	-72.6	-2.066
22	-47.9	-4.946
23	-24.6	-9.367
24	3.6	-15.822
25	29.8	-21.745
26	55.5	-26.491
27	78.6	-28.631
28	102.6	-29.456
29	128.9	-29.821
30	154.3	-30.173
31	179.2	-30.409
32	203.9	-30.513
33	228.0	-30.560
34	252.3	-30.554
35	277.6	-30.501
36	302.8	-30.596
37	328.7	-30.481
38	352.9	-30.376
39	376.6	-30.348
40	401.3	-30.362
41	427.5	-30.302
42	452.7	-30.309
43	477.7	-30.332
44	504.6	-30.360
45	529.1	-30.357
46	554.7	-30.361
47	578.4	-30.380

TABLE. D.4 Derived deflections. Fourth displacement position

Displacement position: 4

Plate displacements Upper: -39.835 -40.021 -40.276
Lower: -39.715 -39.918 -40.165

Average plate displacement: -39.988

Reference	Distance(mm)	Displacement(mm)
1	-566.8	0.009
2	-541.2	-0.008
3	-515.5	-0.009
4	-492.1	0.001
5	-468.0	-0.052
6	-442.8	-0.046
7	-418.8	-0.041
8	-394.1	-0.009
9	-370.1	0.019
10	-345.5	-0.032
11	-321.0	0.094
12	-295.9	0.128
13	-271.3	0.147
14	-246.8	0.148
15	-224.8	0.220
16	-198.8	0.197
17	-172.8	0.217
18	-147.5	0.095
19	-122.8	-0.166
20	-98.2	-0.912
21	-74.1	-2.263
22	-49.4	-5.925
23	-26.1	-11.777
24	2.1	-20.645
25	28.3	-28.919
26	54.0	-35.145
27	77.0	-37.988
28	101.1	-38.909
29	127.4	-39.487
30	152.8	-39.980
31	177.7	-40.266
32	202.4	-40.344
33	226.5	-40.248
34	250.8	-40.370
35	276.1	-40.347
36	301.3	-40.098
37	327.2	-39.953
38	351.4	-39.897
39	375.1	-39.825
40	399.8	-39.813
41	426.0	-39.736
42	451.2	-39.796
43	476.2	-39.737
44	503.1	-39.777
45	527.6	-39.780
46	553.2	-39.912
47	576.9	-39.738

APPENDIX E

Computed linear elastic deflections and bending moments, ductile pipe simulation

TABLE. E.1 Computed linear elastic values. 1st. displacement position

Distance along pipe (mm)	Displacement (mm)	Bending Moment (kN.mm)
-600	-0.013	-0.21
-575	-0.008	-0.29
-550	0.000	-0.36
-525	0.012	-0.44
-500	0.029	-0.51
-475	0.052	-0.55
-450	0.082	-0.56
-425	0.119	-0.51
-400	0.161	-0.37
-375	0.207	-0.11
-350	0.254	0.29
-325	0.298	0.87
-300	0.330	1.67
-275	0.343	2.69
-250	0.323	3.96
-225	0.256	5.45
-200	0.124	7.11
-175	-0.092	8.84
-150	-0.413	10.49
-125	-0.857	11.82
-100	-1.440	12.52
-75	-2.168	12.16
-50	-3.038	10.23
-25	-4.024	6.10
0	-5.079	0.00
25	-6.334	-6.10
50	-7.12	-10.23
75	-7.989	-12.16
100	-8.718	-12.52
125	-9.301	-11.82
150	-9.745	-10.49
175	-10.066	-8.84
200	-10.282	-7.11
225	-10.414	-5.45
250	-10.481	-3.96
275	-10.501	-2.69
300	-10.488	-1.67
325	-10.456	-0.87
350	-10.412	-0.29
375	-10.365	0.11
400	-10.319	0.37
425	-10.276	0.51
450	-10.240	0.56
475	-10.210	0.55
500	-10.187	0.51
525	-10.169	0.44
550	-10.157	0.36
575	-10.149	0.29
600	-10.145	0.21

TABLE. E.2 Computed linear elastic values. 2nd. displacement position

Distance along pipe (mm)	Displacement (mm)	Bending Moment (kN.mm)
-600	-0.025	-0.41
-575	-0.016	-0.55
-550	-0.001	-0.70
-525	0.023	-0.85
-500	0.056	-0.98
-475	0.101	-1.07
-450	0.159	-1.08
-425	0.229	-0.98
-400	0.311	-0.71
-375	0.400	-0.22
-350	0.491	0.56
-325	0.575	1.69
-300	0.639	3.22
-275	0.663	5.21
-250	0.625	7.66
-225	0.495	10.53
-200	0.240	13.74
-175	-0.178	17.09
-150	-0.797	20.28
-125	-1.656	22.85
-100	-2.782	24.20
-75	-4.191	23.50
-50	-5.872	19.77
-25	-7.778	11.80
0	-9.816	0.00
25	-11.854	-11.80
50	-13.761	-19.77
75	-15.441	-23.50
100	-16.850	-24.20
125	-17.976	-22.85
150	-18.835	-20.28
175	-19.454	-17.09
200	-19.872	-13.74
225	-20.127	-10.53
250	-20.257	-7.66
275	-20.295	-5.21
300	-20.271	-3.22
325	-20.208	-1.69
350	-20.124	-0.56
375	-20.032	0.22
400	-19.943	0.71
425	-19.861	0.98
450	-19.791	1.08
475	-19.734	1.07
500	-19.688	0.98
525	-19.655	0.85
550	-19.631	0.70
575	-19.616	0.55
600	-19.607	0.41

TABLE. E.3 Computed linear elastic values. 3rd. displacement position

Distance along pipe (mm)	Displacement (mm)	Bending Moment (kN.mm)
-600	-0.039	-0.63
-575	-0.025	-0.84
-550	-0.002	-1.07
-525	0.034	-1.30
-500	0.086	-1.50
-475	0.155	-1.63
-450	0.243	-1.65
-425	0.350	-1.49
-400	0.475	-1.08
-375	0.611	-0.33
-350	0.751	0.86
-325	0.880	2.58
-300	0.976	4.93
-275	1.013	7.96
-250	0.955	11.70
-225	0.757	16.10
-200	0.367	21.00
-175	-0.272	26.12
-150	-1.219	31.00
-125	-2.531	34.93
-100	-4.253	36.99
-75	-6.406	35.93
-50	-8.974	30.21
-25	-11.888	18.03
0	-15.003	0.00
25	-18.119	-18.03
50	-21.032	-30.21
75	-23.601	-35.93
100	-25.754	-36.99
125	-27.475	-34.93
150	-28.787	-31.00
175	-29.735	-26.12
200	-30.373	-21.00
225	-30.763	-16.10
250	-30.961	-11.70
275	-31.020	-7.96
300	-30.983	-4.93
325	-30.886	-2.58
350	-30.758	-0.86
375	-30.618	0.33
400	-30.481	1.08
425	-30.357	1.49
450	-30.250	1.65
475	-30.161	1.63
500	-30.092	1.50
525	-30.041	1.30
550	-30.005	1.07
575	-29.981	0.84
600	-29.968	0.63

TABLE. E.4 Computed linear elastic values. 4th. displacement position

Distance along pipe (mm)	Displacement (mm)	Bending Moment (kN.mm)
-600	-0.051	-0.84
-575	-0.033	-1.12
-550	-0.002	-1.43
-525	0.046	-1.73
-500	0.115	-1.99
-475	0.207	-2.17
-450	0.324	-2.20
-425	0.667	-1.99
-400	0.633	-1.44
-375	0.815	-0.44
-350	1.001	1.14
-325	1.172	3.44
-300	1.301	6.57
-275	1.350	10.61
-250	1.272	15.59
-225	1.008	21.45
-200	0.489	27.99
-175	-0.362	34.81
-150	-1.624	41.31
-125	-3.373	46.55
-100	-5.667	49.29
-75	-8.536	47.88
-50	-11.960	40.27
-25	-15.842	24.03
0	-19.994	0.00
25	-24.146	-24.03
50	-28.029	-40.27
75	-31.452	-47.88
100	-34.321	-49.29
125	-36.615	-46.55
150	-38.364	-41.31
175	-39.626	-34.81
200	-40.477	-27.99
225	-40.996	-21.45
250	-41.261	-15.59
275	-41.339	-10.61
300	-41.289	-6.57
325	-41.160	-3.44
350	-40.989	-1.14
375	-40.803	0.44
400	-40.621	1.44
425	-40.455	1.99
450	-40.312	2.20
475	-40.195	2.17
500	-40.103	1.99
525	-40.034	1.73
550	-39.986	1.43
575	-39.955	1.12
600	-39.937	0.84

APPENDIX F

Computed inelastic deflections, bending moments,
depth of inelastic front and stress,
ductile pipe simulation

TABLE. F.1 Computed inelastic values. 1st. displacement position

Distance along pipe (mm)	Displacement (mm)	Bending Moment (kN.mm)	Depth of inelastic front (mm)	Stress (N/mm^2)
-600	-0.010	-0.09		-1.50
-575	-0.008	-0.13		-2.14
-550	-0.006	-0.18		-2.87
-525	-0.001	-0.23		-3.65
-500	0.006	-0.28		-4.45
-475	0.017	-0.32		-5.15
-450	0.032	-0.35		-5.65
-425	0.050	-0.36		-5.77
-400	0.073	-0.33		-5.30
-375	0.100	-0.25		-3.97
-350	0.129	-0.09		-1.48
-325	0.159	0.15		2.49
-300	0.187	0.51		8.30
-275	0.209	1.01		16.25
-250	0.219	1.64		26.57
-225	0.209	2.44		39.37
-200	0.169	3.37		54.48
-175	0.090	4.42	0.689	65.18
-150	-0.044	5.53	5.747	68.04
-125	-0.266	6.58	6.254	85.07
-100	-0.688	7.41	6.293	98.57
-75	-1.407	7.70	6.300	103.17
-50	-2.454	6.92	6.275	90.56
-25	-3.741	4.35	0.532	65.17
0	-5.079	0.00		0.00
25	-6.417	-4.35	0.532	-65.17
50	-7.704	-6.92	6.275	-90.56
75	-8.751	-7.70	6.300	-103.17
100	-9.469	-7.41	6.293	-98.57
125	-9.892	-6.58	6.254	-85.07
150	-10.113	-5.53	5.747	-68.04
175	-10.247	-4.42	0.689	-65.18
200	-10.327	-3.37		-54.48
225	-10.366	-2.44		-39.37
250	-10.376	-1.64		-26.57
275	-10.367	-1.01		-16.25
300	-10.345	-0.51		-8.30
325	-10.317	-0.15		-2.49
350	-10.287	0.09		1.48
375	-10.257	0.25		3.97
400	-10.231	0.33		5.30
425	-10.208	0.36		5.77
450	-10.189	0.35		5.65
475	-10.175	0.32		5.15
500	-10.164	0.28		4.45
525	-10.157	0.23		3.65
550	-10.152	0.18		2.87
575	-10.149	0.13		2.14
600	-10.148	0.09		1.50

TABLE. F.2 Computed inelastic values. 2nd. displacement position

Distance along pipe (mm)	Displacement (mm)	Bending Moment (kN.mm)	Depth of inelastic front (mm)	Stress (N/mm^2)
-600	-0.016	-0.08		-1.27
-575	-0.017	-0.13		-2.07
-550	-0.016	-0.19		-3.06
-525	-0.013	-0.26		-4.22
-500	-0.007	-0.34		-5.53
-475	0.003	-0.43		-6.91
-450	0.019	-0.51		-8.23
-425	0.040	-0.58		-9.31
-400	0.068	-0.61		-9.91
-375	0.103	-0.60		-9.71
-350	0.146	-0.51		-8.29
-325	0.194	-0.32		-5.17
-300	0.245	0.01		0.18
-275	0.296	0.52		8.37
-250	0.341	1.24		19.96
-225	0.370	2.19		35.44
-200	0.373	3.41		55.12
-175	0.335	4.89	2.096	65.29
-150	0.236	6.60	6.256	85.27
-125	-0.069	8.43	6.312	115.09
-100	-0.789	10.15	6.325	142.88
-75	-2.117	11.19	6.330	159.75
-50	-4.170	10.59	6.327	150.02
-25	-6.876	6.89	6.274	90.15
0	-9.816	0.00		0.00
25	-12.756	-6.89	6.274	-90.15
50	-15.463	-10.59	6.327	-150.22
75	-17.515	-11.19	6.330	-159.75
100	-18.843	-10.15	6.325	-142.88
125	-19.563	-8.43	6.312	-115.09
150	-19.868	-6.60	6.256	-85.27
175	-19.967	-4.89	2.096	-65.29
200	-20.005	-3.41		-55.12
225	-20.002	-2.19		-35.44
250	-19.973	-1.24		-19.96
275	-19.928	-0.52		-8.37
300	-19.877	-0.01		-0.18
325	-19.826	0.32		5.17
350	-19.778	0.51		8.29
375	-19.736	0.60		9.71
400	-19.700	0.61		9.91
425	-19.672	0.58		9.31
450	-19.651	0.51		8.23
475	-19.636	0.43		6.91
500	-19.625	0.34		5.53
525	-19.619	0.26		4.22
550	-19.616	0.19		3.06
575	-19.615	0.13		2.07
600	-19.616	0.08		1.27

TABLE. F.3 Computed inelastic values. 3rd. displacement position

Distance along pipe (mm)	Displacement (mm)	Bending Moment (kN.mm)	Depth of inelastic front (mm)	Stress (N/mm^2)
-600	-0.023	-0.06		-1.00
-575	-0.026	-0.12		-1.98
-550	-0.027	-0.20		-3.25
-525	-0.026	-0.30		-4.83
-500	-0.021	-0.41		-6.70
-475	-0.012	-0.54		-8.80
-450	0.004	-0.68		-11.02
-425	0.028	-0.81		-13.17
-400	0.062	-0.93		-14.96
-375	0.107	-0.99		-16.00
-350	0.163	-0.98		-15.77
-325	0.231	-0.84		-13.63
-300	0.308	-0.54		-8.80
-275	0.391	-0.02		-0.40
-250	0.474	0.77		12.51
-225	0.547	1.91		30.86
-200	0.596	3.43		55.45
-175	0.604	5.37	4.940	66.21
-150	0.538	7.73	6.300	103.75
-125	0.138	10.42	6.327	147.30
-100	-0.902	13.09	6.335	190.59
-75	-2.885	14.94	6.338	219.43
-50	-6.011	14.53	6.337	214.07
-25	-10.236	9.63	6.322	134.61
0	-15.003	0.00		0.00
25	-19.771	-9.63	6.322	-134.61
50	-23.995	-14.53	6.337	-214.07
75	-27.121	-14.94	6.338	-219.43
100	-29.104	-13.09	6.335	-190.59
125	-30.145	-10.42	6.327	-147.30
150	-30.544	-7.73	6.300	-103.75
175	-30.611	-5.37	4.940	-66.21
200	-30.603	-3.43		-55.45
225	-30.553	-1.91		-30.86
250	-30.480	-0.77		-12.51
275	-30.397	0.02		0.40
300	-30.314	0.54		8.80
325	-30.237	0.84		13.63
350	-30.170	0.98		15.77
375	-30.113	0.99		16.00
400	-30.069	0.93		14.96
425	-30.035	0.81		13.17
450	-30.011	0.68		11.02
475	-29.995	0.54		8.80
500	-29.985	0.41		6.70
525	-29.980	0.30		4.83
550	-29.979	0.20		3.25
575	-29.981	0.12		1.98
600	-29.983	0.06		1.00

TABLE. F.4 Computed inelastic values. 4th. displacement position

Distance along pipe (mm)	Displacement (mm)	Bending Moment (kN.mm)	Depth of inelastic front (mm)	Stress (N/mm^2)
-600	-0.030	-0.04		-0.67
-575	-0.035	-0.11		-1.81
-550	-0.039	-0.21		-3.36
-525	-0.040	-0.33		-5.35
-500	-0.037	-0.48		-7.79
-475	-0.028	-0.66		-10.65
-450	-0.012	-0.85		-13.80
-425	0.015	-1.06		-17.07
-400	0.054	-1.25		-20.13
-375	0.107	-1.39		-22.53
-350	0.178	-1.46		-23.64
-325	0.265	-1.40		-22.65
-300	0.368	-1.15		-18.56
-275	0.484	-0.63		-10.18
-250	0.607	0.23		3.79
-225	0.725	1.53		24.76
-200	0.825	3.34		54.04
-175	0.884	5.74	6.056	71.41
-150	0.833	8.75	6.315	120.19
-125	0.330	12.27	6.333	177.29
-100	-1.024	15.87	6.339	234.03
-75	-3.626	18.52	6.341	279.09
-50	-7.785	18.31	6.341	275.54
-25	-13.471	12.25	6.333	177.06
0	-19.994	0.00		0.00
25	-26.517	-12.25	6.333	-177.06
50	-32.203	-18.31	6.341	-275.54
75	-36.363	-18.52	6.341	-279.09
100	-38.965	-15.87	6.339	-234.03
125	-40.318	-12.27	6.333	-177.29
150	-40.821	-8.75	6.315	-120.19
175	-40.872	-5.74	6.056	-71.41
200	-40.813	-3.34		-54.04
225	-40.714	-1.53		-24.76
250	-40.595	-0.23		-3.79
275	-40.472	0.63		10.18
300	-40.356	1.15		18.56
325	-40.253	1.40		22.65
350	-40.166	1.46		23.64
375	-40.096	1.39		22.53
400	-40.042	1.25		20.13
425	-40.003	1.06		17.07
450	-39.976	0.85		13.80
475	-39.960	0.66		10.65
500	-39.951	0.48		7.79
525	-39.948	0.33		5.35
550	-39.949	0.21		3.36
575	-39.953	0.11		1.81
600	-39.958	0.04		0.67

REFERENCES

1. The water supply of London.
   The Metropolitan Water Board, London, June 1961.

2. Manual of British Water Engineering Practice.
   The Institution of Water Engineers, London, 3rd edition 1961.

3. Report of the sub-committee re-burst water mains to the Works and Stores Committee of The Board.
   The Metropolitan Water Board, London, July 1930.

4. Boden, W.
   Modern cast iron pipes and joints.
   The Stanton Ironworks Company Limited, January 1946.

5. BS 78:1938. Cast iron pipes (vertically cast) for water, gas and sewage and special castings for use therewith.
   British Standards Institution, London.

6. BS 1211:1958. Centrifugally cast (spun) iron pressure pipes for water, gas and sewage.
   British Standards Institution, London.

7. Metropolitan Water Board.
   71st Annual Report, London, March 1974.

8. Spheroidal graphite cast iron.
   The Mond Nickel Company Limited, London.

9. Scholes, J. P. and Fuller, A. G.
The properties of ductile iron pipe and their relevance to modern water supply practice.
British Cast Iron Research Association. Report No. X6, May 1973.

10. BS 4622:1970. Grey iron pipes and fittings.
British Standards Institution, London.

11. BS 4772:1971. Ductile iron pipes and fittings.
British Standards Institution, London.

12. Interim report of the departmental committee on the deterioration of cast iron and spun iron pipes.
Ministry of Health. HMSO, London 1950.

13. Reed, E. C.
Updating of pipe renovation techniques and experience.
International Water Supply Association. 14th Congress, Paris 1980.

14. BS 534:1966. Steel pipes, fittings and specials for water, gas and sewage.
British Standards Institution, London.

15. Concrete pipes and conduits (2nd edition).
Cement and Concrete Association, London.

16. BS 486:1973. Asbestos-cement pressure pipes.
British Standards Institution, London.

17. Plastic pipes and fittings.
Plastic Pipe Manufacturers' Society, Birmingham, February 1965.

18. BS 3505:1968. Unplasticized PVC pipe for cold water services.
British Standards Institution, London.

19. BS 1972:1967. Polythene pipe (type 32) for cold water services.
British Standards Institution, London.

20. BS 3284:1967. Polythene pipe (type 50) for cold water services.
British Standards Institution, London.

21. Report on burst water mains.
Institution of Water Engineers, London. Transactions,
Vol. XXXVI, June 1931.

22. Mabee, W. C.
Breaks in cast iron pipe gridiron systems.
Journal of the American Water Works Association, Vol. 24,
November 1932, pp 1717.- 1737.

23. Garrity, Leo V.
Detroit experience with sulfur compound jointing material.
Journal of the American Water Works Association, Vol. 47,
May 1955, pp 453 - 464.

24. Galler, Sol.
City plans to combat water main break problem.
Public Works, 109, No. 10, October 1978, pp 88 - 89.

25. Bacon, E. S, Langley, J. F. and Roberts, N. P.
A survey of fractures in grey cast iron water mains.
The City University, London, 2nd edition, March 1973.

26. Roberts, N. P. and Regan, T.
Causes of fractures in grey cast iron water mains.
The City University, London, March 1974.

27. Roberts, N. P. and Regan, T.
Pattern of fractures in cast iron mains - The influence of summer 1976.
The City University, London, December 1976.

28. Roberts, N. P. and Regan, T.
Fractures in water mains.
The City University, London, July 1977.

29. Harrison, J. T.
Corrosion and corrosion protection in gas transmission and distribution.
Gas Engineering and Management, December 1976, pp 409 - 420.

30. Gray, D. and Wilkins, R.
Materials preservation through control of corrosion (1).
Pipes and Pipelines International, October 1979, pp 9 - 14.

31. Lacey, R. F.
A statistical investigation of mains breakages and reported escapes from joints in the Metropolitan Division of South East Gas Board 1910 - 1970.
Gas Council Engineering Research Station. Report R 73, Dec 757, DEC/WPL 112, March 1972.

32. Clarke, N. W. B.
Buried pipelines (A manual of structural design and installation).
Maclaren and Sons, London, 1968.

33. Smith, W. Harry.
Frost loadings on underground pipe.
Journal of the American Water Works Association, Vol.68, No.12, December 1976, pp 673 - 674.

34. Monie, William D. and Clark, Curtis, M.
Loads on underground pipe due to frost penetration.
Journal of the American Water Works Association, Vol. 66, No. 6, June 1974, pp 353 - 358.

35. Metropolitan Water Board.
60th Annual Report, London, March 1963.

36. Chandler, T. J.
The Climate of London.
Hutchinson & Company (Publishers) Ltd, London, 1965.

37. Gray, D. and Wilkins, R.
Materials preservation through control of corrosion (2).
Pipes and Pipelines International, Vol. 24, No. 6, December 1979, pp 25 - 30.

38. Regan, T. and Speare, P. R. S.
Fissure corrosion in spun grey iron water mains.
The City University, London, May 1981.

39. Newport, Ray.
Factors influencing the occurrence of bursts in iron water mains.
Aqua. 3, 81, pp 0274 - 0278.

40. Maintenance, renovation and renewal of water mains - Effective management of a deteriorating asset.
The Severn Trent Water Authority, Draft Report, October 1978.

41. Parkinson, R. W.
Stress induced corrosion cracking in spun grey iron water mains.
Water Research Centre, Report LR 1069, September 1979.

42. Coe, A. L.
Water supply and plumbing practice in Continental Europe.
Hutchinson Benham, London, 1978.

43. Hetényi, M.
Beams on elastic foundation.
University of Michigan Press, 1946.

44. P.F.A as a fill.
Central Electricity Generating Board, London.

45. Soil mechanics for road engineers.
HMSO, London, 1952.

46. Terzaghi, Karl.
Evaluation of coefficients of subgrade reaction.
Géotechnique 5: 1955, pp 297 - 326.

47. Morris, Jr, R. E.
Principal causes and remedies of water main breaks.
Journal of the American Water Works Association, Vol. 59, No. 7, July 1967, pp 782 - 798.

48. Symons, I. F.
Ground movements and their influence on shallow buried pipes.
The Public Health Engineer, Vol. 8, No. 4, October 1980, pp 149 - 153 and 172.

49. Pearson, Frank H.
Beam behaviour of buried rigid pipelines.
Journal of the Environmental Engineering Division, American Society of Civil Engineers, Vol. 103, No. EE5, Paper 13253, October, 1977, pp 767 - 783.

50. American National Standard ANSI/AWWA C 101 - 67 (R 1977) for thickness design of cast-iron pipe with tables of pipe thickness (ASA. A21.1)
American Water Works Association, New York, 1977.

51. Kerr, Arnold D.
Elastic and viscoelastic foundation models.
American Society of Mechanical Engineers, Journal of Applied Mechanics, September 1964, pp 491 - 498.

52. Johnson, N. L. and Leone, F. C.
Statistics and experimental design in engineering and physical sciences, Vol. 1.
John Wiley & Sons Inc, 1964.

53. Pipes for water distribution to BS 3505:1968.
Chemidus Plastics Limited, Ashford, Kent, 8th issue,
April, 1971.

54. Spiegel, Murry R.
Theory and problems of advanced calculus.
Schaum Publishing Company, New York, 1963.

55. Smith, J. O. and Sidebottom, O. M.
Inelastic behaviour of load carrying members.
J. Wiley & Sons Inc, 1965.

56. Rolston, A.
A first course in numerical analysis.
McGraw-Hill, 1965.

57. Kemps Engineers Year Book for 1973, Vol. 1.
Morgan-Grampian (Publishers) Ltd, 78th edition, London, 1973.

58. Thoms, Robert L.
Experimental study of beam on elastic foundations.
American Society of Civil Engineers, Journal of the
Engineering Mechanics Division, EM3, 2509, June 1960,
pp 107 - 118.

59. Timoshenko, S.
Strength of Materials, Part II, Advanced Theory and Problems.
3rd edition. Van Nostrand Reinhold Company, 1958.

60. Romanoff, Melvin.
Underground corrosion.
National Bureau of Standards, Circular 579. United States Department of Commerce, April, 1957.

61. Kirby, P. C.
Internal corrosion and loss of strength of iron pipes.
Maintenance of water quality and pipeline integrity,
A Water Research Centre Conference, Water Research Centre,
February, 1979.

62. Shamir, Uri and Howard, Charles D. D.
An analytic approach to scheduling pipe replacement.
Journal of the American Water Works Association, Vol. 70,
No. 4, May 1979, pp 248 - 258.

63. Trewin, R. J, Robinson, B. and Howell, P.
Mains data - A computer system for distribution.
Gas Engineering and Management, November 1976, pp 387 - 404.